



ESCUELA POLITÉCNICA NACIONAL

DOCTORADO EN INGENIERÍA ELÉCTRICA MENCIÓN TELECOMUNICACIONES Y REDES DE LA INFORMACIÓN

SECURE PERFORMANCE OF 5G AND BEYOND NETWORKS UNDER GENERALIZED FADING CONDITIONS

**DOCTORAL THESIS FOR AWARDING THE DEGREE OF DOCTOR OF
ELECTRICAL ENGINEERING**

JOSÉ DAVID VEGA SÁNCHEZ

ADVISOR: Ph.D. MARTHA CECILIA PAREDES PAREDES

CO-ADVISORS: Ph.D. LUIS FELIPE URQUIZA AGUIAR

: Ph.D. DIANA PAMELA MOYA OSORIO

Quito, November 2021



ESCUELA POLITÉCNICA NACIONAL

**DOCTORADO EN INGENIERÍA ELÉCTRICA
MENCIÓN TELECOMUNICACIONES Y REDES DE LA
INFORMACIÓN**

**SECURE PERFORMANCE OF 5G AND BEYOND NETWORKS
UNDER GENERALIZED FADING CONDITIONS**

JOSÉ DAVID VEGA SÁNCHEZ

DIRECTOR: Ph.D. MARTHA CECILIA PAREDES PAREDES

CO-DIRECTOR: Ph.D. LUIS FELIPE URQUIZA AGUIAR

: Ph.D. DIANA PAMELA MOYA OSORIO

Tribunal de Defensa: Juan Manuel Romero Jerez
UMA/DTE/España
Edgar Eduardo Benitez Olivo
UNESP/DEET/Brasil
Soraya Lucia Sinche Maita
EPN/DETRI/Ecuador
Pablo Anibal Lupera Morillo
EPN/DETRI/Ecuador
Felipe Leonel Grijalva Arevalo
EPN/DETRI/Ecuador

Catalogación:

204 páginas; 21 x 15 cm

Línea de Investigación: Comunicaciones Inalámbricas.

Departamento de Electrónica, Telecomunicaciones y Redes de la Información (DETRI).

Primera Edición. Fecha de Catalogación: diciembre 2021

**SECURE PERFORMANCE OF 5G AND BEYOND NETWORKS
UNDER GENERALIZED FADING CONDITIONS**

JOSÉ DAVID VEGA SÁNCHEZ

Tesis de Doctorado

Programa de Doctorado en Ingeniería Eléctrica

Mención: Telecomunicaciones y Redes la Información

ISBN:

eISBN:

ESCUELA POLITÉCNICA NACIONAL, 2021

La reproducción total o parcial de este libro en forma idéntica o modificada, impresa o digital, no autorizada por los editores, viola derechos reservados. Cualquier utilización debe ser previamente solicitada.

© 2021 by Escuela Politécnica Nacional, Quito, Ecuador.

CERTIFICACIÓN

Certifico que el presente trabajo fue desarrollado por José David Vega Sánchez, bajo mi supervisión.

Ph.D. MARTHA CECILIA PAREDES PAREDES
DIRECTOR DE PROYECTO

DECLARACIÓN

Yo, José David Vega Sánchez, declaro bajo juramento que el trabajo aquí descrito es de mi autoría; que no ha sido previamente presentada para ningún grado o calificación profesional; y, que he consultado las referencias bibliográficas que se incluyen en este documento.

A través de la presente declaración cedo mis derechos de propiedad intelectual correspondientes a este trabajo, a la Escuela Politécnica Nacional, según lo establecido por la Ley de Propiedad Intelectual, por su Reglamento y por la normatividad institucional vigente.

José David Vega Sánchez

To my mother María Estela

ACKNOWLEDGEMENTS

First of all, I would like to sincerely thank my supervisors, Prof. Martha Cecilia Paredes and Prof. Luis Urquiza-Aguilar, who have continuously supported me with a deep insightful vision and brilliant thoughtful guidance. I would also like to express my deepest appreciation for having believed in me since the first time we met each other. All good and bad moments we shared in this doctoral journey, helped me to grow immensely.

I would like to give my special thanks to my co-supervisor, Prof. Diana Moya Osorio, for her insightful guidance and support in both research works and my personal life. I have gained a lot of knowledge from discussions with her on academic issues. I really appreciate her involvement in my process of academic training.

Special thanks are due to Prof. F. Javier López-Martínez for his fruitful cooperation. Through his in-depth discussions on random variables and channel models, I managed to develop as a researcher. Also, my unconditional thanks for his valuable friendship.

I would like to acknowledge the dissertation committee members for their constructive suggestions and their precious time in reviewing my dissertation, which helped improve its quality.

Most of all, I deeply thank my beloved mother, María Estela, for her unconditional support, caring, sacrifice, and love at all stages of my life. Everything I am, I owe to her. Thanks to my whole family for being my inspiration to achieve my goals.

In a special way, I would like to thank Erika Paola, a very special person in my life who has always encouraged me to finish this work and pushed me forward.

I am very grateful to all my friends who have accompanied my journey at Escuela Politécnica Nacional (EPN) during my period in the Doctorate program. Especially to José for his genuine friendship.

Finally, I would like to thank EPN for the financial support.

LIST OF NOTATIONS

ACRONYMS

4G	Fourth Generation
5G	Fifth Generation
6G	Sixth Generation
ABEP	Average Bit Error Probability
ASC	Average Secrecy Capacity
ASR	Average Secrecy Rate
AWGN	Additive White Gaussian Noise
BFSK	Binary Frequency-Shift Keying
BPSK	Binary Phase Shift Keying
CCDF	Complementary Cumulative Density Function
CDF	Cumulative Density Function
CF	Characteristic Function
CLT	Central Limit Theorem
CR	Cognitive Radio
CSI	Channel State Information
D2D	Device-to-Device
DBPSK	Binary Phase-Shift Keying
EE	Energy Efficiency
EGC	Equal Gain Combining
EM	Expectation-Maximization

FD	Full-Duplex
FT	Fourier Transform
FTR	Fluctuating Two-Ray
i.i.d.	independent and identically distributed
i.n.i.d.	independent but not identically distributed
LoS	Line-of-Sight
LT	Laplace Transform
MC	Monte Carlo
MGF	Moment Generating Function
MIMO	Multiple-Input Multiple-Output
MoM	Moment Matching Method
MRC	Maximal Ratio Combining
NLoS	Non-Line-of-Sight
NMM	Nakagami- m Mixture Model
NWDP	N-Wave with Diffuse Power
PDF	Probability Density Function
PLS	Physical Layer Security
RF	Radio-Frequency
RIS	Reconfigurable Intelligent Surface
RV	Random Variable
SC	Selection Combining
SE	Spectrum Efficiency
SISO	Single-Input-Single-Output
SNR	Signal-to-noise Ratio

SOP	Secrecy Outage Probability
SPSC	Strictly Positive Secrecy Capacity
TAS	Transmit Antenna Selection
TWDP	Two-Wave with Diffuse Power
UAV	Unmanned Aerial Vehicle

FUNCTIONS

$\Gamma(\cdot)$	Gamma function
$\Gamma(\cdot, \cdot)$	Upper incomplete gamma function
$\psi(\cdot)$	Digamma function
$G_{p,q}^{m,n}[\cdot]$	Meijer G-function
$U(\cdot; \cdot; \cdot)$	Confluent hypergeometric function
${}_1F_1(\cdot; \cdot; \cdot)$	Kummer confluent hypergeometric function
${}_2F_1(\cdot, \cdot; \cdot; \cdot)$	Hypergeometric function
$\mathbb{Q}_z(\cdot, \cdot)$	Marcum Q-function of order z
\mathcal{C}	Euler-Mascheroni constant
$H_{p,q}^{m,n}[\cdot]$	Fox H-function
$\text{erfc}(\cdot)$	Complementary error function
$\Phi_2(\cdot, \cdot; \cdot; \cdot, \cdot)$	Bivariate confluent hypergeometric function
$\Phi_Z(\cdot)$	Characteristic function of the variable Z
E_1	Exponential integral function
$\Upsilon(\cdot, \cdot)$	Lower incomplete gamma function
e	Exponential constant
$L_{(\cdot)}(\cdot)$	Laguerre polynomial
${}_2F_2(\cdot, \cdot; \cdot, \cdot; \cdot)$	Generalized hypergeometric function

SYMBOLS

\approx	“Approximately equal to”
$\phi_i(z, \theta_i)$	i -th PDF component from a mixture model with a parameter vector θ_i of a random variable Z
$\Pr\{\cdot\}$	Probability
\simeq	“Asymptotically equal to”
F_Z	Cumulative density function of Z
f_Z	Probability density function of Z
$f_Z(z, \theta)$	Probability density function of a random variable Z with a parameter vector θ
$ \cdot $	Absolute value
\forall	For all
\mathbb{C}	Complex numbers excluding 0
$\mathbb{E}[\cdot]$	Expectation operator
$\mathbb{R}^+, \mathbb{N}^+$	Positive real and integers numbers excluding 0
$\mathbb{V}[\cdot]$	Variance operator
j	Imaginary unit, $\sqrt{-1}$
$\ \cdot\ $	Modulus

CONTENTS

Resumen	xviii
Abstract	xx
1 INTRODUCTION	1
1.1 Related Work and Motivation	4
1.1.1 Sum of Random Variables	4
1.1.2 Ratio of Random Variables	5
1.1.3 Physical layer security over fading channel models	5
1.1.4 Physical layer security via Reconfigurable Intelligent Surfaces	7
1.2 Hypothesis	7
1.3 Main and Supplementary Objectives	7
1.3.1 Main Objective	7
1.3.2 Supplementary Objectives	8
1.4 Summary of Contributions	8
1.4.1 Thesis Outline	8
1.4.2 List of Publications	10
2 PRELIMINARIES	12
2.1 Fundamentals of Physical Layer Security	12
2.1.1 General System Model	12
2.1.2 Secrecy Metrics	13
2.2 Fading channel models overview	17
2.2.1 Classical fading models	17
2.2.2 Generalized fading models	19
2.3 Diversity Combining Techniques	23
2.3.1 Transmitter Antenna Diversity	24
2.3.2 Receiver Antenna Diversity	25
2.3.3 Performance Metric for Multibranch Combining Receivers	27
2.4 Fundamentals of RIS-assisted wireless communications	29
3 SUM AND RATIO OF RANDOM VARIABLES	31

3.1	Sum of Random Variables	31
3.1.1	Problem Formulation and Exact Solutions	31
3.1.2	Nakagami- m Approximation Approach	33
3.1.3	Generalized Approximation Approach	50
3.1.4	Conclusions	58
3.2	Ratio of Random Variables	59
3.2.1	Exact Solution Statistics	59
3.2.2	Proposed Ratio Statistics Representations	60
3.2.3	Numerical Results	65
3.2.4	Conclusions	68
4	PHYSICAL LAYER SECURITY ENHANCEMENT IN N-WAVE WITH DIFFUSE POWER FADING CHANNELS	69
4.1	System Model	69
4.2	Secrecy Metrics	70
4.2.1	SOP Analysis	70
4.2.2	Asymptotic SOP Analysis	71
4.2.3	ASC Analysis	72
4.2.4	Asymptotic ASC Analysis	73
4.3	Numerical Results and Discussions	74
4.4	Conclusions	82
5	SECURE TRANSMISSION WITH ANTENNA SELECTION IN MIMO κ-μ SHAD- OWED FADING CHANNELS	83
5.1	System and Channel Model Statistics	83
5.1.1	System Model	83
5.1.2	Channel Model	84
5.1.3	Transmission Scheme	86
5.1.4	Channel Statistics for TAS/MRC setup	87
5.2	Secrecy Metrics	89
5.2.1	SOP Analysis	89
5.2.2	Asymptotic SOP Analysis	90
5.2.3	ASC Analysis	91
5.2.4	Asymptotic ASC Analysis	93
5.3	Some Plots and Discussions	94
5.4	Conclusions	99

6	PHYSICAL LAYER SECURITY OF RECONFIGURABLE INTELLIGENT SURFACE-ASSISTED COMMUNICATIONS WITH PHASE ERRORS	101
6.1	System Model	101
6.2	SNR Distributions	103
6.2.1	Distribution of γ_b	103
6.2.2	Distribution of γ_e	104
6.3	PLS Performance Analysis	105
6.3.1	SOP Performance Analysis	106
6.3.2	ASR Performance Analysis	107
6.4	Numerical Results	109
6.5	Conclusions	112
7	CONCLUSIONS	113
7.1	Thesis Conclusions	113
7.2	Future Research Directions	115
8	REFERENCES	116
9	Appendices	i
A	Derivation of the ABEP expressions	ii
A.1	Proofs of Proposition 1	ii
A.2	Proofs of Proposition 2	ii
A.3	Proofs of Proposition 3	iv
B	Derivation of the κ-μ expressions	vii
B.1	Proof of Proposition 4	vii
B.2	Derivation of the Equation System for κ - μ case	vii
C	Derivation of the Ratio Statistics	ix
C.1	Proofs of Proposition 5	ix
C.2	Representation of THE FOX-H FUNCTION AS A SUM OF RESIDUES	xii
C.3	Mathematica Implementation for the Single Fox H-function	xiv
D	Derivation of the Secrecy metrics for the NWDP fading model	xv
D.1	Proofs of Proposition 6	xv
D.1.1	SOP	xv
D.1.2	SOP _A	xvi
D.2	Proofs of Proposition 7	xvii

D.2.1	SOP^∞	xvii
D.3	Proof of Proposition 8	xviii
D.4	Proof of Proposition 9	xxi
E	Derivation of the Secrecy metrics for the $K\text{-}\mu$ shadowed fading model	xxii
E.1	Proof of Proposition 10	xxii
E.2	Proof of Proposition 12	xxvi
E.3	Proof of Proposition 13	xxvii
E.4	Proofs of Proposition 14	xxix
E.5	Proofs of Proposition 15	xxxix
F	Proof of Theorem 1	xxxvii
G	Derivation of the SOP and the Asymptotic SOP Expressions	xxxviii
G.1	Proof of Lemma 1	xxxviii
G.1.1	SOP_{FR}	xxxviii
G.1.2	$SOP_{FR}^\infty (\bar{\gamma}_b \rightarrow \infty)$	xxxix
G.2	Proof of Lemma 2	xxxix
G.2.1	SOP_{BR}	xxxix
G.2.2	$SOP_{BR}^\infty (\bar{\gamma}_b \rightarrow \infty)$	xl
G.3	Proof of Lemma 3	xl
G.3.1	SOP_{NR}	xl
G.3.2	$SOP_{NR}^\infty (\bar{\gamma}_b \rightarrow \infty)$	xli
H	Derivation of the ASR and the Asymptotic ASR Expressions	xlii
H.1	Proof of Lemma 4	xlii
H.1.1	ASR_{S-FR}	xlii
H.1.2	$ASR_{S-FR}^\infty (\bar{\gamma}_b \rightarrow \infty)$	xliii
H.2	Proof of Lemma 5	xliv
H.2.1	ASR_{S-BR}	xliv
H.2.2	$ASR_{S-BR}^\infty (\bar{\gamma}_b \rightarrow \infty)$	xlv
H.3	Proof of Lemma 6	xlvi
H.3.1	ASR_{S-NR}	xlvi
H.3.2	$ASR_{S-NR}^\infty (\bar{\gamma}_b \rightarrow \infty)$	xlvi
I	MATLAB CODE FOR BECKMANN CDF	xlviii
J	MATLAB CODE FOR UPPER INCOMPLETE MOMENT GENERATION FUNCTION OF THE BECKMANN DISTRIBUTION	xlix

LIST OF FIGURES

2.1	The wiretap model with two legitimate nodes and an eavesdropper, based on [66]	12
2.2	Illustration of a combiner in a MISO system, based on [131].	24
2.3	Illustration of a combiner in a SIMO system, based on [131].	25
2.4	Typical IRS-assisted wireless system, based on [132].	29
3.1	Coefficient of variation for the PDF of the sum of six i.n.i.d. Nakagami- m variates with parameters $\Omega_i = 1$, and $(m_1, m_2, m_3, m_4, m_5, m_6) = (0.5, 0.7, 0.9, 1, 1.5, 2)$	35
3.2	PDF of the sum of twenty and thirty n.i.i.d. Nakagami- m RVs. For $M = 20$, $m_i = 0.5$ for $i = 1$ to 3, $m_i = 1$ for $i = 4$ to 6, $m_i = 2$ for $i = 7$ to 9, $m_i = 2.5$ for $i = 8$ to 12, $m_i = 3$ for $i = 13$ to 16, and $m_i = 3.5$ for $i = 17$ to 20. For $M = 30$, $m_i = 0.5$ for $i = 1$ to 6, $m_i = 0.7$ for $i = 7$ to 12, $m_i = 0.9$ for $i = 13$ to 18, $m_i = 1$ for $i = 19$ to 24, and $m_i = 1.5$ for $i = 25$ to 30.	42
3.3	Average Bit Error Probability for coherent and non-coherent modulations of EGC receivers over $M = 3$ Nakagami- m RVs.	44
3.4	Average Bit Error Probability for coherent and non-coherent modulations of EGC receivers over $M = 4, 6$, and 8 Nakagami- m RVs.	45
3.5	SNR regime analysis of the Average Bit Error Probability for coherent and non-coherent modulations of EGC receivers over $M = 4, 6$, and 8 Nakagami- m RVs.	47
3.6	SNR regime analysis of the Average Bit Error Probability for coherent and non-coherent modulations of EGC receivers over $M = 4, 6$, and 8 Nakagami- m RVs.	48
3.7	Average elapsed time for both the PDF and ABEP in EGC varying the number of branches.	49
3.8	Sum of three i.i.d. κ - μ RVs by varying μ_i for $\Omega_i = 1$ and $\kappa_i = 1.7$	56
3.9	Sum of three i.n.i.d. κ - μ RVs for <i>Case I</i> : $(\mu_1, \mu_2, \mu_3) = (0.5, 1.5, 2.5)$, $(\kappa_1, \kappa_2, \kappa_3) = (1.1, 3.1, 7.5)$, $\Omega_i = 1$, and <i>Case II</i> : $(\mu_1, \mu_2, \mu_3) = (1.5, 3.2, 4.5)$, $(\kappa_1, \kappa_2, \kappa_3) = (2.1, 3.2, 3.9)$, $\Omega_i = 1$	57
3.10	PDF and CDF of the ratio of two squared α - μ RVs.	66
3.11	SOP vs. $\bar{\gamma}_B$ by varying α_i and μ_i for $i \in \{B, E\}$	67

4.1	SOP vs. $\bar{\gamma}_B$, for different numbers of dominant specular waves N by considering balanced amplitude scenario (i.e., $V_{n,i} = 1$ for $n = 1, \dots, N_i$). For all curves, the parameter values are: $R_S = 1$ bps/Hz, $\bar{\gamma}_E = 4$ dB, $K_{dB}^E = 10$ dB, $\Omega_i = 1$, and $N_i = N$ for $i \in \{B, E\}$. Dashed lines correspond to asymptotic analysis by using expression (4.6).	75
4.2	SOP in terms of $\bar{\gamma}_B$ for different numbers of dominant specular waves N , by considering unbalanced amplitude case (i.e., $\alpha_{n,i} = \alpha_i = 0.3$). For all cases, the corresponding parameters are set to the following values: $R_S = 1$ bps/Hz, $\bar{\gamma}_E = 1$ dB, $K_{dB}^E = 0$ dB, $\Omega_i = 1$, and $N_i = N$ for $i \in \{B, E\}$	76
4.3	SOP vs. $\bar{\gamma}_B$ for different numbers of dominant specular waves N by considering unbalanced amplitude case (i.e., $\{\alpha_B, \alpha_E\} = \{0.2, 0.9\}$ and $\{\alpha_B, \alpha_E\} = \{0.9, 0.2\}$). For all curves, the values of channel parameters are: $R_S = 1$ bps/Hz, $\bar{\gamma}_E = 8$ dB, $K_{dB}^B = K_{dB}^E = 25$ dB, $\Omega_i = 1$, and $N_i = N$ for $i \in \{B, E\}$	77
4.4	SOP in terms of R_S for different numbers of dominant specular waves of $N_B = \{2, 3, 4, 5\}$ with regard to $N_E = \{2, 3\}$ by considering unbalanced amplitude case (i.e., $\{\alpha_B, \alpha_E\} = \{0.2, 0.3\}$). For all curves, the fading parameters are set as: $\bar{\gamma}_E = 1$ dB, $\bar{\gamma}_B = 8$ dB, $K_{dB}^B = K_{dB}^E = 20$ dB, and $\Omega_i = 1$ for $i \in \{B, E\}$	78
4.5	SOP vs. $\bar{\gamma}_B$ for different numbers of dominant specular waves $N = N_B = N_E$ by varying the value of R_S and assuming unbalanced amplitudes (i.e., $\alpha = \{0.15, 0.30\}$). Also, $\bar{\gamma}_E = 1$ dB, $K_{dB}^B = 25$ dB, and $K_{dB}^E = 0$ dB.	79
4.6	SOP vs. $\bar{\gamma}_B$ for different numbers of dominant specular waves $N = N_B = N_E$ by assuming for all cases $R_S = 1$ bps/Hz, $\Omega_B = \Omega_E = 1$, $\bar{\gamma}_E = 8$ dB, and $K_{dB}^B = 20$ dB, and $K_{dB}^E = 0$ dB.	80
4.7	ASC vs. $\bar{\gamma}_B/\bar{\gamma}_E$ for different configurations of N_E , and α_E with $\Omega_B = \Omega_E = 1$, and $K_{dB}^B = K_{dB}^E = 25$ dB.	81
4.8	ASC vs. $\bar{\gamma}_B/\bar{\gamma}_E$ by varying K_{dB}^B for a fixed $K_{dB}^E = 0$ dB with $\Omega_B = \Omega_E = 1$, and $\bar{\gamma}_E = 10$ dB.	81
5.1	A general TAS/MRC MIMO network consisting of a legitimate pair and one eavesdropper, where the transmitter Alice (A), the receiver Bob (B), and the eavesdropper Eve (E) are equipped with N_A , N_B , and N_E antennas, respectively. This figure is based on [98].	84
5.2	SOP vs. $\bar{\gamma}_B$, for various numbers of transmit antennas, N_A , and a fixed number of receive antennas, $N_B = N_E = 2$. The setting parameter values are: $R_S = 1$ bps/Hz, $\bar{\gamma}_E = 8$ dB, $\mu_i = 2$, $\kappa_i = 2$, and $m_i = 3$ for $i \in \{B, E\}$. Markers denote Monte Carlo simulations.	95

5.3	SOP vs. $\bar{\gamma}_B$, for various numbers of eavesdroppers antennas, N_E , and a fixed number antennas, $N_A = N_B = 2$. Markers denote Monte Carlo simulations, whereas the solid and dash-dotted lines represent analytical solutions.	96
5.4	SOP vs. $\bar{\gamma}_B$, for different numbers of receive antennas, N_B , and unchanged number of: (i) receive antennas, $N_E = 2$, and (ii) transmit antennas, $N_A = 2$. Markers denote Monte Carlo simulations, whereas the solid and dash-dotted lines represent analytical solutions.	96
5.5	SOP vs. $\bar{\gamma}_B$, for $N_A = N_B = 2$, $N_E = 3$, and different received wave clusters, μ_B , and μ_E . The setting parameter values are: $R_S = 2$ bps/Hz, $\bar{\gamma}_E = 8$ dB, $\kappa_i = 4$, and $m_i = 5$ for $i \in \{B, E\}$. The solid and dash-dotted lines represent analytical solutions.	97
5.6	SOP vs. κ_i , with $N_A = 3$, $N_B = N_E = 2$, and fixed $m_i = 3$ for $i \in \{B, E\}$. The setting parameter values are: $R_S = 3$ bps/Hz, $\bar{\gamma}_E = 8$ dB, and $\bar{\gamma}_B = 25$ dB. Markers denote Monte Carlo simulations.	98
5.7	ASC vs. $\bar{\gamma}_B$, for different configurations of N_A , N_B , and N_E . The corresponding parameter values are: $\bar{\gamma}_E = 8$ dB, $\mu_i = 2$, $m_i = 1$, and $\kappa_i = 5$ for $i \in \{B, E\}$. Markers denote Monte Carlo simulations.	99
5.8	ASC vs. $\bar{\gamma}_B$, for different numbers of receive antennas, N_B , and fixed number of antennas, $N_A = N_E = 2$. The corresponding parameter values are: $\bar{\gamma}_E = 8$ dB, and $\mu_i = m_i = 2$ for $i \in \{B, E\}$. Markers denote Monte Carlo simulations, whereas the solid and dash-dotted lines represent analytical solutions.	100
6.1	IRS-aided secure communication from Alice (A) to a legitimate receiver Bob (B) in the presence of an eavesdropper Eve (E). This figure is based on [132].	102
6.2	ASR as a function of $\bar{\gamma}_{0,b}$ for different values of n for $n_b = 1$. Markers correspond to the legitimate and eavesdropper channels computed with (6.2) and (6.5), respectively.	110
6.3	ASR as a function of $\bar{\gamma}_{0,b}$ for different values of n for $n_b = 2$. Markers correspond to the legitimate and eavesdropper channels computed with (6.2) and (6.5), respectively.	110
6.4	SOP as a function of $\bar{\gamma}_{0,b}$ for different values of n for $n_b = 1$. Markers correspond to the legitimate and eavesdropper channels computed with (6.2) and (6.5), respectively.	111
6.5	SOP as a function of $\bar{\gamma}_{0,b}$ for different values of n for $n_b = 2$. Markers correspond to the legitimate and eavesdropper channels computed with (6.2) and (6.5), respectively.	112

RESUMEN

Debido a la naturaleza de transmisión en el medio inalámbrico, los problemas de privacidad y seguridad de la información son aspectos críticos, comúnmente abordados en todas las generaciones de comunicaciones móviles. Recientemente, partiendo de las bases de Teoría de Información, la seguridad a nivel de capa física se ha convertido en un enfoque prometedor para brindar seguridad en redes emergentes (5G y post-5G). Dicha tecnología toma ventaja de la aleatoriedad inherente del canal inalámbrico (por ejemplo, ruido, interferencia, y desvanecimiento) para resguardar los datos de nodos no autorizados. Hoy en día, varios investigadores, han dedicado un esfuerzo considerable para comprender las bases fundamentales de la seguridad a nivel de la capa física sobre diferentes modelos de desvanecimientos en escenarios sujetos a espionaje. En este contexto, es importante destacar que, adecuados modelos de canal de desvanecimiento pueden capturar de forma precisa las propiedades intrínsecas del medio inalámbrico. Varios trabajos propuestos en la literatura concernientes al estudio de la seguridad a nivel de capa física sobre canales de desvanecimiento, se basan principalmente en modelos simplistas. Es decir, dichos modelos de canal no capturan la versatilidad del medio de propagación a corta escala que formarán parte del entorno 5G y post-5G. Por lo que, estudiar y comprender los beneficios de la seguridad a nivel de capa física sobre modelos de canal de desvanecimientos es de primordial importancia para el diseño e implementación de aplicaciones seguras en la próxima red móvil de comunicación.

Esta tesis tiene como objetivo proporcionar un estudio integral del desempeño de la seguridad a nivel de capa física sobre modelos de canales de desvanecimiento generalizados. Cabe mencionar que, se considerará aquellos modelos de desvanecimiento que han demostrado caracterizar con precisión el canal inalámbrico en las comunicaciones que emplean ondas milimétricas (mm-Wave, del inglés millimeter-Wave). En particular, este trabajo se enfoca en investigar el desempeño de la seguridad a nivel de capa física en canales de escuchas para sistemas con una única antena (SISO, del inglés Single-Input Single-Output) y múltiples antenas (MIMO, del inglés Multiple-Input Multiple-Output). Para tal propósito, se utilizarán métricas relativas a la seguridad ampliamente utilizadas en la literatura, entre las cuales, podemos destacar, la probabilidad de corte del secreto de la comunicación (SOP, del inglés Secrecy Outage Probability), y la tasa alcanzable de secreto promedio (ASC, del inglés Average Secrecy Capacity). Además, partiendo del hecho de que: (i) el SOP puede ser interpretado como el cociente de dos variables aleatorias, y (ii) las técnicas de combinación de diversidad (por ejemplo, MIMO) implican la suma de variables aleatorias. Este trabajo también propone nuevas metodologías para aproximar la distribución exacta de las principales estadísticas (por ejemplo, Función Densidad de Probabilidad y Función de Distribución Acumulativa) de la suma y el cociente de variables aleatorias. Con base a estos resultados, posteriormente

se proporcionan formulaciones de métricas relativas de secreto para explorar el desempeño de la seguridad a nivel de capa física de los sistemas propuestos (es decir, canales de escucha SISO y MIMO). Los modelos de canal de desvanecimiento considerados para los escenarios propuestos son κ - μ shadowed y N-Rayos con Potencia Difusa.

Finalmente, inspirados por el potencial prometedor de las comunicaciones inalámbricas asistidas por superficie inteligente reconfigurable (RIS, del inglés Intelligent Reflecting Surface) para redes posteriores a 5G; este trabajo explora la seguridad de la capa física de un sistema inalámbrico que emplea tecnología RIS. Los resultados muestran que la incorporación de la configuración RIS en las redes inalámbricas post-5G aporta una mejora significativa al desempeño de la seguridad a nivel de capa física.

Keywords— Métodos de aproximación, suma de variables aleatorias, radio de variables aleatorias, canales de desvanecimiento generalizado, κ - μ shadowed, N-Rayos con Potencia Difusa, seguridad en capa física, superficies inteligentes reconfigurables.

ABSTRACT

Due to the wireless medium's broadcast nature, privacy and security concerns are critical issues in wireless communications systems. Rooted in information theory, physical layer security by exploiting the inherent randomness (e.g., noise, interference, and fading) of the wireless channel has become a promising approach to providing security in future wireless networks. Nowadays, many researchers have devoted a considerable effort to understand the fundamental basis of physical layer security over different fading wire-tap channel models. Importantly, proper fading channel models can capture the time-varying properties of the wireless environment. Works available in the literature on the study of the physical layer security over fading channels are primarily based on fading models that do not capture the irregularity and heterogeneity of the versatile set of channels that will be part of 5G and post-5G networks. Therefore, understanding physical layer security's performance undergoing more practical fading channel models is of great importance for practical security applications at the physical layer level for the next wireless networks.

This thesis aims to provide a comprehensive study on physical layer security's fundamental performance over generalized fading channel models, which have proven to characterize mm-Wave scenarios in 5G accurately. Specifically, this investigation focuses on the secrecy performance of both the Single-Input Single-Output (SISO) and Multiple-Input Multiple-Output (MIMO) wiretap channels by employing the Secrecy Outage Probability (SOP), Average Secrecy Capacity (ASC) as secrecy metrics. Knowing that: (i) the SOP can be interpreted as the ratio of two random variables, and (ii) the diversity combining techniques used in MIMO systems implies a sum of Random Variables (RVs), analytical approximations for statistics (e.g., PDF and CDF) of both the sum and the ratio of the random variables are derived in the first instance. Based on these results, the secrecy formulations to investigate the secrecy performance of the concerned systems (i.e., SISO and MIMO wiretap channels) over generalized fading channels, namely, κ - μ shadowed, and N-Wave with Diffuse Power are derived. Finally, inspired by the promising potential of Reconfigurable Intelligent Surface (RIS)-aided communications for post-5G networks, a wireless system's physical layer security employing RIS technology is also explored. The results show that incorporating RIS configuration in wireless networks brings a prominent physical layer security enhancement.

Keywords— Approximation methods, sum of random variables, ratio of random variables, generalized fading channels, κ - μ shadowed, N-wave with Diffuse Power fading model, physical layer security, reconfigurable intelligent surfaces.

1 INTRODUCTION

In wireless communications, a large number of factors directly affect the quality of the received signal. Signal strength fluctuates frequently, sometimes providing a good quality signal, sometimes degrading the signal. Some of the physical phenomena that influence the wireless channel include interference, path loss, shadowing, fading, among others [1]. Specifically, fading is caused due to multipath propagation, i.e., the interaction of multiple reflections, scattering, and diffractions of the radio-mobile signal along its pathway. Due to the stochastic nature of the physical factors involved in the fading, it is necessary to characterize it through probability distributions such as Rayleigh, Rice, Hoyt, Weibull, and Nakagami- m . Fading imposes severe performance limitations on wireless communications systems [2]. Therefore, diversity combination methods are used as efficient techniques to combat the fading. The basic principle of these methods is to provide the receiver with multiple replicates of the information signal, called diversity signals or branches, which, when properly combined, provide a less fading resulting signal. Classic diversity combining techniques are Equal Gain Combining (EGC) and Maximum Ratio Combining (MRC) [3]. Such diversity combining schemes are the most relevant instances that imply sums of Random Variables (RVs). Other important applications of the sum of fading RVs include, for instance, outage probability, signal detection, inter-symbol interference, phase jitter, linear equalizers, and error-bound calculations for coding in satellite communications [4], [5]. Unfortunately, the exact analytical evaluation of the sum statistics (i.e., Probability Density Function (PDF), Cumulative Density Function (CDF), and Moment Generation Function (MGF)) may be cumbersome even for statistically independent, well-known fading channel models. For independent RVs, the PDF of the sum can be computed either as the convolution of the individual PDFs of the summands or as the Fourier Transform (FT) of the product of the corresponding Characteristic Functions (CFs) [6]. Although tractable solutions are available for particular fading models and specific numbers of summands, no general closed-form solution exists as yet for an arbitrary number of summands over generalized fading channels. In such cases, one needs to resort to numerical routines by using popular mathematical software packages. However, as the number of summands increases, this approach becomes prone to convergence and instability issues, or even impracticable. To bypass the stated limitation on exact sum statistics, approximate methods for many fading scenarios have emerged in the literature. In this sense, a better knowledge of the statistics of the sum of fading RVs plays a pivotal role in the analytical performance evaluation of many wireless applications.

Nowadays, with the advent of new applications (e.g., autonomous cars, remote surgery, Internet of Thing (IoT), cloud computing, among others), the capacity of the fourth generation (4G) systems will not be able to support the demanding bandwidths and high service quality requirements [7]. In this context, Fifth Generation (5G) technology emerges as a solution to almost everything. Specifically, 5G is supposed to offer enormous data speeds, extreme reliability, and supporting a massive number of things or devices connected for the next decade [8]. The key to the successful development of 5G systems will be the unification of different networking technologies. For instance, some of new scenarios of wireless systems under the umbrella of 5G include millimeter Wave (mm-Wave) communications, Device-to-Device (D2D) systems, machine-type networks, vehicular communications, Unmanned Aerial Vehicle (UAV) communications, and many others [9]. These novel scenarios will create the necessity for wireless nodes to operate over a versatile set of channels ranging from (i) indoor to outdoor; (ii) Line-of-Sight (LoS) to Non-LoS (NLoS), and (iii) homogeneous diffuse scattering to scenarios with clustering of scattered multipath waves [10]. Recent investigations in [11] have shown that none of the well-established fading models (e.g., Rayleigh, Rician, and Nakagami- m) present an accurate fit with the field measurements in mm-Wave communications. One of the reasons for such mismatch is based on the fact that classical fading models heavily rely on the Central Limit Theorem (CLT), which assumes a sufficiently large number of multipath waves arriving at the receiver ends – and such conditions are not always met [12]. In the last years, some efforts have been oriented to formulate more accurate channel models that overcome such limitations. One good example is the α - η - κ - μ fading model [13], which has shown good accuracy to model the short-term fading channel behavior in the mm-Wave band [14]. Another choice are stochastic fading models that explicitly discern between the individual multipath waves classically regarded as LoS components. Such models have been proposed as a way for bridging the gap between CLT-based approaches and purely ray-based models, and may be suited to accommodate to propagation conditions encountered in the mm-Wave band like those emulated by ray-tracing schemes [15], [16]. For instance, Durgin's Two-Wave with Diffuse Power (TWDP) [17] and the Fluctuating Two-Ray (FTR) [18] are known to improve the fit to field measurements in different scenarios, including mm-Wave set-ups [11], [19], compared to conventional fading channel models. Very recently, the author in [20] proposed the generalization of TWDP that was referred to as N-wave with diffuse power (NWDP) in order to deal with the rather unwieldy nature of the wireless channel for the next networks. In this context, another popular model to characterize the propagation medium in emerging practical scenarios is the κ - μ shadowed [21], which relies on the assumption that the signal's dominant components are subject to random fluctuations. Nonetheless, a myriad of challenges must still be overcome so that 5G converges into a reliable, safe, and efficient system. One of the most critical aspects is related to information transmission security, given that 5G is designed to support diverse applications. Consequently, highly confidential and vulnerable data is expected to be transmitted in 5G and beyond networks, which are sensitive to eavesdropping due to their wireless nature. Traditionally, security systems are based on higher layer cryptographic mechanisms, which contemplate mathematically

complex algorithms that demand high energy and computational resources. Such methods pose significant challenges for implementing and managing the 5G wireless networks in practice [22]. Therefore, classical cryptography by itself does not constitute an integral solution to the security problems envisioned for future wireless transmissions. In this sense, Physical Layer Security (PLS) arises as an alternative to providing secure communications at the physical layer by smartly exploiting the randomness (e.g., noise, interference, and fading) of wireless channels [23]. The main advantage of employing PLS for 5G networks compared to cryptography methods is that PLS techniques do not rely on computational complexity. Hence, even if the unauthorized devices in 5G systems are equipped with high power computational resources, secure and reliable communications can still be attained [24]. However, since 5G is a multi-level system with different security levels, using PLS techniques in this complicated environment is challenging. In this regard, the PLS approach should interact with other protocol stack techniques to reach a fair tradeoff between security and Quality of Service (QoS) [25]. PLS's works over wireless fading channels have been extensively investigated in the literature. The vast majority in such studies assume fading channel models that do not adequately characterize the environments in which 5G will be deployed. Therefore, providing useful insights into PLS's performance over generalized fading channel models remains challenging.

By the end of the next decade, future mobile applications will demand stricter technical requirements than those designed to coexist on the 5G platform. Based on this fact, several researchers anticipate exploring what Sixth Generation (6G) would look like in the future communication era [26]. With great certainty, it is expected that 6G will improve 5G in terms of speed, reliability, and availability [27]. While 5G takes us into the IoT to transform the way we communicate; 6G is believed to open the new era of "Internet of Intelligence" with connected people, connected things, and connected intelligence, helping to improve the world we inhabit [27]. Hence, academic 6G research is in search of technologies that greatly enhance what is offered by 5G. For instance, most researchers have addressed their efforts in technologies at the physical and architectural levels [28]. In this context, novel candidate physical layer technologies for 6G have emerged, such as User-centric cell-free Massive MIMO [29], [30], Holographic Radio MIMO [31], [32], and Reconfigurable Intelligent Surface (RIS) [33]. Specifically, RIS arises as an unconventional wireless technology paradigm that can intentionally control the reflection, scattering, and refraction characteristics of electromagnetic waves, i.e., controlling the wireless propagation medium. A typical RIS-based transmission consists of a large number of low-cost, passive elements on an RIS that reflect the arrived signals with an adjustable phase shift in order to increase the achievable rate at the desired receiver [34]. These unique RIS features can enhance incredibly security at the physical layer level for the next wireless networks. Therefore, a PLS study of RIS technology is definitely essential in the state-of-the-art.

1.1 RELATED WORK AND MOTIVATION

This section surveys several works concerning (i) PLS over fading channel models; (ii) sum of RVs; (iii) ratio of two generalized RVs, and (iv) secure wireless communications via RIS, that have been investigated and widely discussed in the literature.

1.1.1 Sum of Random Variables

In the literature, a plethora of work has been done for approximating the statistics (i.e., PDF and CDF) of the sum of RVs. The famous Nakagami in [35] proposed to approximate the sum of an arbitrary number of independent, identically distributed (i.i.d.) Nakagami- m RVs by using another Nakagami- m RV. Based on the results given in [35], the parameters of the approximate Nakagami- m distribution for the sum of two identical and correlated Nakagami- m RVs were obtained in [36]. Authors of [37] presented a finite range multifold integral for PDF of the sum of i.i.d. Nakagami- m RVs, however, its performance in computational terms is as intense as the exact solution. An interesting approach for the evaluation of the CDF via Hermite numerical integration of the weighted sum of M independent Rician and Nakagami- m envelopes with or without the presence of additive White Gaussian noise (AWGN) was presented in [38]. Then, a closed-form expression for the PDF, CDF, and MGF of M Nakagami- m vectors with uniform phases and a restricted m to integers was derived in [39]. Exact infinite summations of hypergeometric functions and gamma for the distribution of the sum of i.i.d. Nakagami- m RVs was shown in [40], although their computation becomes intractable while the number of RVs increases. Aiming to evaluate the error-rate performance of EGC, an efficient approximation to the sum of correlated Nakagami- m RVs with identical, integer-valued m -fading parameters was presented in [41]. In [42], a Gaussian complementary CDF was considered to approximate the sum of Rice RVs. In [43] and [44], closed-form approximations to the PDF of the sum of Rayleigh and Rice RVs were derived, based on a small-argument approximation and the modification of the sum distribution of squared Rice RVs, respectively. In [45]–[47], approximations to the sum of uncorrelated Weibull RVs were proposed to assess the performance of EGC, MRC, and Selection Combining (SC) systems. Several approximations based on the Moment Matching Method (MoM) are available in the literature. In the MoM, the approximate sum distribution parameters are calibrated by matching certain moments of the approximate model to those of the exact sum distribution. For instance, an improved approximation for the PDF of the sum of arbitrary number of independent but not identically distributed (i.n.i.d.) Nakagami- m RVs was derived in [48], [49]. Also via MoM, good approximations were obtained for sums of Weibull [50], Rice [51], Hoyt (Nakagami- q) [52], α - μ [53], and generalized RVs [54]. Very recently, approximations for sums of Malaga and Fisher RVs were proposed in [55] and [56], respectively.

1.1.2 Ratio of Random Variables

Important applications, such as Cognitive Radio (CR), Full-Duplex (FD) relaying, and PLS, are obtained by the ratio of RVs. However, the statistics of the ratio of RVs has been little explored in the literature. Next, the most outstanding works on the ratio of two RVs are reviewed. Approaches concerning the statistics of the ratio between RVs with well-known distributions such as Gamma, Exponential, Weibull, Normal, and the most recent FTR model were presented in [57]–[61], where some application uses were also provided. Regarding generalized distributions, the statistics of the ratio of independent and arbitrary squared α - μ RVs, via series representation, was proposed in [62]. Notwithstanding, in that work, the convergence of the power series was attained by making an strong assumption, more specifically: the values related to the non-linearity of the environment (i.e., to the α parameter, also referred as shape parameter) of each α - μ RV involved in the quotient must be co-prime integers. This fact hinders a more comprehensive insight into the performance analysis of different wireless communication systems. Furthermore, under the same constraint as in [62], the work in [63] provides closed-form expressions for the statistics of the ratio of products of an arbitrary number of independent and non-identically distributed α - μ variates. Recently, the ratio of two generalized RVs was proposed in [64].

1.1.3 Physical layer security over fading channel models

The famous Shannon introduced the first PLS notions from an information-theoretical perspective in his seminal work in [65]. Later, the well-known wiretap channel was proposed by Wyner in [66]. In such a work, Wyner showed that information could be safely transmitted when the wiretap channel is a degraded version (much noisier) of the legitimate link. Subsequently, Wyner's results were extended for the broadcast channel in [67] and for the Gaussian channel in [68]. In the latter work, the secrecy capacity was defined as the difference between the capabilities of the legitimate channel and the wiretap channel. Hence, secure wireless transmissions are possible if and only if the main channel's quality is better than that of the eavesdropper channel. In the last years, works in [67] and [68] have inspired an important amount of recent research activities to explore PLS over different fading channel models. For instance, the first works on PLS performance for conventional Rayleigh fading with SISO-single eavesdropper (also known as SISO-SE channels) were studied in [69], [70]. Next, the probability of strictly positive secrecy capacity (SPSC) was explored for independent log-normal fading channels by assuming single eavesdropper with single antenna devices. SPSC formulations for Rician and Weibull SISO-SE fading channels were investigated in [71] and [72], respectively. The SOP behavior under Nakagami- m SISO-SE channels was reported in [73]. Subsequently, the secrecy performance by assuming mixed fading channels for the legitimate/eavesdropper paths was derived for Rician/Rayleigh [74], and Rician/Nagami- m [75]. From a PLS perspective, secure wireless communications over generalized SISO-SE fading channels have been widely investigated for

α - μ [76]–[78], Fluctuating Beckmann [79], Generalized- K [80], Fisher-Snedecor \mathcal{F} [81], κ - μ [82], α - κ - μ , α - η - μ [83], α - η - κ - μ [84] models. For the specific case of ray-based fading channels, which accommodate very well to propagation conditions encountered in the mm-Wave, few results are available in the literature. In particular, only two specular components (i.e., TWDP and FTR models) were considered for the secrecy performance analysis in [85], [86]. Very recently, in [87], the authors studied the effect on PLS when considering a finite number of scattering waves in the NWDP fading channel model. However, an exhaustive PLS study that considers (i) an arbitrary number of dominant specular components and (ii) sufficiently large diffuse propagating waves for the NWDP model is an appealing research topic in the state-of-the-art.

MIMO wireless systems are conceived to increase reliability or to achieve high data rates. From a secrecy point of view, MIMO set-ups allow enhancing PLS performance by exploiting the multi-antenna diversity at the legitimate nodes. In this context, PLS has gained considerable attention for MIMO wiretap channels in the last years. Key concepts concerning the generalization of the wiretap channels to MIMO systems were investigated in [88], [89]. These pioneering works have motivated various research efforts to improve the secrecy performance in different MIMO topologies. For instance, the utilization of artificial noise (AN) has been proposed to enhance the secrecy performance of MIMO networks [90]. Moreover, the impact of cooperative communications on the secrecy capacity of MIMO wiretap systems were studied in [91], [92]. In [93], the authors focused on the secrecy performance of cognitive MIMO relaying networks. In order to achieve higher secrecy capacities, different beamforming schemes were considered in [94]–[96]. Nevertheless, beamforming-based methods require as many radio-frequency (RF) chains as antenna ports, as well as the use of advanced signal processing algorithms to accurately estimate the channel state information (CSI). These approaches require a high computational demand, which may be infeasible for resource-constrained devices. Alternatively, as optimal antenna selection at the transmitter side only requires a single RF chain compared to classical beamforming schemes [97], Transmit Antenna Selection (TAS) has been adopted to enhance secrecy performance at low-cost and complexity. Therefore, several works have focused on the advantages of TAS in the context of PLS [23], [98]. In those works, PLS metrics were investigated in the combined use of TAS and maximal ratio combining (MRC) receivers affected by Rayleigh and Nakagami- m fading, respectively. Recently, the secrecy performance in MIMO wiretap channels has been analyzed over generalized fading conditions (i.e., α - μ [99] and η - μ [100] fading models). However, the fading channels considered in the works mentioned above are sometimes inaccurate to characterize the propagation medium in emerging practical scenarios for 5G [101]. As pointed out above, generalized and versatile channel models, such as the TWDP, FTR, NWDP, κ - μ shadowed have been proposed to circumvent this issue. Hence, PLS research under generalized fading conditions in scenarios where all nodes have multiple antennas is definitely crucial in the literature.

1.1.4 Physical layer security via Reconfigurable Intelligent Surfaces

Very recently, RIS has drawn full attention for ensuring secure wireless communications in a low complexity manner. Therefore, several researchers have addressed their efforts to investigate PLS on RIS-aided wireless communications systems. Because of the rather complex nature of the RIS composite fading model, the analytical characterization of PLS performance metrics is utterly unfeasible and most works often resort to optimization techniques to maximize the secrecy rate metric [102]–[105]. In such works, the authors maximize the secrecy rate by jointly optimizing the beamformers at the transmitter and the reflecting coefficients at the RIS. Initial results on RIS-aided secure wireless systems with multiple legitimate nodes and multiple eavesdroppers were provided in [106] and [107], respectively. Again, in these works, alternative optimization techniques were used to tackle the non-convexity of the formulated problems. Other existing studies on secrecy RIS include secure wireless communications exploiting deep reinforcement learning [108], secrecy rate maximization for RIS-aided communications [109], programmable wireless environment for PLS [110], and artificial noise to enhance the secrecy rate for RIS-assisted systems [111]. All the works cited above consider only the secrecy rate as a performance metric in their reports. Nevertheless, the SOP is a more suitable metric for practical scenarios since, in this secrecy metric, the Eavesdropper's CSI is not available at the transmitter. In this setup, the eavesdropper intercepts messages and does not communicate with other users on the network. The authors in [112] studied the SOP performance of the RIS-aided wireless communication system, where perfect knowledge of the channel phases is assumed at the RIS. Based on this fact, an in-depth study of different secrecy metrics for RIS-aided communications with more realistic assumptions is an open research topic in the literature.

1.2 HYPOTHESIS

This research work hypothesizes that, integrating enabling 5G and post-5G technologies (e.g., MIMO, RIS) with physical layer security techniques would allow improving the information security of upcoming wireless networks under realistic propagation conditions.

1.3 MAIN AND SUPPLEMENTARY OBJECTIVES

1.3.1 Main Objective

According to the previous statement, the main objective of this research work is:

“To assess the secrecy performance of adversary wireless scenarios empowered by next-generation technologies, through physical layer security techniques assuming generalized fading conditions”.

1.3.2 Supplementary Objectives

The asserted in the main objective is achieved, through the development of the following points:

- To propose a novel methodology for approximating the chief statistics (e.g., PDF, CDF and MGF) of the sum of RV taken from generalized fading models.
- To formalize a pioneering methodology for approximating the chief statistics of the ratio of RV taken from α - μ distributions.
- To model and analyze the performance of physical layer security of MIMO-and SISO-system over generalized fading channels.
- To derive exact, approximate, or asymptotic analytical expressions for the secrecy performance metrics related to the physical layer by assuming realistic propagation conditions.
- To obtain from the exact/asymptotic secrecy metric expressions, easy-to-use security criteria for forthcoming communications networks over generalized fading channels.
- To propose a methodology for characterizing the RIS end-to-end equivalent channel using traditional approximation approaches (e.g., MoM and CLT).
- To compare the secrecy performance of the derived analytical expressions concerning (i) the results obtained through simulations of 5G and post-5G communication systems using the Monte Carlo method; (ii) other approaches reported in the literature.

1.4 SUMMARY OF CONTRIBUTIONS

The major contributions of this thesis are fourfold: 1) First, the PDF for the sum of Nakagami- m RVs is derived in terms of o the Nakagami- m mixture model (NMM). In that case, the parameters of the approximate distribution are estimated by using an expectation-maximization (EM) algorithm; 2) The PDF, CDF, and MGF of the ratio of two RVs taken from the α - μ distribution is derived in exact closed-fashion in terms of the univariate Fox H-function; 3) Secrecy performance metrics, namely, SOP, ASC, Asymptotic SOP, Asymptotic ASC are derived in closed-form expressions over i) NWDP SISO wiretap channels, and i) κ - μ shadowed MIMO wiretap channels; and 4) Closed-form analytical expressions for the average secrecy rate (ASR) and the SOP of an RIS-aided wireless communication system in the presence of an eavesdropping user are also derived in terms of well-known functions in the communication theory.

1.4.1 Thesis Outline

This thesis is organized as follows:

Chapter 2 provides some fundamental concepts concerning PLS. Here, the secrecy metrics most used by researchers as design criteria in order to describe adversary scenarios' security level are reviewed. Specifically, the secrecy capacity, SOP, ASC, Asymptotic SOP, and Asymptotic ASC are reviewed. Furthermore, the generalized fading channel models NWDP and κ - μ shadowed are revisited. Finally, the basic working principles of the diversity combining techniques on both the transmitter (e.g., TAS) and the receiver (e.g., MRC and EGC) to mitigate fading effects are also described.

Chapter 3 presents an accurate approximation for the exact sum PDF of Nakagami- m RVs using a mixture of two Nakagami RVs. In such approximation, the approximate distribution's parameters are calibrated via the EM algorithm. An application example regarding the sum of RVs is also presented. Specifically, an analytical formulation of the Average Bit Error Probability (ABEP) of multibranch EGC receivers is obtained. Furthermore, a novel approach named the "asymptotic matching" method to approximate sums of independent channel envelopes that follow generalized fading models is introduced. Based on the asymptotic matching, an approximate expression for the sum of κ - μ RVs is derived by matching its asymptotic behavior around zero to that of the exact solution. Next, novel closed-form expressions for the PDF, CDF, and MGF of the ratio of two RVs taken from α - μ distribution in terms of the single Fox H-function as well as in terms of simple infinite series are developed. An application example in PLS over α - μ RVs is used to demonstrate the obtained expressions' usefulness.

Chapter 4 analyzes the PLS performance over NWDP SISO wiretap fading channels. In particular, novel closed-form fashions for the SOP, Asymptotic SOP, ASC, and Asymptotic are derived in terms of well-known functions in the communication theory literature. Such analytical expressions have comparable complexity to those obtained in approximate form for the simplified case of the TWDP fading channel model.

Chapter 5 provides new equivalent forms of κ - μ shadowed CDFs, which are very helpful to derive either the maximum or minimum of i.i.d. κ - μ shadowed RVs. Based on these results, secrecy expressions are developed in a TAS/MRC configuration under κ - μ shadowed fading. Specifically, exact closed-form formulations for the SOP and ASC are derived. Also, simple asymptotic expressions for the SOP and the ASC in the high Signal-to-Noise Ratio (SNR) regime are obtained.

Chapter 6 investigates the secrecy performance of RIS-assisted wireless communications with imperfect phase estimation. Novel closed-form formulations for both the SOP and ASR are obtained by leveraging recent formulations of the RIS composite fading channel as an equivalent scalar channel. Analytical asymptotic expressions for the SOP and ASR in the high SNR region are also derived

Chapter 7 provides the main conclusions and indicates opportunities for future research topics.

1.4.2 List of Publications

Journal Articles

- **J. D. Vega Sánchez**, L. Urquiza-Aguiar, M. C. Paredes, and F. Javier López-Martínez, "Expectation-Maximization Learning for Wireless Channel Modeling of Reconfigurable Intelligent Surfaces," *IEEE Wireless Communications Letters*, vol. 10, no. 9, pp. 2051–2055, Sep. 2021.
- **J. D. Vega Sánchez**, D. P. Moya Osorio, F. J. López-Martínez, M. C. Paredes Paredes and L. Urquiza-Aguiar, "Information-Theoretic Security of MIMO Networks under κ - μ Shadowed Fading Channels," *IEEE Transactions on Vehicular Technology*, vol. 70, no. 7, pp. 6302–6318, Jul. 2021.
- **J. D. Vega Sánchez**, L. Urquiza-Aguiar, and M. C. Paredes Paredes, "Fading channel models for mm-Wave communications," *Electronics*, vol. 10, no. 7, pp. 798, Mar. 2021.
- **J. D. Vega Sánchez**, D. P. Moya Osorio, F. J. López-Martínez, M. C. Paredes Paredes and L. Urquiza-Aguiar, "On the Secrecy Performance Over N-Wave with Diffuse Power Fading Channel," *IEEE Transactions on Vehicular Technology*, vol. 69, no. 12, pp. 15137–15148, Dec. 2020.
- **J. D. Vega Sánchez**, P. Ramírez-Espinosa, and F. Javier López-Martínez, "Physical Layer Security of Large Reflecting Surface Aided Communications With Phase Errors," *IEEE Wireless Communications Letters*, vol. 10, no. 2, pp. 325–329, Feb. 2021.
- **J. D. Vega Sánchez**, L. Urquiza-Aguiar, M. C. Paredes Paredes, and D. P. Moya Osorio, "Survey on Physical Layer Security for 5G Wireless Networks," *Springer Annals of Telecommunications*, Sep. 2020.
- **J. D. Vega Sánchez**, D. P. Moya Osorio, E. E. B. Olivo, H. Alves, M. C. Paredes Paredes, and L. Urquiza-Aguiar, "On the Statistics of the Ratio of Non-constrained Arbitrary α - μ Random Variables: A General Framework and Applications," *Transactions on Emerging Telecommunications Technologies*, no. e3832, Feb. 2019.
- **J. D. Vega Sánchez**, L. Urquiza-Aguiar, and M. C. Paredes Paredes, "An Accurate, Fast Approximation for the Sum of Fading Random Variables via Expectation Maximization," *IEEE Access*, vol. 6, pp. 42616–42630, Jul. 2018.

Co-Authored Journal Articles

- I. W. G. da Silva, D. P. M. Osorio, **J. D. Vega Sánchez**, E. E. B. Olivo, and M. Latva-aho, "On the Impact of Self-Energy Recycling and Cooperative Jamming on SWIPT-Based FD Relay Networks with Secrecy Constraints," accepted to publication in *IEEE Access*, 2021.

- J. L. M. Bandera, P. R. Espinosa, **J. D. Vega Sánchez**, and F.J. Lopez-Martinez, "Effect of Correlation on the Capacity of Backscatter Communication Systems," *Electronics Letters*, vol. 56, no. 14, pp. 716–719, Jul. 2020.
- V. Perim, **J. D. Vega Sánchez**, and J. C. S. S. Filho, "Asymptotically Exact Approximations to Generalized Fading Sum Statistics," *IEEE Transactions on Wireless Communications*, vol. 19, no. 1, pp. 205–217, Jan. 2020.

Co-Authored Book Chapter

- D. P. M. Osorio, **J. D. Vega Sánchez**, and H. Alves, "Physical Layer Security for 5G and Beyond," *5G REF: The Essential 5G Reference Online*, John Wiley & Sons, 2019, ch. 1, pp. 1–19.

Conference Articles

- **J. D. Vega Sánchez**, L. Urquiza-Aguiar, M. C. Paredes Paredes, and F. Javier López Martínez, "Secure Systems via Reconfigurable Intelligent Surfaces over Correlated Rayleigh Channels," *2021 IEEE Second Ecuador Technical Chapters Meeting (ETCM)*, Quito, 2021, pp.1–6.
- **J. D. Vega Sánchez**, L. Urquiza-Aguiar, and M. C. Paredes Paredes, "Modelos de Canal de Desvanecimiento para Comunicaciones Millimter-Wave," *Andean Wireless Communications & Applications Workshop (AWCA)*, Quito, 2021, pp.1–6.
- **J. D. Vega Sánchez**, L. Urquiza-Aguiar, and M. C. Paredes Paredes, "Physical Layer Security for 5G Wireless Networks: A Comprehensive Survey," *IEEE 3rd Cyber Security in Networking Conference (CSNet)*, Quito, Ecuador, 2019, pp.122–129.
- **J. D. Vega Sánchez**, L. Urquiza-Aguiar, M. C. Paredes Paredes, and D. J. R. Chisaguano, "A Simple Approximation for the Sum of Fading Random Variables via a Nakagami- m Distribution," *IEEE 90th Vehicular Technology Conference (VTC2019-Fall)*, Honolulu, HI, USA, 2019, pp.1–7.
- **J. D. Vega Sánchez**, L. Urquiza-Aguiar and M. C. Paredes Paredes, "Performance Metrics for Diversity-Combining Techniques over Nakagami- m Fading," *2017 IEEE Second Ecuador Technical Chapters Meeting (ETCM)*, Salinas, 2017, pp.1–6.

2 PRELIMINARIES

This chapter reviews several key notions concerning 1) PLS; 2) fading channels models; 3) diversity combining techniques; and 4) RIS-aided wireless systems, which will serve as background to understand the results obtained in this thesis.

2.1 FUNDAMENTALS OF PHYSICAL LAYER SECURITY

In this section, the essential concepts to understand PLS in wireless communications systems are introduced.

2.1.1 General System Model

As introduced in Wyner's work [66], the wiretap channel consists of three nodes, as illustrated in Fig. 2.1.

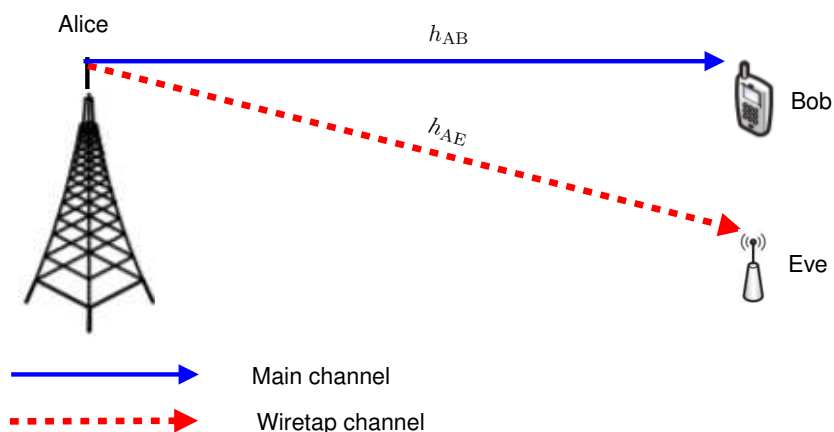


Figure 2.1: The wiretap model with two legitimate nodes and an eavesdropper, based on [66]

The first node is the legitimate transmitter (also known as Alice in network security jargon), the second node is the intended receiver (also known as Bob), and the third node is the eavesdropper (also known as Eve). The channel between Alice and Bob (i.e., h_{AB}) is known as the legitimate channel, while the channel between Alice and Eve is named the wiretap channel (also known as Eavesdropper channel, i.e., h_{AE}). In this setup, Alice transmits confidential information to Bob, while

Eve receives the signal and intends to decode it. Therefore, Alice's goal is to use a transmission approach that can deliver the secret information to Bob while making sure that Eve cannot intercept the transmitted data. Under basic SISO wiretap channel configuration, the received signals at both Bob and Eve are given by [66]

$$y_i = \sqrt{P}h_{Ai}x + n_i, \quad (2.1)$$

where P is the transmit power at Alice, and h_{Ai} with $i \in \{B, E\}$ denotes the channel coefficients for either the main channel or the eavesdropper channel, respectively. Also, n_B and n_E are additive white complex Gaussian noise at the receivers with zero mean and variance σ_i^2 . From (2.1), the corresponding instantaneous SNRs at the receivers can be expressed as

$$\gamma_i = \frac{P|h_{Ai}|^2}{\sigma_i^2}. \quad (2.2)$$

In order to attain secrecy in wireless systems, PLS uses signal processing techniques designed to take advantage of specific features of the channel, including fading, noise, interference, among others [24]. Another relevant factor to take into account in the wiretap channel (see, Fig. 2.1) is the availability of CSI in all the nodes (i.e., Alice, Bob, and Eve). CSI can vary from complete, partial to even null at the nodes. From a secrecy perspective, CSI is of paramount importance because, based on its knowledge, the transmitter can decide whether or not to transmit and at which rate [113]. Thus, this fact will lead to achieving remarkable improvement in the SOP. However, in practice, all nodes can only obtain some kind of information about the channel between them and the other nodes. Alice is generally considered to know Bob's CSI but not Eve's CSI. This is because Eve is typically passive (i.e., Eve monitors the network, intercepts messages, and does not communicate with other users in the network). Furthermore, there are scenarios in which Eve is active and performs some of the following actions: intentional interference (also known as jamming), adulteration and modification, or denial of service [114]. At this point, it is worth mentioning that in our PLS analysis over generalized fading channels, this research focuses on practical adversary scenarios, i.e., passive attacks.

2.1.2 Secrecy Metrics

Here, the most frequently used secrecy performance metrics in the state-of-the-art are revisited. A good understanding of such metrics will facilitate understanding of the contributions addressed in the following chapters.

2.1.2.1 Secrecy Capacity

The secrecy capacity, C_S , for a wiretap wireless channel is the most used metric in PLS evaluation. C_S is defined as the capacity difference between the main and wiretap channels. Mathematically, it

defines the maximum secret rate at which the secret message reliably recovers at transmitter while remaining unrecoverable at Eve [115]. Therefore, the C_S in a quasi-static fading channel case is formulated as in [66] by

$$\begin{aligned} C_S &= \max \{C_B - C_E, 0\} \\ &= \max \{W \log_2(1 + \gamma_B) - W \log_2(1 + \gamma_E), 0\} \end{aligned} \quad (2.3)$$

where γ_i for $i \in \{B, E\}$ is the instantaneous SNR at the receivers given by (2.2), and C_B and C_E are the capacities of the main and wiretap channels, respectively. Without loss of generality, it is considered a normalized bandwidth of $W = 1$ in the capacity formulations mentioned above. Under this scenario, it is possible to attain secure transmissions only if the legitimate link has a better SNR than the eavesdropper link, i.e., [66]

$$C_S = \begin{cases} \log_2 \left(\frac{1 + \gamma_B}{1 + \gamma_E} \right), & \text{if } \gamma_B > \gamma_E \\ 0, & \text{if } \gamma_B \leq \gamma_E, \end{cases} \quad (2.4)$$

Here, it is worth mentioning that the C_S is widely extended by researchers to compute the SOP [70], which is described below.

2.1.2.2 Secrecy Outage Probability

The SOP is defined as the probability that the secrecy capacity falls below a secrecy rate threshold R_S . In other words, when the current C_S is not more than R_S , the secrecy outage occurs, i.e., $R_S > C_S$. This means that the current secrecy rate cannot guarantee the security requirements. On the other hand, in those instants on which $R_S \leq C_S$, secrecy is achieved. This metric is commonly used with silent eavesdroppers, whose CSIs are not available at the source. Therefore, the source decides whether or not to transmit based on the information about the receiver's CSI. In practice, this setup is associated with a passive eavesdropping scenario. According to [116], the exact SOP can be formulated as

$$\begin{aligned} \text{SOP} &= \Pr \{C_S(\gamma_B, \gamma_E) < R_S\} \\ &= \Pr \left\{ \left(\frac{1 + \gamma_B}{1 + \gamma_E} \right) < 2^{R_S} \triangleq \tau \right\} \\ &= \Pr \{ \gamma_B < \tau \gamma_E + \tau - 1 \} \\ &= \int_0^\infty F_{\gamma_B}(\tau \gamma_E + \tau - 1) f_{\gamma_E}(\gamma_E) d\gamma_E. \end{aligned} \quad (2.5)$$

Note that the SOP is a useful performance metric for measuring information leakage. Due to the mathematical complexity of (2.5) when dealing with generalized fading channels, a high SNR ap-

proximation of the SOP defined as SOP_A can be obtained from (2.5) as [99]

$$\begin{aligned}
SOP_A &= \Pr \left\{ \frac{\gamma_B}{\gamma_E} < \tau \right\} \\
&= \Pr \{ \gamma_B < \tau \gamma_E \} \\
&= \int_0^\infty F_{\gamma_B}(\tau \gamma_E) f_{\gamma_E}(\gamma_E) d\gamma_E.
\end{aligned} \tag{2.6}$$

It is worth highlighting that PLS research over different types of fading channels focuses on the computation of (2.6) due to its simpler mathematical tractability with respect to the exact formulation in (2.5). Furthermore, SOP_A is well-known as the ratio of two random variables, namely: γ_B and γ_E , which can follow any fading distribution. Based on this fact, one contribution of this thesis is the derivation of mathematical analytical expression of the ratio of two random variables, which follow α - μ fading channels.

2.1.2.3 Asymptotic Secrecy Outage Probability

This metric is widely used to gain insights into the impact of the fading parameters on the secrecy performance in wiretap channels. The asymptotic measure investigates the behavior of the SOP at high SNR regime. Generally, for the asymptotic analysis, two scenarios are considered: (i) the average received SNRs at both the legitimate and the eavesdropper sides go to infinity, i.e., $\bar{\gamma}_B \rightarrow \infty$, $\bar{\gamma}_E \rightarrow \infty$, while the ratio between these SNRs, i.e., $\bar{\gamma}_B/\bar{\gamma}_E$ is kept unchanged. This scenario corresponds to the case when both the legitimate destination and the eavesdropper are close to the source; (ii) only the average received SNR at the legitimate destination goes to infinity, i.e., $\bar{\gamma}_B \rightarrow \infty$ while $\bar{\gamma}_E$ is kept fixed. Here, this scenario corresponds to the case where the legitimate entity is very close to the source and the eavesdropper is located far away. The goal in the asymptotic analysis is to find an asymptotic SOP expression in the form [117]

$$SOP^\infty \simeq G_c \bar{\gamma}_B^{-G_d} \tag{2.7}$$

where G_c and G_d represent the secrecy array gain and the secrecy diversity order/gain. It is worth mentioning that a challenging task is to derive asymptotic SOP expressions for the generalized fading channels (e.g., κ - μ shadowed, and purely ray-based models).

2.1.2.4 Average Secrecy Capacity

When dealing with active eavesdropping scenarios, where the CSIs of both main and eavesdropper channels are available at the source, the ASC is the most common secrecy metric used to evaluate secrecy performance in wireless communications systems. Unlike the passive eavesdropping scenario, in active eavesdropping case, Alice can now adapt her transmission rate according to any

achievable secrecy rate R_S such that $R_S \leq C_S$. Then, the maximum achievable secrecy rate occurs when $R_S = C_S$. According to [70], the ASC, \bar{C}_S , is defined as the average of the secrecy rate over the instantaneous SNR of the main and eavesdropper channels. For mathematical convenience, throughout this thesis, it is used the formulation of \bar{C}_S proposed in [99, Proposition 3], so it follows that

$$\bar{C}_S = \bar{C}_B - \mathcal{L}(\bar{\gamma}_B, \bar{\gamma}_E), \quad (2.8)$$

where \bar{C}_B is the average capacity of the main link in the absence of an eavesdropper, given by [99]

$$\bar{C}_B = \frac{1}{\ln 2} \int_0^\infty \frac{1 - F_{\gamma_B}(\gamma_E)}{1 + \gamma_E} d\gamma_E, \quad (2.9)$$

or

$$\bar{C}_B = \frac{1}{\ln 2} \int_0^\infty \ln(1 + \gamma_E) f_{\gamma_B}(\gamma_E) d\gamma_E. \quad (2.10)$$

It is worthwhile to mention that the formulations in (2.9), and (2.10) can be used to compute the average secrecy capacity of the eavesdropper link, i.e., \bar{C}_E by replacing the corresponding PDF and CDF distributions of the eavesdropper channel. The $\mathcal{L}(\bar{\gamma}_B, \bar{\gamma}_E)$ term can be interpreted as an ASC loss, defined as [99]

$$\mathcal{L}(\bar{\gamma}_B, \bar{\gamma}_E) = \frac{1}{\ln 2} \int_0^\infty \frac{\bar{F}_{\gamma_E}(\gamma_E) \bar{F}_{\gamma_B}(\gamma_E)}{1 + \gamma_E} d\gamma_E \geq 0, \quad (2.11)$$

in which \bar{F}_{γ_B} and \bar{F}_{γ_E} denote the complementary CDF (CCDF) of the RVs γ_B , and γ_E , respectively.

2.1.2.5 Asymptotic Average Secrecy Capacity

This metric examines the behavior of the ASC in the high-SNR region. As in the Asymptotic SOP case, two scenarios can be studied (i) both $\bar{\gamma}_B$ and $\bar{\gamma}_E$ go to infinity, while the ratio between these SNRs is kept unchanged; (ii) $\bar{\gamma}_B \rightarrow \infty$ while $\bar{\gamma}_E$ is kept fixed. The latter case is the most used in the literature due to its helpfulness in understanding the system behavior when the legitimate link quality is much better than the eavesdropper's link quality. Based on this, the exact asymptotic expression of the ASC can be formulated as [99]

$$\bar{C}_S^\infty \simeq \bar{C}_B^{\bar{\gamma}_B \rightarrow \infty} - \bar{C}_E, \quad (2.12)$$

where \bar{C}_E is calculated by (2.9) or (2.10) with the respective substitutions. It is appropriate to mention that an accurate approximation of \bar{C}_S^∞ in the high-SNR regime can be expressed in the form [118]

$$\bar{C}_B^{\bar{\gamma}_B \rightarrow \infty} \approx \log_2(\bar{\gamma}_T) - t, \quad (2.13)$$

where $\bar{\gamma}_T$ is the total average SNR at the receiver side, and t denotes the capacity loss, which is given by [118]

$$t = -\log_2(e) \left. \frac{d\mathcal{M}(g)}{dg} \right|_{g=0} \quad (2.14)$$

where $\mathcal{M}(g)$ denotes the normalized moments of the RV γ_B given by [118]

$$\mathcal{M}(g) \triangleq \frac{\mathbb{E}[\gamma_B^g]}{\bar{\gamma}_B^g}. \quad (2.15)$$

All these secrecy metrics will be used in the secrecy performance analysis over generalized fading channels subsequently.

2.2 FADING CHANNEL MODELS OVERVIEW

Due to the several uncertainties in the wireless environment, it is convenient to statistically model the channel with fading distributions. In the basic SISO setup, the received signal arises as a constructive or destructive combination of randomly delayed, reflected, scattered, and diffracted multipath waves. This fading type is well-known as fast fading and is responsible for rapidly-varying fluctuations in the received signal. Based on the multipath propagation, the complex base-band signal can be expressed as [17]

$$\tilde{V} = R \exp(j\theta) = \sum_{i=1}^M V_i \exp(j\theta_i), \quad (2.16)$$

where M is the number of the multipath waves, R and θ denotes the the magnitude and phase of \tilde{V} , respectively, $V_i \exp(j\theta_i)$ represents the i -th component having an amplitude V_i and random phase θ_i . Depending on the wireless propagation medium's nature, different fading distributions have been proposed in the literature to describe the signal envelope's statistical behavior. In the next section, the most widely used fading channels to describe the statistical behavior of the received signal amplitude, i.e., $R = \|\tilde{V}\|$ are reviewed. Specifically, both the classical and the generalized fading channels are addressed. Finally, it is worth mentioning that all the system models consider only flat-fading to characterize the fading effects on narrowband wireless communications.

2.2.1 Classical fading models

When a sufficiently large M is assumed in (2.16), the base-band voltage, \tilde{V} , can be regarded as a complex Gaussian RV by virtue of the CLT [119, Sec. 27]. Different classical fading models can be built depending on the choice of the complex Gaussian RV's parameters, i.e., the mean and variance of the in-phase and quadrature components. Based on this fact, the literature's most commonly used conventional fading channel models are described in the following.

2.2.1.1 Rayleigh Fading Model

The Rayleigh model considers that the multipath waves in (2.16) have constant amplitude and independent phases which are uniformly distributed into the interval $[-\pi, \pi)$. Under the CLT assumption, the received signal envelope R is characterized as a zero mean circularly-symmetric complex Gaussian RV by [120]

$$R = \|\sigma X + j\sigma Y\|, \quad (2.17)$$

where X and Y are independent Gaussian RVs, i.e., $X, Y \sim \mathcal{N}(0, 1)$, and $\sigma^2 \in \mathbb{R}^+$ denotes the variance of both in-phase and quadrature components of the complex Gaussian RV. From [120], the PDF and CDF of the channel fading amplitude R are distributed according to

$$f_R(r) = \frac{2r}{\Omega} \exp\left(-\frac{r^2}{\Omega}\right), \quad (2.18)$$

$$F_R(r) = 1 - \exp\left(-\frac{r^2}{\Omega}\right), \quad (2.19)$$

where $\Omega = \mathbb{E}[R^2] = 2\sigma^2$ is the average received power determined by the path loss and shadowing phenomenon. The Rayleigh distribution is widely used for NLoS scenarios. Furthermore, due to the mathematical simplicity of (2.18), several theoretical research on wireless communications have been investigated under the assumption of i.i.d. Rayleigh fading.

2.2.1.2 Rician Fading Model

In contrast to the Rayleigh model, if there is a strong LoS path, the Gaussian RV complex's real and imaginary parts no longer have mean of zero. Again, based on CLT, the received signal R in (2.16) is model as nonzero mean circularly-symmetric complex Gaussian RV by [120]

$$R = \|\sigma X + p + j(\sigma Y + q)\|, \quad (2.20)$$

in which $X, Y \sim \mathcal{N}(0, 1)$, and $\sigma^2 \in \mathbb{R}^+$ denotes the variance of both in-phase and quadrature components of the complex Gaussian RV. Also, p and $q \in \mathbb{R}^+$ are the mean values of the in-phase and quadrature components, respectively. From [121], the amplitude of the received signal of (2.20) is a Rician distribution with PDF and CDF given by

$$f_R(r) = \frac{2r(1+K)}{\Omega} \exp\left(-K - \frac{r^2(1+K)}{\Omega}\right) I_0\left(2r\sqrt{\frac{K(1+K)}{\Omega}}\right), \quad (2.21)$$

$$F_R(r) = 1 - \mathcal{Q}_1\left(\sqrt{2K}, r\sqrt{\frac{2(1+K)}{\Omega}}\right), \quad (2.22)$$

where $\Omega = \mathbb{E}[R^2] = p^2 + q^2 + 2\sigma^2$ is the mean received power, and $K = (p^2 + q^2)/(2\sigma^2)$ is the Rician factor which denotes the ratio between the power of the dominant component and the power of the scattering waves. For $K = 0$, (2.21) reduces to the Rayleigh distribution.

2.2.1.3 Nakagami- m Fading Model

Nakagami fading model was proposed in [35] as a natural generalization of Rayleigh distribution to improve the fitting of experimental measurements for different propagation conditions. The received signal envelope, R , can be formulated from the same underlying complex Gaussian model than the previous fading distributions as [35]

$$R = \sqrt{\sum_{i=1}^m \|\sigma X_i + j\sigma Y_i\|^2}, \quad (2.23)$$

where $m \in \mathbb{N}^+$ is the fading severity parameter, $X_i, Y_i \forall i$ are independent Gaussian RVs, i.e., $X_i, Y_i \sim \mathcal{N}(0, 1)$, and $\sigma^2 \in \mathbb{R}^+$ denotes the variance of both in-phase and quadrature components of the complex Gaussian RV of cluster i . From [35], the PDF and CDF of the received signal envelope, R , are given by

$$f_R(r) = \frac{2m^m r^{2m-1}}{\Gamma(m)\Omega^m} \exp\left(-\frac{mr^2}{\Omega}\right), \quad (2.24)$$

$$F_R(r) = \frac{\Upsilon\left(m, \frac{mr^2}{\Omega}\right)}{\Gamma(m)}, \quad (2.25)$$

where $\Omega = \mathbb{E}[R^2]$ is the mean received power, and $m = \Omega^2/\mathbb{V}[R^2] \geq 1/2$. Note that, the PDF and CDF given in (2.24) and (2.25) respectively, are valid for $m \in \mathbb{R}^+$. Moreover, for $m = 1$, (2.24) reduces to the Rayleigh PDF. An important remark is that the Nakagami- m distribution is often used to approximate the Rician distribution by properly mapping the Rician factor K as $m = (1+K)^2/(1+2K)$. Such approximation dates back from the original paper by Nakagami [35], and has been largely used in communication theory for decades. Even though such approximation is rather popular, it has important limitations when it comes to approximating the asymptotic behavior in outage-related metrics [122].

2.2.2 Generalized fading models

As mentioned early, in order to gain more degrees of freedom (i.e., more flexibility) when attempting to model fading conditions in more intricate environment (e.g., mm-Wave scenarios in 5G), several fading channels models have been proposed in the literature in the last years. Such generalized fading models not only provide an accurate fit with the field measurements in emerging 5G scenarios, but they also encompass distinct classical fading distributions. Next, two general distributions, as well as their connections to other popular fading models are described.

2.2.2.1 The α - μ Fading Model

The α - μ fading distribution was proposed in [123], and its applicability has been tested in various practical scenarios. For instance, field measurements of diverse propagation environments investigated in [124]–[126] have shown that the α - μ distribution suits better statistical variations of the propagated signal than the commonly used fading models. In the α - μ model, the received signal envelope includes an arbitrary number, μ , of multipath components and is observed as a nonlinear function of the modulus of the sum of such components. Assuming that the nonlinearity term is expressed in the form of a power parameter, $\alpha > 0$, so that the resulting envelope R is given by [123]

$$R = \sqrt[\alpha]{\sum_{i=1}^{\mu} \|\sigma X_i + j\sigma Y_i\|^2}, \quad (2.26)$$

where $X_i, Y_i \forall i$ are independent Gaussian RVs, i.e., $X_i, Y_i \sim \mathcal{N}(0, 1)$, and $\sigma^2 \in \mathbb{R}^+$ denotes the variance of both in-phase and quadrature components of the multipath waves of cluster i . From, [123], the corresponding PDF and CDF of R are expressed as

$$f_R(r) = \frac{\alpha \mu^\mu r^{\alpha\mu-1}}{\Gamma(\mu)\Omega^\mu} \exp\left(-\frac{\mu r^\alpha}{\Omega}\right), \quad (2.27)$$

$$F_R(r) = \frac{\Upsilon\left(\mu, \frac{\mu r^\alpha}{\Omega}\right)}{\Gamma(\mu)}, \quad (2.28)$$

where $\Omega = \mathbb{E}[R^\alpha]$ is a scale parameter, and $\mu = \mathbb{E}^2[R^\alpha]/\mathbb{V}[R^\alpha]$. In particular, for $\mu = 1$, (2.27) reduces to the Weibull PDF and, for $\alpha = 2$, to the Nakagami- m PDF.

2.2.2.2 The κ - μ Fading Model

The κ - μ model arises as a natural generalization of the Rician distribution. In such a model, the clusters of the received signal envelope are composed of both scattered and LoS waves. The LoS components' power is assumed to be different in each cluster, but the scattered waves of all clusters have the same power. Therefore, the received signal amplitude R is given by [127]

$$R = \sqrt{\sum_{i=1}^{\mu} \|\sigma X_i + p_i + j(\sigma Y_i + q_i)\|^2}, \quad (2.29)$$

where $X_i, Y_i \forall i$ are independent Gaussian RVs, i.e., $X_i, Y_i \sim \mathcal{N}(0, 1)$, $\sigma^2 \in \mathbb{R}^+$ denotes the variance of both in-phase and quadrature components of the multipath waves of cluster i , and μ is the number of clusters of multipath. Also, p_i and $q_i \in \mathbb{R}^+$ are the mean values of the in-phase and quadrature components of the multipath waves of cluster i , respectively. From [127], the PDF and CDF of R are

given by

$$f_R(r) = \frac{2\mu(1+\kappa)^{\frac{1+\mu}{2}} r^\mu}{\kappa^{\frac{\mu-1}{2}} \Omega^{\frac{\mu+1}{2}} \exp(\mu\kappa)} \exp\left(-\frac{\mu(1+\kappa)r^2}{\Omega}\right) I_{\mu-1}\left(2\mu r \sqrt{\frac{\kappa(1+\kappa)}{\Omega}}\right), \quad (2.30)$$

$$F_R(r) = 1 - \mathbb{Q}_\mu\left(\sqrt{2\kappa\mu}, r \sqrt{\frac{2\mu(1+\kappa)}{\Omega}}\right), \quad (2.31)$$

where

$$\kappa = \frac{\sum_{i=1}^{\mu} p_i^2 + q_i^2}{2\mu\sigma^2}, \quad \Omega = \mathbb{E}[R^2] = \sum_{i=1}^{\mu} p_i^2 + q_i^2 + 2\mu\sigma^2. \quad (2.32)$$

As particular cases, for $(\kappa = K, \mu = 1)$, (2.30) reduces to the Rician PDF and, for $(\kappa = 0, \mu = m)$, to the Nakagami- m PDF. Note that κ is defined in a similar way to that Rice K -factor, corresponding to the ratio between the power of the LoS waves and the power of the diffuse components. Although the physical model of κ - μ in (2.29) forces μ to be a positive integer, the PDF and CDF given in (2.30) and (2.31), respectively, are valid for $\mu \in \mathbb{R}^+$.

2.2.2.3 The κ - μ shadowed Fading Model

The κ - μ shadowed model was proposed in [21] as a generalization of the κ - μ distribution. The κ - μ shadowed model considers a signal composed of clusters of multipath waves, propagating in a non-homogeneous environment. Within each cluster, the multipath waves have scattered diffuse waves with identical power and a specular component with certain arbitrary power. Unlike the conventional κ - μ model, the dominant component of the i -th cluster of the κ - μ shadowed model is allowed to fluctuate randomly. Therefore, the received envelope signal, R , be formulated as [21]

$$R = \sqrt{\sum_{i=1}^{\mu} \|\sigma X_i + j\sigma Y_i + \xi(p_i + jq_i)\|^2}, \quad (2.33)$$

where μ is the number of the multipath clusters, $X_i, Y_i \forall i$ are independent Gaussian RVs, i.e., $X_i, Y_i \sim \mathcal{N}(0, 1)$, $\sigma^2 \in \mathbb{R}^+$ denotes the variance of both in-phase and quadrature components of the multipath waves of cluster i . Also, $\xi p_i + \xi q_i$ represents the dominant component of the i th cluster with power given by $p_i^2 + q_i^2$, where p_i and $q_i \in \mathbb{R}^+$ are the mean values of the in-phase and quadrature components of the multipath waves of cluster i , respectively. The total power of the scattered components for each cluster is $2\sigma^2$. The κ parameter is defined as the ratio between the total power of the dominant components and the total power of the scattered waves can be computed as $\kappa = d^2/(2\sigma^2\mu)$, where $d^2 = \sum_{i=1}^{\mu} p_i^2 + q_i^2$. The specular components for each cluster are subject to the same shadowing fluctuation ξ , which follows a Gamma RV with scale parameter m and spreading parameter $\mathbb{E}\{\xi\} = 1$. From [21], the PDF and CDF of the received signal envelope R are expressed as [21]

$$f_R(r) = \frac{2\mu^{\mu} m^m (1+\kappa)^{\mu} r^{2\mu-1}}{\Omega^{\mu} \Gamma(\mu) (\mu\kappa + m)^m} \exp\left(-\frac{\mu(1+\kappa)r^2}{\Omega}\right) {}_1F_1\left(m; \mu; \frac{\mu^2 \kappa (1+\kappa) r^2}{(\mu\kappa + m)\Omega}\right), \quad (2.34)$$

Table 2.1: Conventional and general fading models derived from the κ - μ shadowed distribution.

Fading Distribution	κ - μ shadowed parameters
One-sided Gaussian	$\underline{\mu} = 0.5, \underline{\kappa} \rightarrow 0, \underline{m} \rightarrow \infty$
Rayleigh	$\underline{\mu} = 1, \underline{\kappa} \rightarrow 0, \underline{m} \rightarrow \infty$
Nakagami- m	$\underline{\mu} = m, \underline{\kappa} \rightarrow 0, \underline{m} \rightarrow \infty$
Rician	$\underline{\mu} = 1, \underline{\kappa} = K, \underline{m} \rightarrow \infty$
κ - μ	$\underline{\mu} = \mu, \underline{\kappa} = \kappa, \underline{m} \rightarrow \infty$
η - μ	$\underline{\mu} = 2\mu, \underline{\kappa} = (1 - \eta)/(2\eta), \underline{m} = \mu$
Hoyt (Nakagami- q)	$\underline{\mu} = 1, \underline{\kappa} = (1 - \eta)/(2\eta), \underline{m} = 0.5$
Rician Shadowed	$\underline{\mu} = 1, \underline{\kappa} = K, \underline{m} = m$

$$F_R(r) = \frac{\mu^{\mu-1} m^m (1 + \kappa)^\mu r^{2\mu}}{\Omega^\mu \Gamma(\mu) (\mu\kappa + m)^m} \Phi_2 \left(\mu - m, m; \mu + 1; -\frac{\mu(1 + \kappa)r^2}{\Omega}, -\frac{\mu(1 + \kappa)mr^2}{\Omega(\mu\kappa + m)} \right), \quad (2.35)$$

where the κ and Ω are given in (2.32). Furthermore, (2.34) and (2.35) are valid for $\mu \in \mathbb{R}^+$. According to the characteristics of the channel described above, the κ - μ shadowed fading model finds great applicability in a range of real-world applications such as D2D communications, Underwater Acoustic Communications (UAC), body-centric fading channels, UAV systems, Land Mobile Satellite (LMS), etc [10]. It is worth mentioning that in [128], the κ - μ shadowed distribution can be characterized as a finite mixture of Nakagami- m RVs under the assumption of having positive integers values for μ and m . Finally, Table 2.1 summarizes the connections between the κ - μ shadowed distribution and other fading channel models. In order to avoid confusion, the parameters corresponding to the κ - μ shadowed distribution are underlined.

2.2.2.4 N-wave with Diffuse Power Fading Model

In the NWDP model, the received envelope signal is represented as a superposition of N multipath waves arising from dominant specular reflections and M additional waves associated with diffuse scattering [20, Eq. (2)]:

$$\tilde{V} = R \exp(j\theta) = \sum_{n=1}^N V_n \exp(j\theta_n) + \sum_{i=1}^M V_i \exp(j\theta_i), \quad (2.36)$$

where \tilde{V} is the received complex base-band signal with magnitude R and phase θ , $V_n \exp(j\theta_n)$ denotes the n -th specular component having a constant amplitude V_n and a uniformly distributed random phase $\theta_n \sim \mathcal{U}[0, 2\pi)$. The random phases for each dominant wave are assumed to be statistically independent. Because each diffuse scattered is able to generate several multipath waves [129], one can safely assume that $M \rightarrow \infty$ and hence the diffuse component tends to be Gaussian distributed, i.e., $\sum_{k=1}^M V_k \exp(j\theta_k) \approx V_d \exp(j\theta_d)$, so that V_d is Rayleigh distributed with $\mathbb{E}\{|V_d|^2\} = 2\sigma^2 = \Omega$. Notice that the consideration of arbitrary N in (2.36) allows for individually accounting for the effect of having multiple specular waves and widely differs from the conventional assumptions in fading modeling, reducing only for $N = 0, 1, 2$ to the Rayleigh, Rician, and TWDP

cases, respectively [17]. According to [20], the corresponding PDF and CDF of the received amplitude signal, R , are given by

$$f_R(r) = 2\epsilon r \exp(-\epsilon r^2) \sum_{z=0}^{\infty} C_z L_z(\epsilon r^2), \quad (2.37)$$

$$F_R(r) = \sum_{z=0}^{\infty} C_z \sum_{k=0}^z \frac{(-1)^k}{k!} \binom{z}{k} \Upsilon(k+1, \epsilon r^2), \quad (2.38)$$

where the constant ϵ and the coefficient C_z are defined as

$$\epsilon = \frac{1}{\sum_{n=0}^N V_n^2 + \Omega}, \quad C_z = \sum_{k=0}^z \frac{(-\epsilon)^k}{k!} \binom{z}{k} u_{N+1}^{(2k)}, \quad (2.39)$$

where

$$u_j^{2k} = \sum_{w=0}^k \binom{k}{w}^2 u_{j-1}^{(2w)} v_j^{(2k-2w)}, \quad \text{for } j = 2, \dots, N+1, \quad (2.40)$$

in which the initial value is $u_1^{2k} = v_1^{2k}$, and

$$v_j^{2k} = \begin{cases} V_j^{2k}, & \text{for } j = 1 \dots N, \\ (1)_k (\Omega)^k, & \text{for } j = N+1. \end{cases} \quad (2.41)$$

It is worth highlighting that two-ray-based models (i.e., FTR and TWDP) have shown good fit to empirical measurements in mm-Wave communications [19], [130]. Therefore, the NWDP model is a promising candidate to improve fading channel modeling in mm-Wave because it includes several degrees of freedom more than FTR and TWDP models.

2.3 DIVERSITY COMBINING TECHNIQUES

Dealing with the damaging effects of multipath propagation is one of the difficult tasks in designing wireless communication systems. There are many techniques for combating these effects, including diversity combining techniques, coding and adaptive equalization, among others [3]. Specifically, diversity techniques have attracted significant attention for their efficiency and relative simplicity of implementation. The principle of diversity establishes that fading in independent channels are independent events. Thus, if specific information is made available with redundancy in a certain number of channels (branches of diversity), the probability that it is affected by a deep fading, simultaneously in all channels, is less than the probability of occurring in one of these channels [120]. Therefore, by combining the different branches' information signals with an appropriate algorithm (i.e., diversity techniques), a resulting signal less deteriorated by the fading that marks each branch individually is obtained. Next, detailed description of the most used diversity combining methods in the literature is provided.

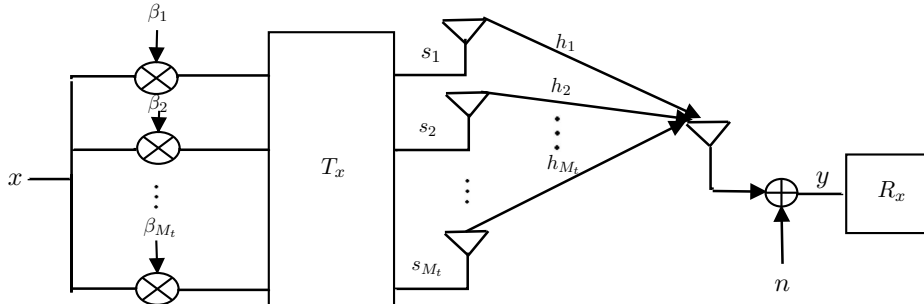


Figure 2.2: Illustration of a combiner in a MISO system, based on [131].

2.3.1 Transmitter Antenna Diversity

For this setup, it is considered that the transmitter is equipped with M_t antennas as depicted in Fig. 2.2, where $x(k)$ is the sequence of data with i.i.d symbols. Based on the particular transmit diversity method, the data is first pre-processed to form a sequence of transmit symbol vector, i.e., $s(k) = [s_1(k), s_2(k), \dots, s_{M_t}(k)]$ to later be transmitted over the M_t antennas in the k -th symbol period. The transmitted signal on the k -th antenna is given by [131]

$$s_i(k) = \beta_i x(k), \quad \text{for } i = 1, \dots, M_t, \quad (2.42)$$

where $\beta_1, \beta_2, \dots, \beta_{M_t}$ are the weighting factors applied on the M_t antennas, respectively. The signal observed at the receiver can be written as [131]

$$y(k) = \sum_{i=1}^{M_t} \sqrt{P} h_i s_i(k) + n(k), \quad (2.43)$$

where P is the total transmit power, h_i is the channel coefficient between the i -th transmit antenna and the receiver, and $n(k)$ is a zero-mean circularly symmetric complex Gaussian RV with variance σ^2 . Here, based on the knowledge of the CSI at the transmitter, different techniques (e.g., transmit Beamforming and TAS) can be used to exploit spatial diversity. The next section focuses on the TAS scheme that will be used later.

2.3.1.1 Transmit Antenna Selection

Suppose that the transmitter can obtain knowledge of the channel amplitude but not the channel phase information (i.e., partial CSI)^[1]. Therefore, the transmitted signal over multiple antennas cannot be co-phased at the receiver side. In this case, it is more efficient to transmit only on the antenna with the best channel to avoid destructive interference. Now, assuming that the i^* -th antenna is the

^[1] Such a case is very common in practice because the phase varies much faster than the channel amplitude, making it more challenging to estimate.

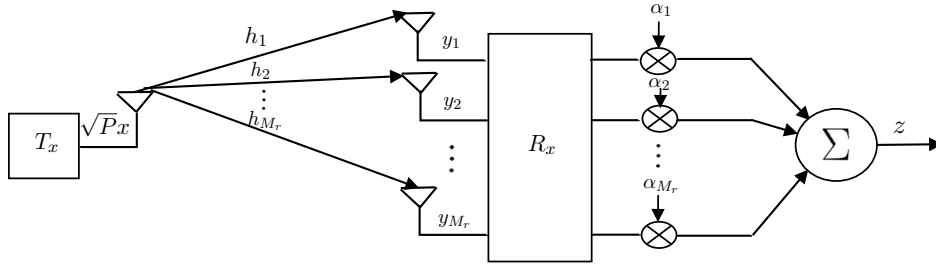


Figure 2.3: Illustration of a combiner in a SIMO system, based on [131].

one experiencing the highest SNR, i.e., [131]

$$i^* = \arg \max_{1 \leq i \leq M_t} \frac{P|h_i\beta_i|^2}{\sigma^2}, \quad (2.44)$$

and is chosen to transmit, so that [131]

$$\beta_i = \begin{cases} 1, & \text{for } i = i^*, \\ 0, & \text{for } i \neq i^*. \end{cases} \quad (2.45)$$

Therefore, (2.43) can be rewritten as [131]

$$y(k) = \sqrt{P}h_{i^*}x(k) + n(k). \quad (2.46)$$

From (2.46), the resulting SNR for the TAS scheme is expressed by [131]

$$\gamma_{\text{TAS}} = \frac{P|h_{i^*}|^2}{\sigma^2} = \max_{1 \leq i \leq M_t} \frac{P|h_i|^2}{\sigma^2}. \quad (2.47)$$

It is worth mentioning that the TAS/MRC setup is an excellent choice in the performance analysis of wireless systems with multiple antennas due to its low implementation complexity compared to Transmit Beamforming/MRC schemes.

2.3.2 Receiver Antenna Diversity

When the receiver is equipped with multiple antennas (i.e., SIMO setup), the system performance can be improved using spatial diversity at the receiver side. Consider the configuration where the transmitter with single-antenna sends information to a receiver equipped with M_r antennas, as illustrated in Fig. 2.3. In such a scheme, the received signal at i -th branch can be expressed as [131]

$$y_i(k) = \sqrt{P}h_i x(k) + n_i(k), \quad \text{for } i = 1, \dots, M_r, \quad (2.48)$$

where $x(k)$ is the symbol to be transmitted in the k -th symbol period, P is the transmit power, h_i is the channel coefficient observed by the i -th received antenna, and $n_i(k)$ is a zero-mean circularly

symmetric complex Gaussian RV with same variance σ_i^2 at the i -th antenna. The channel coefficient h_i can be expressed in terms of its amplitude $|h_i|$ and phase θ_i as [131]

$$h_i = |h_i| \exp(j\theta_i), \quad \text{for } i = 1, \dots, M_r. \quad (2.49)$$

From (2.48), the SNR at the i -th antenna is defined as [131]

$$\gamma_i = \frac{P |h_i|^2}{\sigma_i^2}. \quad (2.50)$$

By assuming that the CSI of the channel coefficients is available at the receiver side. Therefore, before performing signal detection, the receiver combines the received signals with the respective weighting factors, i.e., $\alpha_i \forall i$ (see Fig. 2.3), to obtain the resulting signal at the combiner output as [131]

$$z(k) = \sum_{i=1}^{M_r} \alpha_i y_i(k). \quad (2.51)$$

Here, depending on the weighting factors' values, two different signal combining techniques are introduced below.

2.3.2.1 Equal Gain Combining

In this technique, the received signals on M_r branches are each multiplied by a complex weighting factor for the phase rotation of the channel. Such weighting factors are given by [131]

$$\alpha_i = \exp(-j\theta_i), \quad \text{for } i = 1, \dots, M_r. \quad (2.52)$$

Note that the magnitudes of the weighting factor, i.e. $|\alpha_i| \forall i$, are equal to unity. This fact reduces the implementation complexity compared to the MRC to be introduced later on. Substituting (2.52) into (2.51), the signal output of the EGC is given by [131]

$$z_{\text{EGC}}(k) = \sqrt{P} \left(\sum_{i=1}^{M_r} |h_i| \right) x(k) + \sum_{i=1}^{M_r} \exp(-j\theta_i) n_i(k) \quad (2.53)$$

From (2.53), the resulting SNR at the output of the EGC combiner can be expressed as [131]

$$\begin{aligned} \gamma_{\text{EGC}} &= \frac{P \left(\sum_{i=1}^{M_r} |h_i| \right)^2}{\sum_{i=1}^{M_r} \sigma_i^2} \\ &= \frac{P \left(\sum_{i=1}^{M_r} |h_i| \right)^2}{M_r \sigma_i^2} \end{aligned} \quad (2.54)$$

With the help of (2.50), (2.54) can be rewritten in compact form as

$$\gamma_{\text{EGC}} = \frac{1}{M_r} \left(\sum_{i=1}^{M_r} \sqrt{\gamma_i} \right)^2. \quad (2.55)$$

2.3.2.2 Maximal Ratio Combining

Although EGC uses CSI to determine their weighting factors, such values are no optimized in any sense. Therefore, to fully exploit the spatial diversity in multiple receive antennas, it is necessary to choose the weighting factors to maximize the received SNR. Based on this, given the CSI, the weighting factors of the MRC can be formulated as [131]

$$\alpha_i = h_i^* / \sigma_i^2 = |h_i| \exp(-j\theta_i) / \sigma_i^2, \quad \text{for } i = 1, \dots, M_r. \quad (2.56)$$

Note that the received signals are weighted based on their channel quality and are co-phased to achieve the phase-coherent addition of signals at the receiver. In other words, branches with a strong signal are further amplified, while weak signals are attenuated. Substituting (2.56) into (2.51), the signal output of the MRC is given by [131]

$$z_{\text{MRC}}(k) = \sqrt{P} \left(\sum_{i=1}^{M_r} \frac{|h_i|}{\sigma_i^2} \right) x(k) + \sum_{i=1}^{M_r} \frac{h_i^*}{\sigma_i^2} n_i(k). \quad (2.57)$$

From (2.57), the resulting SNR at the output of the MRC combiner can be expressed as [131]

$$\begin{aligned} \gamma_{\text{MRC}} &= \frac{P \left(\sum_{i=1}^{M_r} |h_i|^2 / \sigma_i^2 \right)^2}{\sum_{i=1}^{M_r} |h_i|^2 / \sigma_i^2} \\ &= \sum_{i=1}^{M_r} \frac{P |h_i|^2}{\sigma_i^2} \end{aligned} \quad (2.58)$$

Again, with the help of (2.50), (2.58) can be rewritten in compact form as

$$\gamma_{\text{MRC}} = \sum_{i=1}^{M_r} \gamma_i. \quad (2.59)$$

Notice that (2.59) is essentially the sum of the received SNRs at all branches.

2.3.3 Performance Metric for Multibranch Combining Receivers

Several metrics to assess the performance of diversity combining techniques over different fading channels have been proposed in the literature [120]. Among these metrics, the ABEP is the most commonly used to evaluate communications systems' performance because of its straightforward

interpretation. Specifically, the formulations for the ABEP at the output of EGC multibranch receivers for coherent and non-coherent modulation techniques are revisited in the following. This performance metric will be incorporated as an application for sums of RVs in Chapter 3.

2.3.3.1 Average Bit Error Probability

Here, the exact formulations of the ABEP at the output of multibranch EGC receiver associated with coherent and non-coherent modulation techniques are revisited. In particular, the exact solution for the ABEP in EGC reception can be defined as in [120] by

$$\bar{P}_e = \int_0^{\infty} P_e(r) f_R(r) dr, \quad (2.60)$$

where $f_R(r)$ is the PDF of the sum of fading amplitudes at the output of the EGC combiner. The combiner output envelope R can be obtained from (2.55) using a standard transformation of variables, i.e., $R = \sqrt{\gamma_{\text{EGC}}}$. Therefore, it follows that [49]

$$R = \frac{1}{\sqrt{M_r}} \sum_{i=1}^{M_r} R_i. \quad (2.61)$$

Also, $P_e(r)$ denotes the conditional bit error probability. Considering non-coherent Modulations, $P_e(r)$ can be expressed as in [120] by

$$P_e(r) = \frac{1}{2} \exp(-g r^2 E_b / N_0), \quad (2.62)$$

where N_0 is the one-sided AWGN variance, E_b is the bit energy, and g is a modulation dependent parameter such that $g = 1$ for Differential Binary Phase-Shift Keying (DBPSK), and $g = 1/2$ for non-coherent Binary Frequency-Shift Keying (BFSK). For coherent Modulations, $P_e(r)$ can be defined as in [120] by

$$P_e(r) = \frac{1}{2} \operatorname{erfc} \left(r \sqrt{g E_b / N_0} \right), \quad (2.63)$$

where $g = 1$ for coherent Binary Phase Shift keying (BPSK), $g = 1/2$ for coherent BFSK, and $g = 0.715$ for coherent BFSK with minimum correlation. In general, the main difficulty associated with evaluating the ABEP in (2.60) is related to the requirement of obtaining the PDF of the sum of RVs given in (2.61). Such PDF requires the convolution (as will be seen later) of the individual PDFs R_i and can often be challenging to evaluate. Therefore, one of this thesis's contributions is to provide simple and accurate approximations for the sum of RVs to facilitate wireless systems' performance analysis with multiple antennas.

2.4 FUNDAMENTALS OF RIS-ASSISTED WIRELESS COMMUNICATIONS

In this section, in order to understand the motivation behind the PLS of RIS-aided communications, a theoretical background on how a basic communication system works with the help of RIS technology is introduced.

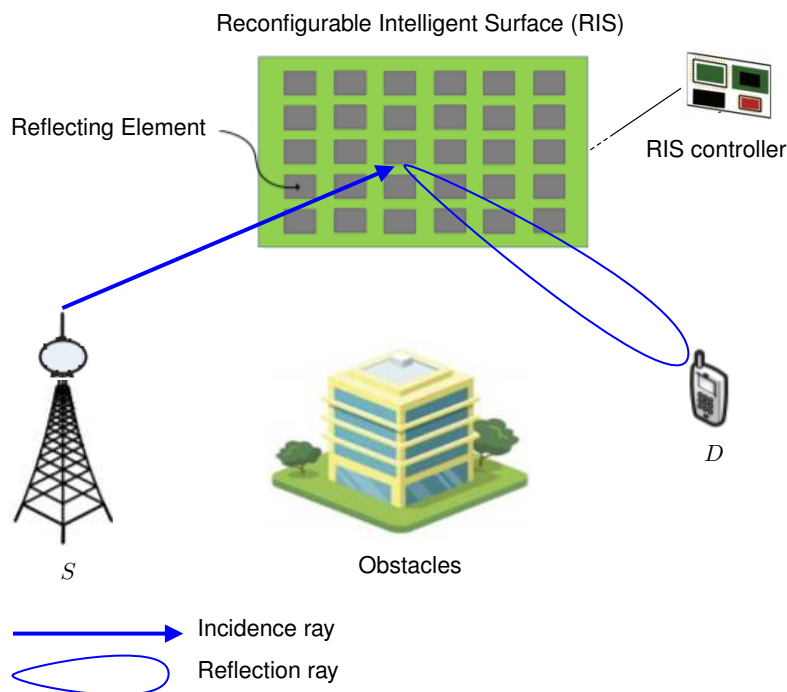


Figure 2.4: Typical IRS-assisted wireless system, based on [132].

RIS technology has emerged as a new beyond MIMO paradigm for 6G to noticeably improve the performance of post-5G networks in terms of Spectrum Efficiency (SE) and Energy Efficiency (EE) [132]. RIS is a meta-surface that consists of a large number of low-cost passive reflecting electronic units that can be programmed to alter the electromagnetic fields in order to obtain favorable environments. RIS's element can adaptively adjust the amplitude reflection and/or the phase shift of the incident signals in a customizable way. Unlike other comparable technologies, such as relays and MIMO beamforming, RIS technology does not need any power source and complex encoding and decoding methods. These programmable features make RISs attractive to be integrated into the infrastructure of beyond 5G networks [133].

A typical RIS-based SISO communication scheme consists of one source (S), one RIS with n reflecting elements, and one destination (D), where S and D are equipped with one antenna, as illustrated in Fig. 2.4. In this setup, S communicates with the D via RIS technology. By assuming that the phase shifts induced by the composite fading channels are available at the RIS, the reflecting elements' phases can be set so that the signals can be combined coherently at the destination side. Neverthe-

less, the perfect phase estimation of the reflection phases is unfeasible in practice. Therefore, one contribution of this thesis is to study the impact of imperfect phase estimation on the communications system's secrecy performance through an RIS technology.

It is worth mentioning that, the assumption in Fig. 2.4 related to neglecting the direct link between the source and the receiver is because one of RIS technology's key uses is to overcome NLoS scenarios [134]. Furthermore, it is important to rule out that very recently, the work in [135] provides channel modeling formulations to analyze the performance of RIS-assisted communications in the existence of a direct link between the transmitter and receiver sides. These results will undoubtedly bring a broad study of RIS-aided communications for LoS scenarios. Finally, it is worth highlighting that, this work will focus on the PLS analysis of RIS-assisted wireless communications assuming NLoS scenarios.

3 SUM AND RATIO OF RANDOM VARIABLES

In this chapter, analytic closed-form expressions for (i) the sum of both classic and generalized RVs; and (ii) the ratio of two RVs taken from α - μ distributions are derived. Specifically, two approaches are introduced for the sum of RVs. In the first, the exact distribution of the sum of Nakagami- m RVs is approximated by a mixture of two Nakagami- m RV, where the adjustment parameters are estimated using the EM algorithm. For the second approach, the chief statistics of the sum of generalized RVs are approximated by using another generalized RV in which the fit parameters are calibrated through the asymptotic matching method. Concerning the ratio of two α - μ RVs, the exact PDF, CDF and MGF are derived in terms of the univariate Fox H-function. Based on these results, a practical application example in PLS over α - μ fading channels is also provided.

3.1 SUM OF RANDOM VARIABLES

Before tackling the proposed approximations, the formulation of the problem of the sum of RVs and two classical frameworks to obtain the exact PDF of a sum of independent RVs are revisited. In the first approach, the exact PDF emerges as the convolution of the individual PDFs. For the second method, the sum PDF arises from the FT of the product of the marginal CFs. Furthermore, it is essential to mention that computing the exact sum PDF even for classical distributions is challenging.

3.1.1 Problem Formulation and Exact Solutions

3.1.1.1 Formulation

Let R be the sum of an arbitrary number M of i.n.i.d. fading (non-negative) RVs R_i [49]

$$R = \sum_{i=1}^M R_i. \quad (3.1)$$

Here, it is considered that, each summand R_i can follow a generalized or classic fading model. In particular, two cases are addressed: (i) R_i follows a Nakagami- m distribution, and (ii) R_i can be taken from α - μ , κ - μ , η - μ , and κ - μ shadowed models. The goal is to find, for any given sum, a

good approximation to the PDF of R or, equivalently, to its CDF. Next, the conventional analytical frameworks to obtain the exact PDF solution are reviewed.

3.1.1.2 Exact Solution Framework

As mentioned earlier, the exact mathematical evaluation for the PDF of the sum of independent RVs can be achieved by two means. Therefore, these standard procedures are introduced in the following.

Convolution of Densities and Brennan's Integral: The PDF and CDF of R can be computed as the convolution of the marginal PDFs of R_i . Alternatively, when the summands are non-negative RVs (like in our case of fading envelopes), it is possible to reformulate the sum PDF by means of a geometric approach, as proposed by Brennan in [136]. Both the convolution and Brennan's approach are written in a similar fashion, as an multiple-fold integral formula in terms of the product of marginal PDFs. Hence, the resultant PDF and CDF of R in (3.1) can be written as [136]

$$f_R(r) = \int_0^r \int_0^{r-r_M} \dots \int_0^{r-\sum_{i=3}^M r_i} f_{R_1, \dots, R_M}(r - \sum_{i=2}^M r_i, r_2, \dots, r_M) dr_2 \dots dr_{M-1} dr_M, \quad (3.2a)$$

$$F_R(r) = \int_0^r \int_0^{r-r_M} \dots \int_0^{r-\sum_{i=3}^M r_i} \int_0^{r-\sum_{i=2}^M r_i} f_{R_1, \dots, R_M}(r_1, r_2, \dots, r_M) dr_2 \dots dr_{M-1} dr_M. \quad (3.2b)$$

As pointed out in [136], (3.2) is valid even for correlated summands. For this case, the correlation matrix is included the joint PDF of R_1, \dots, R_M . In our context, since the summands are assumed to be independent, the joint PDF in (3.2) reduces to the product of marginal PDFs [136]

$$f_{R_1, \dots, R_M}(r_1, \dots, r_M) = \prod_{i=1}^M f_{R_i}(r_i). \quad (3.3)$$

Regrettably, the multi-fold integral in (3.2) is quite as frightful as it appears, and its evaluation presents a closed-form solution only for particular fading models. The computation of (3.2) through numerical integration using standard computing software such as Mathematica and Matlab can be unfeasible and very time-consuming for the sum of more than five RVs.

Product of Characteristics Functions: The CF of R_i is presented as the Inverse FT of its PDF as: $\Phi_i(\omega) \triangleq \mathbb{E}[\exp(j\omega R_i)]$ [137]. Knowing that in the time domain the PDF of R is given as the convolution of individual PDFs, the $\Phi_R(\cdot)$ of R in the frequency domain can be achieved through the product of marginal CFs of R_i as [137]

$$\Phi_R(\omega) = \prod_{i=1}^M \Phi_{R_i}(\omega). \quad (3.4)$$

Consequently, the exact PDF in (3.2a) can be obtained from its CF by using Fourier transform [137]

$$f_R(r) = \frac{1}{2\pi} \int_{-\infty}^{+\infty} \prod_{i=1}^M \Phi_{R_i}(w) \exp(-j\omega r) d\omega. \quad (3.5)$$

The downside of this solution is that closed-form expressions for the marginal CFs, i.e., $\Phi_{R_i}(\cdot)$, are known only for a few fading models. For instance, the CF of a branch R_i that follows a Nakagami- m PDF is given by [120]

$$\Phi_{R_i}(\omega) = {}_1F_1\left(m_i; \frac{1}{2}; -\frac{\Omega_i \omega^2}{4m_i}\right) + j\omega \frac{\Gamma(m_i + \frac{1}{2})}{\Gamma(m_i)} \sqrt{\frac{\Omega_i}{m_i}} {}_1F_1\left(m_i; \frac{1}{2}; -\frac{\Omega_i \omega^2}{4m_i}\right). \quad (3.6)$$

Based on this, a closed-form solutions of (3.4) exist only for particular cases (e.g., Rayleigh and Nakagami- m cases). Furthermore, the marginal CFs are often rather oscillatory functions, especially for the CFs available in generalized fading models. This fact makes the numerical evaluation of (3.4) prone to convergence issues and impracticable as the number of summands increases.

For informative purposes, an alternative approach to compute the exact sum PDF that is not covered in this section is that (3.1) can also be obtained in terms of the marginal MGFs — the Laplace Transform (LT) of the marginal PDFs. The MGF of R is the product of the MGFs of R_i , the inverse LT of which gives the PDF of R . Although the MGF approach avoids the oscillatory issues of the CF approach, the approach still deals with the inverse LT that is hardly computed in closed-form, requiring as before numerical routines.

3.1.2 Nakagami- m Approximation Approach

Here, the sum of M i.n.i.d. Nakagami- m RVs is approximated by using a mixture of two Nakagami- m RVs. For this sum, the exact distribution R can be calculated with the help of (3.1), where each summand R_i follows a Nakagami- m distribution. From (2.24), R_i can be rewritten as [35]

$$f_{R_i}(r; \boldsymbol{\theta}_i) = \frac{2m_i^{m_i} r^{2m_i-1}}{\Gamma(m_i)\Omega_i^{m_i}} \exp\left(-\frac{m_i r^2}{\Omega_i}\right), \quad (3.7)$$

where $\boldsymbol{\theta}_i = (\Omega_i, m_i)$ is the vector of parameters corresponding at the i -th branch of the sum^[1]. Here, the goal is to find a good approximation to the PDF of R . To understand the motivation behind the proposed approximation, a theoretical background is introduced below.

[1] Through this section, bold typeface symbols represent vectors.

3.1.2.1 Background

This section introduces a theoretical basis concerning the EM algorithm and the Monte Carlo (MC) approach. These methods are required to calibrate the parameters of the Nakagami- m mixture model.

Monte Carlo Method: MC simulations describe any technique of computation that uses a large number of pseudo-random samples to achieve a certain result. They are often the only practical way to evaluate mathematical problems and they are useful when it is difficult or unfeasible to use other mathematical tools. MC methods are mainly employed in three distinct problem classes: numerical integration, optimization and generating samples from probability distributions [138]. For the problem dealt in this work, the sum of generalized RVs given by multidimensional integrals can easily be translated from the continuous multiple integrals to the discrete sum of pseudo-random samples by using the MC method. Therefore, the sample space of the observations of the resulting PDF R in (3.1) can be expressed by

$$\mathbf{X} = \sum_{i=1}^M X_i. \quad (3.8)$$

where each pseudo-random sequence X_i contains a vector of n samples that follows a Nakagami- m distribution. To generate sequences of random numbers needed in (3.8), several mathematical methods have been proposed in [139]. In addition, the random number generation routines in Wolfram Mathematica and Matlab called *RandomVariate* [140], and *makedist* [141], respectively, implement fast algorithms to obtain Nakagami- m samples. So, for our approximation, these tools are employed. Alternatively, after a careful study of the works reported on developing of approximate expressions [142]–[144] to generate X_i having Nakagami- m distribution, this research work uses the approach in [144], due to its easy implementation in any standard computer language. Having mentioned the two ways of obtaining the desired sequence X_i , the estimation of the sample size in MC simulations is explained in detail below.

As mentioned previously, the main idea on MC simulation is to create series of experimental samples using pseudo-random numbers. Hence, it is necessary to establish the appropriate number of samples that ensures a good accuracy in the results. For this purpose, according to the central limit theorem, the statistics such as mean (μ), and standard deviation (σ) can be used through the coefficient of variation ($CV = \frac{\sigma}{\mu}$) as an indicator of estimation of iterations when the number of samples is large enough [145]. Consequently, the coefficients of variation are depicted in Fig 3.1, as a function of the number of MC realizations from the whole set of 30.000 MC simulations in the sum of six i.n.i.d. Nakagami- m variates. This figure also reports an estimate about the number of simulations required to improve the accuracy of predictions in MC method. Therefore, based on Fig 3.1, 20.000 samples for each X_i for the MC simulations are used.

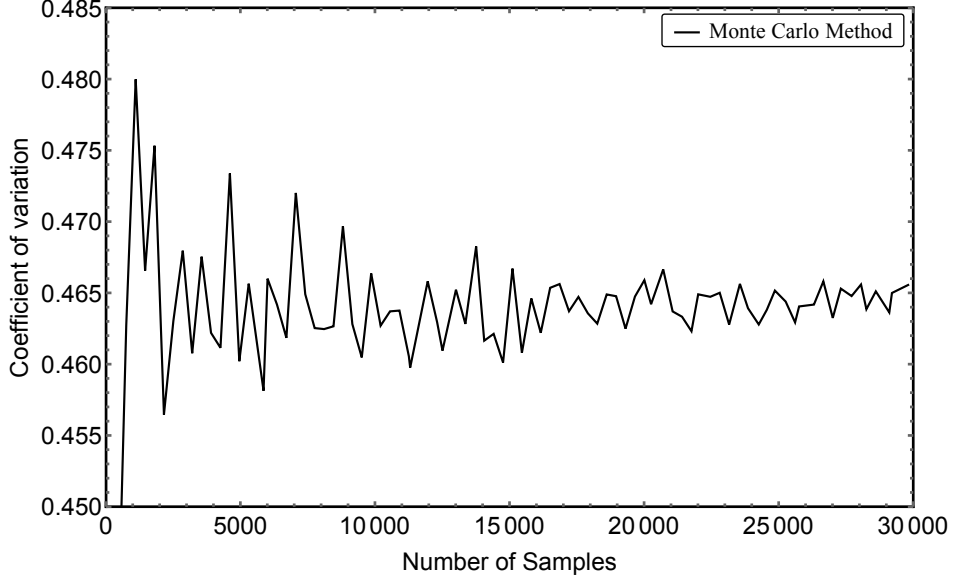


Figure 3.1: Coefficient of variation for the PDF of the sum of six i.n.i.d. Nakagami- m variates with parameters $\Omega_i = 1$, and $(m_1, m_2, m_3, m_4, m_5, m_6) = (0.5, 0.7, 0.9, 1, 1.5, 2)$.

Expectation Maximization Algorithm With Mixture Model: EM is an iterative method that can be used to fit a mixture model of a parametric PDF. In the EM algorithm, it is assumed that the approximate PDF of (3.1) can be modeled as a weighted sum of other p numbers of PDFs. The parameters of those PDFs can be estimated using n samples taken from the distribution of X , where ($p \ll n$). EM maximizes the likelihood function of the mixture respect to the weight coefficients using the provided statistical samples. Therefore, EM with mixture model can be defined as in [146] by

$$f_X(x; \Psi) = \sum_{i=1}^p \omega_i \phi_i(x; \theta_i), \quad (3.9)$$

where ω_i , $i \in \{1, \dots, p\}$ denote the mixture weights, and $\phi_i(x; \theta_i)$ represents the density of the i -th mixture component of the mixture model. An important constraint on this estimation is to have $\sum_{i=1}^p \omega_i = 1$, and $0 \leq \omega_i \leq 1$ to satisfy the unity integral of (3.9). Let $\Psi = \{\omega_1, \dots, \omega_{p-1}, \theta_1, \dots, \theta_p\}$ be the set of all unknown parameters of the mixture model, where θ_i is a vector containing the unknown parameters of the i -th component density. Next, in the mixture model with EM procedure, one starts with any feasible values of θ_i , and ω_i , then the parameters, and the weighting coefficients are updated in each iteration by alternating between the following two steps until a convergence condition is met:

Expectation step (E step): To establish notation, let $\Psi^{(k)}$ denotes the current estimate of Ψ after the k -th iteration of the EM algorithm. This stage evaluates the k -th responsibility value $\tau_{ij}^{(k)}$ that the data point $x_j \in X$ (obtained from (3.8)) belongs to the i -th weighted PDF, given the current parameter estimates ω_i , and θ_i . Using Bayes' Rule, this responsibility can be computed as in [147] by

$$\tau_{ij}^{(k)} = \frac{\omega_i \phi_i(x_j; \theta_i)}{\sum_{l=1}^p \omega_l \phi_l(x_j; \theta_l)}, \quad i = 1, 2, \dots, p, \quad j = 1, 2, \dots, n, \quad (3.10)$$

where p is the number of weighted PDFs, and n is the whole set of samples. *Maximization step (M step)*: On the $(k + 1)$ -th iteration of the M-step, the current estimate of Ψ , named $\Psi^{(k)}$, is updated to $\Psi^{(k+1)}$. The new parameters $\Psi^{(k+1)}$ are estimated by maximizing the log-likelihood function $L(\mathbf{X} | \Psi)$ of each distribution $\phi_i(x; \theta_i)$ weighted by the responsibilities, from a sample data set $\mathbf{X} = \{x_j\}_{j=1}^n$ obtained through the MC method. So, the $L(\mathbf{X} | \Psi)$ function is defined as in [147] by

$$L(\mathbf{X} | \Psi)^{(k+1)} = \sum_{j=1}^n \sum_{i=1}^p \tau_{ij}^{(k)} \log [\omega_i \phi_i(x_j; \theta_i)]. \quad (3.11)$$

Let θ_{it} denotes the t -th element of the parameter vector θ_i . The EM updating parameters are derived from the gradient of $L(\mathbf{X} | \Psi)$ equal to zero. Thus, the maximum likelihood estimator of the element $\theta_{it} \in \theta_i \in \Psi$ is given by:

$$\frac{\partial L(\mathbf{X} | \Psi)^{(k+1)}}{\partial \theta_{it}} = \sum_{j=1}^n \tau_{ij}^{(k)} \frac{\partial}{\partial \theta_{it}} \log [\omega_i \phi_i(x_j; \theta_i)] = 0. \quad (3.12)$$

The estimate of the element $\omega_i \in \Psi$, is given by

$$\frac{\partial L(\mathbf{X} | \Psi)^{(k+1)}}{\partial \omega_i} = \sum_{j=1}^n \tau_{ij}^{(k)} \frac{\partial}{\partial \omega_i} \log [\omega_i \phi_i(x_j; \theta_i)] = 0, \quad (3.13)$$

where, the weighting coefficients ω_i can be updated as in [147] by:

$$\omega_i^{(k+1)} = \frac{\sum_{j=1}^n \tau_{ij}^{(k)}}{n}. \quad (3.14)$$

Typically, the iterations in the EM procedure are performed until the changes in the relative difference of the PDFs parameters are less than some pre-established threshold ϵ . It is worth mentioning that, the accuracy of the EM algorithm depends both on the threshold and the number of weighted PDFs. Furthermore, the time for convergence increases on two factors; as the number of mixture distributions rises and with decreasing of ϵ . Interested readers can revise [148] for further guidance about convergence and the accuracy of the EM algorithm.

3.1.2.2 Proposed Approximation

Herein, this research proposes to approximate the PDF of R given in (3.1) by two weighted envelopes given in (3.9), for which appropriate parameters must be determined to render this method a good approximation. The development of such an approach is derived in detail below.

In our approach all ϕ_i are Nakagami- m density functions given in (3.7), hence, all $\theta_i = (\Omega_i, m_i)$. Now, putting (3.7) in (3.12) for $\Omega_i \in \theta_i$, it follows that

$$\sum_{j=1}^n \tau_{ij}^{(k)} \frac{\partial}{\partial \Omega_i} \log \left[\frac{\omega_i 2m_i^{m_i} x_j^{2m_i-1}}{\Gamma(m_i) \Omega_i^{m_i}} \exp \left(-\frac{m_i x_j^2}{\Omega_i} \right) \right] = 0. \quad (3.15)$$

Solving the equality (3.15), yields

$$\begin{aligned} \sum_{j=1}^n \tau_{ij}^{(k)} \left[\frac{m_i x_j^2}{\Omega_i^2} - \frac{m_i}{\Omega_i} \right] &= 0 \\ \frac{\sum_{j=1}^n \tau_{ij}^{(k)} m_i x_j^2}{\Omega_i^2} &= \frac{\sum_{j=1}^n \tau_{ij}^{(k)} m_i}{\Omega_i}. \end{aligned} \quad (3.16)$$

From (3.16), the EM updating equation to estimate the Ω_i posteriori (i.e., $\Omega_i^{(k+1)}$) is given by

$$\Omega_i^{(k+1)} = \frac{\sum_{j=1}^n \tau_{ij}^{(k)} x_j^2}{\sum_{j=1}^n \tau_{ij}^{(k)}}. \quad (3.17)$$

Note that in (3.17), the $\Omega_i^{(k+1)}$ value is updated in $(k+1)$ -th iteration of the M-step until a convergence condition is reached (i.e., the parameters' variation between $k-1$, and k iteration is lower than a certain threshold).

Likewise, substituting (3.7) in (3.12) and solving for $m_i \in \theta_i$, the equation to estimate m_i , can be expressed as follows

$$\sum_{j=1}^n \tau_{ij}^{(k)} \frac{\partial}{\partial m_i} \log \left[\frac{\omega_i 2m_i^{m_i} x_j^{2m_i-1}}{\Gamma(m_i) \Omega_i^{m_i}} \exp \left(-\frac{m_i x_j^2}{\Omega_i} \right) \right] = 0. \quad (3.18)$$

After some mathematical manipulations in (3.18), it follows that

$$\sum_{j=1}^n \tau_{ij}^{(k)} - \sum_{j=1}^n \tau_{ij}^{(k)} \underbrace{\frac{x_j^2}{\Omega_i}} + \sum_{j=1}^n \tau_{ij}^{(k)} \log(m_i) - \sum_{j=1}^n \tau_{ij}^{(k)} \log(\Omega_i) + \sum_{j=1}^n \tau_{ij}^{(k)} \log(x_j^2) - \sum_{j=1}^n \tau_{ij}^{(k)} \psi(m_i) = 0. \quad (3.19)$$

It is worth noting that the underlined Ω_i in (3.19) refers to (3.17). Thus, by replacing Ω_i from (3.17) in second term of (3.19), yields $-\sum_{j=1}^n \tau_{ij}^{(k)}$. Therefore, the simplified expression is given by

$$\sum_{j=1}^n \tau_{ij}^{(k)} \left[\log(\Omega_i) - \log(x_j^2) \right] = \sum_{j=1}^n \tau_{ij}^{(k)} \left[\log(m_i) - \psi(m_i) \right]. \quad (3.20)$$

Rearranging (3.20) with respect to m_i , it obtains that

$$\log(m_i) - \psi(m_i) = \frac{\sum_{j=1}^n \tau_{ij}^{(k)} \left[\log(\Omega_i) - \log(x_j^2) \right]}{\sum_{j=1}^n \tau_{ij}^{(k)}}. \quad (3.21)$$

Now, (3.21) can be rewritten as

$$\log(m_i) - \psi(m_i) = \Delta_i^k, \quad (3.22)$$

where

$$\Delta_i^k = \frac{\sum_{j=1}^n \tau_{ij}^{(k)} \left[\overbrace{\log(\Omega_i) - \log(x_j^2)}^h \right]}{\sum_{j=1}^n \tau_{ij}^{(k)}}. \quad (3.23)$$

Here, note that (3.23) requires knowledge of Ω_i , which was computed previously by using (3.17). In addition, notice that the term h in (3.23) is the difference of arithmetic and geometric means, hence Δ_i^k will always assume only positive values^[2]. Now, to find the m_i parameter, it is necessary to solve the nonlinear equation (3.22), which does not lead to a closed-form solution. Because of this, the term $\psi(z)$ is approximated by an asymptotic expansion defined as in [149, Eq. (6.3.18)] by

$$\psi(z) \sim \log(z) - \frac{1}{2z} - \frac{1}{12z^2} + \frac{1}{120z^4} - \frac{1}{252z^6} + \dots \quad (3.24)$$

By using the second order approximation $\psi(z) \approx \log(z) - \frac{1}{2z} - \frac{1}{12z^2}$ into (3.22), and solving the quadratic equation for m_i , this parameter is obtained in a straightforward manner by

$$m_i^{(k+1)} = \frac{1 + \sqrt{1 + \frac{4\Delta_i^k}{3}}}{4\Delta_i^k}. \quad (3.25)$$

Due to the fact that the parameter m_i only assumes positive values, the negative solution is discarded. Furthermore, it is necessary that $m_i > 0$. Therefore, since both h and the responsibilities τ_{ij} are positive in (3.23), the non-negativity of Δ_i^k is guaranteed in (3.25). For more information about non-negative property of the logarithmic ratio of the arithmetic mean to the geometric mean in (3.23), the reader can refer to [149, Eq. (3.2.1)].

Algorithm 1 depicts our Nakagami- m Mixture Model based on EM. Here, note that both the responsibility τ_{2j}^k and the weighting coefficient ω_2^{k+1} are computed from the difference between the unit and the τ_{1j}^k , and ω_1^{k+1} parameters, respectively. This is because the algorithm uses the EM-NMM for mixing two Nakagami- m distributions, so it turns out that $\omega_1 + \omega_2 = 1$. In addition, the relative tolerance method is employed as a stop criterion. Also, this approach computes the difference between the new estimation and the old one for each of the variables, and divide it by the previous (old) value of the variable. The algorithm stops when a relative tolerance in both variables is lower than the threshold. For our approximation, a threshold value of 1×10^{-3} is considered to ensure that there is no significant change between the current and the old parameter estimate over successive iterations. Finally, as will be shown later, the proposed approximation can directly be extended to the performance analysis evaluation in which sum of RVs occurs.

^[2] As will be seen later, the non-negativity of Δ_i^k is necessary to be able to solve the equation in (3.22)

Algorithm 1: EM procedural algorithm to estimate ω_i , Ω_i , and m_i of Nakagami- m Finite Mixture weighted PDFs

Input: observed data $\rightarrow X$, threshold $\rightarrow \epsilon$, ω_1 , Ω_i , and m_i , for $i = 1, 2$.

Output: ω_i , Ω_i , and m_i , for $i = 1, 2$.

$\omega_2 = 1 - \omega_1$;

$k = 1$;

$n = \text{length}(X)$;

while $\Delta\Omega_i$ && $\Delta m_i < \epsilon$ **do**

E step:

for $j = 1; j < n; j++$ **do**

$$\mathcal{P}_{1j} = \phi_1(X_j; \Omega_1^k, m_1^k);$$

$$\mathcal{P}_{2j} = \phi_2(X_j; \Omega_2^k, m_2^k);$$

$$\tau_{1j}^k = \frac{\omega_1^k \times \mathcal{P}_{1j}}{\omega_1^k \times \mathcal{P}_{1j} + \omega_2^k \times \mathcal{P}_{2j}};$$

$$\tau_{2j}^k = 1 - \tau_{1j}^k;$$

end

M step:

$$\Delta_1^k = \frac{\sum_{l=1}^n \tau_{1l}^k (\log(\Omega_1^k) - \log(X_l^2))}{\sum_{l=1}^n \tau_{1l}^k};$$

$$\Delta_2^k = \frac{\sum_{l=1}^n \tau_{2l}^k (\log(\Omega_2^k) - \log(X_l^2))}{\sum_{l=1}^n \tau_{2l}^k};$$

$$\Omega_1^{k+1} = \frac{\sum_{l=1}^n \tau_{1l}^k \times X_l^2}{\sum_{l=1}^n \tau_{1l}^k};$$

$$\Omega_2^{k+1} = \frac{\sum_{l=1}^n \tau_{2l}^k \times X_l^2}{\sum_{l=1}^n \tau_{2l}^k};$$

$$m_1^{k+1} = \frac{1 + \sqrt{1 + \frac{4\Delta_1^k}{3}}}{4\Delta_1^k};$$

$$m_2^{k+1} = \frac{1 + \sqrt{1 + \frac{4\Delta_2^k}{3}}}{4\Delta_2^k};$$

$$\omega_1^{k+1} = \sum_{l=1}^n \tau_{1l}^k / n;$$

$$\omega_2^{k+1} = 1 - \omega_1^{k+1};$$

$k = k + 1$;

end

Stop Criterion Notation:

$$\Delta m_i = | (m_i^{(k+1)} - m_i^{(k)}) / m_i^k |$$

$$\Delta \Omega_i = | (\Omega_i^{(k+1)} - \Omega_i^{(k)}) / \Omega_i^k |$$

3.1.2.3 Application: Average Bit Error Probability

ABEP approximations

As shown in section (2.3.3.1), the exact solution of the ABEP for multibranch combining receivers involves multiple integrals in its evaluation. Therefore, a simple and tight approximations of the ABEP for coherent and non-coherent modulation schemes is introduced. For this purpose, one can replace the exact PDF $f_R(r)$ in (2.60) by the approximate PDF $f_X(x; \Psi)$ obtained in (3.9) and $P_e(r)$ by (2.62) and (2.63) for non-coherent and coherent modulations, respectively. Next, the ABEP approximations for non-coherent and coherent modulations are given by the following proposition.

Proposition 1. *The ABEP for non-coherent and coherent modulations of EGC multibranch receivers can be obtained as (3.26) and (3.27), respectively.*

$$P_e \approx \sum_{i=1}^2 \frac{\frac{\omega_i}{2} \left(\frac{m_i}{\Omega_i}\right)^{m_i}}{\left(\frac{E_b g}{N_0} + \frac{m_i}{\Omega_i}\right)^{m_i}}, \quad (3.26)$$

$$P_e \approx \sum_{i=1}^2 \frac{\omega_i \Gamma(2m_i) {}_2F_1\left(m_i, \frac{1}{2} + m_i; 1 + m_i; -\frac{1}{\frac{\Omega_i g E_b}{m_i N_0}}\right)}{\Gamma(m_i) \left(\frac{4\Omega_i g E_b}{m_i N_0}\right)^{m_i}}. \quad (3.27)$$

Proof. The proof is provided in Appendix A.1. □

Note that our ABEP formulations in terms of mathematical complexity are as treatable as those approaches that use a single distribution for the approximation to the sum of RVs, because NMM is a linear combination of independent Nakagami- m distributions.

High and Low SNR Regime Analysis In order to simplify the SNR analysis, the main concern in this section is to derive both asymptotic closed-form expressions for high SNR, and formulations at low SNR regime for P_e shown in (3.26) and (3.27). It is worth mentioning that the asymptotic analysis has been widely studied in both Outage Probability and Bit Error Probability at high SNR regime (see, for example, [150], [151], and the references therein). So, this approach mainly focuses on the asymptotic analysis in the high SNR regime for the ABEP in both coherent and non-coherent modulations. Furthermore, the expressions for the aforesaid modulations in the low SNR regime are also derived. These results are presented as follows.

Proposition 2. *The ABEP expression for non-coherent and coherent modulations in low SNR regime can be obtained as (3.28) and (3.29), respectively.*

$$P_e \approx \sum_{i=1}^2 \frac{\omega_i/2}{1 + g\Omega_i \left(\frac{E_b}{N_0}\right) + \frac{g^2(m_i-1)\Omega_i^2}{2m_i} \left(\frac{E_b}{N_0}\right)^2}, \quad (3.28)$$

$$P_e \approx \sum_{i=1}^2 \frac{\omega_i \Gamma(2m_i) \left[\frac{\Gamma(\frac{1}{2})}{\Gamma(m_i + \frac{1}{2})} \right]}{\Gamma(m_i) 4^{m_i} (z+1)^{m_i}}. \quad (3.29)$$

Proof. The proof is provided in Appendix A.2. □

Proposition 3. *The ABEP expression for non-coherent and coherent modulations in high SNR regime can be formulated as (3.30) and (3.31), respectively.*

$$P_e \approx \frac{1}{\left(\frac{E_b}{N_0}\right)^m} \left[\frac{\omega}{2} \left(\frac{m}{g\Omega}\right)^m \right], \quad (3.30)$$

$$P_e \approx \frac{1}{\left(\frac{E_b}{N_0}\right)^m} \left[\frac{\omega \Gamma(2m)}{\Gamma(m) \left(\frac{4g\Omega}{m}\right)^m \Gamma(1+m)} \right]. \quad (3.31)$$

where m is equal to the lower value between the parameters m_1 , and m_2 , i.e., $m = \min\{m_1, m_2\}$. Correspondingly, the coefficients ω and Ω are associated with the m parameter index that meets the aforementioned condition.

Proof. The proof is provided in Appendix A.3. □

Note that for the ABEP expression for coherent modulations in low and high SNR regimes, the hypergeometric function, i.e., ${}_2F_1(\cdot, \cdot; \cdot; \cdot)$ disappears concerning the ABEP approximation given in (3.27). This fact makes such formulations mathematically more treatable than the proposed ABEP approximation.

Remark 1. *In the high-SNR region, the ABEP can be characterized by the diversity order G_d and the coding gain G_c . Therefore, from (2.7), it is defined $P_e^\infty \approx (G_c \frac{E_b}{N_0})^{-G_d}$. In this context, based on (3.30), it can be inferred that $G_c = (\frac{g\Omega}{m})(\frac{\omega}{2})^{-1/m}$, and $G_d = m$. Likewise, from (3.31), it results that $G_c = \left[\frac{\omega \Gamma(2m)}{\Gamma(m) \left(\frac{4g\Omega}{m}\right)^m} \right]^{-1/m}$, and $G_d = m$. These parameters play a fundamental role in designing wireless communication system. For instance, the diversity order D_o determines the slope of the ABEP versus average SNR curve, at high SNR, in a log-log scale. Moreover, the coding gain G_c (in dB) determines the shift of the curve in SNR relative to a benchmark ABEP curve of $(\frac{E_b}{N_0})^{-G_d}$.*

3.1.2.4 Numerical Examples and Discussions

In this section, in order to check the accuracy of our proposed approximations, numerical examples for EGC receivers over Nakagami- m fading channels in terms of ABEP are presented. The exact sum statistics have been computed via numerical integration with the use of (3.2a) and (3.5). Likewise, the exact solutions for the ABEP in EGC reception are also plotted via numerical integration

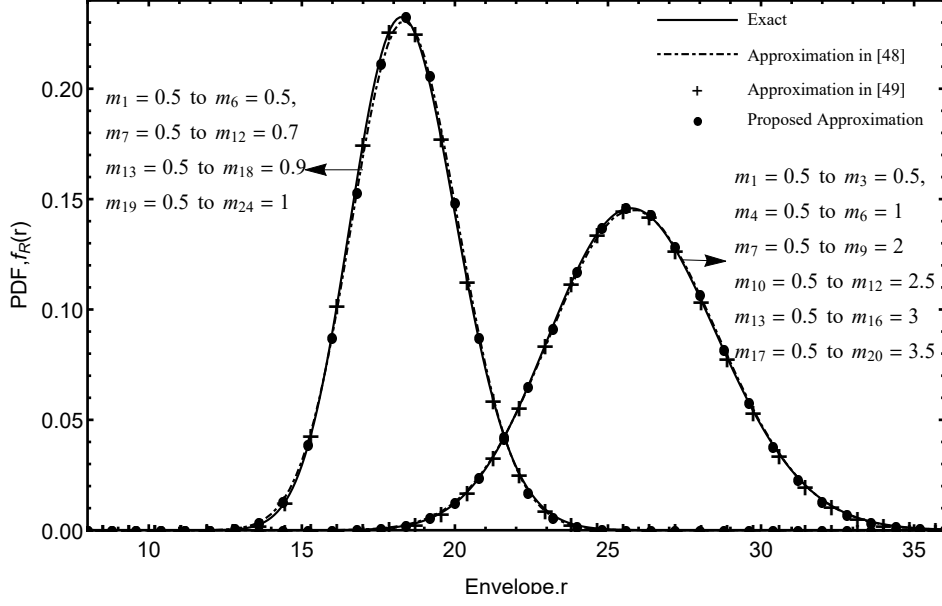


Figure 3.2: PDF of the sum of twenty and thirty n.i.i.d. Nakagami- m RVs. For $M = 20$, $m_i = 0.5$ for $i = 1$ to 3, $m_i = 1$ for $i = 4$ to 6, $m_i = 2$ for $i = 7$ to 9, $m_i = 2.5$ for $i = 8$ to 12, $m_i = 3$ for $i = 13$ to 16, and $m_i = 3.5$ for $i = 17$ to 20. For $M = 30$, $m_i = 0.5$ for $i = 1$ to 6, $m_i = 0.7$ for $i = 7$ to 12, $m_i = 0.9$ for $i = 13$ to 18, $m_i = 1$ for $i = 19$ to 24, and $m_i = 1.5$ for $i = 25$ to 30.

from (2.60) with their respective substitutions. The comparison of our NMM approximation against the approaches given in [48] and [49] for the sum of Nakagami- m RVs is also shown in the figures. In all the cases of this section, it is employed envelopes with unit-power, and the samples values of m_i have been selected to cover a wide range of fading. It is noteworthy that, here, only the i.n.i.d. cases are plotted, because for the i.i.d. cases, the proposed approximations are practically indistinguishable from the exact solutions.

Firstly, to demonstrate the ability of NMM approach to evaluate the expressions for large M , non-identical summands are considered in Fig. 3.2, where the number of RV is set to 20, and 30. For these scenarios, the corresponding fading parameters are given by: *Case I* ($M = 20$): $m_i = 0.5$ for $i = 1$ to 3, $m_i = 1$ for $i = 4$ to 6, $m_i = 2$ for $i = 7$ to 9, $m_i = 2.5$ for $i = 8$ to 12, $m_i = 3$ for $i = 13$ to 16, and $m_i = 3.5$ for $i = 17$ to 20, and *Case II* ($M = 30$): $m_i = 0.5$ for $i = 1$ to 6, $m_i = 0.7$ for $i = 7$ to 12, $m_i = 0.9$ for $i = 13$ to 18, $m_i = 1$ for $i = 19$ to 24, and $m_i = 1.5$ for $i = 25$ to 30. As can be seen for $M = 20$, the differences among the exact, the approach of [49], the proposal of [48], and our approximate curves are almost imperceptible. Notice that the small difference are reduced even further as M increases. On the other hand, for the case of $M = 30$, the results of the proposed approximate in [48] (e.g., $16 < r < 18$) are slightly poorer than the others.

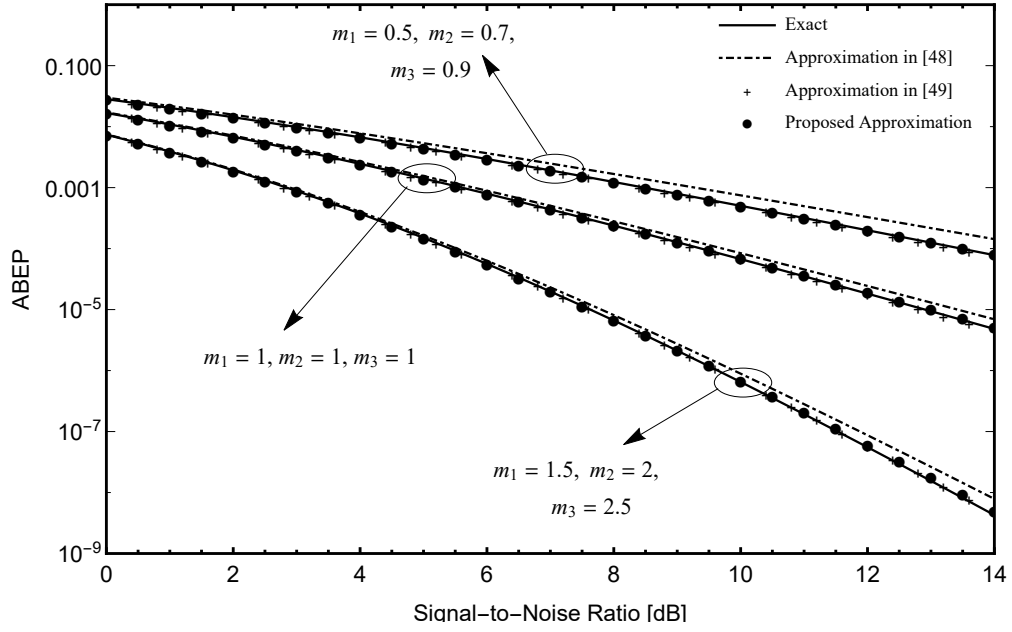
Next, Figs. 3.3a and 3.3b show the ABEP against the average output SNR for BFSK (coherent), and DBPSK (non-coherent) modulations for EGC receivers, respectively. For both figures, it is considered three branches (i.e., $M = 3$) with different values of m_i to cover the special cases of fading in the Nakagami- m distribution as follows: *Case III*: $(m_1, m_2, m_3) = (0.5, 0.7, 0.9)$, *Case IV (Rayleigh)*: $(m_1, m_2, m_3) = (1, 1, 1)$, and *Case V*: $(m_1, m_2, m_3) = (1.5, 2, 2.5)$. Note that when the signals have

smaller fading severities, the proposed NMM approximation, and the approach in [49] are excellent. In the opposite scenario, i.e., signals with greater fading severities, there are a small gap regarding the exact solution; however, both approximate solutions are still very good. Therefore, the behavior of our approaches is very accurate in all of three cases, and outperforms the approximation given in [48]. In short, the proposed approximation presents a similar behavior to the results in [49] for all fading scenarios considering the same order of diversity (i.e., $M = 3$) in all the cases shown.

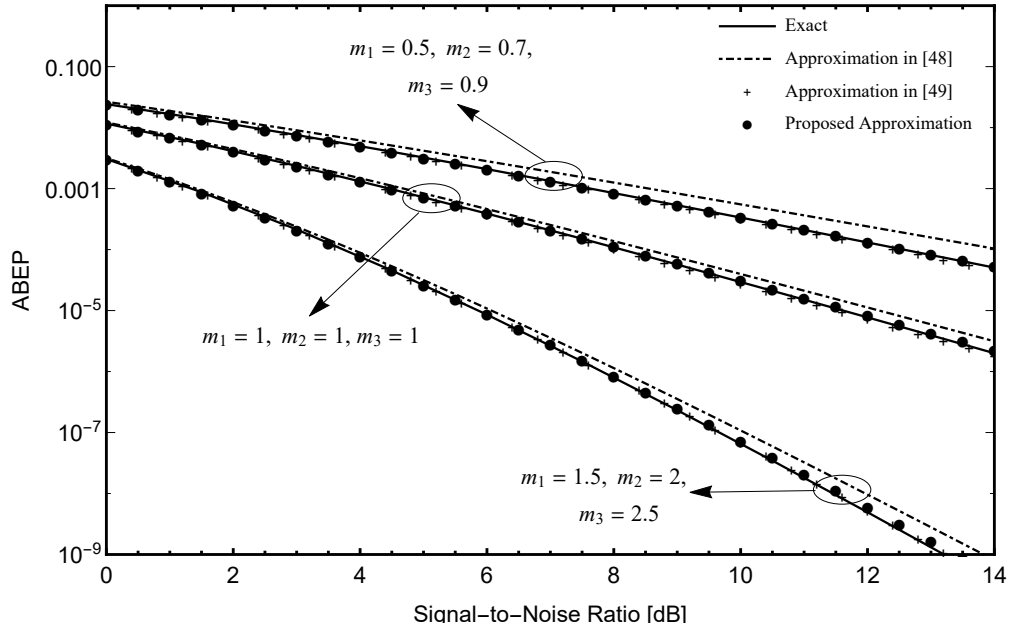
Then, the ABEP at the output of an ECG combiner with $M = 4, 6$, and 8 diversity branches is analyzed. Figs. 3.4a and 3.4b show the results of these cases for coherent and non-coherent modulation schemes respectively. Here, in order to demonstrate the robustness of the proposed approximations, it is considered only small values of fading. Based on this, for both figures, the corresponding fading parameters are given by: *Case VI*: $(m_1, m_2, m_3, m_4) = (0.5, 0.7, 0.9, 1)$, *Case VII*: $(m_1, m_2, m_3, m_4, m_5, m_6) = (0.5, 0.7, 0.9, 1, 1.5, 2)$, and *Case VIII*: $(m_1, m_2, m_3, m_4, m_5, m_6, m_7, m_8) = (0.5, 0.7, 0.9, 1, 1.5, 2, 2.5, 3)$. As can be seen in all cases, the approximations achieved with our MNM agree completely with the exact solution. Here, it is worth mentioning that in all scenarios our approximations behave similarly to those presented in [49] for low values of diversity, but slightly worse than that given by [49] as the number of branches increases. The reason for this small difference is because the $\alpha-\mu$ distribution used in [49] to approximate the sum of Nakagami- m RVs has one degree of freedom more than Nakagami- m . On the other hand, the approach of [48], although good, again is notably outperformed by our proposal. Moreover, from both figures, it is interesting to note that the ABEP performance improves rapidly for high values of branches or high values of SNR at output receiver, while for low values of diversity, the ABEP increases significantly.

Henceforth, only the approach in [49], and our approximations are presented. The reason for this decision is that these approximations are perfectly matched with the exact solutions as can be seen in the previous analysis (see, for instance, Figs. 3.3 and 3.4). Figs. 3.5 and 3.6 denote the SNR regime analysis for both coherent and non-coherent modulations, considering the cases VI, VII, and VIII previously presented. In Figs. 3.5b and 3.6b, the ABEP at high SNR is plotted for coherent and non-coherent modulations respectively. It is shown that the asymptotic performances are well aligned to both the approach in [49], and our approximations. As expected, the ABEP decreases with the increase of M . In the same figures, the diversity order, theoretically defined as $D = \lim_{SNR \rightarrow \infty} [-\log(P_e)/\log(SNR)]^{[3]}$ [152] is also shown as a function of the SNR for different values of M . As depicted in these figures, as the SNR goes to infinity, the diversity order D approaches $G_d = \min\{m_1, m_2\}$ (with $M = \{4, 6, 8\}$), verifying the mathematical results presented in Remark 1.

^[3] It is worth noting that the term P_e in the expression for diversity order D refers to (3.28), and (3.29).

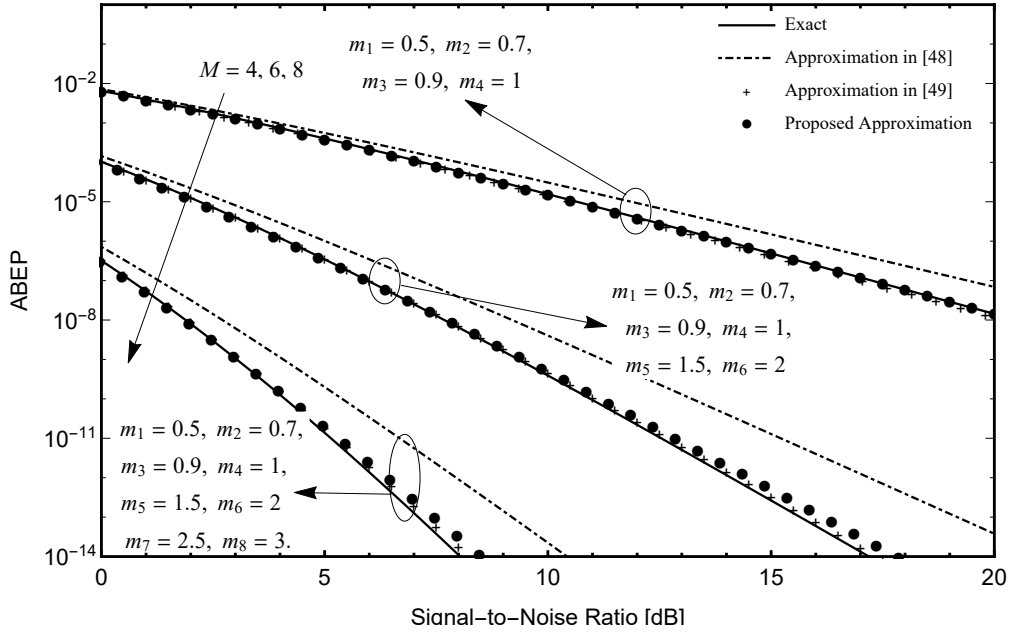


(a) Average Bit Error Probability for coherent Binary Frequency-Shift Keying of EGC receivers operating on $M = 3$ n.i.i.d. Nakagami- m fading channels, assuming $\Omega_i = 1$, and varying m_i .

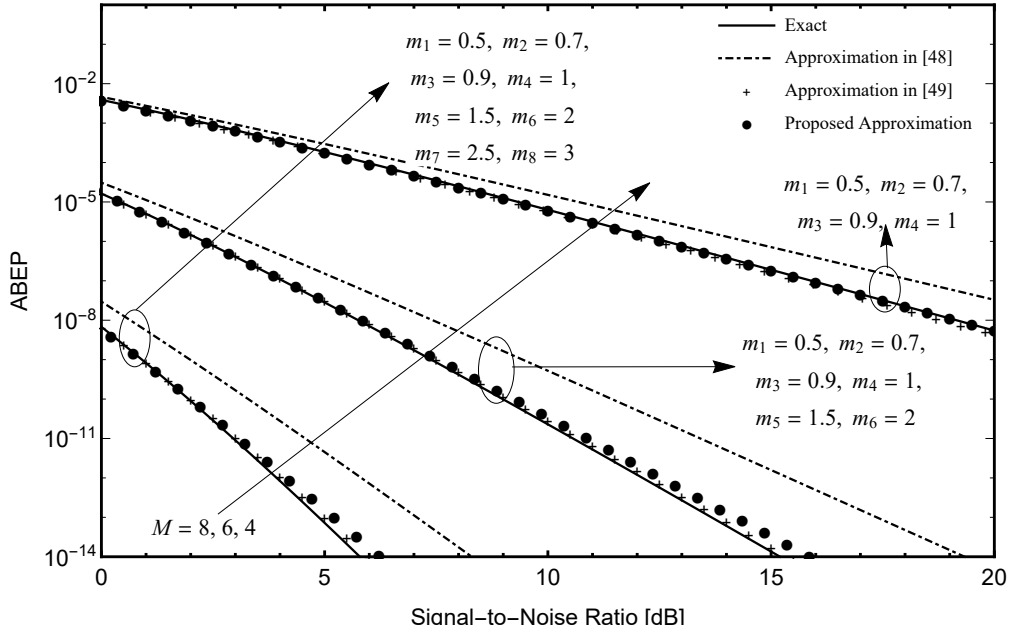


(b) Average Bit Error Probability for Differential Binary Phase-Shift Keying of EGC receivers operating on $M = 3$ n.i.i.d. Nakagami- m fading channels, assuming $\Omega_i = 1$, and varying m_i .

Figure 3.3: Average Bit Error Probability for coherent and non-coherent modulations of EGC receivers over $M = 3$ Nakagami- m RVs.



(a) Average Bit Error Probability for coherent Binary Frequency-Shift Keying of EGC receivers operating on $M = 4, 6,$ and 8 n.i.i.d. Nakagami- m fading channels, assuming $\Omega_i = 1$, and varying m_i .



(b) Average Bit Error Probability for Differential Binary Phase-Shift Keying of EGC receivers operating on $M = 4, 6,$ and 8 n.i.i.d. Nakagami- m fading channels, assuming $\Omega_i = 1$, and varying m_i .

Figure 3.4: Average Bit Error Probability for coherent and non-coherent modulations of EGC receivers over $M = 4, 6,$ and 8 Nakagami- m RVs.

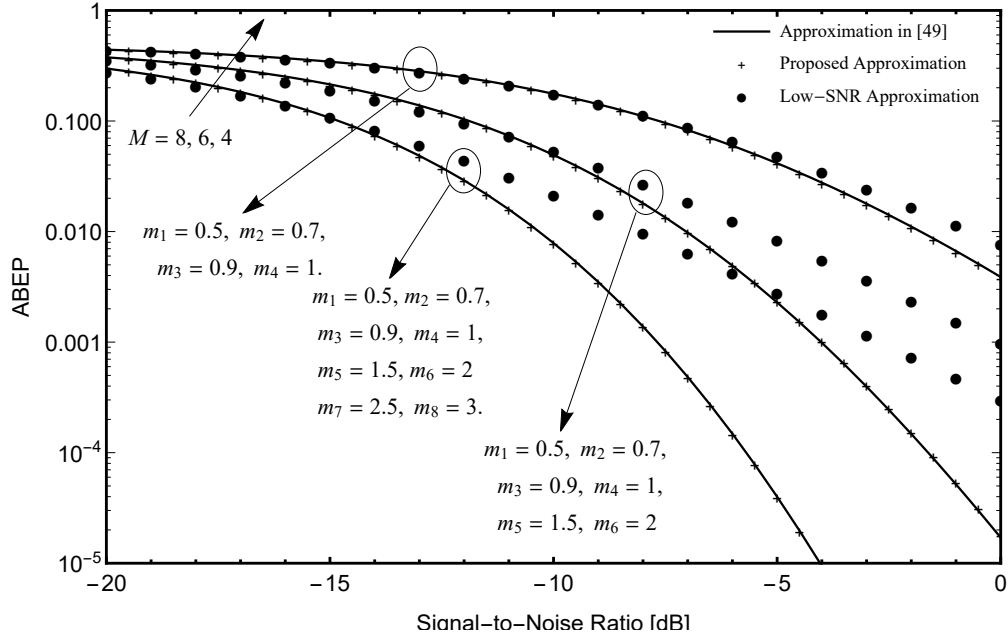
Table 3.1: Comparison of computational efforts between the exact and approximate solutions.

Statistic	Average Elapsed Time (sec.)		
	Exact Solution	Proposed Approximation	Reduction Percentage (%)
PDF			
$M = 20$	609.90	2.44	99.60
$M = 30$	2,229.67	2.63	99.88
ABEP			
$M = 3$	217.31	2.14	99.02
$M = 4$	786.73	2.17	99.72
$M = 6$	49,281.55	2.19	100
$M = 8$	277,555.92	2.24	100

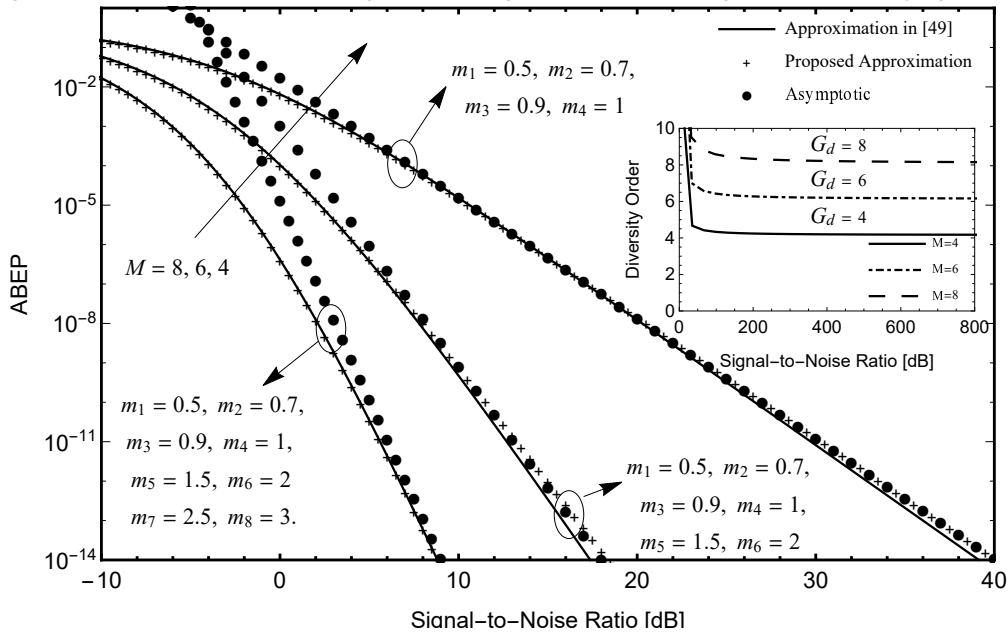
Regarding the proposed expressions at low SNR regime, the Figs. 3.5a and 3.6a show the ABEP for non-coherent and coherent modulation schemes respectively. Note that the observed performances of the formulations for this scenario lose their accuracy with respect to the solutions given in (3.28) and (3.29). However, it is encouraged the use of these latter expressions, since they are mathematically as treatable as those solutions derived for low SNR regime. In summary, the results show the expected behavior, that is, the ABEP metric improves by increasing the diversity order and/or improving the fading/shadowing conditions. It is worth mentioning that the carried out tests for other fading conditions showed an excellent fitting in all the cases investigated.

For informative purposes, the Fig. 3.7 presents the computational consuming time of all the approaches shown above. In this context, to circumvent very long simulation times in the evaluation of the exact solution, parallel processing has been used with Wolfram Mathematica. The box plots in Figs. 3.7a and 3.7b denote the Average elapsed time to obtain the combined envelope for $M = \{20, 30\}$, and the ABEP for $M = \{4, 6, 8\}$ in EGC respectively. From both figures, the reader can observe that approach in [48] corresponds to the fastest envelope computation, but certainly its performance is the worst among all approximations. Likewise, the approach in [49] shows an excellent computational speed in all cases, and its behavior is as good as the proposed approximation in this work. Furthermore, it is clear in both figures that the average times of the approaches in [48] and [49] tend to grow rapidly with the number of branches. For instance, the average elapsed times to compute the PDF for $M = 20$, and $M = 30$ RVs for both the approach in [49], and our approximation are (Case $M = 20$: 1.51 sec., and 2.23 sec.), and (Case $M = 30$: 7.45 sec., and 2.58 sec.), respectively. So, it is clear that the simulation time of our approximation for the complete set of examples is practically constant in the range of 2.2-2.6 seconds, being independent of the number of RVs.

In order to verify the speed of real-time computations, a complete summary between the exact and the proposed approximation has been made in Table 3.1 for both the resulting PDF and the ABEP in EGC technique. It is worth noting that, our proposed method reduces the computational effort above 99% in all the illustrated examples with respect the exact solution.

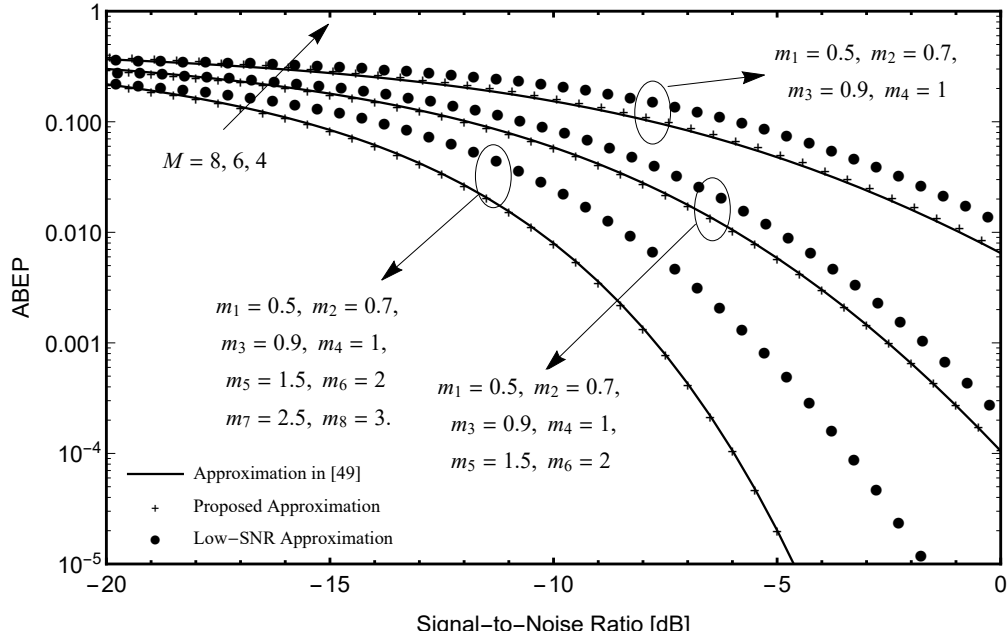


(a) Low-SNR analysis of Average Bit Error Probability for Differential Binary Phase-Shift Keying of EGC receivers operating on $M = 4, 6,$ and 8 n.i.i.d. Nakagami- m fading channels, assuming $\Omega_i = 1$, and varying m_i .

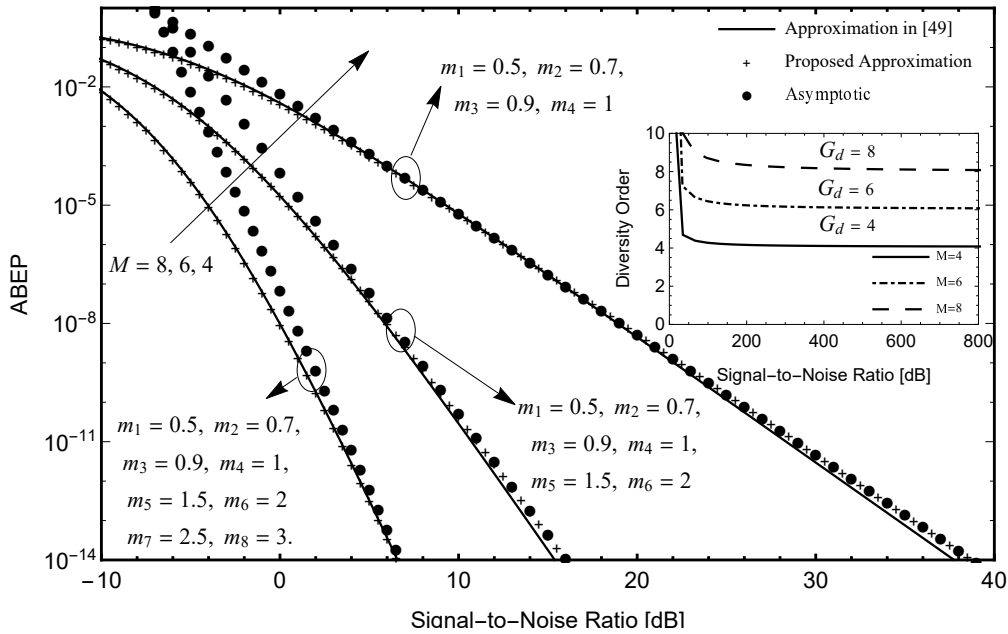


(b) High-SNR analysis of Average Bit Error Probability for coherent Binary Frequency-Shift Keying of EGC receivers operating on $M = 4, 6,$ and 8 n.i.i.d. Nakagami- m fading channels, assuming $\Omega_i = 1$, and varying m_i .

Figure 3.5: SNR regime analysis of the Average Bit Error Probability for coherent and non-coherent modulations of EGC receivers over $M = 4, 6,$ and 8 Nakagami- m RVs.

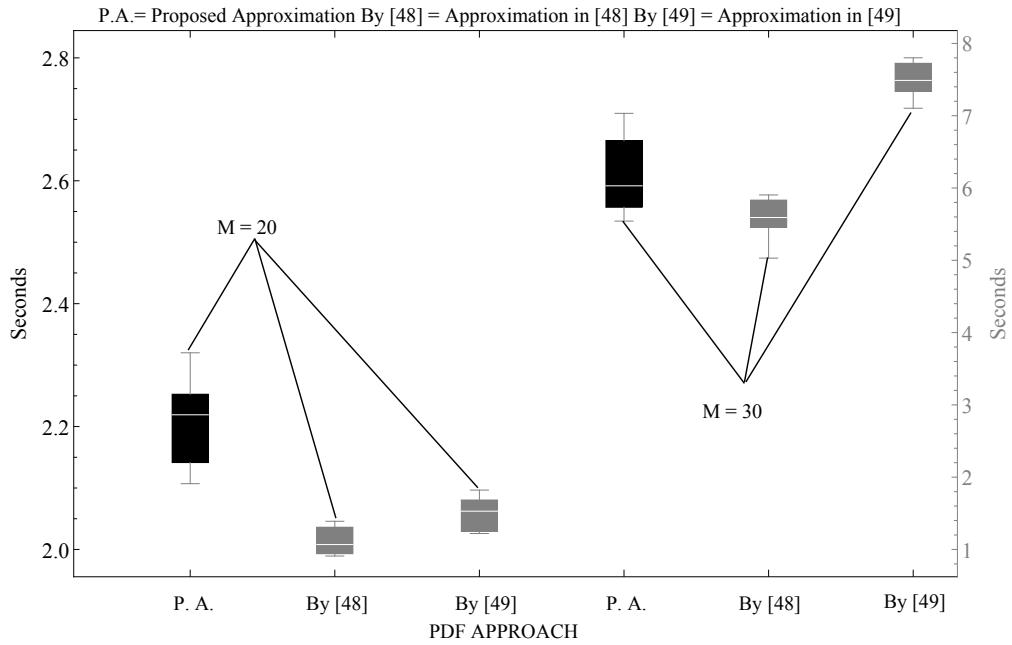


(a) Low-SNR analysis of Average Bit Error Probability for coherent Binary Frequency-Shift Keying of EGC receivers operating on $M = 4, 6,$ and 8 n.i.i.d. Nakagami- m fading channels, assuming $\Omega_i = 1$, and varying m_i .

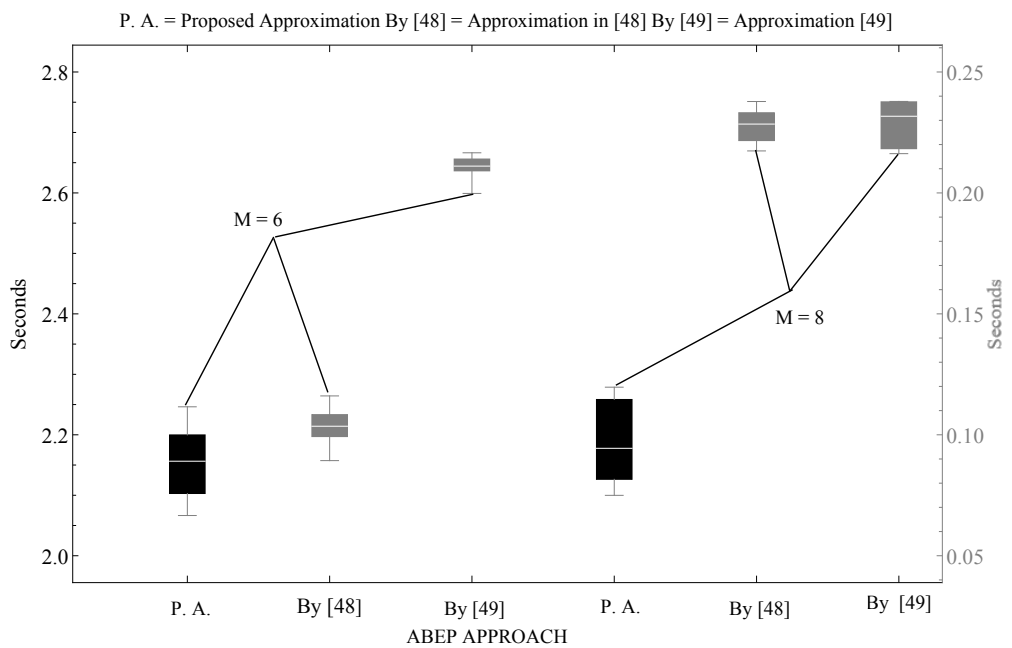


(b) High-SNR analysis of Average Bit Error Probability for Differential Binary Phase-Shift Keying of EGC receivers operating on $M = 4, 6,$ and 8 n.i.i.d. Nakagami- m fading channels, assuming $\Omega_i = 1$, and varying m_i .

Figure 3.6: SNR regime analysis of the Average Bit Error Probability for coherent and non-coherent modulations of EGC receivers over $M = 4, 6,$ and 8 Nakagami- m RVs.



(a) Average elapsed time to compute the resulting PDF for $M = 20$, and 30 n.i.i.d. Nakagami- m RVs.



(b) Average elapsed time to evaluate the ABEP of EGC receivers operating on $M = 6$, and 8 n.i.i.d. Nakagami- m RVs.

Figure 3.7: Average elapsed time for both the PDF and ABEP in EGC varying the number of branches.

Finally, the results of our approaches in the evaluation of both the PDF and the ABEP with large M prove to be the fastest in real-time computations those presented in [48] and [49]. This fact, makes our NMM proposal attractive in applications for which sum of RVs occur such as Multiple Input Multiple Output (MIMO), Single Input Multiple Output (SIMO) among others.

3.1.3 Generalized Approximation Approach

Here, this work proposes a unified approach to approximate the PDF and CDF of the exact sum given in (3.1), where R_i follows a generalized fading model. Specifically, given any chosen model, the approximate solution's parameters are fit by matching its asymptotic behavior around zero to that of the exact sum. Based on this, this approach is called *asymptotic matching*. In addition, if the approximate solution has three or more parameters to be calibrated, one or more moments of the exact and approximate sum are also matched to one another (method well-known as MoM). Before introducing the proposed approximation, both the statistical properties and the asymptotic characterization of a generalized fading model are revisited.

3.1.3.1 Background Statistics

The asymptotic matching method can be applied to generalized fading models, including α - μ , κ - μ , η - μ , κ - μ shadowed, among others. Without loss of generality, this work focuses on approximating the sum of κ - μ RVs. However, the theoretical framework developed in this section can be used to approximate the sum of any fading model mentioned above.

Summands' Statistics Here, for a better understanding, the κ - μ fading model associated to the summands are introduced. From (2.30), the PDF of each κ - μ summand R_i in (3.1) is give by

$$f_{R_i}(r) = \frac{2\mu_i(1+\kappa_i)^{\frac{1+\mu_i}{2}} r^{\mu_i}}{\kappa_i^{\frac{\mu_i-1}{2}} \Omega_i^{\frac{\mu_i+1}{2}} \exp(\mu_i \kappa_i)} \exp\left(-\frac{\mu_i(1+\kappa_i)r^2}{\Omega_i}\right) I_{\mu_i-1}\left(2\mu_i r \sqrt{\frac{\kappa_i(1+\kappa_i)}{\Omega_i}}\right). \quad (3.32)$$

The n -th moment of R_i in (3.32) can be obtained as [127]

$$\mathbb{E}[R_i^n] = \frac{\Gamma\left(\mu_i + \frac{n}{2}\right) \exp[-\kappa_i \mu_i] \Omega_i^{\frac{n}{2}}}{\Gamma(\mu_i) [(1+\kappa_i) \mu_i]^{n/2}} {}_1F_1\left(\mu_i + \frac{n}{2}; \mu_i; \kappa_i \mu_i\right). \quad (3.33)$$

Summands' Asymptotic Statistics Here, it is obtained Maclaurin series representations for the κ - μ PDF. This representation is essential to the asymptotic matching approach. Assume that the PDF of R_i has a Maclaurin series representation written as

$$f_{R_i}(r) = \sum_{n=0}^{\infty} a_{i,n} r_i^{b_{i,n}}, \quad (3.34)$$

in which $b_{i,n}$ is a monotonically increasing function with respect to n and the coefficients $a_{i,n}$ and $b_{i,n}$ depend on the fading model used. Specifically, for the κ - μ case, the Maclaurin series representation is given in the following proposition.

Proposition 4. *The Maclaurin series coefficients $a_{i,n}$ and $b_{i,n}$ for κ - μ distribution are given by*

$$a_{i,n} = \frac{2\mu_i (1 + \kappa_i)^{\frac{1+\mu_i}{2}} (-1)^n}{\kappa_i^{\frac{\mu_i-1}{2}} \Omega_i^{\frac{\mu_i+1}{2}} \exp(\mu_i \kappa_i) \Gamma(1+n)^2 \Gamma(n+\mu_i)} \left(\frac{\mu_i(1+\kappa_i)}{\Omega_i} \right)^n \left(\mu_i \sqrt{\frac{\kappa_i(1+\kappa_i)}{\Omega_i}} \right)^{2n+\mu_i-1} \quad (3.35a)$$

$$b_{i,n} = 2(\mu_i + 2n) - 1. \quad (3.35b)$$

Proof. The proof is provided in Appendix B.1. □

As shall become apparent, our asymptotic-matching approach turns out to depend solely on the first term of the above series, i.e., on $a_{i,0}$ and $b_{i,0}$. This occurs because this term has the smallest exponent in the series ($= b_{i,0}$) and thus dominates the asymptotic behavior around zero, i.e., in the left tail of the PDF. Recall that the PDF's asymptote around zero governs the high-SNR performance of a communication system operating over a channel modeled by that PDF, as shown in [117]. Therefore, ultimately, the goal is to achieve a good fit at medium to high SNR.

Summands-to-Sum Asymptotic Mapping

Now, consider the Maclaurin series representation for the PDF of the exact sum R given in (3.1) as:

$$f_R(r) = \sum_{n=0}^{\infty} a_n r^{b_n}. \quad (3.36)$$

Here, the approach is interested in the first term alone, which rules the asymptotic behavior around zero, i.e.,

$$f_R(r) \simeq a_0 r^{b_0}. \quad (3.37)$$

Next, closed-form expressions for a_0 and b_0 as a function of the coefficients $a_{i,0}$ and $b_{i,0}$ for the summands are derived. Since the PDF of R is given as the convolution of the individual PDFs of R_i , it can be represented in terms of the corresponding Maclaurin series in (3.34) as

$$f_R(r) = \sum_{n_1=0}^{\infty} \sum_{n_2=0}^{\infty} \cdots \sum_{n_M=0}^{\infty} a_{1,n_1} r^{b_{1,n_1}} \otimes a_{2,n_2} r^{b_{2,n_2}} \otimes \cdots \otimes a_{M,n_M} r^{b_{M,n_M}}. \quad (3.38)$$

Also, it can be shown that, for each set of terms in (3.38), $a_{1,n_1} r^{b_{1,n_1}}, \dots, a_{M,n_M} r^{b_{M,n_M}}$, the convolution among them results in a term with the same format, i.e.,

$$a_{1,n_1} r^{b_{1,n_1}} \otimes \dots \otimes a_{M,n_M} r^{b_{M,n_M}} = ar^b$$

$$\stackrel{\Delta}{=} a_{(n_1, n_2, \dots, n_M)} r^{b_{(n_1, n_2, \dots, n_M)}}. \quad (3.39)$$

Note that each term resulting from the convolution has contributions of all summands, so one can express a and b as a function of n_1, n_2, \dots, n_M . As known, this convolution can be expressed as a product in the Laplace domain, the inverse of which gives ar^b . By taking the Laplace transform of each summand term in (3.39), it follows that

$$\mathcal{L} \left\{ a_{i,n_i} r^{b_{i,n_i}} \right\} = \frac{a_{i,n_i} \Gamma(1 + b_{i,n_i})}{s^{1+b_{i,n_i}}}. \quad (3.40)$$

Therefore, from (3.40), (3.39) can be rewritten as

$$ar^b = \mathcal{L}^{-1} \left\{ \prod_{i=1}^M \frac{a_{i,n_i} \Gamma(1 + b_{i,n_i})}{s^{1+b_{i,n_i}}} \right\}$$

$$= \frac{\prod_{i=1}^M a_{i,n_i} \Gamma(1 + b_{i,n_i})}{\Gamma(M + \sum_{i=1}^M b_{i,n_i})} r^{(M-1) + \sum_{i=1}^M b_{i,n_i}}, \quad (3.41)$$

so the coefficients a and b are obtained as

$$a = \frac{\prod_{i=1}^M [a_{i,n_i} \Gamma(1 + b_{i,n_i})]}{\Gamma(M + \sum_{i=1}^M b_{i,n_i})} \quad (3.42a)$$

$$b = (M - 1) + \sum_{i=1}^M b_{i,n_i}. \quad (3.42b)$$

Considering that each term b_{i,n_i} is a monotonically increasing function with respect to n_i , the smallest value of b in (3.42b) occurs for $n_1 = n_2 = \dots = n_M = 0$. Accordingly, a_0 and b_0 can be finally calculated as

$$a_0 = \frac{\prod_{i=1}^M [a_{i,0} \Gamma(1 + b_{i,0})]}{\Gamma(M + \sum_{i=1}^M b_{i,0})} \quad (3.43a)$$

$$b_0 = (M - 1) + \sum_{i=1}^M b_{i,0}. \quad (3.43b)$$

This result plays a pivotal role in our proposed approximation.

Summands-to-Sum Moment Mapping

As mentioned previously, if the approximate distribution has three or more parameters to be fit (e.g., κ - μ case), the n -th moment of the exact sum is needed. From [48, Eq. (6)], the n -th moment of R can be expressed in terms of the individual moments of the summands as

$$\mathbb{E}[R^n] = \sum_{n_1=0}^n \sum_{n_2=0}^{n_1} \cdots \sum_{n_{M-1}=0}^{n_{M-2}} \binom{n}{n_1} \binom{n_1}{n_2} \cdots \binom{n_{M-2}}{n_{M-1}} \mathbb{E}[R_1^{n-n_1}] \mathbb{E}[R_2^{n_1-n_2}] \cdots \mathbb{E}[R_M^{n_{M-1}}], \quad (3.44)$$

where the required individual moments $\mathbb{E}[R_i^n]$ for the κ - μ case is given in (3.33).

3.1.3.2 Proposed Framework and Approximation

In this section, an approach that can be used to calibrate the distribution parameters of any candidate statistical model expected to approximate a sum of i.n.i.d., non-negative RVs is presented. As seen later, the proposed approach can be used when dealing with sums of κ - μ RVs.

Let \tilde{R} be the RV whose PDF is assumed to approximate the PDF of the exact sum R . To avoid confusion, \tilde{R} refers to the approximate sum. In addition, let $\tilde{a}_0 r^{\tilde{b}_0}$ be the asymptote — i.e., the first term of the Maclaurin series — of $f_{\tilde{R}}(r)$. The essence of our approach is to adjust the parameters of $f_{\tilde{R}}(r)$ so that its asymptote matches that of $f_R(r)$, i.e., $\tilde{a}_0 r^{\tilde{b}_0} = a_0 r^{b_0}$. This is the reason because the approach is named asymptotic matching.

The asymptotic matching provides two equations to calibrate the parameters of a chosen approximate distribution: $\tilde{a}_0 = a_0$ and $\tilde{b}_0 = b_0$. So these equations suffice when the approximate distribution has only two parameters, such as the Weibull and Nakagami- m approximations. But certain approximate distributions may have three or more parameters. For instance, the α - μ , κ - μ , η - μ approximate distributions have three parameters each, namely and respectively, $(\tilde{\alpha}, \tilde{\mu}, \tilde{\Omega})$, $(\tilde{\kappa}, \tilde{\mu}, \tilde{\Omega})$, and $(\tilde{\eta}, \tilde{\mu}, \tilde{\Omega})$. In these cases, an extra equation is needed to calibrate the parameters. Here, it is suggested that this equation be obtained by matching a certain n -th moment of the approximate sum to that of the exact sum, i.e., by forcing $\mathbb{E}[\tilde{R}^n] = \mathbb{E}[R^n]$, with n integer. It is noteworthy that, whereas the asymptotic matching ensures an excellent fit — asymptotically perfect, indeed — in the left tail of the PDF, the extra moment matching improves the fit in its right tail. More generally, for approximate distributions containing $L > 3$ parameters (e.g., shadowed versions of the generalized fading models), these can be calibrated using two equations from the asymptotic matching ($\tilde{a}_0 = a_0$ and $\tilde{b}_0 = b_0$) and $L - 2$ equations by matching multiple moments: $\mathbb{E}[\tilde{R}^{n_1}] = \mathbb{E}[R^{n_1}], \dots, \mathbb{E}[\tilde{R}^{n_{L-2}}] = \mathbb{E}[R^{n_{L-2}}]$. Here again, the values of n_1, \dots, n_{L-2} can be chosen somewhat arbitrarily. Also, the higher these values, the better the fit in the right tail of the PDF.

In short, this research proposes to calibrate the parameters of any selected two-parameter approximate sum distribution by forcing the first two of the constraints

$$\tilde{a}_0 = a_0 \quad (3.45a)$$

$$\tilde{b}_0 = b_0 \quad (3.45b)$$

$$\mathbb{E}[\tilde{R}^n] = \mathbb{E}[R^n], \quad (3.45c)$$

and to adjust the parameters of any selected three-parameter approximate distribution by forcing all three constraints. Notice that the terms on the right-hand side of (3.45), namely, a_0 , b_0 , and $\mathbb{E}[R^n]$, refer to the exact sum, being given in (3.43a), (3.43b), and (3.44), and depending ultimately on the distribution parameters of the summands at hand. As for the terms on the left-hand side of (3.45), namely, \tilde{a}_0 , \tilde{b}_0 , and $\mathbb{E}[\tilde{R}^n]$, these must be obtained as a function of the parameters of the approximate distribution under consideration.

Next, as an illustrative example, consider the left-hand side of (3.45) for the κ - μ distribution. It is worth mentioning that for approximate distributions that have only two parameters of adjustment (e.g., Nakagami- m and Weibull cases), the solution is obtained in closed-form fashion. Conversely, for approximate distributions with three or more parameters of fit (e.g., α - μ , η - μ , κ - μ , κ - μ shadowed cases), transcendental equations appear that have to be solved numerically, e.g., by using built-in routines of computing software such as Matlab and Mathematica.

Sum of κ - μ Random Variables

Here, the proposed framework is employed to approximate the exact sum distribution given in (3.1), where R_i is given by (3.32). Specifically, the sum of κ - μ RVs is approximated by using another κ - μ RV. Therefore, \tilde{R} is assumed to follow a κ - μ PDF, given by

$$f_{\tilde{R}}(r) = \frac{2\tilde{\mu}(1+\tilde{\kappa})^{\frac{1+\tilde{\mu}}{2}} r^{\tilde{\mu}}}{\tilde{\kappa}^{\frac{\tilde{\mu}-1}{2}} \tilde{\Omega}^{\frac{\tilde{\mu}+1}{2}} \exp(\tilde{\mu}\tilde{\kappa})} \exp\left(-\frac{\tilde{\mu}(1+\tilde{\kappa})r^2}{\tilde{\Omega}}\right) I_{\tilde{\mu}-1}\left(2\tilde{\mu}r\sqrt{\frac{\tilde{\kappa}(1+\tilde{\kappa})}{\tilde{\Omega}}}\right), \quad (3.46)$$

where $\tilde{\kappa}$, $\tilde{\mu}$, and $\tilde{\Omega}$ being the parameters to be determined by solving (3.45). For this purpose, \tilde{a}_0 and \tilde{b}_0 can be obtained from (3.35), with $n = 0$, this yields

$$\tilde{a}_0 = \frac{2\tilde{\mu}\tilde{\kappa}^{\frac{1-\tilde{\mu}}{2}} (1+\tilde{\kappa})^{\frac{1+\tilde{\mu}}{2}}}{\Gamma(\tilde{\mu})\tilde{\Omega}^{\frac{\tilde{\mu}+1}{2}} \exp(\tilde{\mu}\tilde{\kappa})} \left(\tilde{\mu}\sqrt{\frac{\tilde{\kappa}(1+\tilde{\kappa})}{\tilde{\Omega}}}\right)^{\tilde{\mu}-1} \quad (3.47a)$$

$$\tilde{b}_0 = 2\tilde{\mu} - 1, \quad (3.47b)$$

and from (3.33), the n -th moment of the approximate distribution is given by

$$\mathbb{E}[\tilde{R}^n] = \frac{\Gamma\left(\tilde{\mu} + \frac{n}{2}\right) \exp[-\tilde{\kappa}\tilde{\mu}]\tilde{\Omega}^{\frac{n}{2}}}{\Gamma(\tilde{\mu}_i) [(1+\tilde{\kappa})\tilde{\mu}]^{n/2}} {}_1F_1\left(\tilde{\mu} + \frac{n}{2}; \tilde{\mu}; \tilde{\kappa}\tilde{\mu}\right). \quad (3.48)$$

Using (3.47) and (3.48) with $n = 2$ into (3.45), the solution for the κ - μ case reduces to^[4]

^[4] For complete detail of how to arrive at (3.49), please check Appendix B.

$$\tilde{\mu} = \sum_{i=1}^M \mu_i \quad (3.49a)$$

$$\tilde{\Omega} = \mathbb{E}[R^2] \quad (3.49b)$$

$$\frac{2\tilde{\kappa}^{\frac{1-\tilde{\mu}}{2}} (1+\tilde{\kappa})^{\frac{1+\tilde{\mu}}{2}}}{\Gamma(\tilde{\mu})\tilde{\Omega}^{\frac{\tilde{\mu}+1}{2}} \exp(\tilde{\mu}\tilde{\kappa})} \left(\tilde{\mu} \sqrt{\frac{\tilde{\kappa}(1+\tilde{\kappa})}{\tilde{\Omega}}} \right)^{\tilde{\mu}-1} = \frac{\prod_{i=1}^M \left[\frac{2\kappa_i^{\frac{1-\mu_i}{2}} (1+\kappa_i)^{\frac{1+\mu_i}{2}} \Gamma(2\mu_i)}{\Gamma(\mu_i)\Omega_i^{\frac{\mu_i+1}{2}} \exp(\mu_i\kappa_i)} \left(\mu_i \sqrt{\frac{\kappa_i(1+\kappa_i)}{\Omega_i}} \right)^{\mu_i-1} \right]}{\Gamma\left(2\sum_{i=1}^M \mu_i\right)}, \quad (3.49c)$$

where $\mathbb{E}[R^2]$ is given in (3.44) and only (3.49c) remaining to be solved numerically for $\tilde{\kappa}$. Note that the parameters $\tilde{\mu}$ and $\tilde{\Omega}$ are given in a closed-form fashion.

3.1.3.3 Numerical Examples and Discussions

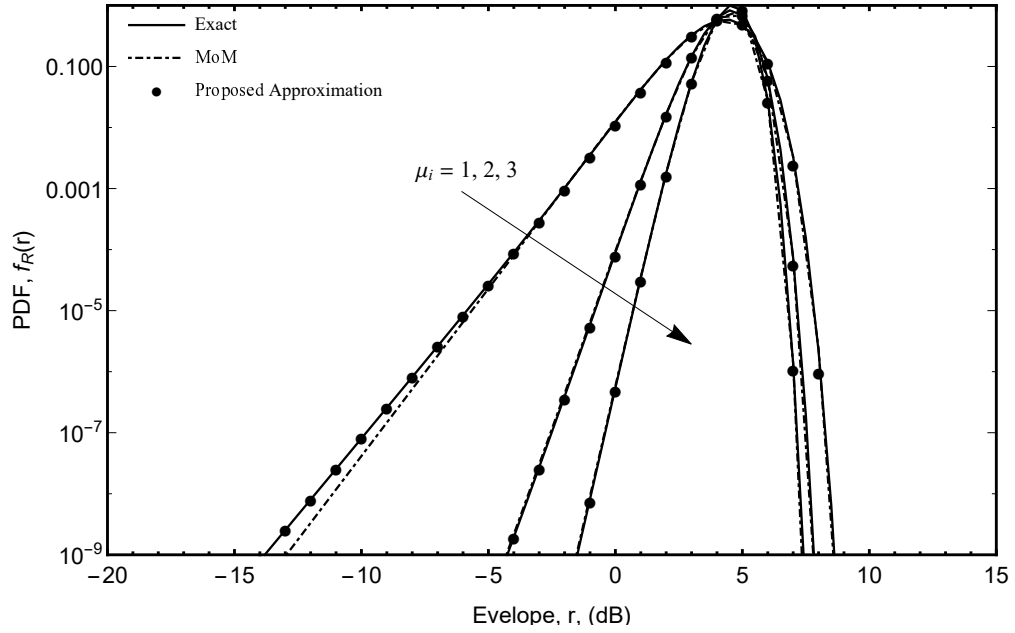
This section checks the accuracy of the proposed approximation through some numerical examples. The exact sum statistics are computed via numerical integration with the use of (3.2). As a term of comparison, the approximation in [51] based solely on MoM for the sum of κ - μ RVs is also included. Next, the curves for both the PDF and the CDF are provided.

Before presenting the numerical results, an important remark is in order. It is necessary to provide some clear evidence that, for engineering purposes^[5], the proposed framework (asymptotic matching and, secondarily, moment matching) outperforms the traditional one (moment matching only) in calibrating the parameters of any distribution model selected to approximate a given fading sum. As mentioned before, the asymptote of the channel PDF around zero governs the high-SNR performance of a communications system operating over that channel, e.g., in terms of important metrics such as outage probability and bit-error rate [117]. So, by matching the asymptotes of the approximate and exact sums, a very good fit (asymptotically exact) is expected for such performance metrics at medium to high SNR — a paramount regime in practice. In such applications, the distribution's body and right tail play a minor role, if any.

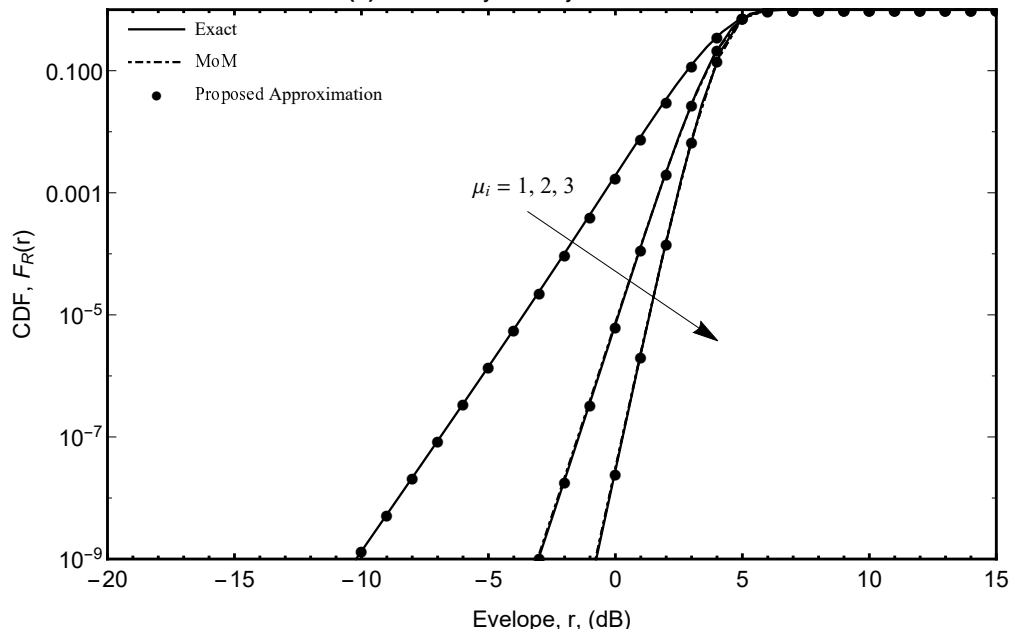
All curves are presented as a function of the envelope r . In addition, the exact solutions are plotted with solid lines; the proposed approximations, with markers; and the MoM approximations [51], with dash-dotted lines.

Fig. 3.8 shows the PDF and CDF for the sum of three i.i.d. κ - μ RVs by varying μ_i for shape parameters $\Omega_i = 1$, $\kappa_i = 1.7$. First, note in Fig. 3.8 that, our proposed approximations render an excellent, asymptotically optimal fit at the left tail of the curves. This region becomes medium to high SNR

[5] By “engineering purposes” it means “regarding the performance of communications systems”.

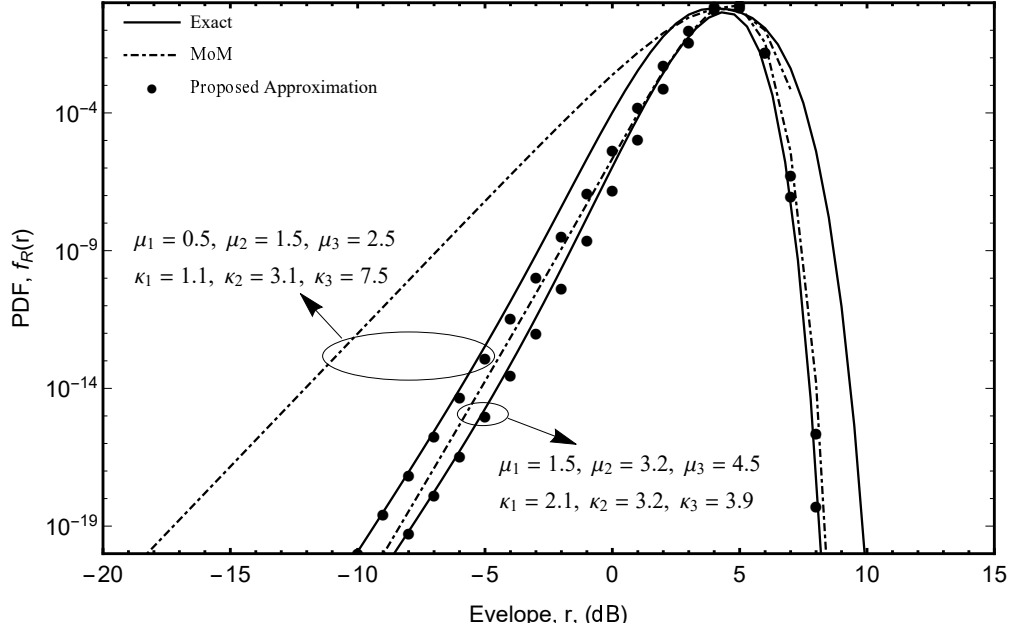


(a) Probability density function.

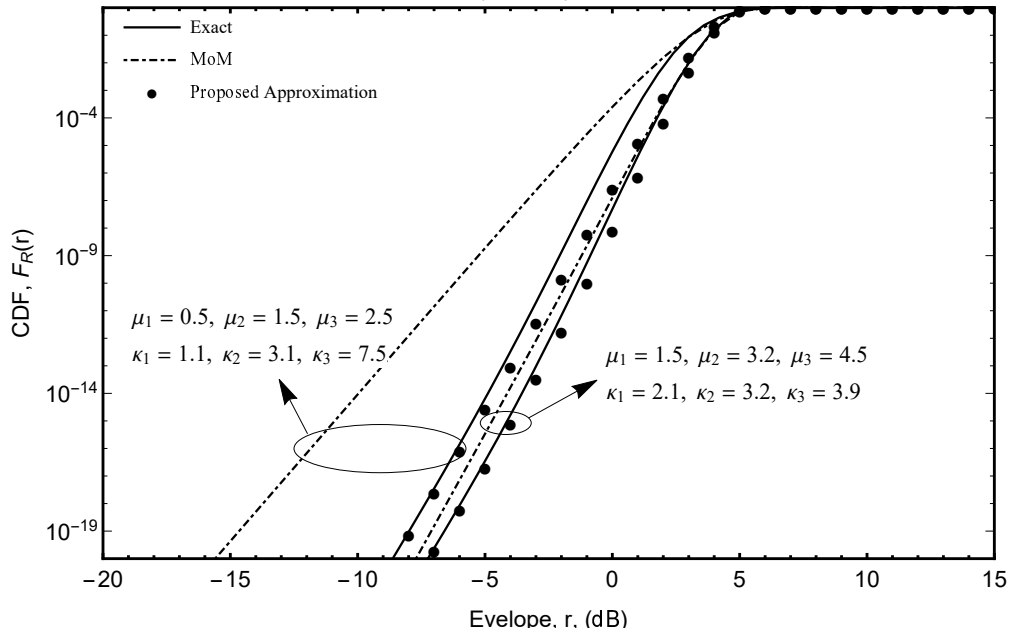


(b) Cumulative distribution function.

Figure 3.8: Sum of three i.i.d. κ - μ RVs by varying μ_i for $\Omega_i = 1$ and $\kappa_i = 1.7$.



(a) Probability density function.



(b) Cumulative distribution function.

Figure 3.9: Sum of three i.n.i.d. κ - μ RVs for *Case I*: $(\mu_1, \mu_2, \mu_3) = (0.5, 1.5, 2.5)$, $(\kappa_1, \kappa_2, \kappa_3) = (1.1, 3.1, 7.5)$, $\Omega_i = 1$, and *Case II*: $(\mu_1, \mu_2, \mu_3) = (1.5, 3.2, 4.5)$, $(\kappa_1, \kappa_2, \kappa_3) = (2.1, 3.2, 3.9)$, $\Omega_i = 1$.

when power sums (i.e., $\Upsilon \triangleq R^2/\sigma^2$ with σ^2 being the noise power) come into play. On the other hand, the κ - μ MoM approximation keeps good track of the exact sum distribution at high SNR (left tail of the distributions). It is worth mentioning that, as a rule, the MoM approximations outperform the proposed approximations at the right tail (this region becomes low SNR regime). This fact will be more evident in the i.n.i.d. case (vide Fig. 3.9). Yet this low SNR range is of little or no concern to practical applications such as estimating the outage probability or error rate at desirable operational levels (e.g., below 10^{-4}). At medium to high SNR, such metrics are also dominated by the channel asymptote around zero [117], mimicking the general trend of the CDF curves in Fig. 3.8b.

More extremely, Fig. 3.9 addresses the sum of three i.n.i.d. κ - μ RVs. For these scenarios, the corresponding fading parameters are given by: *Case I*: $(\mu_1, \mu_2, \mu_3) = (0.5, 1.5, 2.5)$, $(\kappa_1, \kappa_2, \kappa_3) = (1.1, 3.1, 7.5)$, $\Omega_i = 1$, and *Case II*: $(\mu_1, \mu_2, \mu_3) = (1.5, 3.2, 4.5)$, $(\kappa_1, \kappa_2, \kappa_3) = (2.1, 3.2, 3.9)$, $\Omega_i = 1$. In all instances, the same general observations made for Fig. 3.8 still hold true, except that no longer any MoM approximation keeps reasonable track of the exact sum distribution at the left tail of the curves (recall this region denotes the high SNR). It is worth pointing out that our curves ensure a very good fit at the left tail of both PDF and CDF. However, contrary to the MoM approximations, our proposed approach present poor fit at the right tail of the curves (see Fig 3.9a). As mentioned above, this region is not very meaningful in the performance analysis of wireless systems.

3.1.4 Conclusions

3.1.4.1 Nakagami- m Approximation

In this approach, a novel closed-form expression to approximate the PDF of the sum of independent RVs by using a mixture of two Nakagami- m distributions was introduced. The parameters of the approximate distribution have been estimated by implementing the completely unsupervised EM learning algorithm. Our results find applicability in many important communications scenarios where sums of RVs occur. For instance, simple closed-form approximate expressions for ABEP of EGC for both coherent and non-coherent modulations schemes were derived. The asymptotic behavior of the ABEP in the high SNR regime was analyzed with representative examples. Additionally, analytical expressions have also been obtained for ABEP at low SNR regime. Results for ABEP performance for EGC method were presented from representative cases (i.e., low and high fading severity/branches) for both low and high SNR regimes. Finally, our approach can be easily extended to approximate the sum of more general fading distributions, facilitating the performance analysis of wireless communications in emerging environments (e.g., mm-Wave, D2D, UAV, among others).

3.1.4.2 Generalized Approximation

In this approach, a novel framework to approximate a given sum of non-negative independent RVs was proposed. Our main goal was to provide a more effective way (instead of MoM) to calibrate the approximate solution parameters. Specifically, our method have matched the asymptotic behavior around zero between the approximation and the exact sum. Because of this, the method is called *asymptotic matching*. The approach capitalized on the novel technique to estimate the κ - μ model's parameters for the sum of i.i.d. and i.n.i.d. κ - μ RVs. The results showed a much better fit at the left tail of curves compared to the classical MoM. Finally, our approach can be readily extended to sums of fading powers also occurring in wireless applications (i.e., outage probability, bit-error rate).

3.2 RATIO OF RANDOM VARIABLES

The performance analysis of some scenarios considered key technologies (CR, FD, and PLS) for future wireless networks involves calculating the signal's power ratio. As mentioned previously, generalized fading distributions are better suitable than conventional models to fit field data of emerging scenarios in 5G and beyond networks. Therefore, the distribution of the ratio of two α - μ RVs is of particular interest in the analytical evaluation of wireless systems. In light of the above considerations, this section derives closed-form exact expressions for the main statistics (i.e., PDF, CDF, and MGF) of the ratio of independent and i.n.i.d. squared α - μ RVs. Unlike approaches available in the literature, our ratio expressions' fading parameters can be non-constrained arbitrary positive real numbers. This way, our formulations relieve the strong assumption (parameters associated with positive integer numbers) considered in [62] and [63] for the ratio of two squared α - μ RVs. Furthermore, a simple practical application example in PLS, namely SOP is also provided. Before addressing the proposed ratio expressions, the exact statistics of the ratio of two independent RVs are revisited.

3.2.1 Exact Solution Statistics

Let γ_1 and γ_2 be two statistically independent RVs and $X = \gamma_1/\gamma_2$ their ratio. Thus, from standard statistical procedures [137], the exact PDF of X can be obtained by

$$f_X(x) = \int_0^{\infty} y f_{\gamma_1}(xy) f_{\gamma_2}(y) dy. \quad (3.50)$$

The CDF of X can be formulated as [137]

$$F_X(x) = \Pr\{X \leq x\} = \Pr\left\{\frac{\gamma_1}{\gamma_2} \leq x\right\} = \int_0^{\infty} F_{\gamma_1}(xy) f_{\gamma_2}(y) dy. \quad (3.51)$$

From (3.50), the n -th order moment of the RV X is defined as [137]

$$\mathbb{E}[X^n] \triangleq \int_0^{\infty} x^n f_X(x) dx. \quad (3.52)$$

The MGF of X can be obtained, by definition, as [153]

$$\mathcal{M}_X(s) \triangleq \mathbb{E}[\exp(-sX)] = \int_0^{\infty} \exp(-sx) f_X(x) dx. \quad (3.53)$$

Henceforth, it is assumed that the RVs γ_1 and γ_2 are taken from the α - μ distributions.

3.2.2 Proposed Ratio Statistics Representations

Here, closed-form expressions for the PDF, CDF, MGF and higher order moments of the ratio $X = \gamma_1/\gamma_2$ are provided.

Let $\gamma \triangleq \gamma_t R^2$ be the received SNR through an α - μ fading channel, where $\gamma_t \triangleq P/N_0$ is defined as the transmit SNR, with P being the transmit power and N_0 being the mean power of the AWGN. Hence, the corresponding PDF and CDF can be obtained from (2.27) by performing a transformation of variables as [53, Eqs. (8) and (10)]

$$f_\gamma(\gamma) = \frac{\alpha \gamma^{(\alpha\mu/2)-1}}{2\beta^{\alpha\mu/2} \Gamma(\mu)} \exp\left[-\left(\frac{\gamma}{\beta}\right)^{\alpha/2}\right], \quad (3.54)$$

$$F_\gamma(\gamma) = \frac{1}{\Gamma(\mu)} \Upsilon\left(\mu, \left(\frac{\gamma}{\beta}\right)^{\alpha/2}\right), \quad (3.55)$$

where $\beta = \bar{\gamma} \Gamma(\mu) / \Gamma(\mu + 2/\alpha)$, with $\bar{\gamma}$ being the average received SNR, so that

$$\begin{aligned} \bar{\gamma} &= \mathbb{E}[\gamma] d^{-\eta} \\ &= \Omega^2 \frac{\Gamma(\mu + 2/\alpha)}{\mu^{2/\alpha} \Gamma(\mu)} \gamma_t d^{-\eta}, \end{aligned} \quad (3.56)$$

in which d is the propagation distance, and η is path-loss exponent. Now, by using the Meijer G-function representation of the lower incomplete gamma function $\Upsilon(\cdot, \cdot)$ [154, Eq. (06.09.26.0006.01)] and the exponential function $\exp(\cdot)$ [154, Eq. (01.03.26.0004.01)]

$$\exp(-z) = G_{0,1}^{1,0} \left[z \middle| 0 \right], \quad (3.57a)$$

$$\Upsilon(a, z) = z^a G_{1,2}^{1,1} \left[z \middle| 1-a, 0, -a \right], \quad (3.57b)$$

into (3.54) and (3.55), the PDF and CDF of γ can be rewritten as

$$f_{\Upsilon}(\gamma) = \frac{\alpha\gamma^{(\alpha\mu/2)-1}}{2\beta^{\alpha\mu/2}\Gamma(\mu)} G_{0,1}^{1,0} \left[\left(\frac{\gamma}{\beta} \right)^{\alpha/2} \middle| 0 \right]. \quad (3.58)$$

$$F_{\Upsilon}(\gamma) = \frac{1}{\Gamma(\mu)} \left(\frac{\gamma}{\beta} \right)^{\frac{\mu\alpha}{2}} G_{1,2}^{1,1} \left[\left(\frac{\gamma}{\beta} \right)^{\frac{\alpha}{2}} \middle| 1-\mu, -\mu \right]. \quad (3.59)$$

Next, the PDF, CDF, MGF, and the n -th moment of the ratio of two independent squared α - μ RVs are given in terms of the univariate Fox H-function in the following proposition. It is worth mentioning that, it is assumed $\alpha_1, \alpha_2 \in \mathbb{R}^+$, $k = \frac{\alpha_1}{\alpha_2}$, $\mu_1, \mu_2 \in \mathbb{R}^+$, and $x \in \mathbb{R}^+$.

Proposition 5. *Let γ_1 and γ_2 be i.n.i.d. squared α - μ distributed RVs with density functions given in (3.54) and (3.55). The PDF, CDF, and MGF of the ratio $X = \gamma_1/\gamma_2$ are respectively given by*

$$f_X(x) = \frac{\alpha_1 x^{\frac{\alpha_1\mu_1}{2}-1} \beta_2^{\frac{\alpha_1\mu_1}{2}}}{2\beta_1^{\frac{\alpha_1\mu_1}{2}} \Gamma(\mu_2)\Gamma(\mu_1)} \underbrace{H_{1,1}^{1,1} \left[\left(\frac{x\beta_2}{\beta_1} \right)^{\frac{\alpha_1}{2}} \middle| \begin{matrix} (1-\mu_2-k\mu_1, k) \\ (0, 1) \end{matrix} \right]}_{H_1}, \quad (3.60)$$

$$F_X(x) = \frac{1}{\Gamma(\mu_2)\Gamma(\mu_1)} \left(\frac{x\beta_2}{\beta_1} \right)^{\frac{\alpha_1\mu_1}{2}} \underbrace{H_{2,2}^{1,2} \left[\left(\frac{x\beta_2}{\beta_1} \right)^{\frac{\alpha_1}{2}} \middle| \begin{matrix} (1-\mu_1, 1), (1-\mu_1 k - \mu_2, k) \\ (0, 1), (-\mu_1, 1) \end{matrix} \right]}_{H_2}, \quad (3.61)$$

$$\mathcal{M}_X(s) = \frac{\alpha_1}{2\Gamma(\mu_2)\Gamma(\mu_1)} \left(\frac{\beta_2}{s\beta_1} \right)^{\frac{\alpha_1\mu_1}{2}} \underbrace{H_{2,1}^{1,2} \left[\left(\frac{\beta_2}{s\beta_1} \right)^{\frac{\alpha_1}{2}} \middle| \begin{matrix} (1-\mu_2-k\mu_1, k), (1-\frac{\mu_1\alpha_1}{2}, \frac{\alpha_1}{2}) \\ (0, 1) \end{matrix} \right]}_{H_3}. \quad (3.62)$$

$$\mathbb{E}[X^n] = \frac{(\Omega_1\Omega_2)^{2n} \Gamma\left(\mu_1 + \frac{2n}{\alpha_1}\right) \Gamma\left(\mu_2 - \frac{2n}{\alpha_2}\right)}{\mu_1^{2n/\alpha_1} \mu_2^{2n/\alpha_2} \Gamma(\mu_1) \Gamma(\mu_2)}, \quad \text{for } n > \mu_i\alpha_i, \quad i \in \{1, 2\}. \quad (3.63)$$

Proof. The proof is provided in Appendix C.1. □

Remark 2. *Notice that contrary to previous works [62], [63], the results of Proposition 5 are general, since no constraints are imposed on the parameters of γ_1 and γ_2 .*

Remark 3. *It is worth mentioning that currently the Fox H-function is not implemented in mathematical software packages such as Wolfram Mathematica. However, the Fox H-function can be evaluated using either numerical evaluations in the form of a Mellin–Barnes integral [155] or by applying calculus of residues. In the former, a portable implementation of the Fox H-function in MATHEMATICA@Wolfram is provided in Appendix C. The code is simple, efficient, highly accurate and its convergence is always attained. Here, it is worth mentioning that the overall convergence speed of the proposed code is achieved faster for small values of the argument, namely “z” (see (C.16)), and influenced by the fading parameters of the distribution in matter. Moreover, tests were carried out for different fading conditions, from which the average elapsed time to obtain a desired accuracy (e.g.,*

Table 3.2: PDF of the Ratio for particular cases of the α - μ model.

Ratio	PDF
Nakagami- m /Nakagami- m	$f_X(x) = \frac{x^{\mu_1-1}\beta_2^{\mu_1}}{\beta_1^{\mu_1}\Gamma(\mu_2)\Gamma(\mu_1)} G_{1,1}^{1,1} \left[\frac{x\beta_2}{\beta_1} \middle \begin{matrix} 1 - \mu_2 - \mu_1 \\ 0 \end{matrix} \right]$
Nakagami- m /Weibull	$f_X(x) = \frac{x^{\mu_1-1}\beta_2^{\mu_1}}{\beta_1^{\mu_1}\Gamma(\mu_2)} H_{1,1}^{1,1} \left[\frac{x\beta_2}{\beta_1} \middle \begin{matrix} (-\frac{2\mu_1}{\alpha_2}, \frac{2}{\alpha_2}) \\ (0, 1) \end{matrix} \right]$
Nakagami- m /Rayleigh	$f_X(x) = \frac{x^{\mu_1-1}\beta_2^{\mu_1}}{\beta_1^{\mu_1}\Gamma(\mu_1)} G_{1,1}^{1,1} \left[\frac{x\beta_2}{\beta_1} \middle \begin{matrix} -\mu_1 \\ 0 \end{matrix} \right]$
Weibull/Weibull	$f_X(x) = \frac{\alpha_1 x^{\frac{\alpha_1}{2}-1} \beta_2^{\frac{\alpha_1}{2}}}{2\beta_1^{\frac{\alpha_1}{2}}} H_{1,1}^{1,1} \left[\left(\frac{x\beta_2}{\beta_1} \right)^{\frac{\alpha_1}{2}} \middle \begin{matrix} (-k, k) \\ (0, 1) \end{matrix} \right]$
Weibull/Nakagami- m	$f_X(x) = \frac{\alpha_1 x^{\frac{\alpha_1}{2}-1} \beta_2^{\frac{\alpha_1}{2}}}{2\beta_1^{\frac{\alpha_1}{2}} \Gamma(\mu_2)} H_{1,1}^{1,1} \left[\left(\frac{x\beta_2}{\beta_1} \right)^{\frac{\alpha_1}{2}} \middle \begin{matrix} (1 - \mu_2 - \frac{\alpha_1}{2}, \frac{\alpha_1}{2}) \\ (0, 1) \end{matrix} \right]$
Weibull/Rayleigh	$f_X(x) = \frac{\alpha_1 x^{\frac{\alpha_1}{2}-1} \beta_2^{\frac{\alpha_1}{2}}}{2\beta_1^{\frac{\alpha_1}{2}}} H_{1,1}^{1,1} \left[\left(\frac{x\beta_2}{\beta_1} \right)^{\frac{\alpha_1}{2}} \middle \begin{matrix} (-\frac{\alpha_1}{2}, \frac{\alpha_1}{2}) \\ (0, 1) \end{matrix} \right]$
Rayleigh/Rayleigh	$f_X(x) = \frac{\beta_2}{\beta_1} G_{1,1}^{1,1} \left[\frac{x\beta_2}{\beta_1} \middle \begin{matrix} -1 \\ 0 \end{matrix} \right]$
Rayleigh/Nakagami- m	$f_X(x) = \frac{\beta_2}{\beta_1 \Gamma(\mu_2)} G_{1,1}^{1,1} \left[\frac{x\beta_2}{\beta_1} \middle \begin{matrix} -\mu_2 \\ 0 \end{matrix} \right]$
Rayleigh/Weibull	$f_X(x) = \frac{\beta_2}{\beta_1} H_{1,1}^{1,1} \left[\frac{x\beta_2}{\beta_1} \middle \begin{matrix} (-\frac{2}{\alpha_2}, \frac{2}{\alpha_2}) \\ (0, 1) \end{matrix} \right]$

10^{-8} in our tests) was ~ 4.5 s. Unlike other codes available in the literature for the implementation of the Fox H -function, our algorithm is valid for the evaluation of any univariate Fox H -function without any mathematical constraint. In the latter, an alternative method to compute the results presented here is given by the series representation for the Fox H -functions H_1 , H_2 , and H_3 as in (3.64), (3.65) and (3.66), respectively. It is important to emphasize that (3.64), (3.65) and (3.66) converge adequately and correctly as long as the convergence condition with regard to parameter k is fulfilled. Moreover, these series yield accurate results and the evaluation time is negligible. For instance, exhaustive tests have shown that the number of terms to arrive at the desired accuracy (e.g., 10^{-9}) were around 40 and the time taken varied approximately from 0.8 s to 6.5 s depending on the choice of the fading parameters. The mathematical derivation of the referred expressions is provided in Appendix C.

$$H_1 = \begin{cases} \sum_{h=0}^{\infty} \frac{z^h \Gamma(k(h+\mu_1)+\mu_2)}{(-1)^h h!}, & k \leq 1, \text{ if } k = 1 \rightarrow |z| < 1. \\ \sum_{h=0}^{\infty} \frac{z^{-\frac{h+k\mu_1+\mu_2}{k}} \Gamma(\frac{h+k\mu_1+\mu_2}{k})}{(-1)^h k h!}, & k \geq 1, \text{ if } k = 1 \rightarrow |z| > 1. \end{cases} \quad (3.64)$$

Table 3.3: CDF of the Ratio for particular cases of the α - μ model.

Ratio	CDF
Nakagami- m /Nakagami- m	$F_X(x) = \frac{1}{\Gamma(\mu_2)\Gamma(\mu_1)} \left(\frac{x\beta_2}{\beta_1}\right)^{\mu_1} G_{2,2}^{1,2} \left[\frac{x\beta_2}{\beta_1} \mid \begin{matrix} 1 - \mu_1, 1 - \mu_1 - \mu_2 \\ 0, -\mu_1 \end{matrix} \right]$
Nakagami- m /Weibull	$F_X(x) = \frac{1}{\Gamma(\mu_1)} \left(\frac{x\beta_2}{\beta_1}\right)^{\mu_1} H_{2,2}^{1,2} \left[\frac{x\beta_2}{\beta_1} \mid \begin{matrix} (1 - \mu_1, 1), (-\frac{2\mu_1}{\alpha_2}, \frac{2}{\alpha_2}) \\ (0, 1), (-\mu_1, 1) \end{matrix} \right]$
Nakagami- m /Rayleigh	$F_X(x) = \frac{1}{\Gamma(\mu_1)} \left(\frac{x\beta_2}{\beta_1}\right)^{\mu_1} G_{2,2}^{1,2} \left[\frac{x\beta_2}{\beta_1} \mid \begin{matrix} 1 - \mu_1, -\mu_1 \\ 0, -\mu_1 \end{matrix} \right]$
Weibull/Weibull	$F_X(x) = \left(\frac{x\beta_2}{\beta_1}\right)^{\frac{\alpha_1}{2}} H_{2,2}^{1,2} \left[\left(\frac{x\beta_2}{\beta_1}\right)^{\frac{\alpha_1}{2}} \mid \begin{matrix} (0, 1), (-k, k) \\ (0, 1), (-1, 1) \end{matrix} \right]$
Weibull/Nakagami- m	$F_X(x) = \frac{1}{\Gamma(\mu_2)} \left(\frac{x\beta_2}{\beta_1}\right)^{\frac{\alpha_1}{2}} H_{2,2}^{1,2} \left[\left(\frac{x\beta_2}{\beta_1}\right)^{\frac{\alpha_1}{2}} \mid \begin{matrix} (0, 1), (1 - k - \mu_2, k) \\ (0, 1), (-1, 1) \end{matrix} \right]$
Weibull/Rayleigh	$F_X(x) = \left(\frac{x\beta_2}{\beta_1}\right)^{\frac{\alpha_1}{2}} H_{2,2}^{1,2} \left[\left(\frac{x\beta_2}{\beta_1}\right)^{\frac{\alpha_1}{2}} \mid \begin{matrix} (0, 1), (-\frac{\alpha_1}{2}, \frac{\alpha_1}{2}) \\ (0, 1), (-1, 1) \end{matrix} \right]$
Rayleigh/Rayleigh	$F_X(x) = \frac{x\beta_2}{\beta_1} G_{2,2}^{1,2} \left[\frac{x\beta_2}{\beta_1} \mid \begin{matrix} 0, -1 \\ 0, -1 \end{matrix} \right]$
Rayleigh/Nakagami- m	$F_X(x) = \frac{x\beta_2}{\beta_1\Gamma(\mu_2)} G_{2,2}^{1,2} \left[\frac{x\beta_2}{\beta_1} \mid \begin{matrix} 0, -\mu_2 \\ 0, -1 \end{matrix} \right]$
Rayleigh/Weibull	$F_X(x) = \frac{x\beta_2}{\beta_1} H_{2,2}^{1,2} \left[\frac{x\beta_2}{\beta_1} \mid \begin{matrix} (0, 1), (-\frac{2}{\alpha_2}, \frac{2}{\alpha_2}) \\ (0, 1), (-1, 1) \end{matrix} \right]$

$$H_2 = \begin{cases} \sum_{h=0}^{\infty} \frac{z^h \Gamma(k(h+\mu_1)+\mu_2)}{(-1)^h (h+\mu_1)\Gamma(1+h)}, & k \leq 1, \text{ if } k = 1 \rightarrow |z| < 1. \\ \sum_{h=0}^{\infty} \frac{z^{-h-\mu_1} \Gamma(h+\mu_1)\Gamma(-hk+\mu_2)}{(-1)^{h-2}\Gamma(1-h)h!} + \sum_{h=0}^{\infty} \frac{z^{-\frac{h}{k}-\mu_1-\frac{\mu_2}{k}} \Gamma(\frac{-h-\mu_2}{k})\Gamma(\frac{h+k\mu_1+\mu_2}{k})}{(-1)^{h-2}\Gamma(\frac{-h+k-\mu_2}{k})kh!}, & k \geq 1, \text{ if } k = 1 \rightarrow |z| > 1. \end{cases} \quad (3.65)$$

$$H_3 = \begin{cases} \sum_{h=0}^{\infty} \frac{\Gamma(hk+k\mu_X+\mu_Y)z^h}{(-1)^h h!}, & k \leq 1, \text{ if } k = 1 \rightarrow |z| < 1. \\ \sum_{h=0}^{\infty} \frac{\Gamma(\frac{h+k\mu_X+\mu_Y}{k})z^{-\frac{h+k\mu_X+\mu_Y}{k}}}{(-1)^h kh!}, & k \geq 1, \text{ if } k = 1 \rightarrow |z| > 1. \end{cases} \quad (3.66)$$

In short, the formulations derived in (3.60) to (3.63) are general results that can be reduced to particular models, such as Rayleigh, Nakagami- m , and Weibull by setting the parameters of the α - μ distribution (see section 2.2.2.1). Therefore, the PDF, CDF, and MGF for the distribution of the ratio of two squared of the aforementioned distributions are given in Table 3.2, 3.3 and 3.4, respectively.

3.2.2.1 Application: Physical Layer Security

Here, the utility of the new formulations derived for the ratio of two squared α - μ RVs is demonstrated by analyzing a high SNR approximation of the SOP for a wiretap channel configuration. Thus, consider the Wyner's wiretap channel as depicted in Fig. 2.1, where both the main and eavesdropper

Tabla 3.4: MGF of the Ratio for particular cases of the α - μ model.

Ratio	MGF
Nakagami- m /Nakagami- m	$\mathcal{M}_X(s) = \frac{1}{2\Gamma(\mu_2)\Gamma(\mu_1)} \left(\frac{\beta_2}{s\beta_1}\right)^{\mu_1} G_{2,1}^{1,2} \left[\frac{\beta_2}{s\beta_1} \mid \begin{matrix} 1 - \mu_2 - \mu_1, 1 - \mu_1 \\ 0 \end{matrix} \right]$
Nakagami- m /Weibull	$\mathcal{M}_X(s) = \frac{1}{\Gamma(\mu_1)} \left(\frac{\beta_2}{s\beta_1}\right)^{\mu_1} H_{2,1}^{1,2} \left[\frac{\beta_2}{s\beta_1} \mid \begin{matrix} (-\frac{2\mu_1}{\alpha_2}, \frac{2}{\alpha_2}), (1 - \mu_1, 1) \\ (0, 1) \end{matrix} \right]$
Nakagami- m /Rayleigh	$\mathcal{M}_X(s) = \frac{1}{\Gamma(\mu_1)} \left(\frac{\beta_2}{s\beta_1}\right)^{\mu_1} G_{2,1}^{1,2} \left[\frac{\beta_2}{s\beta_1} \mid \begin{matrix} -\mu_1, 1 - \mu_1 \\ 0 \end{matrix} \right]$
Weibull/Weibull	$\mathcal{M}_X(s) = \frac{\alpha_1}{2} \left(\frac{\beta_2}{s\beta_1}\right)^{\frac{\alpha_1}{2}} H_{2,1}^{1,2} \left[\left(\frac{\beta_2}{s\beta_1}\right)^{\frac{\alpha_1}{2}} \mid \begin{matrix} (-k, k), (1 - \frac{\alpha_1}{2}, \frac{\alpha_1}{2}) \\ (0, 1) \end{matrix} \right]$
Weibull/Nakagami- m	$\mathcal{M}_X(s) = \frac{\alpha_1}{2\Gamma(\mu_2)} \left(\frac{\beta_2}{s\beta_1}\right)^{\frac{\alpha_1}{2}} H_{2,1}^{1,2} \left[\left(\frac{\beta_2}{s\beta_1}\right)^{\frac{\alpha_1}{2}} \mid \begin{matrix} (1 - \mu_2 - \frac{\alpha_1}{2}, \frac{\alpha_1}{2}), (1 - \frac{\alpha_1}{2}, \frac{\alpha_1}{2}) \\ (0, 1) \end{matrix} \right]$
Weibull/Rayleigh	$\mathcal{M}_X(s) = \frac{\alpha_1}{2} \left(\frac{\beta_2}{s\beta_1}\right)^{\frac{\alpha_1}{2}} H_{2,1}^{1,2} \left[\left(\frac{\beta_2}{s\beta_1}\right)^{\frac{\alpha_1}{2}} \mid \begin{matrix} (-\frac{\alpha_1}{2}, \frac{\alpha_1}{2}), (1 - \frac{\alpha_1}{2}, \frac{\alpha_1}{2}) \\ (0, 1) \end{matrix} \right]$
Rayleigh/Rayleigh	$\mathcal{M}_X(s) = \frac{\beta_2}{s\beta_1} G_{2,1}^{1,2} \left[\frac{\beta_2}{s\beta_1} \mid \begin{matrix} -1, 0 \\ 0 \end{matrix} \right]$
Rayleigh/Nakagami- m	$\mathcal{M}_X(s) = \frac{\beta_2}{s\beta_1\Gamma(\mu_2)} G_{2,1}^{1,2} \left[\frac{\beta_2}{s\beta_1} \mid \begin{matrix} -\mu_2, 0 \\ 0 \end{matrix} \right]$
Rayleigh/Weibull	$\mathcal{M}_X(s) = \frac{\beta_2}{s\beta_1} H_{2,1}^{1,2} \left[\frac{\beta_2}{s\beta_1} \mid \begin{matrix} (-\frac{2}{\alpha_2}, \frac{2}{\alpha_2}), (0, 1) \\ (0, 1) \end{matrix} \right]$

channels are subject to experience independent α - μ distributed fading.

Notice that the CDF of the ratio of two squared α - μ RVs in (3.51) is defined in a similar way that the SOP_A in (2.6). Based on this, the SOP_A can be expressed as

$$SOP_A = F_X(\tau), \quad (3.67)$$

where $\tau = 2^{R_S}$ with R_S being the secrecy rate threshold (for more details see Section 2.1.2.2), $X = \gamma_B/\gamma_E$ for γ_i , $i \in \{B, E\}$ represents the main and the eavesdropper channels, respectively, and $F_X(\cdot)$ is a CDF of the ratio obtained in (3.61). In the literature, (3.67) is also known as the lower bound of the SOP, which results very tight at high SNR, as shall be shown in Section 3.2.3. It is noteworthy that, our formulation for the lower bound of the SOP is valid for non-constrained arbitrary values of the fading parameters corresponding to the main channel and eavesdropper channel (i.e., α_i and μ_i , for $i \in \{B, E\}$). This is in contrast to previous works [76], [77] related to the performance analysis of physical layer security over single-input single-output (SISO) α - μ fading channels, where constraints on the fading parameter values were considered (more specifically, $\alpha_B = \alpha_E$ in [77], and α_B, α_E must be co-prime integers in [76]). Therefore, our expressions are a generalization of the aforementioned approaches. It is worth mentioning that the secrecy performance analysis over MIMO wiretap α - μ

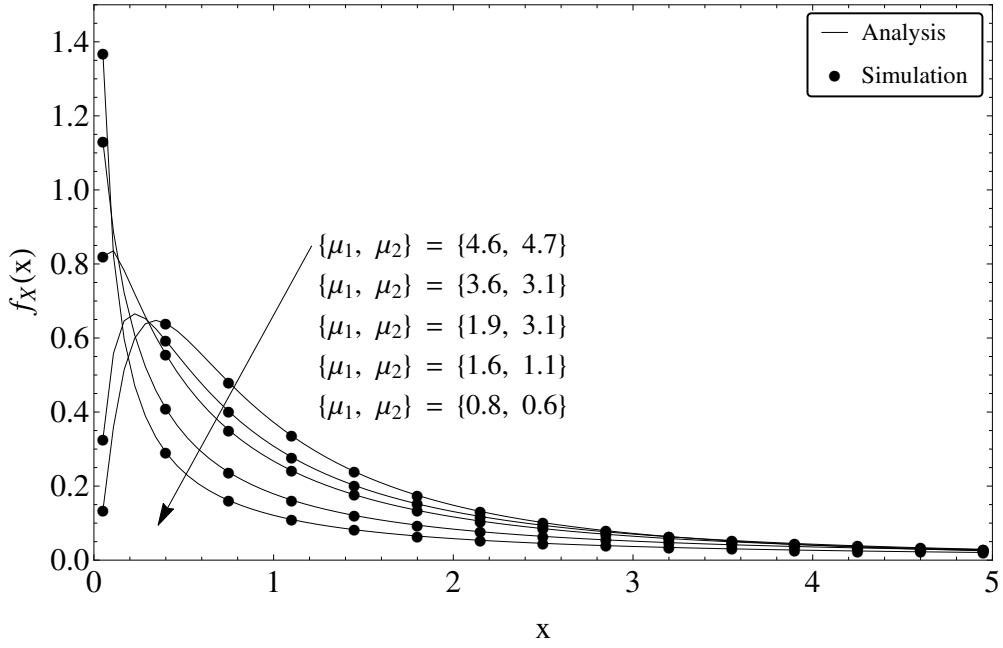
fading channels was derived in terms of the Fox H-function in [99].

3.2.3 Numerical Results

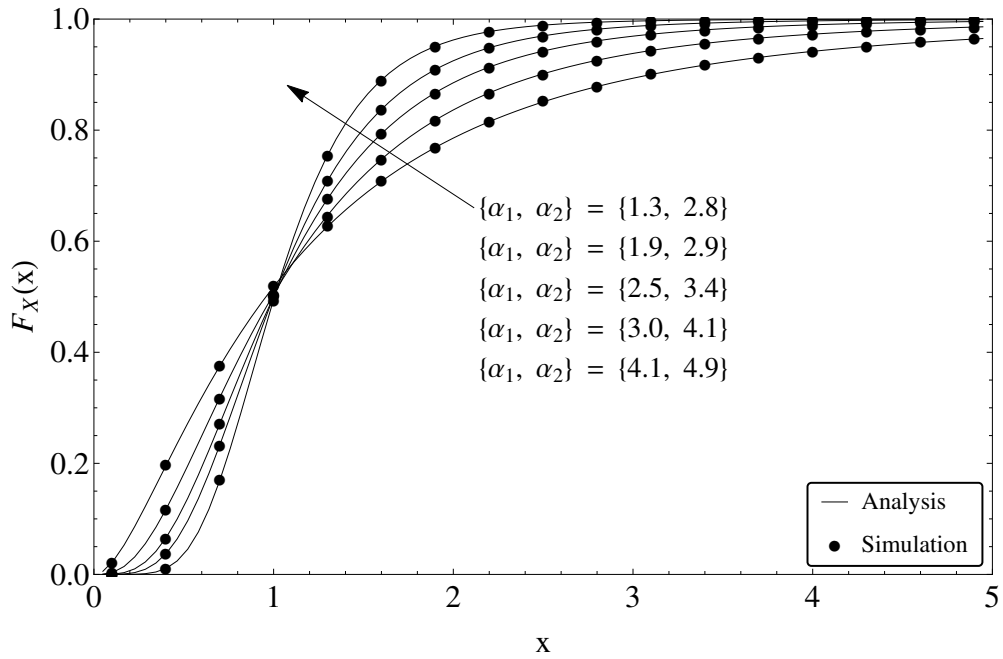
In this section, in order to validate the accuracy of the proposed expressions for some representative cases, Monte Carlo simulations are also plotted. Without loss of generality, the propagation distance d_i , with $i \in \{1, 2\}$ is normalized to unity.

Fig. 3.10 shows the PDF and CDF obtained for the ratio of two squared α - μ RVs, by considering different values of fading parameters. In both figures, the values of the fading parameters are chosen to show the wide range of shapes that the distribution of the ratio can assume. Fig. 3.10a illustrates the resulting PDF for different values of $\{\mu_1, \mu_2\}$, with $\{\alpha_1, \alpha_2\} = \{1.5, 1.1\}$ and $\bar{\gamma}_1 = \bar{\gamma}_2 = 0$ dB. It can be observed that our expressions perfectly match the Monte Carlo simulations, thus validating our results. Fig. 3.10b shows the resulting CDF for distinct values of $\{\alpha_1, \alpha_2\}$, with $\{\mu_1, \mu_2\} = \{3.5, 2.8\}$ and $\bar{\gamma}_1 = \bar{\gamma}_2 = 0$ dB. Once again, it is observed that our expressions perfectly match the Monte Carlo simulations. It can also be noticed from the cases presented in those figures that our expressions allow non-constrained arbitrary values of fading.

Then, Fig. 3.11 evaluates the SOP vs. $\bar{\gamma}_B$ for different combinations of fading parameters α_i, μ_i with $i \in \{B, E\}$. For both figures, the fading parameters are set to: $R_S = 1$ bps/Hz, and $\bar{\gamma}_E = 10$ dB. In Fig. 3.11a, the impact on the secrecy performance when the main and eavesdropper channels experience mild and severe fading conditions is explored. Hence, the fading parameters are given by: $\{\mu_B, \mu_E\} = \{3.5, 0.5\}, \{2.5, 1.5\}, \{1.5, 2.5\}, \{0.5, 3.5\}$, and fixed $\alpha_i = 2.7$ for $i \in \{B, E\}$. For all cases, it can be noticed that the proposed lower bound is very tight to the exact SOP obtained by Monte Carlo simulations. It is observed that as μ_B increases and μ_E decreases, the security performance of the system improves. This is because high values of μ_B and low values of μ_E indicate light and heavy fading on the legitimate and eavesdropper channels, respectively. Now, in Fig. 3.11a, it is investigated how parameter α_i for $i \in \{B, E\}$ affects PLS performance. The fading parameters for this cases are set to: $\{\alpha_B, \alpha_E\} = \{3.5, 0.5\}, \{2.5, 1.5\}, \{1.5, 2.5\}, \{0.5, 3.5\}$, and fixed $\mu_i = 4.2$ for $i \in \{B, E\}$. Again, note that in all instances, our analytical expressions match with Monte Carlo simulations. Besides, it is observed that the α_i presents a similar behavior to μ_i (for $i \in \{B, E\}$) from a secrecy perspective. That is, having an α_B much larger than α_E turns out to be beneficial for PLS. Finally, from both figures, it is evident that the fading conditions can be used to prevent the information from being overheard by an eavesdropper.

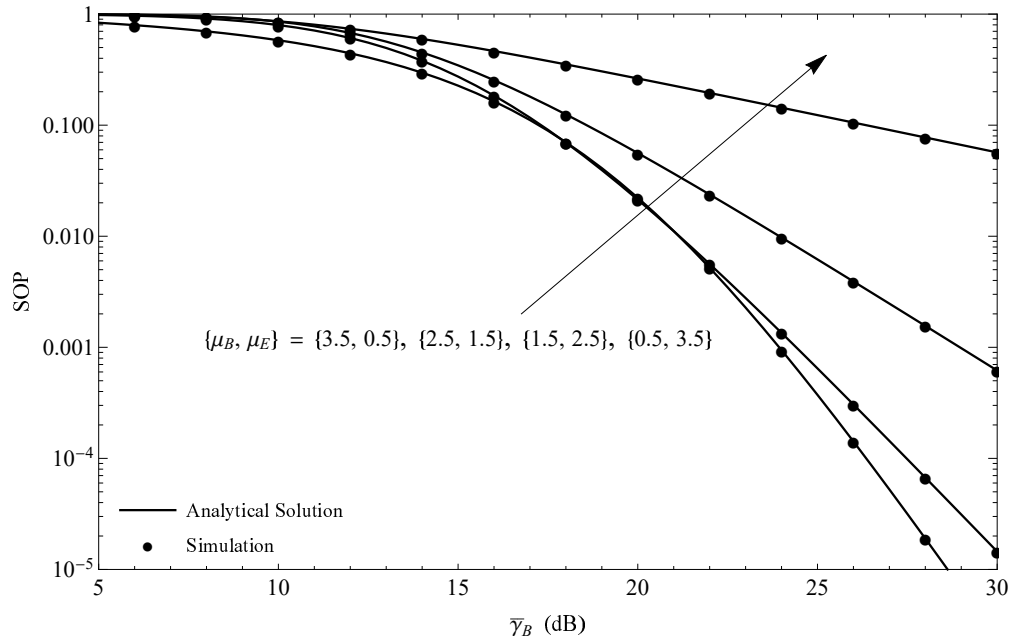


(a) PDF of the ratio of two squared α - μ RVs for different values of $\{\mu_1, \mu_2\}$, with $\{\alpha_1, \alpha_2\} = \{1.5, 1.1\}$ and $\bar{\gamma}_1 = \bar{\gamma}_2 = 0$ dB.

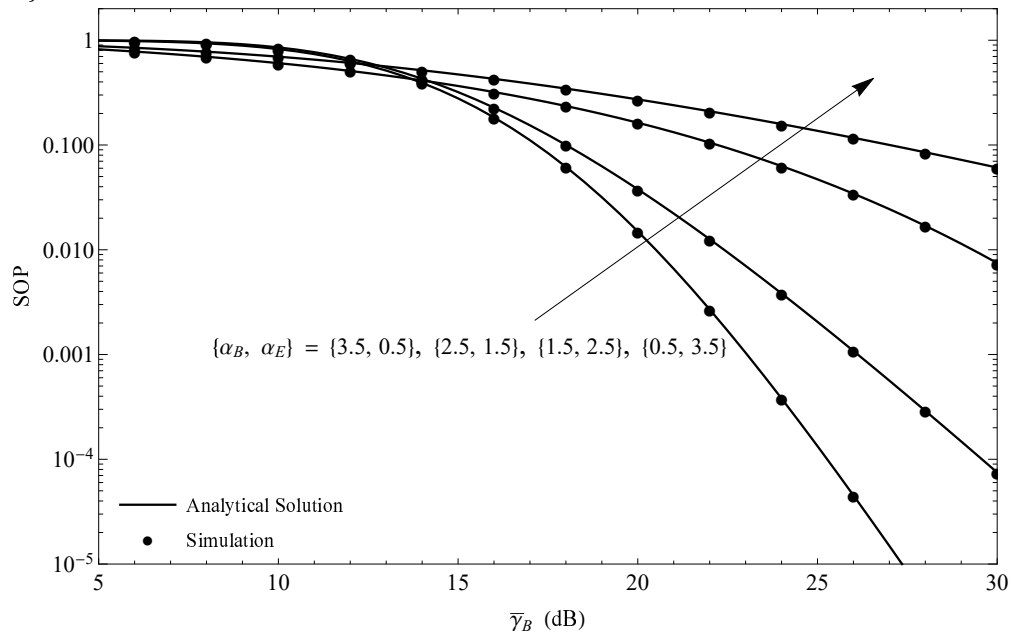


(b) CDF of the ratio of two squared α - μ RVs for different values of $\{\alpha_1, \alpha_2\}$, with $\{\mu_1, \mu_2\} = \{3.5, 2.8\}$ and $\bar{\gamma}_1 = \bar{\gamma}_2 = 0$ dB.

Figure 3.10: PDF and CDF of the ratio of two squared α - μ RVs.



(a) SOP vs. $\bar{\gamma}_B$ with different combinations of $\{\mu_B, \mu_E\}$ for $\bar{\gamma}_E = 10$ dB, $R_S = 1$ bps/Hz, and $\alpha_i = 2.7$ for $i \in \{B, E\}$.



(b) SOP vs. $\bar{\gamma}_B$ with different combinations of $\{\alpha_B, \alpha_E\}$ for $\bar{\gamma}_E = 10$ dB, $R_S = 1$ bps/Hz, and $\mu_i = 4.2$ for $i \in \{B, E\}$.

Figure 3.11: SOP vs. $\bar{\gamma}_B$ by varying α_i and μ_i for $i \in \{B, E\}$.

3.2.4 Conclusions

In this section, novel exact analytical expressions for the PDF, CDF, MGF, and higher order moments of the ratio of two squared α - μ RVs in terms of the Fox H-function were derived. Importantly, these expressions, unlike previous related works, are valid for any values of the fading parameters α and μ . Additionally, a series representation for the formulations are also provided. Based on these results, analytical expressions for the statistics of the ratio of well-known distributions, such as Nakagami- m , Weibull, and Rayleigh, were also provided as byproducts. These novel statistics represent a useful tool to assess the performance of wireless communication schemes considering generalized fading-channel models with applicability in scenarios for next-generation wireless networks. For illustration purposes, the SOP for PLS-based wireless networks was analyzed. Finally, it is worth mentioning that our analytical expressions can be evaluated in a straightforward and efficient manner through mathematical software packages. In this context, an implementation of the Fox H-function was also provided.

4 PHYSICAL LAYER SECURITY ENHANCEMENT IN N-WAVE WITH DIFFUSE POWER FADING CHANNELS

This chapter investigates the effect of considering realistic propagation conditions that differ from the classic Rice and Rayleigh fading from a PLS perspective. Specifically, this work studies how the superposition of a number of dominant specular waves and diffusely propagating components impacts the achievable secrecy performance compared to conventional assumptions relying on the central limit theorem. Analytical expressions for the SOP and the ASC are derived by assuming an arbitrary number of dominant waves at the desired and eavesdropping ends, as well as simplified approximations that become asymptotically tight in the high-SNR regime. Our expressions have similar complexity to other alternatives in the literature derived in terms of well-known elementary and special functions for simpler fading models. Very useful insights on the impact on physical layer security by varying (i) the number; (ii) the relative amplitudes and (iii) the overall power of the dominant specular components are also provided. This research shows that it is possible to obtain remarkable improvements on the system secrecy performance when: (a) the relative amplitudes of the dominant specular components for the legitimate channel are more unbalanced compared to those of the eavesdropper's channel, and (b) the power of the dominant components for the main channel is significantly larger than the power of the dominant components for the wiretap channel. The goal is to perform a fine-grain characterization of the role of individual multipath waves of the NWDP model on the secrecy performance, and to support our findings with analytical results.

4.1 SYSTEM MODEL

Consider the classic Wyner's wiretap channel, as depicted in Fig. 2.1. In this setup, it is assumed that the main and eavesdropper channels experience independent quasi-static fading, and that all nodes are equipped with a single antenna. The signal at each of the receiving ends is expressed as a superposition of N multipath waves arising from dominant specular reflections, and M additional waves associated to diffuse scattering, i.e., Bob and Eve are subject to NWDP fading channels (see Section 2.2.2.4).

Let $\gamma \triangleq \gamma_t R^2$ be the instantaneous received SNR, where $\gamma_t \triangleq P/N_0$ is defined as the transmit SNR, with P being the transmit power and N_0 being the mean power of the AWGN. Note that γ can also be

redefined for the sake of convenience as $\gamma = \bar{\gamma}|h|^2$, where h denotes any normalized fading channel, i.e., $\mathbb{E}\{|h|^2\} = 1$ and $\bar{\gamma}$ representing the average receive SNR. Departing from (2.37) and following the standard procedure of transformation of variables, i.e., $f_\gamma(\gamma) = \frac{1}{2\sqrt{\gamma\bar{\gamma}}}f_R\left(\sqrt{\frac{\gamma}{\bar{\gamma}}}\right)$, the PDF and CDF of γ over NWDP fading channels are given by [20]

$$f_i(\gamma_i) = \frac{1}{\bar{\gamma}_i} \exp\left(-\frac{\gamma_i}{\bar{\gamma}_i}\right) \sum_{z_i=0}^{\infty} C_{z_i} L_{z_i}\left(\frac{\gamma_i}{\bar{\gamma}_i}\right), \quad (4.1a)$$

$$F_i(\gamma_i) = \sum_{z_i=0}^{\infty} C_{z_i} \sum_{k_i=0}^{z_i} \frac{(-1)^{k_i}}{k_i!} \binom{z_i}{k_i} \Upsilon\left(k_i + 1, \frac{\gamma_i}{\bar{\gamma}_i}\right), \quad (4.1b)$$

where the fading parameters (i.e., the number of dominant components N_i , power of diffuse waves Ω_i , and amplitudes of specular waves $V_{n,i}$ for $n = 1, \dots, N_i$) are embedded in the coefficient C_{z_i} , in which $i \in \{B, E\}$ represents either the main channel or the eavesdropper channel, and $\bar{\gamma}_i$ is the average received SNR at B or E as previously stated, given by

$$\bar{\gamma}_i = \gamma_t \mathbb{E}\left[R_i^2\right] r_i^{-\eta_i} = \gamma_t \left(\sum_{n=0}^{N_i} V_{n,i}^2 + \Omega_i\right) r_i^{-\eta_i}, \quad (4.2)$$

where η_i is the path-loss exponent, and r_i is the propagation distance^[1]. Also, C_{z_i} is given by [20]

$$C_{z_i} = \sum_{k_i=0}^{z_i} \frac{(-\epsilon_i)^{k_i}}{k_i!} \binom{z_i}{k_i} u_{N_i+1}^{(2k_i)}, \quad (4.3)$$

where ϵ_i and $u_{N_i+1}^{(2k_i)}$ are given by (2.39) and (2.40), respectively. Next, the secrecy metrics under NWDP fading channels in terms of well-known functions in the communication theory are found.

4.2 SECRECY METRICS

This section derives analytical expressions for the SOP, ASC and high-SNR approximations of the SOP and ASC over NWDP fading channels.

4.2.1 SOP Analysis

Here, it is considered a passive eavesdropping attack, so Eve's CSI is not available at Alice. Therefore, Alice can only encode the confidential messages into codewords at a constant secrecy rate R_S .

[1] Here, as in the LoS ball blockage model, it is assumed that r_i lies within a sphere of fixed radius r_B . Interested readers can revise [156] for further guidance about simplification of the LoS region as a fixed equivalent LoS ball in mm-Wave cellular networks.

For this configuration, the exact formulations of the SOP and a high-SNR approximation of the SOP are given by (2.5) and (2.6), respectively. Based on this, these metrics are introduced in the following proposition.

Proposition 6. *The SOP and the SOP_A over NWDP fading channels can be obtained as*

$$\begin{aligned}
SOP = & 1 - \sum_{z_B=0}^{\infty} C_{z_B} \sum_{k_B=0}^{n_B} (-1)^{k_B} \binom{z_B}{k_B} \left(\frac{1}{\bar{\gamma}_E}\right) \sum_{z_E=0}^{\infty} C_{z_E} \sum_{q=0}^{k_B} \frac{1}{q!} \left(\frac{1}{\bar{\gamma}_B}\right)^q \exp\left(-\frac{\tau-1}{\bar{\gamma}_B}\right) \sum_{a=0}^q \binom{q}{a} \\
& \times (\tau-1)^{q-a} \tau^a \left(\frac{1}{\bar{\gamma}_E} + \frac{\tau}{\bar{\gamma}_B}\right)^{-1-a} \Gamma(1+a) {}_2F_1\left(1+a, -z_E; 1; \frac{\bar{\gamma}_B}{\bar{\gamma}_B + \bar{\gamma}_E \tau}\right) \quad (4.4)
\end{aligned}$$

$$\begin{aligned}
SOP_A = & 1 - \sum_{z_B=0}^{\infty} C_{z_B} \sum_{k_B=0}^{z_B} (-1)^{k_B} \binom{z_B}{k_B} \sum_{z_E=0}^{\infty} C_{z_E} \sum_{q=0}^{k_B} \frac{(\bar{\gamma}_E \tau)^q \bar{\gamma}_B}{(\bar{\gamma}_B + \tau \bar{\gamma}_E)^{q+1}} {}_2F_1\left(-z_E, 1+q; 1; \frac{\bar{\gamma}_B}{\bar{\gamma}_B + \bar{\gamma}_E \tau}\right) \quad (4.5)
\end{aligned}$$

Proof. See Appendix D.1. □

It is worth mentioning that the derived analytical expressions for both the SOP and SOP_A are expressed in terms of infinite series representations. This is also the case of the analysis in [86] for TWDP based on the *approximate* PDF in [17], which arises as a special case of our analysis.

4.2.2 Asymptotic SOP Analysis

In order to provide useful insights on the role of NWDP model fading parameters in the context of PLS, the main concern in this section is to derive asymptotic expressions of the SOP. For this purpose, the behavior of the SOP given in (2.5) in the high-SNR regime is explored. Here, it is assumed that $\bar{\gamma}_B \rightarrow \infty$ while $\bar{\gamma}_E$ is kept fixed. As mentioned in Section 2.1.2.3, this scenario corresponds to the case in which the transmitter (Alice) is very close to the legitimate receiver (Bob) and the eavesdropper (Eve) is located far away. our goal is to derive asymptotic SOP expressions in the form of (2.7). Next, the corresponding asymptotic expressions of the SOP over NWDP fading channels are given in the following Proposition.

Proposition 7. *The asymptotic expressions of the SOP over NWDP fading channels for $\bar{\gamma}_B \rightarrow \infty$ can be formulated as*

$$\text{SOP}^\infty \simeq \sum_{z_B=0}^{\infty} C_{z_B} \sum_{k_B=0}^{z_B} (-1)^{k_B} \binom{z_B}{k_B} \left(\frac{\tau \bar{\gamma}_E}{\bar{\gamma}_B} \right)^{k_B+1} \sum_{z_E=0}^{\infty} C_{z_E} {}_2F_1(k_B+2, -z_E; 1; 1) \quad (4.6)$$

$$\text{SOP}^\infty \simeq \frac{K_{N_B} + 1}{\bar{\gamma}_B} \exp(-K_{N_B}) \mathbb{E}_\theta \left[\exp\left(-\frac{2f(\theta)}{\Omega_B}\right) \right] G_e. \quad (4.7)$$

where

$$G_e = \sum_{z_E=0}^{\infty} C_{z_E} \sum_{h=0}^{z_E} \frac{(-1)^h}{h!} \binom{z_E}{z_E-h} \left(-1 + (1 + \bar{\gamma}_E(1+h))\tau \right). \quad (4.8)$$

denotes a constant secrecy gain attributed to the eavesdropper channel.

Proof. See Appendix D.2. □

Remark 4. For diversity order analysis, important observations are in order: (i) Comparing (2.7), i.e., $\text{SOP}^\infty \simeq G_c \bar{\gamma}_B^{-G_d}$ with respect to (4.7), it is evident that the derived secrecy diversity order, $G_d = 1$, is affirmed by Fig. 4.6 where the slope of the SOP remains identical regardless of the fading parameters (e.g., $V_{n,B}$, N_B , and K_{dB}^B) considered at the legitimate path; (ii) Again, by comparing (2.7), i.e., $\text{SOP}^\infty \simeq G_c \bar{\gamma}_B^{-G_d}$ with respect to (4.6), notice that the secrecy diversity order for such asymptotic expression includes some terms of the form $G_d = (k_B + 1)$, for $k_B = 0 \dots \infty$. This indicates that the decaying slope of the SOP can be steeper before the true secrecy diversity order captured by (4.7) effectively kicks in. This will be later discussed in the Numerical Results section.

4.2.3 ASC Analysis

Unlike SOP analysis, this section focuses on active eavesdropping cases since the CSI of both Bob and Eve channels is available at Alice. As pointed out in Section 2.1.2.4, the ASC's exact formulation is given by (2.8). Based on this, the ASC expression under NWDP fading channels is given in the following proposition.

Proposition 8. The ASC expression over NWDP fading channels can be expressed as

$$\begin{aligned}
\bar{C}_S = & \frac{1}{\ln 2} \left[\exp\left(\frac{1}{\bar{\gamma}_B}\right) \mathbf{E}_1\left(\frac{1}{\bar{\gamma}_B}\right) - \sum_{z_B=1}^{\infty} C_{z_B} \left(\Gamma(z_B) U\left(z_B, 0, \frac{1}{\bar{\gamma}_B}\right) - \sum_{k_B=0}^{z_B} \frac{(-1)^{k_B}}{k_B!} \binom{z_B}{k_B} k_B! \exp\left(\frac{1}{\bar{\gamma}_E}\right) \right. \right. \\
& \times \left. \left(\mathbf{E}_1\left(\frac{1}{\bar{\gamma}_E}\right) - \exp\left(\frac{1}{\bar{\gamma}_B}\right) \sum_{d=0}^{k_B} \frac{1}{d!} \left(\frac{1}{\bar{\gamma}_B}\right)^d \Gamma(1+d) \Gamma\left(-d, \frac{1}{\bar{\gamma}_B} + \frac{1}{\bar{\gamma}_E}\right) \right) \right] - \exp\left(\frac{1}{\bar{\gamma}_B} + \frac{1}{\bar{\gamma}_E}\right) \\
& \times \mathbf{E}_1\left(\frac{1}{\bar{\gamma}_B} + \frac{1}{\bar{\gamma}_E}\right) + \sum_{z_E=1}^{\infty} C_{z_E} \sum_{k_E=0}^{z_E} \frac{(-1)^{k_E}}{k_E!} \binom{z_E}{k_E} k_E! \exp\left(\frac{1}{\bar{\gamma}_B}\right) \left(\mathbf{E}_1\left(\frac{1}{\bar{\gamma}_B}\right) - \sum_{w=0}^{k_E} \frac{1}{w!} \left(\frac{1}{\bar{\gamma}_E}\right)^w \right. \\
& \times \exp\left(\frac{1}{\bar{\gamma}_E}\right) \Gamma(1+w) \Gamma\left(-w, \frac{1}{\bar{\gamma}_B} + \frac{1}{\bar{\gamma}_E}\right) \left. \right) - \sum_{z_B=1}^{\infty} \exp\left(\frac{1}{\bar{\gamma}_B} + \frac{1}{\bar{\gamma}_E}\right) C_{z_B} \sum_{k_B=0}^{z_B} \frac{(-1)^{k_B}}{k_B!} \binom{z_B}{k_B} \\
& \times \frac{1}{(1+k_B)} \left(\frac{1}{\bar{\gamma}_B}\right)^{k_B+1} \sum_{z_E=1}^{\infty} C_{z_E} \sum_{k_E=0}^{z_E} \frac{(-1)^{k_E}}{k_E!} \binom{z_E}{k_E} \frac{1}{(1+k_E)} \left(\frac{1}{\bar{\gamma}_E}\right)^{k_E+1} \sum_{g=0}^{\infty} \frac{(1)_g}{g! (k_B+2)_g} \left(\frac{1}{\bar{\gamma}_B}\right)^g \\
& \times \sum_{c=0}^{\infty} \frac{(1)_c}{c! (k_E+2)_c} \left(\frac{1}{\bar{\gamma}_E}\right)^c \Gamma(3+k_E+k_B+g+c) \Gamma\left(-2-k_B-k_E-g-c, \frac{1}{\bar{\gamma}_B} + \frac{1}{\bar{\gamma}_E}\right) \left. \right].
\end{aligned} \tag{4.9}$$

Proof. See Appendix D.3. □

It is worth mentioning that although (4.9) is an elongated formulation, it is given in terms of well-known functions, facilitating its implementation in mathematical software packages.

4.2.4 Asymptotic ASC Analysis

Here, an asymptotic ASC formulation to evaluate the secrecy performance in the high-SNR regime is derived. Similarly to the asymptotic SOP analysis, it is assumed that $\bar{\gamma}_B$ goes to infinity, while $\bar{\gamma}_E$ is kept fixed. An asymptotic ASC approximation is given in (2.12). Based on this formulation, the asymptotic ASC under NWDP channels is given below.

Proposition 9. *The asymptotic expressions of ASC over NWDP fading channels is given by*

$$\begin{aligned}
\bar{C}_S^\infty \simeq & \log_2(\bar{\gamma}_B) + \log_2(e) \sum_{z_B=0}^{\infty} C_{z_B} \sum_{b=0}^{\infty} \frac{(-z_B)_b}{b!} \psi(1+b) - \frac{1}{\ln 2} \left[\exp\left(\frac{1}{\bar{\gamma}_E}\right) \mathbf{E}_1\left(\frac{1}{\bar{\gamma}_E}\right) \right. \\
& \left. - \sum_{z_E=1}^{\infty} C_{z_E} \Gamma(z_E) U\left(z_E, 0, \frac{1}{\bar{\gamma}_E}\right) \right].
\end{aligned} \tag{4.10}$$

Proof. See Appendix D.4. □

4.3 NUMERICAL RESULTS AND DISCUSSIONS

In this section, the accuracy of the proposed expressions are validated via Monte Carlo simulations, for some representative cases. Without loss of generality, the propagation distance r_i , with $i \in \{B, E\}$ is normalized to unity. Also, it is defined a power ratio parameter similar to the well-known Rician K parameter, i.e., $K_{N_i} \triangleq \frac{\Omega_{N_i}}{\Omega_i}$, with $\Omega_{N_i} = \sum_{n=0}^{N_i} V_{n,i}^2$ being the total average power of the specular components. For the sake of comparison, the Rayleigh case (i.e., $N_B = N_E = 0$) is included as a reference in the SOP analysis.

Before getting into numerical examples, important remarks are in order. 1) It is important to providing clear evidence to identify the impact of increasing/decreasing the number and power of the dominant specular waves over the secrecy performance. In other words, the goal is to determine to what extent it is worth that each of the individual specular waves is treated separately, or it can be safely incorporated into the diffuse component. 2) Depending on the value of the involved channel parameters, the solutions given in (4.4)-(4.10) require a different number of terms to attain an accurate approximation. In this context, the overall convergence speed of these series is achieved faster for small values of both dominant rays (e.g., N_B , and N_E) and power of Bob's dominant specular components (i.e., K_{N_B}). For instance, exhaustive tests have shown that the number of terms to arrive at the desired accuracy (e.g., 10^{-6}) varied from 20 to 30 at Bob and from 4 to 10 at Eve, and the average elapsed times to obtain the accuracy mentioned above were $\sim \{14.1, 27.5, 81.7, 103.5, 114.6\}$ seconds for $N = \{1, \dots, 5\}$, respectively. Moreover, the mathematical representation of the derived series consists of well-known elementary and special functions, which can be easily implemented in software for numerical evaluation.

Fig. 4.1 shows the SOP as a function of $\bar{\gamma}_B$ for different values of dominant specular components $N_B = N_E = N$, by considering the case of balanced amplitudes, i.e., $V_{n,B} = V_{n,E} \forall n$, $n = \{1, \dots, N\}$. For this scenario, the corresponding fading parameters are given by: $K_{dB}^B = 10 \log_{10}(K_B = K_{N_B}) \in \{15, 25\}$ dBs with $K_{dB}^E = 10$ dB, $R_S = 1$ bps/Hz, and $\bar{\gamma}_E = 4$ dB. Note that in all instances, Monte Carlo simulations perfectly match with our derived results. It can be seen that the secrecy performance does not monotonically increase with the number of specular components; instead, notice that the cases with $N_B = 1$ and $N_B = 2$ bound the secrecy performance for a given K_{dB}^B . Also, it is observed that the SOP performance improves with increasing the power of Bob's dominant specular components (i.e., K_{dB}^B) only for odd numbers of rays (i.e., $N = 1, 3$). In the opposite scenario, i.e., increase K_{dB}^B for even numbers of dominant specular waves (i.e., $N = 2, 4$) can be regarded as a worst-case situation in terms of secrecy performance. This is in coherence with the fact that for an even number of dominant specular components of equal amplitudes, the probability of total cancellation between them is larger than when an odd number is considered [157]. This increases fading severity for the desired link more relevantly for large K , which ultimately degrades the SOP. Also, note that for $N = 4$, the performance is very similar to the Rayleigh case. Regarding the asymptotic behavior, it can be noticed that the asymptotic plots accurately approximate the SOP curves in the

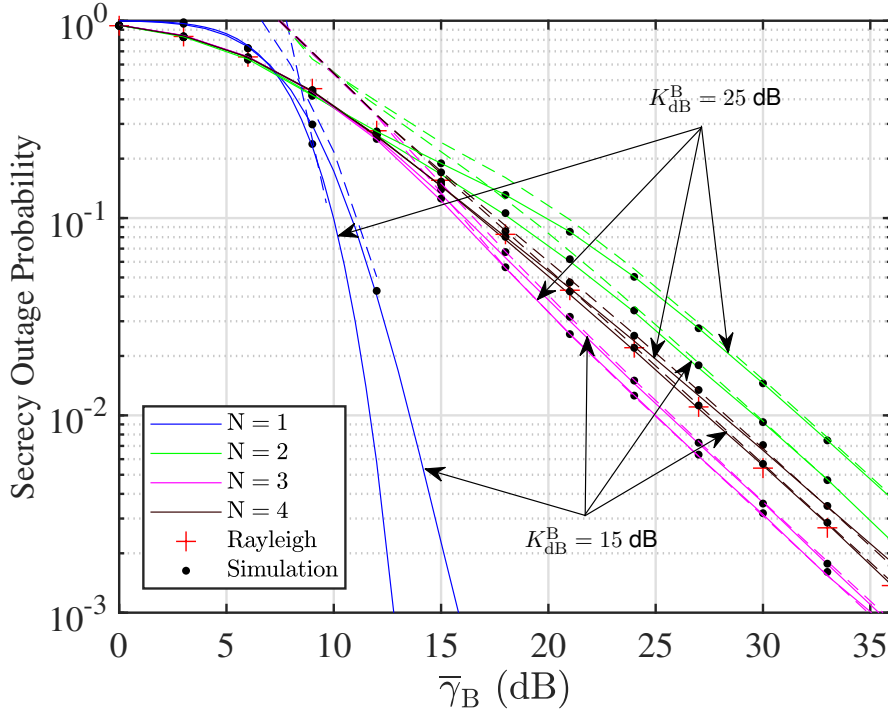


Figure 4.1: SOP vs. $\bar{\gamma}_B$, for different numbers of dominant specular waves N by considering balanced amplitude scenario (i.e., $V_{n,i} = 1$ for $n = 1, \dots, N_i$). For all curves, the parameter values are: $R_S = 1$ bps/Hz, $\bar{\gamma}_E = 4$ dB, $K_{dB}^E = 10$ dB, $\Omega_i = 1$, and $N_i = N$ for $i \in \{B, E\}$. Dashed lines correspond to asymptotic analysis by using expression (4.6).

high-SNR regime. However, all curves have different slopes. The reason for this behavior will be discussed later.

In Fig. 4.2, it is evaluated the SOP vs. $\bar{\gamma}_B$ for different numbers of dominant specular components $N_B = N_E = N$ by considering an unbalanced amplitudes scenario. For seeking of readability, yet without loss of generality, the amplitudes of successive rays are expressed in terms of the amplitude of the first dominant component, as proposed in [87], that is, $V_{n,i} = \alpha_{n,i} V_{1,i}$ for $n = \{2, \dots, N_i\}$, with $0 < \alpha_{n,i} < 1$ and $i \in \{B, E\}$. Considering this, the parameters are set to: $\alpha_{n,i} = \alpha_B = \alpha_E = 0.3$ with $K_{dB}^B \in \{8, 25\}$ dBs, $K_{dB}^E = 0$ dB, $R_S = 1$ bps/Hz, and $\bar{\gamma}_E = 1$ dB. Here, the impact of increasing both the number and the power of Bob's dominant rays for the case of unbalanced amplitudes is investigated. It can be observed in all traces that, unlike on the balanced counterpart, the SOP performance now monotonically improves when rising K_{dB}^B or lowering N , regardless of whether it is even or odd. Notice that a reduced number of dominant specular components at Bob is now benefiting from a secrecy perspective. Also, it can be seen that in all cases, the SOP performance is always better than its Rayleigh counterpart.

Fig. 4.3 evaluates both the SOP and the SOP_A as a function of $\bar{\gamma}_B$, in order to understand the interplay between the number of dominant specular components $N_B = N_E = N$, the amplitude imbalance and the power of the dominant components. The system parameters are set to: $\{\alpha_B, \alpha_E\} \in$

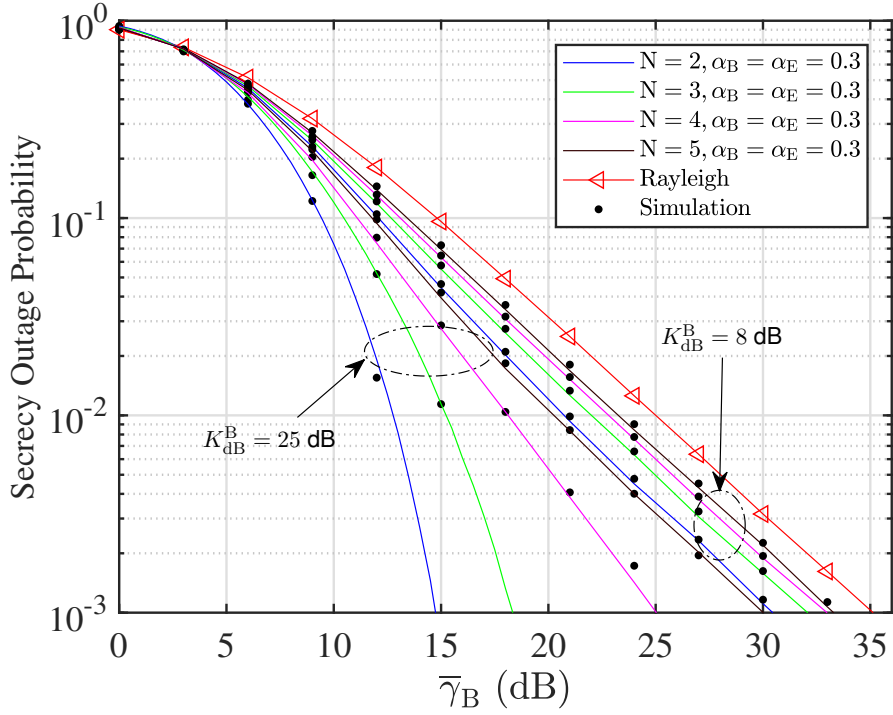


Figure 4.2: SOP in terms of $\bar{\gamma}_B$ for different numbers of dominant specular waves N , by considering unbalanced amplitude case (i.e., $\alpha_{n,i} = \alpha_i = 0.3$). For all cases, the corresponding parameters are set to the following values: $R_S = 1$ bps/Hz, $\bar{\gamma}_E = 1$ dB, $K_{dB}^E = 0$ dB, $\Omega_i = 1$, and $N_i = N$ for $i \in \{B, E\}$.

$\{(0.2, 0.9), (0.9, 0.2)\}$, $R_S = 1$ bps/Hz, $\bar{\gamma}_E = 8$ dB, and $K_{dB}^B = K_{dB}^E = 25$ dB. It can be observed that the worst secrecy performance is attained for cases where the imbalance for the legitimate user α_B is greater than that of α_E , i.e. ($\alpha_B = 0.9, \alpha_E = 0.2$), which is explained as follows: because the amplitudes for the legitimate link are balanced, this is translated into a more severe fading; conversely, the unbalanced amplitudes for the eavesdropper's link indicate a lower fading severity compared to the Rayleigh case. Combining the two effects, the overall SOP performance is hence worse than when assuming Rayleigh fading for both links.

On the other hand, for the cases where α_B is lower than α_E , it can be obtained the desired secrecy performance (i.e., a target SOP) for a lower average SNR at Bob. In such case, some other interesting observations can be made: *i* the secrecy performance for ($\alpha_B = 0.2, \alpha_E = 0.9$), N_i with $i \in \{B, E\}$ is much better than the Rayleigh case. Also, for these scenarios, the increase in the number of dominant specular rays arriving at both Bob and Eve is detrimental from a PLS perspective; and *ii* unlike the ($\alpha_B = 0.2, \alpha_E = 0.9$) case, the worst secrecy performance for ($\alpha_B = 0.9, \alpha_E = 0.2$) is obtained when the number of arriving dominant components at the receiver ends is equal to two, i.e., $N = 2$. Regarding to the high SNR approximation of the SOP, it is clear that its performance is sufficiently tight with regard the exact analytical solution. It is also expected that the SOP_A gradually approximates the exact SOP with higher accuracy as $\bar{\gamma}_E$ increases.

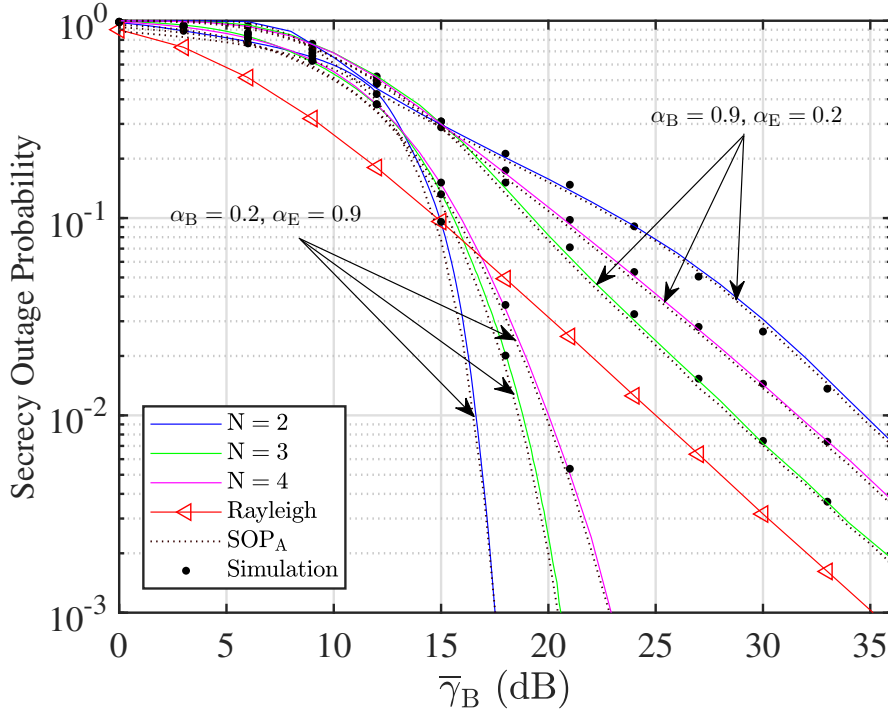


Figure 4.3: SOP vs. $\bar{\gamma}_B$ for different numbers of dominant specular waves N by considering unbalanced amplitude case (i.e., $\{\alpha_B, \alpha_E\} = \{0.2, 0.9\}$ and $\{\alpha_B, \alpha_E\} = \{0.9, 0.2\}$). For all curves, the values of channel parameters are: $R_S = 1$ bps/Hz, $\bar{\gamma}_E = 8$ dB, $K_{dB}^B = K_{dB}^E = 25$ dB, $\Omega_i = 1$, and $N_i = N$ for $i \in \{B, E\}$.

Fig. 4.4 presents the evolution of the SOP as a function of R_S , considering the following channel settings: $\bar{\gamma}_E = 1$ dB, $\bar{\gamma}_B = 8$ dB, $K_{dB}^B = K_{dB}^E = 20$ dB, and $\{\alpha_B, \alpha_E\} = \{0.2, 0.3\}$. Herein, the effect of having a different number of dominant specular rays at both Bob and Eve over the secrecy performance is analyzed. For this purpose, it is assumed a fixed number of rays for the eavesdropper channel, with gradually increasing the number of rays received at Bob. The following cases are considered: $N_E = \{2, 3\}$ and $N_B = \{2, 3, 4, 5\}$, and for the sake of comparison, the figures also include the case $N_B = N_E$. Once again, it can be seen that having a larger number of multipath waves at the legitimate receiver in this unbalanced scenario effectively increases channel variability, causing the SOP to deteriorate when transmitting at a certain secrecy rate R_S . From all curves, out the following two cases as detrimental to the SOP: (i) a fixed N_B , with increasing the number of rays on the eavesdropper's channel and (ii) a fixed N_E , with increasing the number of rays on the Bob's channel. This can be understood by recalling that in the presence of a single dominant specular component for each link and a strong LoS condition, the set-up almost reduces to the AWGN case, for which the SOP is zero as $\bar{\gamma}_B > \bar{\gamma}_E$. Hence, having a reduced number of rays and a dominant component much larger than the remaining specular waves turn out to be beneficial for PLS. Besides, smaller values of R_S can improve the secrecy performance of the system, as expected. Finally, all curves present a better SOP behavior than the Rayleigh fading case.

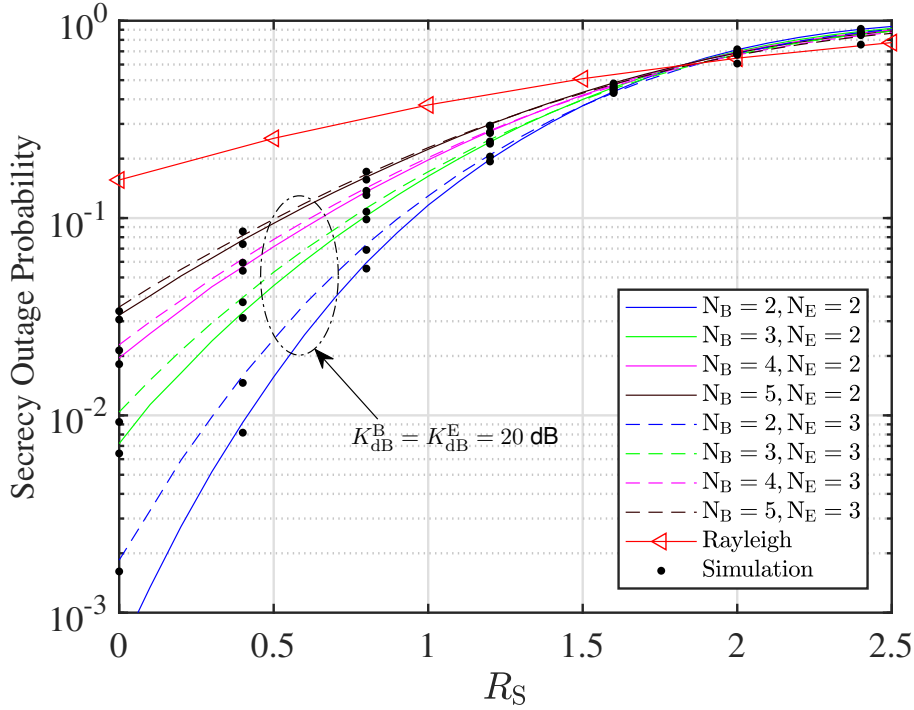


Figure 4.4: SOP in terms of R_S for different numbers of dominant specular waves of $N_B = \{2, 3, 4, 5\}$ with regard to $N_E = \{2, 3\}$ by considering unbalanced amplitude case (i.e., $\{\alpha_B, \alpha_E\} = \{0.2, 0.3\}$). For all curves, the fading parameters are set as: $\bar{\gamma}_E = 1$ dB, $\bar{\gamma}_B = 8$ dB, $K_{dB}^B = K_{dB}^E = 20$ dB, and $\Omega_i = 1$ for $i \in \{B, E\}$.

Next, Fig. 4.5 illustrates the SOP vs. $\bar{\gamma}_B$ for different numbers of rays $N_B = N_E = N$ with $\bar{\gamma}_E = 1$ dB, $K_{dB}^B = 25$ dB, and $K_{dB}^E = 0$ dB. Moreover, the fading parameters are set as: $R_S = \{1, 2.5\}$ with $\alpha = \alpha_B = \alpha_E = 0.15$ and $\alpha = \alpha_B = \alpha_E = 0.30$ for $N = 2, \dots, 4$, and $N = 5$, respectively. From all instances, it can be observed that both the relative amplitudes and the number of the dominant waves play a pivotal role on the secrecy performance. For instance, notice that the decay of the SOP is rather abrupt for $\alpha = 0.15$ and $N = 1, \dots, 4$ regardless of the choice of $R_S = \{1, 2.5\}$. However, when both the number of rays and the relative amplitudes of the rays are increased (say $\alpha = 0.3$ and $N = 5$), then the SOP is dramatically impaired and the decay is now similar to the Rayleigh case. This is in coherence with the observations made in [87] in the limit case of the absence of diffuse scattering, as $\alpha(N_B - 1) < 1$. This finding confirms that the relative amplitudes of the dominant components play a pivotal role in the security design criteria. Finally, all curves over NWDP fading outperform the SOP performance to its corresponding Rayleigh fading cases for the proposed scenarios.

Next, Fig. 4.6 plots the SOP vs. $\bar{\gamma}_B$ and the two asymptotic results given in (4.6), (4.7), respectively. In all the cases, it is employed equal numbers of rays at both B and E, i.e., $N = N_B = N_E$, $R_S = 1$ bps/Hz, $\Omega_B = \Omega_E = 1$, $\bar{\gamma}_E = 8$ dB, $K_{dB}^B = 20$ dB, and $K_{dB}^E = 0$ dB. Also, yet without loss of generality, it is assumed the following cases: *Case I* ($N = 2$): Bob, $V_{2,B} = \alpha_{2,B}V_{1,B}$ with $V_{1,B} = 1$, and $\alpha_{2,B} = 0.2$. Eve, $V_{2,E} = \alpha_{2,E}V_{1,E}$ with $V_{1,E} = 1$, and $\alpha_{2,E} = 0.9$; *Case II* ($N = 3$): Bob, $V_{n,B} = \alpha_{n,B}V_{1,B}$ with

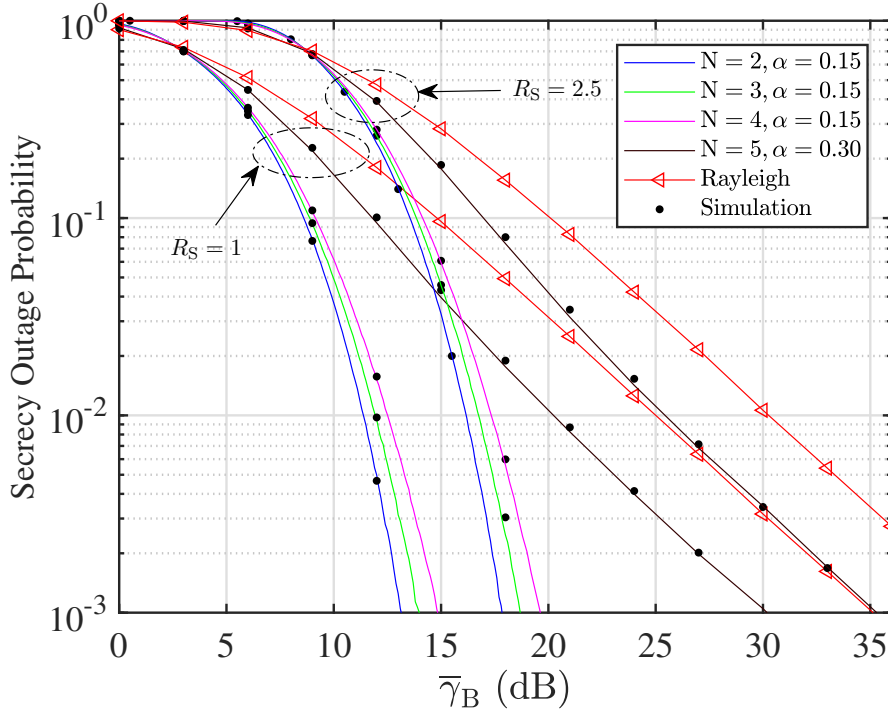


Figure 4.5: SOP vs. $\bar{\gamma}_B$ for different numbers of dominant specular waves $N = N_B = N_E$ by varying the value of R_S and assuming unbalanced amplitudes (i.e., $\alpha = \{0.15, 0.30\}$). Also, $\bar{\gamma}_E = 1$ dB, $K_{dB}^B = 25$ dB, and $K_{dB}^E = 0$ dB.

$V_{1,B} = 1$, $\alpha_{n,B} = 0.5$ for $n = \{2, 3\}$. Eve, $V_{n,E} = 1$ for $n = \{1, 2, 3\}$; **Case III** ($N = 4$): Bob, $V_{n,B} = \alpha_{n,B} V_{1,B}$ with $V_{1,B} = 1$, $\alpha_{n,B} = 0.25$ for $n = \{2, 3, 4\}$. Eve, $V_{n,E} = 1$ for $n = \{1, 2, 3, 4\}$. Here, our primary aim is to analyze the secrecy diversity order of the main links in the proposed scenarios. Firstly, based on the asymptotic expression in (4.7), it can be seen that the secrecy diversity order is one in all instances (see Remark 4). Specifically, the SOP in *Case II* quickly reaches the secrecy diversity order. Conversely, in *Case I* and *III*, it can be pointed out before the SOP curves reach the slope equal to unity, they experience a faster decay (i.e., a steeper slope) for operational ranges of SOP. For instance, if the target SOP is set to 10^{-3} , the exact and asymptotic SOP in *Case I* and *III* are rather dissimilar; hence, the diversity order is not representative of the actual behavior of the SOP. This could be somehow interpreted as an *equivalent* increased secrecy diversity order offered by the fading parameters (i.e., $V_{n,B}$, N_B , and K_{dB}^B) of the NWDP model for some range of SNRs. As mentioned above, such slope's behavior depends on the particular configuration of the parameters of the NWDP model. In those situations on which the condition $\alpha_B (N_B - 1) < 1$ is met, the decay of the SOP is rather steep and behaves similarly as if no diffuse component was present [87] for a certain range of SNR values. In other circumstances, the slope of the SOP rapidly becomes one and the secrecy diversity order dominates the behavior for the operational range of secrecy outage probabilities. On the other hand, from (4.6), it can be observed that the exponents for the $\bar{\gamma}_B$ terms depend on one of the summation indexes (i.e., $(k_B + 1)$). This suggests that each of these terms contributes in different ways to the decay of the SOP, which explains that the slope of the SOP is

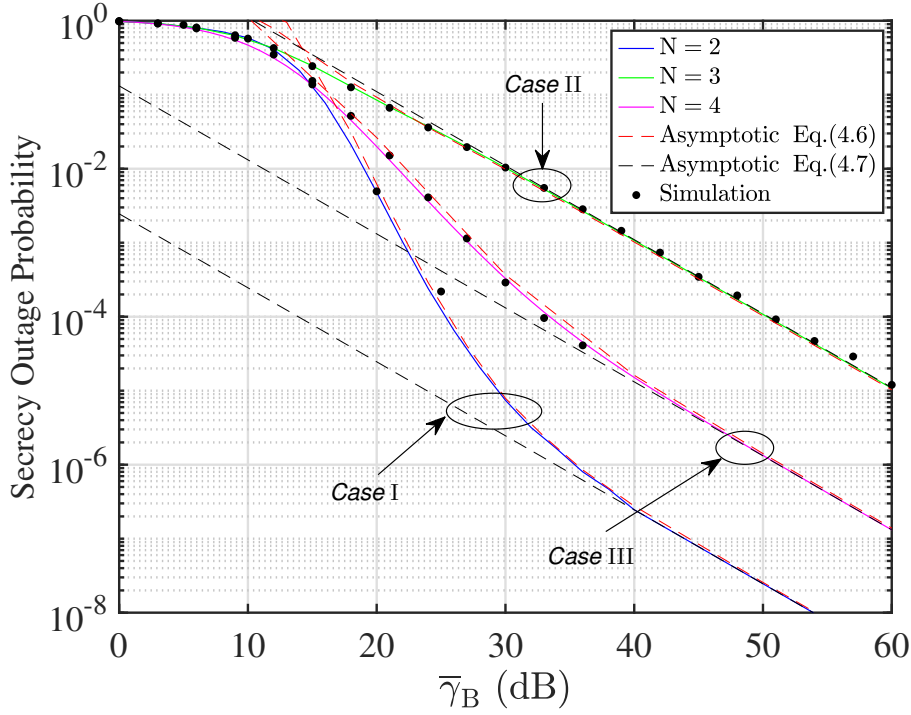


Figure 4.6: SOP vs. $\bar{\gamma}_B$ for different numbers of dominant specular waves $N = N_B = N_E$ by assuming for all cases $R_S = 1$ bps/Hz, $\Omega_B = \Omega_E = 1$, $\bar{\gamma}_E = 8$ dB, and $K_{dB}^B = 20$ dB, and $K_{dB}^E = 0$ dB.

different depending on the range of values of $\bar{\gamma}_B$. As the SNR is increased, it is only the first term of the series, which contributes to the SOP, revealing a diversity secrecy order of one (see the red curves in Fig. 4.6). Finally, notice that the asymptotic analytical in (4.6) is tighter than the asymptotic one given in (4.7) for low-SNR values.

Then, Fig. 4.7 shows the ASC vs. $\bar{\gamma}_B/\bar{\gamma}_E$ for different configurations of N_E , and α_E with $\Omega_B = \Omega_E = 1$, and $K_{dB}^B = K_{dB}^E = 25$ dB. Here, it is assumed the following scenarios: *Case IV* ($N_B = 3, N_E = 2$): Bob, $V_{n,B} = \alpha_{n,B}V_{1,B}$ with $V_{1,B} = 1$, and $\alpha_{n,B} = 0.1$ for $n = \{2, 3\}$. Eve, $V_{2,E} = \alpha_{2,E}V_{1,E}$ with $V_{1,E} = 1$, $\alpha_{2,E} \in \{0.1, 0.5, 1\}$, and $\bar{\gamma}_E = 25$ dB; *Case V* ($N_B = 2, N_E \in \{1, 2, 3, 4\}$): Bob, $V_{n,B} = 1$ for $n = \{1, 2\}$. Eve, $N_E = 1$: $V_{1,E} = 1$, $N_E = 2$: $V_{2,E} = \alpha_{2,E}V_{1,E}$ with $\alpha_{2,E} = 0.9$, $N_E = 3$: $V_{n,E} = \alpha_{n,E}V_{n,E}$ with $\alpha_{n,E} = 0.9$, for $n = \{2, 3\}$, $N_E = 4$: $V_{n,E} = \alpha_{n,E}V_{n,E}$ with $\alpha_{n,E} = 0.9$, for $n = \{2, 3, 4\}$ and $\bar{\gamma}_E = 15$ dB. Also, with the above-described scenarios, the goal is to investigate the impact of the eavesdropper's fading parameters on the ASC performance. To this end, first, note in *Case IV* that, the combination of more specular components in Bob than Eve and the low amplitude values related to such dominant rays at Eve derives into a poor ASC performance. Conversely, high amplitude values of the specular components at the eavesdropper lead to better ASC performance, as expected. On the other hand, for the proposed scenario in *Case IV*, it can be observed that the increase in the number of specular components at Eve practically does not influence the ASC performance. One of the reasons for this behavior is that the amplitudes of Eve's rays take high values regardless of the number of dominant components. This fact results in fading, which prevents improving the quality of the wiretap channel.

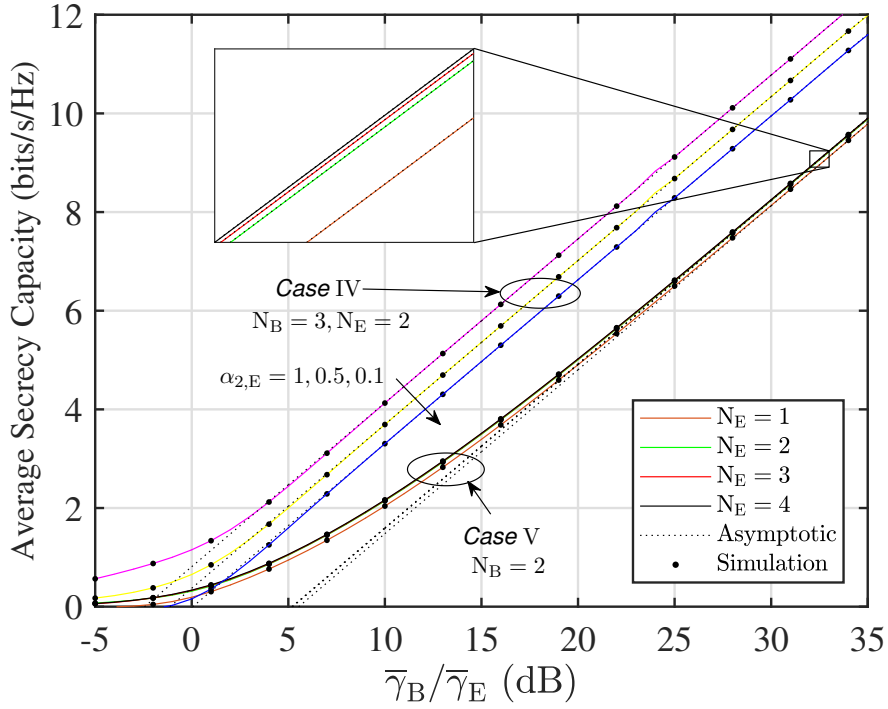


Figure 4.7: ASC vs. $\bar{\gamma}_B/\bar{\gamma}_E$ for different configurations of N_E , and α_E with $\Omega_B = \Omega_E = 1$, and $K_{dB}^B = K_{dB}^E = 25$ dB.

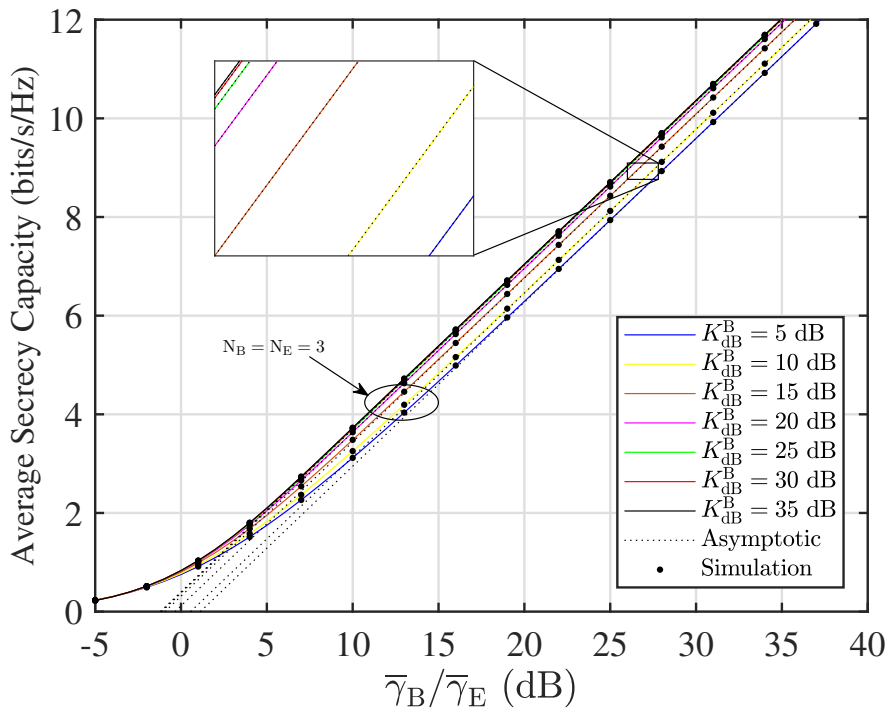


Figure 4.8: ASC vs. $\bar{\gamma}_B/\bar{\gamma}_E$ by varying K_{dB}^B for a fixed $K_{dB}^E = 0$ dB with $\Omega_B = \Omega_E = 1$, and $\bar{\gamma}_E = 10$ dB.

Finally, Fig. 4.8 shows the ASC as a function of $\bar{\gamma}_B/\bar{\gamma}_E$ by varying K_{dB}^B for a fixed $K_{\text{dB}}^E = 0$ dB with $\Omega_B = \Omega_E = 1$, and $\bar{\gamma}_E = 10$ dB. The remainder parameters are set to: Bob ($N_B = 3$), $V_{n,B} = \alpha_{n,B}V_{1,B}$ with $V_{1,B} = 1$, $\alpha_{n,B} = 0.1$ for $n = \{2, 3\}$. Eve ($N_E = 3$), $V_{n,E} = 1$ for $n = \{1, 2, 3\}$. Here, the goal is to explore the impact of increase the power of Bob's dominant components on the ASC performance. Therefore, based on all curves, it can be seen that the K_{dB}^B configuration contributes to improving the ASC performance proportionally. However, this behavior happens up to a particular K_{dB}^B value (i.e., 30 dB); after that, the ASC remains identical. From a secrecy perspective, this result is a good insight into future mobile networks' design criteria. Finally, from all the instances in Fig. 4.7 and Fig. 4.8, it can be observed how for high-SNR values, the ASC curves exhibit a linear behavior in a log-scale, which are perfectly captured by the asymptotic ASC expressions.

4.4 CONCLUSIONS

This work explored how the explicit consideration of the incident waves arriving at the receiver ends may impact PLS performance in the context of wireless fading channels. The analytical expressions derived here complement and generalize those previously reported works in the literature concerning generalized fading channel models. Our findings also support the need for using ray-based fading models in those environments in which conventional fading models cannot adequately characterize an arbitrary number of dominant specular waves (e.g., mm-Wave communications). The main take-aways of our work can be summarized as: (i) abundant dominant specular rays impair the SOP, so scenarios with a reduced number of rays arriving at both Bob and Eve are beneficial whenever $\bar{\gamma}_B > \bar{\gamma}_E$; (ii) balanced amplitudes for the eavesdropper's link and unbalanced amplitudes for the desired link are the most favorable case from a PLS perspective; (iii) a significant increase on the power of Bob's dominant specular components with respect to the power of Eve's dominant specular components (i.e., $K_B \gg K_E$), in the case of balanced amplitudes, is a worst-case scenario for secrecy performance; (iv) the combined effect of decreasing the relative amplitudes at Eve, i.e., α_E and low values of relative amplitudes at the legitimate receiver, i.e. α_B , leads to worse the ASC performance (see Case IV in Fig 4.7).

5 SECURE TRANSMISSION WITH ANTENNA SELECTION IN MIMO κ - μ SHADOWED FADING CHANNELS

This chapter investigates the impact of considering realistic propagation conditions on the achievable PLS performance of a MIMO system in the presence of an eavesdropper equipped with multiple antennas. Specifically, this research concentrates on the κ - μ shadowed fading model because its physical underpinnings capture a wide range of propagation conditions, while, at the same time, it allows for a much better tractability than other state-of-the-art fading models. By considering TAS and MRC reception at the legitimate and eavesdropper's receiver sides, two relevant scenarios are studied, namely, (i) the transmitter does not know the eavesdropper's CSI, and (ii) the transmitter has knowledge of the CSI of the eavesdropper link. To this end, due to the antenna selection procedure, new and tractable expressions for the PDF and CDF of the maximum of i.i.d. RVs associated with the legitimate paths under κ - μ shadowed fading are derived. Based on these results, novel closed-form expressions for the SOP and the ASC are found in a TAS/MRC configuration to assess the PLS performance in both passive and active eavesdropping scenarios. Moreover, analytical asymptotic expressions of the SOP and ASC are performed in the high-SNR regime. Based on these formulations, some valuable insights on how the fading parameters and the numbers of antennas at the receiver ends (i.e., Bob and Eve) impact the secrecy performance of the MIMO system are also provided.

5.1 SYSTEM AND CHANNEL MODEL STATISTICS

5.1.1 System Model

Based on the TAS/MRC configuration given in Section 2.3, it is considered the classic three-node model, as illustrated in Fig. 5.1, where a source node Alice (A) sends confidential information to a legitimate destination node Bob (B), while an eavesdropper Eve (E) attempts to intercept this information through the eavesdropper channel. In this system, all nodes, i.e., the transmitter, the receiver, and the eavesdropper, are equipped with multiple antennas denoted by N_A , N_B , and N_E , respectively.

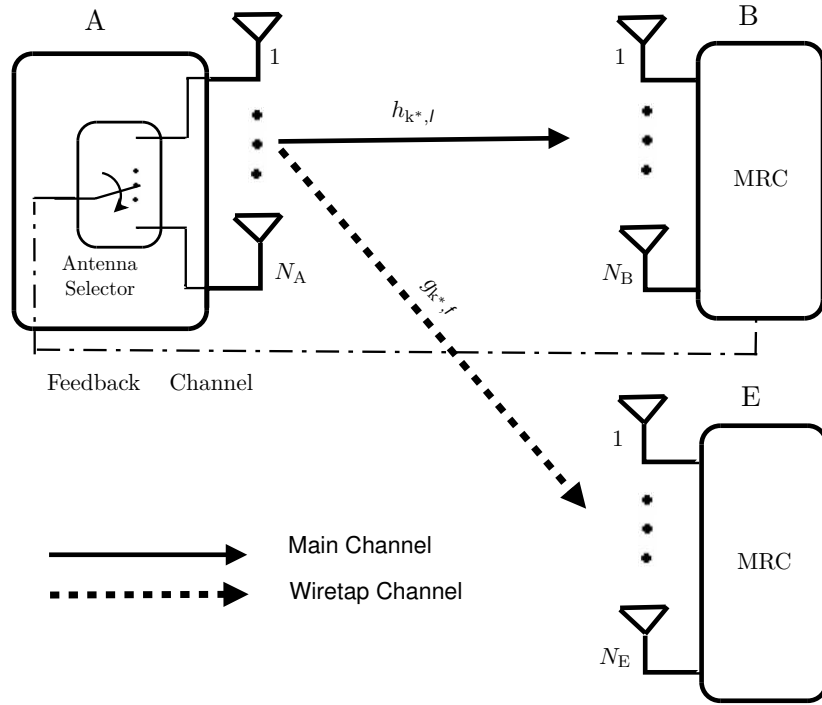


Figure 5.1: A general TAS/MRC MIMO network consisting of a legitimate pair and one eavesdropper, where the transmitter Alice (A), the receiver Bob (B), and the eavesdropper Eve (E) are equipped with N_A , N_B , and N_E antennas, respectively. This figure is based on [98].

5.1.2 Channel Model

Here, it is assumed that both the legitimate and eavesdropper channels experience i.i.d. quasi-static κ - μ shadowed fading. Therefore, the corresponding PDF and CDF of the instantaneous SNR of the RV γ following κ - μ shadowed fading can be expressed as a finite mixture of gamma distributions by [128]^[1]

□ **If** $m < \mu$

$$f_\gamma(\gamma) = \sum_{j=1}^{\mu-m} A_{1,j} f_\gamma^G(\omega_{A1}; \mu - m - j + 1; \gamma) + \sum_{j=1}^m A_{2,j} f_\gamma^G(\omega_{A2}; m - j + 1; \gamma), \quad (5.1a)$$

$$F_\gamma(\gamma) = 1 - \sum_{j=1}^{\mu-m} A_{1,j} \exp\left(-\frac{\gamma}{\Delta_1}\right) \sum_{r=0}^{\mu-m-j} \frac{1}{r!} \left(\frac{\gamma}{\Delta_1}\right)^r - \sum_{j=1}^m A_{2,j} \exp\left(-\frac{\gamma}{\Delta_2}\right) \sum_{r=0}^{m-j} \frac{1}{r!} \left(\frac{\gamma}{\Delta_2}\right)^r, \quad (5.1b)$$

□ **If** $m \geq \mu$

^[1] Noteworthy, the PDF and CDF of the κ - μ shadowed distribution can be represented in many ways (*i*) hypergeometric functions as proposed in its original format [21]; (*ii*) an infinite series in terms of Laguerre polynomials [10], and (*iii*) an infinite [158] and finite [128] mixture of gamma distributions. This work sticks to the last one because of its mathematically tractable expressions, well-suited to dealing with TAS/MRC systems.

$$f_\gamma(\gamma) = \sum_{j=0}^{m-\mu} B_j f_\gamma^G(\omega_B; m-j; \gamma), \quad (5.2a)$$

$$F_\gamma(\gamma) = 1 - \sum_{j=0}^{m-\mu} B_j \exp\left(-\frac{\gamma}{\Delta_2}\right) \sum_{r=0}^{m-j-1} \frac{1}{r!} \left(\frac{\gamma}{\Delta_2}\right)^r, \quad (5.2b)$$

where $f_X^G(\bar{\gamma}; \tilde{m}; x)$ denotes the PDF of a RV X that follows a gamma distribution, defined as

$$f_X^G(\bar{\gamma}; \tilde{m}; x) = \left(\frac{\tilde{m}}{\bar{\gamma}}\right)^{\tilde{m}} \frac{x^{\tilde{m}-1}}{(\tilde{m}-1)!} \exp\left(-\frac{x\tilde{m}}{\bar{\gamma}}\right), \quad (5.3)$$

and

$$\begin{aligned} A_{1,j} &= (-1)^m \binom{m+j-2}{j-1} \left(\frac{m}{\mu\kappa+m}\right)^m \left(\frac{\mu\kappa}{\mu\kappa+m}\right)^{-m-j+1}, \\ A_{2,j} &= (-1)^{j-1} \binom{\mu-m+j-2}{j-1} \times \left(\frac{m}{\mu\kappa+m}\right)^{j-1} \left(\frac{\mu\kappa}{\mu\kappa+m}\right)^{m-\mu-j+1}, \\ B_j &= \binom{m-\mu}{j} \left(\frac{m}{\mu\kappa+m}\right)^j \left(\frac{\mu\kappa}{\mu\kappa+m}\right)^{m-\mu-j}, \end{aligned} \quad (5.4)$$

and

$$\begin{aligned} \omega_{A1} &= \Delta_1 (\mu - m - j + 1), \\ \omega_{A2} &= \Delta_2 (m - j + 1), \\ \omega_B &= \Delta_2 (m - j), \end{aligned} \quad (5.5)$$

where

$$\begin{aligned} \Delta_1 &= \frac{\bar{\gamma}}{\mu(1+\kappa)}, \\ \Delta_2 &= \frac{\mu\kappa+m}{m} \frac{\bar{\gamma}}{\mu(1+\kappa)}. \end{aligned} \quad (5.6)$$

In the above formulations, $\bar{\gamma} = \mathbb{E}[\gamma]$ is the average SNR. Besides, μ , m , and κ are the fading parameters that denote the number of the multipath clusters, the shadowing severity index, and the ratio between the total power of the dominant components associated to the LoS and the total power of the scattered waves, respectively (for more details see Section 2.2.2.3). Finally, it is worth mentioning that due to the antenna selection procedure, the CDFs given in (5.1b) and (5.2b) should be reformulated in order to derive the maximum of i.i.d. κ - μ shadowed RVs, as will be seen in Appendix E.1.

5.1.3 Transmission Scheme

As mentioned in section 2.3.1.1, for the proposed MIMO wiretap system, the optimum TAS protocol selects the strongest antenna between the legitimate entities for transmission, i.e. the antenna that maximizes the instantaneous SNR between Alice and Bob. From a secrecy perspective, this allows to maximize the channel capacity and fully exploit the multi-antenna diversity at the transmitter, while the optimum TAS for Bob corresponds to a random transmit antenna for Eve. Moreover, in an effort to exploit the antenna diversity at the receiver ends, it is assumed that the MRC technique is employed at both Bob and Eve. Therefore, from (2.44), the index of the selected antenna at the transmitter, here for notational convenience denoted by k^* , is given by

$$k^* = \arg \max_{1 \leq k \leq N_A} \sum_{l=1}^{N_B} |h_{k,l}|^2, \quad (5.7)$$

where $h_{k,l}$ is the channel coefficient of the link between k -th transmitting antenna at Alice and l -th receive antenna at Bob. The index of the selected antenna is reported to Alice through a feedback channel. Based on the TAS/MRC setup, the received signals at the l -th antenna of Bob and at the r -th ($1 \leq f \leq N_E$) antenna of Eve are given by

$$y_{B,l} = \sqrt{P} h_{k^*,l} x + n_l, \quad (5.8a)$$

$$y_{E,f} = \sqrt{P} g_{k^*,f} x + n_f, \quad (5.8b)$$

where P is the average transmit power, x denotes the secret message to be transmitted, $h_{k^*,l}$ is the κ - μ shadowed channel coefficients of the link between the selected antenna k^* at Alice and the l -th receive antenna at Bob. Likewise, $g_{k^*,f}$ is the κ - μ shadowed channel coefficient of the link between the selected antenna k^* at Alice, and the f -th receive antenna at Eve. Besides, n_l and n_f are AWGN noise at the receivers of the l -th antenna of Bob and at the f -th antenna of Eve with zero mean and variance σ_w^2 with $w \in \{B, E\}$, respectively. Based on (5.8), the corresponding instantaneous SNRs at the receivers can be expressed as

$$\gamma_B = \frac{P \sum_{l=1}^{N_B} |h_{k^*,l}|^2}{\sigma_B^2}, \quad (5.9a)$$

$$\gamma_E = \frac{P \sum_{f=1}^{N_E} |g_{k^*,f}|^2}{\sigma_E^2}. \quad (5.9b)$$

5.1.4 Channel Statistics for TAS/MRC setup

Here, the theoretical framework used to obtain the PDF and CDF of the main and the eavesdropper channels under the TAS/MRC configuration is introduced. These formulations will be used on the secrecy analysis in the next sections.

Concerning the eavesdropper channel, it is defined $\gamma_{k^*,f} = \frac{P|g_{k^*,f}|^2}{\sigma_E^2}$ as the instantaneous received SNR of the f -th diversity branch of the MRC receiver at Eve. Now, by considering N_E i.i.d. κ - μ shadowed RVs, i.e., $\gamma_{k^*,f}(\bar{\gamma}_E, \kappa_E, \mu_E, m_E)$ for $f = \{1, \dots, N_E\}$, the sum of these RVs is another κ - μ shadowed RV with scaled parameters, i.e., [21, Proposition 1]

$$\sum_{f=1}^{N_E} \gamma_{k^*,f}(\bar{\gamma}_E, \kappa_E, \mu_E, m_E) = \gamma_E(N_E \bar{\gamma}_E, \kappa_E, N_E \mu_E, N_E m_E) \quad (5.10)$$

Departing from (5.2) and applying the relationship given in (5.10), the PDF and CDF at Eve are given by

□ **If** $m_E < \mu_E$

$$f_{\gamma_E}(\gamma_E) = \sum_{j=1}^{\eta_E} A_{1,j}^E f_G(\omega_{A1}^E; \eta_E - j + 1; \gamma_E) + \sum_{j=1}^{\nu_E} A_{2,j}^E f_G(\omega_{A2}^E; \nu_E - j + 1; \gamma_E), \quad (5.11a)$$

$$F_{\gamma_E}(\gamma_E) = 1 - \sum_{j=1}^{\eta_E} A_{1,j}^E \exp\left(-\frac{\gamma_E}{\Delta_1^E}\right) \sum_{r=0}^{\eta_E-j} \frac{1}{r!} \left(\frac{\gamma_E}{\Delta_1^E}\right)^r - \sum_{j=1}^{\nu_E} A_{2,j}^E \exp\left(-\frac{\gamma_E}{\Delta_2^E}\right) \sum_{r=0}^{\nu_E-j} \frac{1}{r!} \left(\frac{\gamma_E}{\Delta_2^E}\right)^r, \quad (5.11b)$$

where $\eta_E = N_E(\mu_E - m_E)$, and $\nu_E = N_E m_E$.

□ **If** $m_E \geq \mu_E$

$$f_{\gamma_E}(\gamma_E) = \sum_{j=0}^{\beta_E} B_j^E f_G(\omega_B^E; \nu_E - j; \gamma_E), \quad (5.12a)$$

$$F_{\gamma_E}(\gamma_E) = 1 - \sum_{j=0}^{\beta_E} B_j^E \exp\left(-\frac{\gamma_E}{\Delta_2^E}\right) \sum_{r=0}^{\nu_E-j-1} \frac{1}{r!} \left(\frac{\gamma_E}{\Delta_2^E}\right)^r, \quad (5.12b)$$

where $\beta_E = N_E(m_E - \mu_E)$. For notational convenience, all the coefficients marked with superscripts E (e.g., Δ_1^E) refer to the fading parameters at Eve, which can be obtained from (5.4) to (5.6) by substituting $\bar{\gamma}$, μ , m and κ by $N_E \bar{\gamma}_E$, $N_E \mu_E$, $N_E m_E$, and κ_E , respectively.

Regarding the legitimate link, it is defined $\gamma_{k^*,l} = \frac{P|h_{k^*,l}|^2}{\sigma_B^2}$ for $f = \{1, \dots, N_B\}$ as the instantaneous received SNR of the l -th diversity branch of the MRC receiver at Bob. Based on this, the CDF and PDF of $\gamma_B = \sum_{l=1}^{N_B} \gamma_{k^*,l}$ are respectively given in the following propositions.

Proposition 10. *The CDF of γ_B is given by*

□ If $m_B < \mu_B$

$$\begin{aligned}
F_{\gamma_B}(\gamma_B) = & 1 + \sum_{k=1}^{N_A} (-1)^k \binom{N_A}{k} \sum_{c=0}^k \binom{k}{c} \sum_{\rho(c, \nu_B)} \frac{c!}{p_1! \cdots p_{\nu_B}!} \left[\prod_{q=1}^{\nu_B} \left(\frac{\left(\frac{1}{\Delta_2^B}\right)^{\nu_B - q}}{(\nu_B - q)!} \sum_{z=\nu_B+1-q}^{\nu_B} A_{2, \nu_B+1-z}^B \right)^{p_q} \right] \\
& \times \exp\left(-\gamma_B \left(\frac{k-c}{\Delta_1^B}\right)\right) \sum_{\rho(k-c, \eta_B)} \frac{(k-c)!}{s_1! \cdots s_{\eta_B}!} \left[\prod_{t=1}^{\eta_B} \left(\frac{\left(\frac{1}{\Delta_1^B}\right)^{\eta_B - t}}{(\eta_B - t)!} \sum_{z=\eta_B+1-t}^{\eta_B} A_{1, \eta_B+1-z}^B \right)^{s_t} \right] \\
& \times \exp\left(-\gamma_B \left(\frac{c}{\Delta_2^B}\right)\right) \gamma_B^{\sum_{t=1}^{\eta_B} (\eta_B - t) s_t + \sum_{q=1}^{\nu_B} (\nu_B - q) p_q}, \tag{5.13}
\end{aligned}$$

where $\eta_B = N_B(\mu_B - m_B)$, $\nu_B = N_B m_B$. As in the previous case, all the coefficients marked with superscripts B (e.g., Δ_1^B) refer to the fading parameters at Bob, which can be obtained from (5.4) to (5.6) by substituting $\bar{\gamma}$ for $N_B \bar{\gamma}_B$, μ for $N_B \mu_B$, m for $N_B m_B$, and κ for κ_B . Also, based on the multinomial theorem [149, Eq. (24.1.2)], it follows that $\rho(k-c, \eta_B) = \left\{ (s_1, s_2, \dots, s_{\eta_B}) : s_t \in \mathbb{N}, \sum_{t=1}^{\eta_B} s_t = k-c \right\}$, and similarly $\rho(c, \nu_B) = \left\{ (p_1, p_2, \dots, p_{\nu_B}) : p_q \in \mathbb{N}, \sum_{q=1}^{\nu_B} p_q = c \right\}$.

□ If $m_B \geq \mu_B$

$$\begin{aligned}
F_{\gamma_B}(\gamma_B) = & 1 + \sum_{k=1}^{N_A} (-1)^k \binom{N_A}{k} \sum_{\rho(k, \nu_B)} \frac{k!}{s_1! \cdots s_{\nu_B}!} \left[\prod_{t=1}^{\nu_B} \left(\frac{\left(\frac{1}{\Delta_2^B}\right)^{\nu_B - t}}{(\nu_B - t)!} \sum_{z=\beta_B+1-\mathcal{T}(j-1)}^{\beta_B} B_{\beta_B-z}^B \right)^{s_t} \right] \\
& \times \exp\left(-\gamma_B \left(\frac{k}{\Delta_2^B}\right)\right) \gamma_B^{\sum_{t=1}^{\nu_B} (\nu_B - t) s_t}, \tag{5.14}
\end{aligned}$$

where $\rho(k, \nu_B) = \left\{ (s_1, s_2, \dots, s_{\nu_B}) : s_t \in \mathbb{N}, \sum_{t=1}^{\nu_B} s_t = k \right\}$ and $\beta_B = N_B(m_B - \mu_B)$.

Proof. See Appendix E.1. □

Proposition 11. *By taking the derivative of (5.13) and (5.14) with respect to γ_B , the PDFs at Bob can be obtained as*

□ If $m_B < \mu_B$

$$\begin{aligned}
f_{\gamma_B}(\gamma_B) &= \sum_{k=1}^{N_A} (-1)^k \binom{N_A}{k} \sum_{c=0}^k \binom{k}{c} \sum_{\rho(c, \nu_B)} \frac{c!}{p_1! \cdots p_{\nu_B}!} \left[\prod_{q=1}^{\nu_B} \left(\frac{\left(\frac{1}{\Delta_2^B}\right)^{\nu_B-q}}{(\nu_B-q)!} \sum_{z=\nu_B+1-q}^{\nu_B} A_{2, \nu_B+1-z}^B \right)^{p_q} \right] \\
&\times \frac{\exp\left(-\gamma_B \left(\frac{k-c}{\Delta_1^B} + \frac{c}{\Delta_2^B}\right)\right)}{\Delta_1^B \Delta_2^B} \sum_{\rho(k-c, \eta_B)} \frac{(k-c)!}{s_1! \cdots s_{\eta_B}!} \left[\prod_{t=1}^{\eta_B} \left(\frac{\left(\frac{1}{\Delta_1^B}\right)^{\eta_B-t}}{(\eta_B-t)!} \sum_{z=\eta_B+1-t}^{\eta_B} A_{1, \eta_B+1-z}^B \right)^{s_t} \right] \\
&\times \gamma_B^{-1 + \sum_{t=1}^{\eta_B} (\eta_B-t)s_t + \sum_{q=1}^{\nu_B} (\nu_B-q)p_q} \left(\Delta_1^B \Delta_2^B \left(\sum_{t=1}^{\eta_B} (\eta_B-t)s_t + \sum_{q=1}^{\nu_B} (\nu_B-q)p_q \right) \right. \\
&\left. - \gamma_B \left(\Delta_1^B c - \Delta_2^B (c-k) \right) \right). \tag{5.15}
\end{aligned}$$

□ If $m_B \geq \mu_B$

$$\begin{aligned}
f_{\gamma_B}(\gamma_B) &= \sum_{k=1}^{N_A} (-1)^k \binom{N_A}{k} \sum_{\rho(k, \nu_B)} \frac{k!}{s_1! \cdots s_{\nu_B}!} \left[\prod_{t=1}^{\nu_B} \left(\frac{\left(\frac{1}{\Delta_2^B}\right)^{\nu_B-t}}{(\nu_B-t)!} \sum_{z=\beta_B+1-\mathcal{T}(j-1)}^{\beta_B} B_{\beta_B-z}^B \right)^{s_t} \right] \\
&\times \frac{\exp\left(-\frac{k\gamma_B}{\Delta_2^B}\right)}{\Delta_2^B} \gamma_B^{-1 + \sum_{t=1}^{\nu_B} (\nu_B-t)s_t} \left(\Delta_2^B \sum_{t=1}^{\nu_B} (\nu_B-t)s_t - k\gamma_B \right). \tag{5.16}
\end{aligned}$$

5.2 SECRECY METRICS

In this section, based on the above formulations given in 5.1.4, analytical expressions for the SOP, ASC and high-SNR approximations of the SOP and ASC under TAS/MRC configuration by assuming κ - μ shadowed fading channels are derived.

5.2.1 SOP Analysis

As in the SOP analysis for the NWDP model, it is considered a silent eavesdropper whose CSI is not available for Alice. Therefore, Alice selects a constant secrecy rate R_S to transmit information to Bob. In practice, this configuration is associated with a passive eavesdropping attack (see Section 2.1.2.2). By using (5.11a),(5.13) and (5.12a),(5.14) into (2.5), the SOP expressions can be obtained as stated in the following Proposition.

Proposition 12. *The SOP for $m_i < \mu_i$ and $m_i \geq \mu_i$ with $i \in \{B, E\}$ over i.i.d. κ - μ shadowed fading channels can be obtained as (5.17) and (5.18), respectively.*

$$\begin{aligned}
\text{SOP} &= \sum_{k=0}^{N_A} (-1)^k \binom{N_A}{k} \sum_{c=0}^k \binom{k}{c} \sum_{\rho(k-c, \eta_B)} \frac{(k-c)!}{s_1! \cdots s_{\eta_B}!} \left[\prod_{t=1}^{\eta_B} \left(\frac{\left(\frac{1}{\Delta_1^B}\right)^{\eta_B-t}}{(\eta_B-t)!} \sum_{z=\eta_B+1-t}^{\eta_B} A_{1, \eta_B+1-z}^B \right)^{s_t} \right] \\
&\times \sum_{\rho(c, \nu_B)} \frac{c!}{p_1! \cdots p_{\nu_B}!} \left[\prod_{q=1}^{\nu_B} \left(\frac{\left(\frac{1}{\Delta_2^B}\right)^{\nu_B-q}}{(\nu_B-q)!} \sum_{z=\nu_B+1-q}^{\nu_B} A_{2, \nu_B+1-z}^B \right)^{p_q} \right] \exp \left(-(\tau-1) \left(\frac{k-c}{\Delta_1^B} + \frac{c}{\Delta_2^B} \right) \right) \\
&\times \sum_{b=0}^{\sum_{t=1}^{\eta_B} (\eta_B-t)s_t + \sum_{q=1}^{\nu_B} (\nu_B-q)p_q} \binom{\sum_{t=1}^{\eta_B} (\eta_B-t)s_t + \sum_{q=1}^{\nu_B} (\nu_B-q)p_q}{b} (\tau-1)^{\sum_{t=1}^{\eta_B} (\eta_B-t)s_t + \sum_{q=1}^{\nu_B} (\nu_B-q)p_q - b} \\
&\times (\tau)^b \left[\sum_{j=1}^{\eta_E} \left(\frac{\eta_E - j + 1}{\omega_{A1}^E} \right)^{\eta_E - j + 1} \frac{A_{1,j}^E}{(\eta_E - j)!} \left(\frac{\tau(k-c)}{\Delta_1^B} + \frac{\tau c}{\Delta_2^B} + \frac{\eta_E - j + 1}{\omega_{A1}^E} \right)^{-1-b+j-\eta_E} \right. \\
&\times \Gamma(1+b-j+\eta_E) + \sum_{j=1}^{\nu_E} \frac{A_{2,j}^E}{(\nu_E - j)!} \left(\frac{\tau(k-c)}{\Delta_1^B} + \frac{\tau c}{\Delta_2^B} + \frac{\nu_E - j + 1}{\omega_{A1}^E} \right)^{-1-b+j-\nu_E} \Gamma(1+b-j+\nu_E) \\
&\left. \times \left(\frac{\nu_E - j + 1}{\omega_{A2}^E} \right)^{\nu_E - j + 1} \right]. \tag{5.17}
\end{aligned}$$

$$\begin{aligned}
\text{SOP} &= \sum_{k=0}^{N_A} (-1)^k \binom{N_A}{k} \exp \left(-k \frac{(\tau-1)}{\Delta_2^B} \right) \sum_{\rho(k, \nu_B)} \frac{k!}{s_1! \cdots s_{\nu_B}!} \left[\prod_{t=1}^{\nu_B} \left(\frac{\left(\frac{1}{\Delta_2^B}\right)^{\nu_B-t}}{(\nu_B-t)!} \sum_{z=\beta_B+1-\mathcal{T}(j-1)}^{\beta_B} B_{\beta_B-z}^B \right)^{s_t} \right] \\
&\times \sum_{b=0}^{\sum_{t=1}^{\nu_B} (\nu_B-t)s_t} \tau^b \binom{\sum_{t=1}^{\nu_B} (\nu_B-t)s_t}{b} (\tau-1)^{\sum_{t=1}^{\nu_B} (\nu_B-t)s_t - b} \sum_{j=0}^{\beta_E} \frac{B_j^E}{\nu_E - j - 1} \left(\frac{\nu_E - j}{\omega_B^E} \right)^{\nu_E - j} \Gamma(b-j+\nu_E) \\
&\times \left(\frac{k\tau}{\Delta_2^B} + \frac{\nu_E - j}{\omega_B^E} \right)^{j-b-\nu_E}. \tag{5.18}
\end{aligned}$$

Proof. See Appendix E.2. □

5.2.2 Asymptotic SOP Analysis

Here, an asymptotic closed-form formulation of the SOP is derived to gain more insights into the impact of the κ - μ shadowed's fading parameters on the PLS performance of TAS/MRC configuration. For that purpose, it is considered the behaviour at the high SNR regime of the legitimate link, where $\bar{\gamma}_B \rightarrow \infty$ while $\bar{\gamma}_E$ is kept fixed, i.e., the case in which Alice (A) is very close to Bob (B) and Eve (E) is located far away (see Section 2.1.2.3). Our aim is to express the asymptotic SOP expression in

the form (2.7). Therefore, the expression for the asymptote of the SOP over κ - μ shadowed fading channels is given in the following Proposition.

Proposition 13. *The asymptotic closed-form expression of the SOP over i.i.d. κ - μ shadowed can be obtained as*

$$\begin{aligned} \text{SOP}^\infty &\simeq \left(\frac{m_B^{N_B m_B} (1 + \kappa_B)^{N_B \mu_B} \mu_B^{N_B \mu_B - 1} \tau^{N_B \mu_B}}{N_B \bar{\gamma}_B^{N_B \mu_B} (m_B + \kappa_B \mu_B)^{N_B m_B} \Gamma(N_B \mu_B)} \right)^{N_A} \frac{m_E^{N_E m_E}}{\Gamma(N_E \mu_E) (\mu_E \kappa_E + m_E)^{N_E m_E}} \\ &\times \left(\frac{\mu_E (1 + \kappa_E)}{\bar{\gamma}_E} \right)^{-N_A N_B \mu_B} {}_2F_1 \left(N_E m_E, N_A N_B \mu_B + N_E \mu_E, N_E \mu_E, \frac{\kappa_E \mu_E}{m_E + \kappa_E \mu_E} \right) \\ &\times \Gamma(N_A N_B \mu_B + N_E \mu_E). \end{aligned} \quad (5.19)$$

Proof. See Appendix E.3. □

Remark 5. *Comparing (2.7), i.e., $\text{SOP}^\infty \simeq G_c \bar{\gamma}_B^{-G_d}$ with respect to (5.19), it can be noticed that the secrecy diversity gain is given by $G_d = N_A N_B \mu_B$. This means that, the secrecy diversity gain is directly affected by the number of antennas (i.e., N_A and/or N_B) or the number of wave clusters arriving at Bob. Interestingly, neither the LoS condition through κ_B nor the LoS fluctuation through m_B affect the secrecy diversity order. This fact plays a pivotal role in the secrecy performance of the system (as will be discussed in Numerical Results Section). On the other hand, notice that the fading parameter μ_E corresponding to the eavesdropper channel does not affect the secrecy diversity gain of the underlying system (see Fig. 5.5).*

5.2.3 ASC Analysis

In this section, it is assumed an active eavesdropping scenario, where the CSIs of both main and eavesdropper channels are known at Alice. Unlike the passive eavesdropping scenario, in an active case, Alice can now adapt her transmission rate according to any achievable secrecy rate R_S such that $R_S \leq C_S$ (see Section 2.1.2.4). Next, by substituting the necessary formulations in (2.8) that were derived in Section 5.1.4, the ASC expressions over i.i.d. κ - μ shadowed fading channels under TAS/MRC system are given as stated in the following Proposition.

Proposition 14. *The ASC closed-form expressions for $m_i \geq \mu_i$ and $m_i < \mu_i$ with $i \in \{B, E\}$ over i.i.d. κ - μ shadowed fading channels can be formulated as (5.20), and (5.21), respectively.*

$$\begin{aligned}
\bar{C}_S &= \frac{1}{\ln 2} \sum_{k=1}^{N_A} (-1)^{k+1} \binom{N_A}{k} \sum_{\rho(k, \nu_B)} \frac{k!}{s_1! \cdots s_{\nu_B}!} \left[\prod_{t=1}^{\nu_B} \left(\frac{\left(\frac{1}{\Delta_2^B}\right)^{\nu_B-t}}{(\nu_B-t)!} \sum_{z=\beta_B+1-\mathcal{T}(j-1)}^{\beta_B} B_{\beta_B-z}^B \right)^{s_t} \right] \exp\left(\frac{k}{\Delta_2^B}\right) \\
&\times \Gamma\left(1 + \sum_{t=1}^{\nu_B} (\nu_B-t)s_t\right) \Gamma\left(-\sum_{t=1}^{\nu_B} (\nu_B-t)s_t, \frac{k}{\Delta_2^B}\right) - \frac{1}{\ln 2} \sum_{k=1}^{N_A} (-1)^{k+1} \binom{N_A}{k} \sum_{\rho(k, \nu_B)} \frac{k!}{s_1! \cdots s_{\nu_B}!} \\
&\times \left[\prod_{t=1}^{\nu_B} \left(\frac{\left(\frac{1}{\Delta_2^B}\right)^{\nu_B-t}}{(\nu_B-t)!} \sum_{z=\beta_B+1-\mathcal{T}(j-1)}^{\beta_B} B_{\beta_B-z}^B \right)^{s_t} \right] \sum_{j=0}^{\beta_E} B_j^E \sum_{r=0}^{\nu_E-j-1} \frac{1}{r!} \left(\frac{1}{\Delta_2^E}\right)^r \exp\left(\frac{k}{\Delta_2^B} + \frac{1}{\Delta_2^E}\right) \\
&\times \Gamma\left(1 + r + \sum_{t=1}^{\nu_B} (\nu_B-t)s_t\right) \Gamma\left(-r - \sum_{t=1}^{\nu_B} (\nu_B-t)s_t, \frac{k}{\Delta_2^B} + \frac{1}{\Delta_2^E}\right). \tag{5.20}
\end{aligned}$$

$$\begin{aligned}
\bar{C}_S &= \frac{1}{\ln 2} \sum_{k=1}^{N_A} (-1)^{k+1} \binom{N_A}{k} \sum_{c=0}^k \binom{k}{c} \sum_{\rho(c, \nu_B)} \frac{c!}{p_1! \cdots p_{\nu_B}!} \left[\prod_{q=1}^{\nu_B} \left(\frac{\left(\frac{1}{\Delta_2^B}\right)^{\nu_B-q}}{(\nu_B-q)!} \sum_{z=\nu_B+1-q}^{\nu_B} A_{2, \nu_B+1-z}^B \right)^{p_q} \right] \\
&\times \sum_{\rho(k-c, \eta_B)} \frac{(k-c)!}{s_1! \cdots s_{\eta_B}!} \left[\prod_{t=1}^{\eta_B} \left(\frac{\left(\frac{1}{\Delta_1^B}\right)^{\eta_B-t}}{(\eta_B-t)!} \sum_{z=\eta_B+1-t}^{\eta_B} A_{1, \eta_B+1-z}^B \right)^{s_t} \right] \exp\left(\frac{k-c}{\Delta_1^B} + \frac{c}{\Delta_2^B}\right) \\
&\times \Gamma\left(1 + \sum_{t=1}^{\eta_B} (\eta_B-t)s_t + \sum_{q=1}^{\nu_B} (\nu_B-q)p_q\right) \Gamma\left(-\sum_{t=1}^{\eta_B} (\eta_B-t)s_t - \sum_{q=1}^{\nu_B} (\nu_B-q)p_q, \frac{\Delta_2^B(k-c) + \Delta_1^B c}{\Delta_1^B \Delta_2^B}\right) \\
&- \frac{1}{\ln 2} \sum_{k=1}^{N_A} (-1)^{k+1} \binom{N_A}{k} \sum_{c=0}^k \binom{k}{c} \sum_{\rho(c, \nu_B)} \frac{c!}{p_1! \cdots p_{\nu_B}!} \left[\prod_{q=1}^{\nu_B} \left(\frac{\left(\frac{1}{\Delta_2^B}\right)^{\nu_B-q}}{(\nu_B-q)!} \sum_{z=\nu_B+1-q}^{\nu_B} A_{2, \nu_B+1-z}^B \right)^{p_q} \right] \\
&\times \sum_{\rho(k-c, \eta_B)} \frac{(k-c)!}{s_1! \cdots s_{\eta_B}!} \left[\prod_{t=1}^{\eta_B} \left(\frac{\left(\frac{1}{\Delta_1^B}\right)^{\eta_B-t}}{(\eta_B-t)!} \sum_{z=\eta_B+1-t}^{\eta_B} A_{1, \eta_B+1-z}^B \right)^{s_t} \right] \exp\left(\frac{k-c}{\Delta_1^B} + \frac{c}{\Delta_2^B}\right) \left(\sum_{j=1}^{\eta_E} A_{1,j}^E\right) \\
&\times \sum_{r=0}^{\eta_E-j} \frac{1}{r!} \left(\frac{1}{\Delta_1^E}\right)^r \exp\left(\frac{1}{\Delta_1^E}\right) \Gamma\left(-r - \sum_{t=1}^{\eta_B} (\eta_B-t)s_t - \sum_{q=1}^{\nu_B} (\nu_B-q)p_q, \frac{k-c}{\Delta_1^B} + \frac{c}{\Delta_2^B} + \frac{1}{\Delta_1^E}\right) \\
&\times \Gamma\left(1 + r + \sum_{t=1}^{\eta_B} (\eta_B-t)s_t + \sum_{q=1}^{\nu_B} (\nu_B-q)p_q\right) + \sum_{j=1}^{\nu_E} \sum_{r=0}^{\nu_E-j} \Gamma\left(1 + r + \sum_{t=1}^{\eta_B} (\eta_B-t)s_t + \sum_{q=1}^{\nu_B} (\nu_B-q)p_q\right) \\
&\times \frac{A_{2,j}^E}{r!} \left(\frac{1}{\Delta_2^E}\right)^r \exp\left(\frac{1}{\Delta_2^E}\right) \Gamma\left(-r - \sum_{t=1}^{\eta_B} (\eta_B-t)s_t - \sum_{q=1}^{\nu_B} (\nu_B-q)p_q, \frac{k-c}{\Delta_1^B} + \frac{c}{\Delta_2^B} + \frac{1}{\Delta_1^E}\right). \tag{5.21}
\end{aligned}$$

Proof. See Appendix E.4. □

It is worth mentioning that although the ASC expressions presented in this apart are long-drawn, they are given in terms of known functions, facilitating their implementation in mathematical software packages such as MATLAB and Wolfram Mathematica.

5.2.4 Asymptotic ASC Analysis

This section derives a closed-form asymptotic ASC expression to assess the system performance in the high-SNR regime. Herein, as in the asymptotic SOP analysis, it is considered the scenario where $\bar{\gamma}_B$ goes to infinity, while $\bar{\gamma}_E$ is kept unchanged. Plugging the respective formulations obtained in Section 5.1.4 into (2.12), the asymptotic ASC expressions under κ - μ shadowed are given in the following Proposition.

Proposition 15. *The asymptotic ASC expressions for $m_i < \mu_i$ and $m_i \geq \mu_i$ with $i \in \{B, E\}$ over i.i.d. κ - μ shadowed fading channels are given in (5.22) and (5.23), respectively.*

$$\begin{aligned}
\bar{C}_S^\infty &\simeq \log_2(\bar{\gamma}_B N_B) + \log_2(e) \sum_{k=1}^{N_A} \binom{N_A}{k} \sum_{c=0}^k \binom{k}{c} \sum_{\rho(c, \nu_B)} \frac{(-1)^k c!}{p_1! \cdots p_{\nu_B}!} \left[\prod_{q=1}^{\nu_B} \left(\frac{\left(\frac{N_B \bar{\gamma}_B}{\Delta_2^B}\right)^{\nu_B - q}}{(\nu_B - q)!} \sum_{z=\nu_B+1-q}^{\nu_B} A_{2, \nu_B+1-z}^B \right)^{p_q} \right] \\
&\times \sum_{\rho(k-c, \eta_B)} \frac{(k-c)!}{s_1! \cdots s_{\eta_B}!} \left[\prod_{t=1}^{\eta_B} \left(\frac{\left(\frac{N_B \bar{\gamma}_B}{\Delta_1^B}\right)^{\eta_B - t}}{(\eta_B - t)!} \sum_{z=\eta_B+1-t}^{\eta_B} A_{1, \eta_B+1-z}^B \right)^{s_t} \right] \mathcal{U} \left(\sum_{t=1}^{\eta_B} (\eta_B - t) s_t + \sum_{q=1}^{\nu_B} (\nu_B - q) p_q \right) \\
&- \frac{1}{\ln 2} \left(\exp\left(\frac{1}{\Delta_1^E}\right) \sum_{j=1}^{\eta_E} A_{1,j}^E \sum_{r=0}^{\eta_E - j} \frac{\Gamma(-r, \frac{1}{\Delta_1^E})}{r!} \left(\frac{1}{\Delta_1^E}\right)^r \Gamma(1+r) + \exp\left(\frac{1}{\Delta_2^E}\right) \sum_{j=1}^{\nu_E} A_{2,j}^E \sum_{r=0}^{\nu_E - j} \frac{\Gamma(-r, \frac{1}{\Delta_2^E})}{r!} \right) \\
&\times \left(\frac{1}{\Delta_2^E}\right)^r \Gamma(1+r). \tag{5.22}
\end{aligned}$$

$$\begin{aligned}
\bar{C}_S^\infty &\simeq \log_2(N_B \bar{\gamma}_B) + \log_2(e) \sum_{k=1}^{N_A} \binom{N_A}{k} \sum_{\rho(k, \nu_B)} \frac{(-1)^k k!}{s_1! \cdots s_{\nu_B}!} \left[\prod_{t=1}^{\nu_B} \left(\frac{\left(\frac{N_B \bar{\gamma}_B}{\Delta_2^B}\right)^{\nu_B - t}}{(\nu_B - t)!} \sum_{z=\beta_B+1-\mathcal{T}(j-1)}^{\beta_B} B_{\beta_B-z}^B \right)^{s_t} \right] \\
&\times \mathcal{W} \left(\sum_{t=1}^{\nu_B} (\nu_B - t) s_t \right) - \frac{1}{\ln 2} \exp\left(\frac{1}{\Delta_2^E}\right) \sum_{j=0}^{\beta_E} B_j^E \sum_{r=0}^{\nu_E - j - 1} \frac{1}{r!} \left(\frac{1}{\Delta_2^E}\right)^r \Gamma(1+r) \Gamma\left(-r, \frac{1}{\Delta_2^E}\right). \tag{5.23}
\end{aligned}$$

where $\mathcal{U}(u)$ and $\mathcal{W}(w)$ are obtained by

$$\mathcal{U}(u) = \begin{cases} \mathcal{C} + \ln \left(\frac{(k-c)N_B\bar{\gamma}_B}{\Delta_1^B} + \frac{cN_B\bar{\gamma}_B}{\Delta_2^B} \right), & \text{for } u = 0 \\ - \left(\frac{N_B\bar{\gamma}_B(c\Delta_1^B + (k-c)\Delta_2^B)}{\Delta_1^B\Delta_2^B} \right)^{- \left(\sum_{t=1}^{\eta_B} (\eta_B - t)s_t + \sum_{q=1}^{\nu_B} (\nu_B - q)p_q \right)} \\ \quad \times \Gamma \left(\sum_{t=1}^{\eta_B} (\eta_B - t)s_t + \sum_{q=1}^{\nu_B} (\nu_B - q)p_q \right), & \text{otherwise.} \end{cases}$$

and

$$\mathcal{W}(w) = \begin{cases} \mathcal{C} + \ln \left(\frac{kN_B\bar{\gamma}_B}{\Delta_2^B} \right), & \text{for } w = 0 \\ - \left(\frac{kN_B\bar{\gamma}_B}{\Delta_2^B} \right)^{- \left(\sum_{t=1}^{\nu_B} (\nu_B - t)s_t \right)} \Gamma \left(\sum_{t=1}^{\nu_B} (\nu_B - t)s_t \right), & \text{otherwise.} \end{cases} \quad (5.24)$$

Proof. See Appendix E.5. □

5.3 SOME PLOTS AND DISCUSSIONS

This section provides illustrative numerical results along with Monte Carlo simulations to verify the proposed analytical derivations. In all plots, as a consequence of using the κ - μ shadowed fading statistics proposed in [128], it is considered that the fading severity parameters (i.e., μ_i and m_i for $i \in \{B, E\}$) take integer values. Indeed, it is assumed integer values for the following reasons: (i) the shape parameter $\mu_{B,E}$ was originally defined in the κ - μ fading model as the number of clusters of multipath waves propagating in a certain environment [127]. So, as asserted in [127], the consideration that the parameters, $\mu_{B,E}$ to take integer values is related to the physical model for the κ - μ distribution; and (ii) in practice, the impact of restricting the fading parameter $m_{B,E}$ to take integer values is noticeable only in severe shadowing environments (i.e., low values of $m_{B,E}$). For medium to mild shadowing scenarios (i.e., high values of $m_{B,E}$), the impact of constraining $m_{B,E}$ to take integer values is even more negligible [128]. Furthermore, in all curves, Monte Carlos simulations are denoted with markers.

Fig. 5.2 compares the SOP as a function of $\bar{\gamma}_B$ for different numbers of transmit antennas, N_A , and a fixed number of receiving antennas, i.e., $N_B = N_E = 2$. Also, the fading parameters are set as: $R_S = 1$ bps/Hz, $\bar{\gamma}_E = 8$ dB, $\mu_i = 2$, $\kappa_i = 2$, and $m_i = 3$ for $i \in \{B, E\}$. Note that in all instances, our analytical expressions, for exact and asymptotic SOP, perfectly match with Monte Carlo simulations. Here, our goal is to analyze the impact of N_A on the secrecy diversity gain of the legitimate channels for the considered cases. Therefore, based on the asymptotic plots, it can be seen that the antenna configuration at Alice clearly contributes to the slope of the SOP in a proportional way. On one hand, this means that the decay of the SOP is steeper (i.e., better secrecy performance) as the number of transmit antennas increases. On the other hand, as the number of transmit antennas decreases the SOP is impaired and the decay is not so pronounced. These results are in coherence with the insights provided in Remark 5.

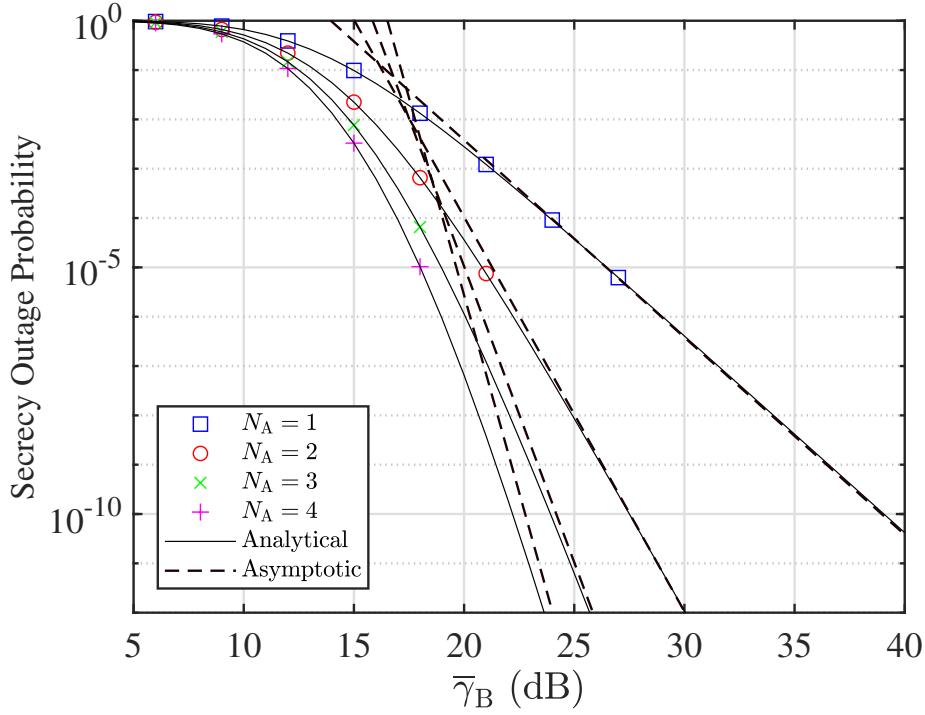


Figure 5.2: SOP vs. $\bar{\gamma}_B$, for various numbers of transmit antennas, N_A , and a fixed number of receive antennas, $N_B = N_E = 2$. The setting parameter values are: $R_S = 1$ bps/Hz, $\bar{\gamma}_E = 8$ dB, $\mu_i = 2$, $\kappa_i = 2$, and $m_i = 3$ for $i \in \{B, E\}$. Markers denote Monte Carlo simulations.

Fig. 5.3 presents the SOP vs. $\bar{\gamma}_B$ for different numbers of eavesdroppers antennas, N_E , and fixed number of antennas at the legitimate nodes, $N_A = N_B = 2$. The remainder parameters are set to: $R_S = 1$ bps/Hz, $\bar{\gamma}_E = 8$ dB, $\mu_i = 3$, and $\kappa_i = 5$, for $i \in \{B, E\}$. In this scenario, the goal is to explore the impact of having light ($m_B = m_E = 10$) or heavy ($m_B = m_E = 1$) shadowing on the LoS components at both Bob and Eve in an environment with multiple antennas. From all curves, it can be observed that the combination of mild shadowing in the LoS components with a reduced number of antennas at Eve derives into a better secrecy performance, as expected. Conversely, secrecy performance always worsens when the shadowing is heavy in the LoS components at Bob or many antennas are used at the eavesdropper. In short, considering the following factors at the eavesdropper side: (i) a reduced number of antennas, and (ii) heavy shadowing in the LoS components is beneficial from the PLS perspective.

Fig. 5.4 illustrates the SOP as a function of $\bar{\gamma}_B$ by considering different numbers of receiving antennas N_B , and fixed number of antennas $N_A = N_E = 2$. The other parameters are setting as follows: $R_S = 2$ bps/Hz, $\bar{\gamma}_E = 8$ dB, $\mu_i = 1$, and $m_i = 2$ for $i \in \{B, E\}$. In this scenario, it is considered small ($\kappa_B = \kappa_E = 1.5$) and large ($\kappa_B = \kappa_E = 10$) LoS components on the received wave clusters for a different number of antennas at Bob. From all instances, it can be observed that the joint effect of increasing the number of Bob's antennas (which improves the secrecy diversity gain) and strong LoS components ($\kappa_B = \kappa_E = 10$) leads to a significant improvement on the secrecy performance.

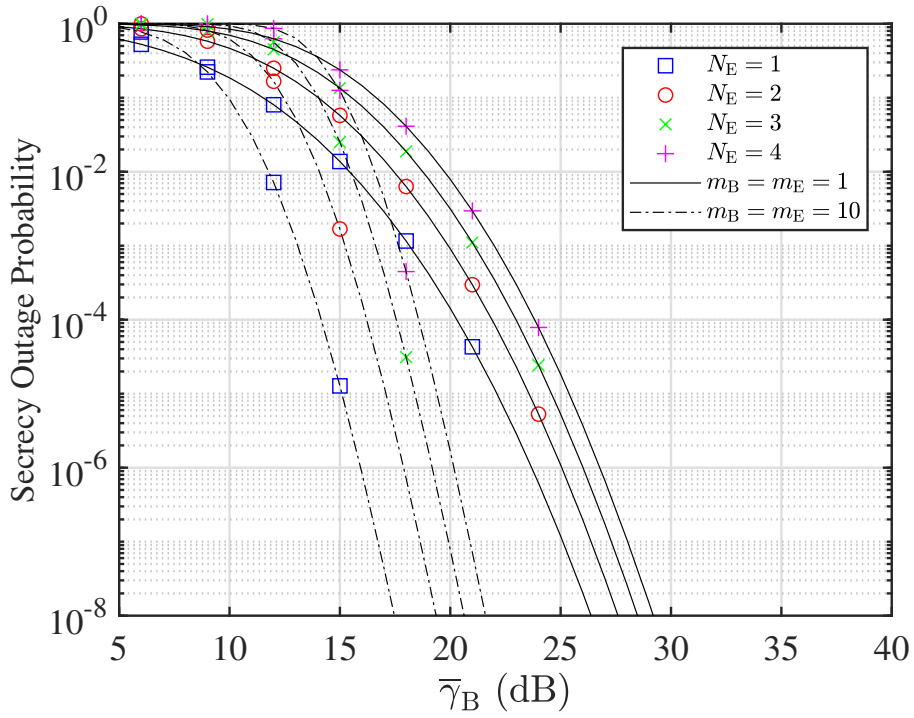


Figure 5.3: SOP vs. $\bar{\gamma}_B$, for various numbers of eavesdroppers antennas, N_E , and a fixed number antennas, $N_A = N_B = 2$. Markers denote Monte Carlo simulations, whereas the solid and dash-dotted lines represent analytical solutions.

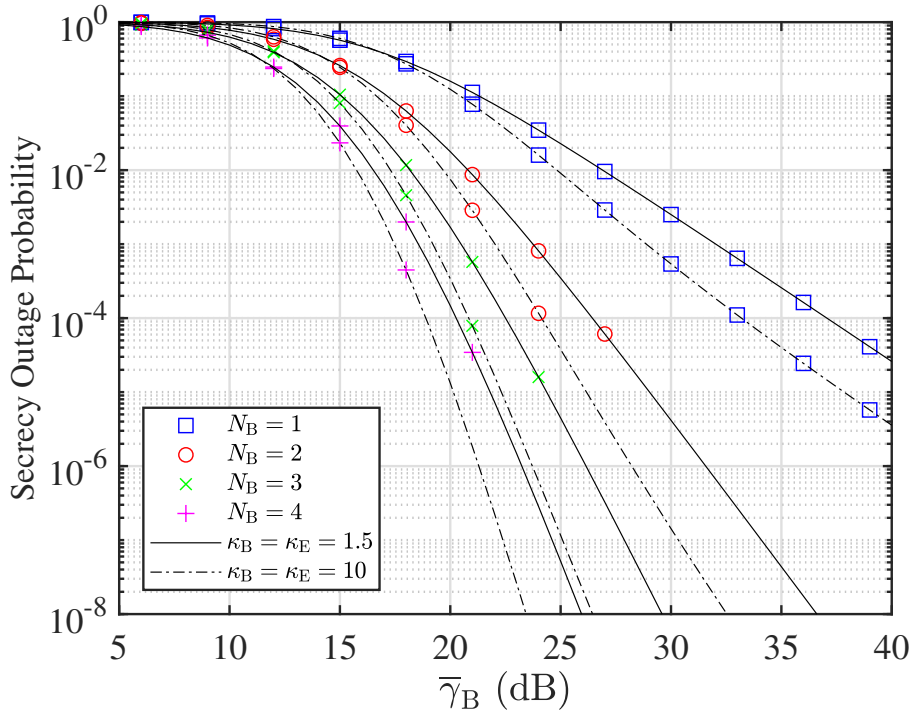


Figure 5.4: SOP vs. $\bar{\gamma}_B$, for different numbers of receive antennas, N_B , and unchanged number of: (i) receive antennas, $N_E = 2$, and (ii) transmit antennas, $N_A = 2$. Markers denote Monte Carlo simulations, whereas the solid and dash-dotted lines represent analytical solutions.

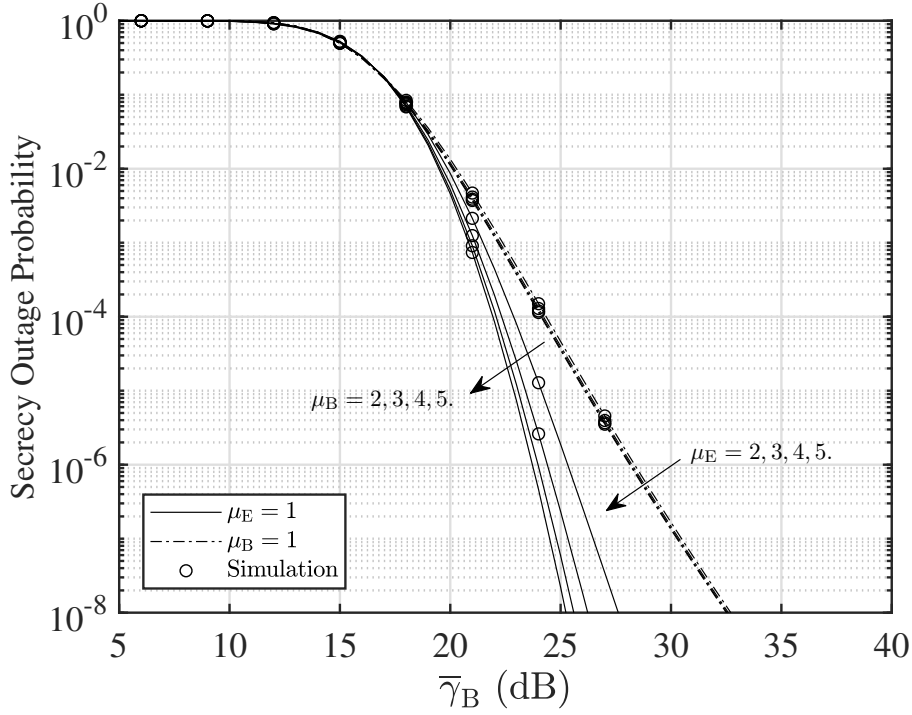


Figure 5.5: SOP vs. $\bar{\gamma}_B$, for $N_A = N_B = 2$, $N_E = 3$, and different received wave clusters, μ_B , and μ_E . The setting parameter values are: $R_S = 2$ bps/Hz, $\bar{\gamma}_E = 8$ dB, $\kappa_i = 4$, and $m_i = 5$ for $i \in \{B, E\}$. The solid and dash-dotted lines represent analytical solutions.

This result is linked to the fact that N_B directly influences the slope of the SOP, as shown in Remark 5. However, in the opposite scenario (wherein both N_B and κ_i for $i \in \{B, E\}$ decrease), note that the secrecy performance significantly deteriorates.

Fig. 5.5 shows the SOP vs. $\bar{\gamma}_B$ for $N_A = N_B = 2$, $N_E = 3$ for different clusters, μ_B and μ_E . The parameters are set to: $R_S = 2$ bps/Hz, $\bar{\gamma}_E = 8$ dB, $\kappa_i = 4$, and $m_i = 5$ for $i \in \{B, E\}$. For the scenarios, the aim is to investigate the influence of the number of wave clusters at the receiver nodes on the secrecy performance. Here, it is considered two cases: (i) μ_E is kept fixed, whereas μ_B goes from 2 to 5; (ii) μ_B is kept unchanged, whereas μ_E goes from 2 to 5. In the former case, it is observed that the secrecy performance improves as μ_B decreases. This fact confirms our finding in Remark 5, where μ_B impacts in the secrecy diversity order of the system. In the latter case, notice that regardless of the μ_E value, the slope of the SOP remains identical. This fact corroborates that the secrecy diversity order of the system is not affected by the number of received wave clusters at the eavesdropper (see Remark 5). From a secrecy perspective, this result provides valuable insight into the design and implementation criteria of future mobile networks over generalized fading conditions.

Then, Fig. 5.6 shows the SOP against the κ_i values with fixed fluctuation in the LoS components of each cluster at the receiver sides, i.e., $m_i = 3$ for $i \in \{B, E\}$. For all curves, the configuration parameters are as follows: $N_A = 3$, $N_B = N_E = 2$, $R_S = 3$ bps/Hz, $\bar{\gamma}_E = 8$ dB, and $\bar{\gamma}_B = 25$ dB. Here, the goal is to investigate the achievable SOP when the LoS components, i.e. κ_i (for

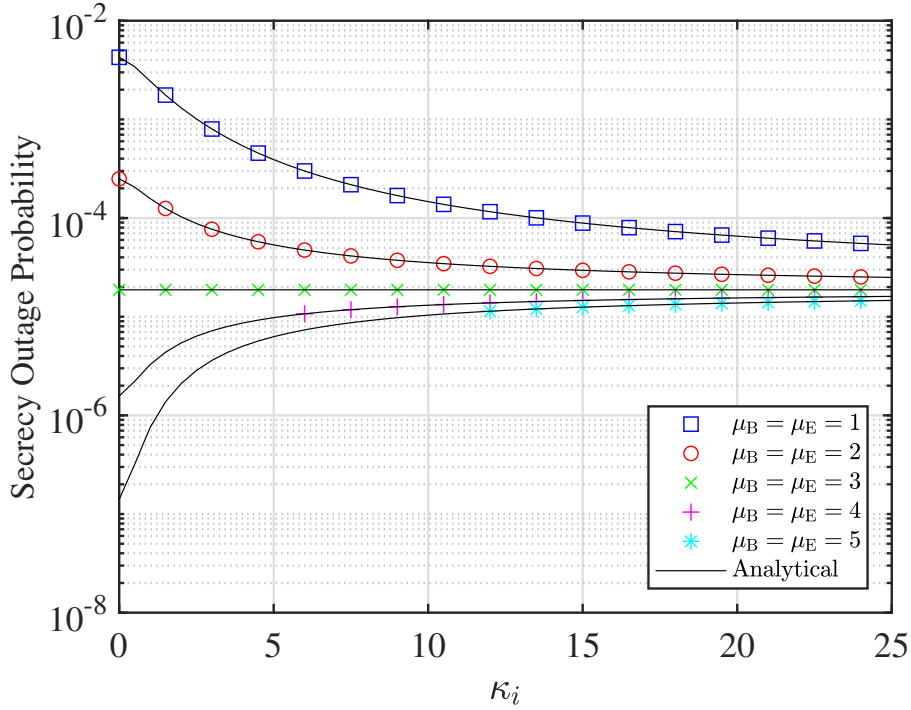


Figure 5.6: SOP vs. κ_i , with $N_A = 3$, $N_B = N_E = 2$, and fixed $m_i = 3$ for $i \in \{B, E\}$. The setting parameter values are: $R_S = 3$ bps/Hz, $\bar{\gamma}_E = 8$ dB, and $\bar{\gamma}_B = 25$ dB. Markers denote Monte Carlo simulations.

$i \in \{B, E\}$) increase. From all curves, it can be seen three scenarios for the SOP behavior regarding the configuration of parameters. For instance, for $\mu_i > m_i$ (with $i \in \{B, E\}$), increasing the received power through the LoS components is detrimental for the secrecy performance, which may seem counter-intuitive at a first glance. In fact, the case with $\mu_B > m_B$ (note that μ_E becomes irrelevant as indicated in Fig. 5.5) indicates that the dominant components associated to LoS are affected by a larger fading severity than the scattering diffuse counterpart. Hence, the secrecy performance worsens as κ_B increases. Conversely, when $\mu_i < m_i$ (with $i \in \{B, E\}$), the SOP is enhanced as the LoS components increase. For the specific case where $\mu_i = m_i$ (with $i \in \{B, E\}$), notice that the SOP does not vary according to the parameter κ_i (for $i \in \{B, E\}$). Such an observation is because if $\mu_i = m_i$ (for $i \in \{B, E\}$), this implies that both the scattering and the shadowed LoS components in each cluster experience the same fading severity. Thus, SOP becomes independent of κ_i in this configuration.

Fig. 5.7 depicts the ASC vs. $\bar{\gamma}_B$, for different setups of N_A , N_B , and N_E . The parameters are set to: $\bar{\gamma}_E = 8$ dB, $\mu_i = 2$, $m_i = 1$ (high fluctuation), and $\kappa_i = 5$ (LoS case) for $i \in \{B, E\}$. From all figures, it is straightforward to see that for the scenarios with severe fluctuation in the LoS components, an excellent strategy to improve the \bar{C}_S is to equip Bob with more antennas than Alice. In the opposite scenario, when Eve's capabilities (e.g., more antennas) are better than those of legitimate peers, the secrecy performance is compromised.

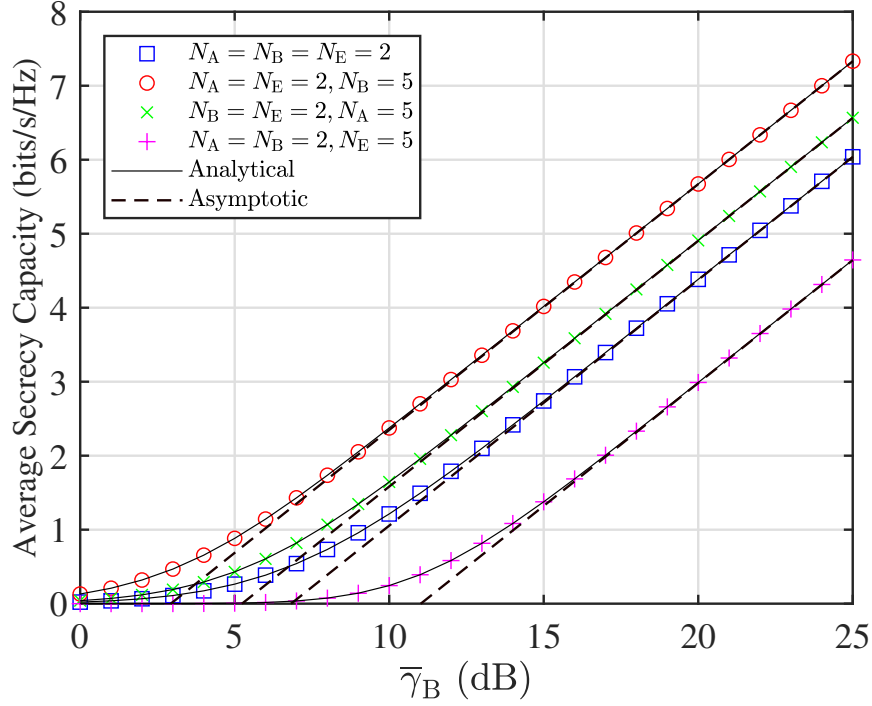


Figure 5.7: ASC vs. $\bar{\gamma}_B$, for different configurations of N_A , N_B , and N_E . The corresponding parameter values are: $\bar{\gamma}_E = 8$ dB, $\mu_i = 2$, $m_i = 1$, and $\kappa_i = 5$ for $i \in \{B, E\}$. Markers denote Monte Carlo simulations.

Finally, Fig. 5.8 shows the ASC as a function of $\bar{\gamma}_B$, considering different numbers of receiving antennas at Bob, i.e., N_B , and a fixed number of antennas at both source and eavesdropper, i.e., $N_A = N_E = 2$. The remainder parameters are set to: $\bar{\gamma}_E = 8$ dB, and $\mu_i = m_i = 2$ for $i \in \{B, E\}$. From all instances, notice that \bar{C}_S is not affected by increasing the power of the LoS components at the receiver sides ($\kappa_i = 1.5$ to $\kappa_i = 10$ for $i \in \{B, E\}$). This result confirms that an increase in the power of the LoS components does not always favor the \bar{C}_S performance. This observation is linked to the discussions in Fig. 5.6, so \bar{C}_S is independent of the κ_i value. Obviously, this channel behavior changes when $m_i \geq \mu_i$ or $m_i < \mu_i$ (for $i \in \{B, E\}$). In addition, in Fig. 5.7 and Fig. 5.8, it can be seen that the asymptotic ASC curves tightly approximate the Monte Carlo simulations and the exact analytical values in the high-SNR regime.

5.4 CONCLUSIONS

This chapter have explored how different propagation mechanisms such as LoS condition (i.e., weak or strong), LoS fluctuation, and clustering of the scattered multipath waves impact on the secrecy performance of MIMO wiretap channels. Specifically, the analyzed results have shown that the effect of combining strong LoS components with a weak fluctuation and a rich scattering condition in the legitimate channel favors the system's secrecy performance. However, whenever the LoS components arriving at Bob suffer a more considerable fading severity than the multipath clustering counterpart

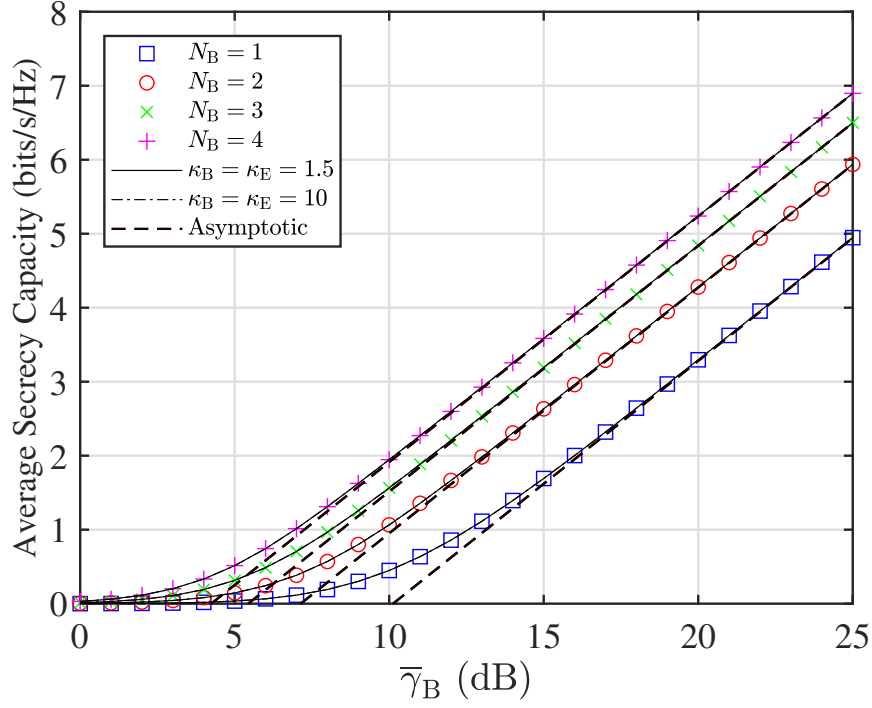


Figure 5.8: ASC vs. $\bar{\gamma}_B$, for different numbers of receive antennas, N_B , and fixed number of antennas, $N_A = N_E = 2$. The corresponding parameter values are: $\bar{\gamma}_E = 8$ dB, and $\mu_i = m_i = 2$ for $i \in \{B, E\}$. Markers denote Monte Carlo simulations, whereas the solid and dash-dotted lines represent analytical solutions.

(i.e. $m_B < \mu_B$), the secrecy performance worsens as κ_B is increased. Furthermore, it was observed that the asymptotic behavior of the system depends not only on the number of antennas of the legitimate pairs (as expected) but also on the scattering environment (i.e., μ_B) of the legitimate link. Conversely, the multipath waves on the eavesdropper's (i.e., μ_E) side play no role in the asymptotic performance in the TAS/MRC configuration. These findings are crucial insights to be taken into account in the design criteria of the next networks over generalized fading conditions. Finally, it was verified that the role of the fading parameters at the eavesdropper becomes less important as $\bar{\gamma}_B > \bar{\gamma}_E$.

6 PHYSICAL LAYER SECURITY OF RECONFIGURABLE INTELLIGENT SURFACE-ASSISTED COMMUNICATIONS WITH PHASE ERRORS

This chapter explores the secrecy performance of a reconfigurable intelligent surface (RIS)-assisted wireless communication system in the presence of an eavesdropper node. Specifically, knowing that the perfect phase estimation of the phase shifts induced by the composite propagation channels through the RIS is unfeasible in practice, the aim is to study the secrecy transmission via RIS with phase errors. Scaling laws of the legitimate and eavesdroppers signal-to-noise ratios with different numbers of reflecting elements show an excellent secrecy performance even in assuming imperfect phase estimation at the RIS. The overall results show the great potential of RIS-aided communications to improve PLS in post-5G networks.

6.1 SYSTEM MODEL

As illustrated in Fig. 6.1, it is considered an RIS-aided wireless communication scenario consisting of one source node Alice (A), one legitimate node Bob (B), one eavesdropper Eve (E), and an RIS, which assists the legitimate communication. The RIS helps the source's transmission by passively reflecting the signal to the legitimate destination. However, due to the wireless medium's broadcast nature, the incident signals could be intercepted by the eavesdropper. Hence, RIS's primary task is to adjust the phase shift of the signals by using reflecting elements to increase the information rate at the destination but decrease the information leakage at the eavesdropper. In the setup, it is assumed that the direct link is neglected, and all nodes are equipped with a single antenna, while the RIS has n low-cost passive reflecting units $R_1 \dots R_n$. Also, $H_{i,1}$ denotes the fading channel coefficient between the source A and the reflecting element R_i , whereas $H_{i,b}$ and $H_{i,e}$ are the fading channel coefficients between R_i and the legitimate receiver B and the eavesdropper E, respectively. Without loss of generality, the fading coefficients are normalized with unitary power, and the corresponding average magnitudes are given $\forall i = 1 \dots n$ by $a_1 = \mathbb{E}\{|H_{i,1}|\}$, $a_{2,b} = \mathbb{E}\{|H_{i,b}|\}$ and $a_{2,e} = \mathbb{E}\{|H_{i,e}|\}$. Notice that $\{a_1, a_{2,b}, a_{2,e}\} \leq 1$ in all instances, where the equality only holds in the limit of a deterministic fading channel, i.e., in the absence of fading. Also, $a_b = \sqrt{a_1 a_{2,b}}$ is defined. According to [159], the

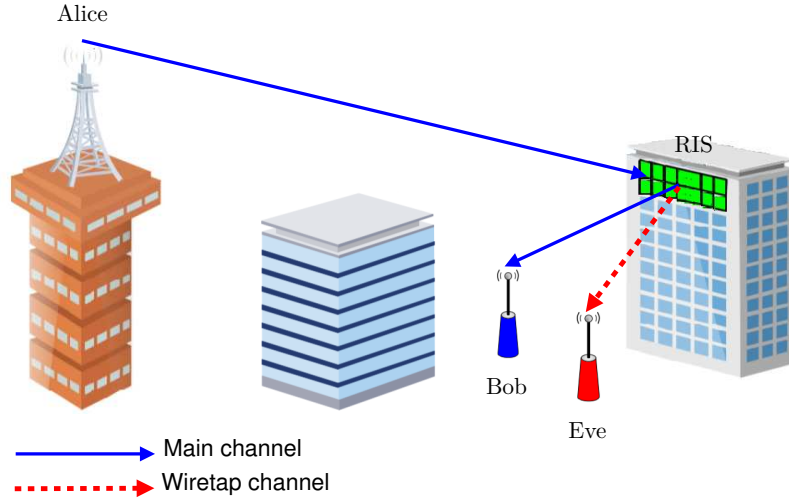


Figure 6.1: IRS-aided secure communication from Alice (A) to a legitimate receiver Bob (B) in the presence of an eavesdropper Eve (E). This figure is based on [132].

received signal at the legitimate destination (i.e., B) can be formulated as

$$Y_b = \sqrt{P_T L_b} \sum_{i=1}^n H_{i,1} e^{j\phi_i} H_{i,b} X + W_b, \quad (6.1)$$

where X is the transmitted symbol, P_T indicates the transmit power at A, L_b encompasses the path losses for the A-R and R-B links, the antenna gains and reflection losses, and W_b is the *AWGN* term with N_0 power.

Ideally, given the phases $\angle H_{i,1}$ and $\angle H_{i,b}$, the RIS designs the phase shifts ϕ_i in (6.1) so as to cancel the overall phase shift $\angle H_{i,1} + \angle H_{i,b}$, which maximizes the SNR at the legitimate receiver [160]. However, in practice, due to the imperfect phase estimation and the limited quantization of phase state at the RIS, a residual random phase error Θ_i persists, i.e., $\phi_i = -\angle H_{i,1} - \angle H_{i,b} + \Theta_i$. Thus, the complex channel at the legitimate receiver can be expressed as

$$H_b = \frac{1}{n} \sum_{i=1}^n |H_{i,1}| |H_{i,b}| e^{j\Theta_i}, \quad (6.2)$$

and (6.1) can be rewritten as

$$Y_b = n\sqrt{\gamma_{0,b}} H_b X + W_b. \quad (6.3)$$

On the other hand, the received signal at the eavesdropper's side can be formulated as

$$Y_e = \sqrt{\gamma_{0,e}} \sum_{i=1}^n H_{i,1} e^{j\phi_i} H_{i,e} X + W_e, \quad (6.4)$$

where $\gamma_{0,e} = P_T L_e / N_0$ denotes the average SNR at the eavesdropper in the case of a single reflector RIS, i.e., $n = 1$, and the parameter L_e is defined in a similar way as L_b . Now, it is worth mentioning that due to the phase shifts ϕ_i are designed by the RIS to compensate for the effects of the fading

channels of the legitimate path, the residual phase error Ψ_i at the eavesdropper path with certainty will be much large than the legitimate link and, whenever $\angle H_{i,e} \sim \mathcal{U}[-\pi, \pi)$, so $\Psi_i \sim \mathcal{U}[-\pi, \pi)$ [161] regardless of the generic phase distribution of $\angle H_{i,1}$. Based on this, the complex channel observed by the eavesdropper is given by

$$H_e = \frac{1}{n} \sum_{i=1}^n |H_{i,1}| |H_{i,e}| e^{j\Psi_i}, \quad (6.5)$$

thus (6.4) can reformulated as

$$Y_e = n\sqrt{\gamma_{0,e}} H_e X + W_e. \quad (6.6)$$

Here, even though the legitimate and eavesdropper's links share the A-R links, As will be seen later, under some premises H_e and H_b are independent. Next, the instantaneous SNR at both the legitimate and the eavesdropper links are given by

$$\gamma_b = n^2 \bar{\gamma}_{0,b} |H_b|^2, \quad (6.7)$$

$$\gamma_e = n^2 \bar{\gamma}_{0,e} |H_e|^2, \quad (6.8)$$

where $\bar{\gamma}_{0,b} = P_T L_b / N_0$ and $\bar{\gamma}_{0,e} = P_T L_e / N_0$ are the average SNRs at both the legitimate and the eavesdropper sides in the case of a single reflector RIS, i.e., $n = 1$. With the previous definitions, the SNRs distributions of both the legitimate and the eavesdropper paths are derived below.

6.2 SNR DISTRIBUTIONS

6.2.1 Distribution of γ_b

As proved by the authors in [159], for sufficiently large n , the distribution of H_b is that of a non-circularly symmetric complex Gaussian RV with $U_b = \Re(H_b)$ and $V_b = \Im(H_b)$, so that $U_b \sim \mathcal{N}(\mu, \sigma_{U_b}^2)$ and $V_b \sim \mathcal{N}(0, \sigma_{V_b}^2)$, where the scaled parameters are $\mu = \varphi_1 a_b^2$, $\sigma_{U_b}^2 = \frac{1}{2n} (1 + \varphi_2 - 2\varphi_1^2 a_b^4)$ and $\sigma_{V_b}^2 = \frac{1}{2n} (1 - \varphi_2)$, and φ_j are the j^{th} circular moments of Θ_i . This fact implies that $R_b = |H_b|$ follows the Beckmann distribution [162] and then, the average SNR at the legitimate receiver γ_b follows a (squared) Beckmann distribution given by

$$f_{\gamma_b}(\gamma) = \frac{c}{4\pi q} \int_0^{2\pi} e^{-\frac{c \left(\sqrt{\gamma} \cos(\theta) - \sqrt{\frac{K\bar{\gamma}_b}{K+1}} \right)^2}{2q^2} - \frac{cg \sin^2(\theta)}{2}} d\theta, \quad (6.9)$$

where $K = \mu^2/(\sigma_{U_b}^2 + \sigma_{V_b}^2)$, $q = \sigma_{U_b}/\sigma_{V_b}$ and $\bar{\gamma}_b = \mathbb{E}\{\gamma_b\}$. Now, by replacing the above definitions in the set of Beckmann's parameters [1], it follows that

$$K = n \frac{\varphi_1^2 a_b^4}{1 - \varphi_1^2 a_b^4}, \quad (6.10)$$

$$q = \sqrt{\frac{1 + \varphi_2 - 2\varphi_1^2 a_b^4}{1 - \varphi_2}}, \quad (6.11)$$

$$\bar{\gamma}_b = n^2 \bar{\gamma}_{0,b} \left[\varphi_1^2 a_b^4 + \frac{1}{n} \left(1 - \varphi_1^2 a_b^4 \right) \right]. \quad (6.12)$$

Note that in (6.12), as claimed by the authors in [159], the average SNR of the legitimate link scales with n^2 . Also, it can be observed that the LoS condition of the equivalent scalar channel is characterized by K that grows with n . Notably, the non-circular symmetry caused by the phase errors captured by $q \in [1, \infty)$ is independent of the number of elements of the RIS. Notice that in the lack of phase errors, H_b becomes a real Gaussian RV and then $|H_b|$ follows a folded normal (FN), which is a particular case of the κ - μ distribution when $\mu_{\kappa-\mu} = 1/2$. Therefore, the PDF of the FN model is given by [163, Eq. (2)]

$$f_{\gamma_b}(\gamma) = \frac{1/2(1+K)^{\frac{3}{4}} \gamma^{-\frac{1}{4}} \exp\left(-\frac{(1+K)\gamma}{2\bar{\gamma}_b}\right) I_{-1/2}\left(\sqrt{\frac{K(1+K)\gamma}{\bar{\gamma}_b}}\right)}{K^{-\frac{1}{4}} \bar{\gamma}_b^{\frac{3}{4}} \exp\left(\frac{K}{2}\right)}, \quad (6.13)$$

where the parameters K and $\bar{\gamma}_b$ are given by (6.10) with $\varphi_1 = 1$, and (6.12), respectively. Also, the distribution of R_b is well approximated by a Nakagami- m distribution in [159], and hence γ_b can be approximated by a gamma distribution denoted by

$$f_{\gamma_b}(\gamma) = \frac{m^m \gamma^{m-1} \exp\left(-\frac{m\gamma}{\bar{\gamma}_b}\right)}{\Gamma(m) \bar{\gamma}_b^m}, \quad (6.14)$$

in which the shape parameter $m = \frac{n}{2} \frac{\varphi_1^2 a_b^4}{1 + \varphi_2 - 2\varphi_1^2 a_b^4}$ and scale parameter $\bar{\gamma}_b = n^2 \bar{\gamma}_{0,b} \varphi_1^2 a_b^4$ [159]. It is worth mentioning that due to the dissimilar behavior of the FN, the Beckmann and the Nakagami- m distributions in terms of diversity order [117], it is considered all such distributions in the derivation of the PLS secrecy metrics, in order to obtain insights on when these distributions are useful to approximate the true distribution of γ_b given in (6.7).

6.2.2 Distribution of γ_e

As mentioned beforehand, RIS technology designs its phase shifts according to the legitimate path. Therefore, the phase distributions for each of the eavesdropper's R-E paths are uniformly distributed, as pointed in [161]. Based on this fact, the distribution of $R_e = |H_e|$ follows a Rayleigh model with

[1] The entire mathematical derivation to arrive at the set of parameters K , q , and $\bar{\gamma}_b$ for the scenario under consideration is given in [159].

PDF given by

$$f_{R_e}(r) = \frac{2r}{\bar{\gamma}_e} \exp\left(-\frac{r^2}{\bar{\gamma}_e}\right), \quad (6.15)$$

where according to [159, Corol. 2], it follows that $\mathbb{E}\{R_e^2\} = 1/n$. Now, by using a standard change of variables, $\gamma_e = R_e^2$, i.e., $f_{\gamma_e}(\gamma) = \frac{f_{R_e}(\sqrt{\gamma})}{2\sqrt{\gamma}}$, the distribution of γ_e follows an exponential distribution, expressed as

$$f_{\gamma_e}(\gamma) = \frac{1}{\bar{\gamma}_e} \exp\left(-\frac{\gamma}{\bar{\gamma}_e}\right), \quad (6.16)$$

wherein $\bar{\gamma}_e = n\bar{\gamma}_{0,e}$.

Remark 6 (Scaling law for $\bar{\gamma}_e$). *Distinctly, the average SNR at the eavesdropper scales with n , whereas the average SNR at the legitimate receiver scales with n^2 . Therefore, the scaling law for the ratio of legitimate and wiretap SNRs is*

$$\frac{\bar{\gamma}_b}{\bar{\gamma}_e} \Big|_{n \uparrow} = n \frac{\bar{\gamma}_{0,b}}{\bar{\gamma}_{0,e}} \left[\varphi_1^2 a_b^4 + \frac{1}{n} \left(1 - \varphi_1^2 a_b^4 \right) \right] \quad (6.17)$$

A useful insight from (6.17) is that the use of sufficiently large n (i.e., RIS's elements) can provide an enormous improvement of the SNR of the legitimate path compared to the eavesdropper's counterpart.

Finally, notice that (6.2) and (6.5) reveals that the legitimate and eavesdropper's links share a common part through, i.e., $H_{i,1}$. However, both channels were proven to be equivalent and statistically independent. Therefore, the PLS problem can be reformulated as a simpler one based on scalar channel representations given above, with tractable analytical expressions, as stated in the next Section.

Theorem 1 (Independence of legitimate and eavesdropper paths). *Let us consider the equivalent legitimate and eavesdropper channels in (6.2) and (6.5). Therefore, H_b and H_e are independent if $\angle H_{i,e} \sim \mathcal{U}[-\pi, \pi)$. Indeed, this is the case of considering Rayleigh fading channels for the RIS to eavesdropper's links.*

Proof. See Appendix F. □

6.3 PLS PERFORMANCE ANALYSIS

This section derives analytical closed-form solutions for the chief PLS secrecy metrics defined previously. Three different scenarios are considered in our analysis, namely: (a) no phase errors – FN/Rayleigh case; (b) with phase errors – Beckmann/Rayleigh case; (c) with phase errors – Nakagami/Rayleigh case.

6.3.1 SOP Performance Analysis

Here, the SOP metrics for the FN/Rayleigh, Nakagami/Rayleigh and Beckmann/Rayleigh scenarios are introduced below.

Lemma 1. *The SOP and the asymptotic SOP expressions (i.e., $\bar{\gamma}_b \rightarrow \infty$) for the FN/Rayleigh (FR) scenario in the absence of phase errors for RIS-aided communications are given by*

$$SOP_{FR} = 1 - Q_{0.5} \left(\sqrt{K}, \sqrt{\frac{(1+K)\gamma}{\bar{\gamma}_b}} \right) + e^{\frac{\tau-1}{\tau\bar{\gamma}_e} + \frac{K\bar{\gamma}_b s}{K+1-2\bar{\gamma}_b s}} \sqrt{\frac{(K+1)}{K+1-2\bar{\gamma}_b s}} \\ \times Q_{0.5} \left(\sqrt{\frac{K(K+1)}{K+1-2\bar{\gamma}_b s}}, \sqrt{2 \left(\frac{K+1}{2\bar{\gamma}_b} - s \right) (\tau-1)} \right), \quad (6.18)$$

$$SOP_{FR}^{\infty} \simeq e^{-K/2 + \frac{\tau-1}{\tau\bar{\gamma}_e}} \sqrt{\frac{\tau\bar{\gamma}_e(1+K)}{2\bar{\gamma}_b}} \tilde{\Gamma} \left(1.5, \frac{\tau-1}{\tau\bar{\gamma}_e} \right), \quad (6.19)$$

in which $\tau = 2^{Rs}$, and $s = -\frac{1}{\tau\bar{\gamma}_e}$. It is worth mentioning that the Marcum Q -function of order 0.5 can be easily computed with the help of the Gaussian Q function as $Q_{0.5}(a, b) = Q(b-a) + Q(b+a)$.

Proof. See Appendix G.1. □

Lemma 2. *The SOP and the asymptotic SOP expressions (i.e., $\bar{\gamma}_b \rightarrow \infty$) for Beckmann/Rayleigh (BR) scenario considering phase errors in the RIS-aided communications are given by*

$$SOP_{BR} = F_{\gamma_b}(\tau-1) + \exp\left(\frac{\tau-1}{\tau\bar{\gamma}_e}\right) \mathcal{M}_{\gamma_b}^u \left(-\frac{1}{\tau\bar{\gamma}_e}, \tau-1 \right). \quad (6.20)$$

$$SOP_{BR}^{\infty} \simeq \exp\left(-\frac{K(1+q^2)}{2q^2}\right) \frac{(1+K)(1+q^2)(\bar{\gamma}_e\tau + \tau - 1)}{2q\bar{\gamma}_b} \quad (6.21)$$

where $F_{\gamma_b}(\cdot)$ denotes the CDF of a squared Beckmann distribution [164, Eq. (7)], which is computed through Matlab code given in appendix I. Also $\mathcal{M}_{\gamma_b}^u(\cdot, \cdot)$ is the upper-incomplete moment generating function (IMGF) [164, Eq. (3)] of the RV γ_b , which follows a squared Beckmann distribution. The $\mathcal{M}_{\gamma_b}^u(\cdot, \cdot)$ is carried out numerically through an inverse Laplace transformation [165] as in [164, Eq. 4]. So, an efficient algorithm in Matlab for the implementation of $\mathcal{M}_{\gamma_b}^u(\cdot, \cdot)$ is provided in appendix J.

Proof. See Appendix G.2. □

Lemma 3. *The SOP and the asymptotic SOP expressions (i.e., $\bar{\gamma}_b \rightarrow \infty$) for Nakagami/Rayleigh scenario (NR) considering phase errors in the RIS-aided communications can be expressed as*

$$SOP_{NR} = \tilde{\gamma} \left(m, \frac{(\tau-1)m}{\bar{\gamma}_b} \right) + e^{\frac{\tau-1}{\tau\bar{\gamma}_e}} \frac{\tilde{\Gamma} \left(m, (\tau-1) \left(\frac{m}{\bar{\gamma}_b} + \frac{1}{\tau\bar{\gamma}_e} \right) \right)}{\left(1 + \frac{\bar{\gamma}_b}{m\tau\bar{\gamma}_e} \right)^m}, \quad (6.22)$$

$$SOP_{NR}^{\infty} \simeq \frac{2^{R_S m} \Gamma(1+m) m^{m-1}}{\Gamma(m)} \left(\frac{\bar{\gamma}_e}{\bar{\gamma}_b} \right)^m. \quad (6.23)$$

Proof. See Appendix G.3. □

Note that all secrecy metrics in Lemmas 1-3, are given in closed-form fashion except for the Beckmann/Rayleigh case in (6.20). Now, from [166, Table I] the secrecy diversity order for each of the approximations are given by $\mu_{\kappa-\mu} = 1/2, 1$ and m for the FR, BR and NR cases, respectively. The implications arising from this observation will be discussed in the Numerical Results Section.

6.3.2 ASR Performance Analysis

In this section, the ASR metrics in the FN/Rayleigh, Nakagami/Rayleigh and Beckmann/Rayleigh scenarios are formulated.

Lemma 4. *The ASR and the asymptotic ASR expressions (i.e., $\bar{\gamma}_b \rightarrow \infty$) over FN/Rayleigh (FR) scenario in the absence of phase errors for RIS-aided communications are formulated by*

$$\begin{aligned} \bar{\mathcal{R}}_{S-FR} &\approx \frac{1}{\ln 2} \frac{0.5(1+K)^{3/4}}{\bar{\gamma}_b^{3/4} K^{-1/4} \exp(0.5K)} \sum_{z=0}^{\infty} \frac{1}{z! \Gamma(0.5+z)} \left(0.5 \sqrt{\frac{K(1+K)}{\bar{\gamma}_b}} \right)^{2z-1/2} \\ &\times G_{2,3}^{3,1} \left[\begin{matrix} (1+K) \\ 2\bar{\gamma}_b \end{matrix} \middle| \begin{matrix} (-0.5-z), (0.5-z) \\ (0), (-0.5-z), (-0.5-z) \end{matrix} \right] - \frac{1}{\ln 2} \sum_{l=0}^{\infty} \frac{(0.5K)^l}{l! \exp(0.5K)} \\ &\times \sum_{z=0}^{\text{Floor}(l-0.5)} \frac{1}{z!} \left(\frac{0.5(1+K)}{\bar{\gamma}_b} \right)^z \exp \left(\frac{1}{\bar{\gamma}_e} + \frac{0.5(1+K)}{\bar{\gamma}_b} \right) \Gamma(1+z) \\ &\times \Gamma \left(-z, \frac{1}{\bar{\gamma}_e} + \frac{0.5(1+K)}{\bar{\gamma}_b} \right) \end{aligned} \quad (6.24)$$

$$\bar{\mathcal{R}}_{S-FR}^{\infty} \approx \log_2 \left(\frac{\bar{\gamma}_b}{1+K} \right) + \log_2(e) \left[\psi \left(\frac{1}{2} \right) + K {}_2F_2 \left(1, 1; 2, \frac{3}{2}; -\frac{K}{2} \right) \right] - \frac{e^{1/\bar{\gamma}_e}}{\ln 2} E_1 \left(\frac{1}{\bar{\gamma}_e} \right) \quad (6.25)$$

where

$$\begin{aligned}
f_1(x) = & \frac{\exp(x) E_1(x)}{\left[\left((1+K)(1+q^2) + 2x\bar{\gamma}_b \right) \left((1+K)(1+q^2) + 2q^2x\bar{\gamma}_b \right) \right]^{5/2} \left[\frac{(1+q^2)}{(1+K)^{-1}} \right]} \\
& \times \exp \left(-\frac{K\bar{\gamma}_b(1+q^2)x}{(1+K)(1+q^2) + 2q^2x\bar{\gamma}_b} \right) \bar{\gamma}_b \left((1+K)(1+q^2) + 2x\bar{\gamma}_b \right) \\
& \times \left[\frac{(1+q^2)^3}{(1+K)^{-3}} + \frac{2(1+q^2)}{(1+K)^{-1}} \left(K + (3+K)q^2 + q^4 \right) x\bar{\gamma}_b + 8q^4x^2\bar{\gamma}_b^2 \right] \quad (6.26)
\end{aligned}$$

$$f_2(x) = \frac{\exp \left(\frac{K\bar{\gamma}_b(1+q^2)\phi}{(1+K)(1+q^2) - 2\phi\bar{\gamma}_b} \right) (1+K)(1+q^2) \exp(\phi)}{\sqrt{\left((1+K)(1+q^2) - 2\phi\bar{\gamma}_b \right) \left((1+K)(1+q^2) - 2q^2\phi\bar{\gamma}_b \right) (1-e^{-x})}} \quad (6.27)$$

and $\phi = \frac{-1}{(1-e^{-x})\bar{\gamma}_e}$.

Proof. See Appendix H.1. □

Lemma 5. *The ASR and the asymptotic ASR expressions (i.e., $\bar{\gamma}_b \rightarrow \infty$) for Beckmann/Rayleigh (BR) scenario considering phase errors in the RIS-aided communications are given by*

$$\bar{\mathcal{R}}_{S-BR} \approx \frac{1}{\ln 2} \left[\sum_{i=1}^h w_i f_1(k_i) - e^{1/\bar{\gamma}_e} E_1 \left(\frac{1}{\bar{\gamma}_e} \right) + e^{1/\bar{\gamma}_e} \sum_{i=1}^h w_i f_2(k_i) \right] \quad (6.28)$$

$$\bar{\mathcal{R}}_{S-BR}^\infty \approx \frac{1}{\ln 2} \left[\sum_{i=1}^h w_i f_1(k_i) - e^{1/\bar{\gamma}_e} E_1 \left(\frac{1}{\bar{\gamma}_e} \right) \right] \quad (6.29)$$

Proof. See Appendix H.2. □

Lemma 6. *The ASR and the asymptotic ASR expressions (i.e., $\bar{\gamma}_b \rightarrow \infty$) for Nakagami/Rayleigh scenario (NR) considering phase errors in the RIS-aided communications can be expressed as*

$$\begin{aligned}
\bar{\mathcal{R}}_{S-NR} \approx & \frac{1}{\ln 2} \sum_{z=0}^{\text{Floor}(m-1)} \frac{1}{z!} \left(\frac{m}{\bar{\gamma}_b} \right)^z \exp \left(\frac{m}{\bar{\gamma}_b} \right) \Gamma(1+z) \left[\Gamma \left(-z, \frac{m}{\bar{\gamma}_b} \right) - \exp \left(\frac{1}{\bar{\gamma}_e} \right) \right. \\
& \left. \times \Gamma \left(-z, \frac{m}{\bar{\gamma}_b} + \frac{1}{\bar{\gamma}_e} \right) \right] \quad (6.30)
\end{aligned}$$

$$\bar{\mathcal{R}}_{S-NR}^\infty \approx \log_2(\bar{\gamma}_b) + \log_2(e) \left[\psi(m) - \ln(m) \right] - \frac{e^{1/\bar{\gamma}_e}}{\ln 2} E_1 \left(\frac{1}{\bar{\gamma}_e} \right). \quad (6.31)$$

Proof. See Appendix H.3. □

Notice that all secrecy metrics in Lemmas 4-6, are given in analytical closed-form expression including the Beckmann/Rayleigh case. In the next section, some secrecy metrics are evaluated to explore the impact of the phases errors in wireless communications via RIS technology.

6.4 NUMERICAL RESULTS

Here, the main goal is to assess the effect of phase errors on the secrecy performance metrics for the proposed scenarios, as well as the goodness of the scalar approximations for the equivalent composite channel in RIS-assisted communications. For the links between Alice and the RIS, and between the RIS and Bob, it is considered Rician fading, i.e, the shape parameter $K = 1$. The links between the RIS and Eve are assumed to be Rayleigh distributed, so that $a_{1,b} = a_{2,b} = \sqrt{\pi/(4(K+1))} {}_1F_1(-1/2, 1, -K)$, and $a_{2,e} = \sqrt{\pi}/2$.^[2] In our analysis, it is assumed phase errors due to the finite number of phase shifts available at the RIS. Therefore, only 2^{n_b} phases for $n_b \geq 1$ can be configured at the RIS, where n_b is the number of quantization bits used to encode the phase shifts [159]. In this sense, Θ_i in (6.2) is assumed to be uniformly distributed over the interval $[-2^{-n_b}\pi, 2^{-n_b}\pi]$. Consequently, it follows that $\varphi_1 = \frac{\sin(2^{-n_b}\pi)}{2^{-n_b}\pi}$ and $\varphi_2 = \frac{\sin(2^{-n_b+1}\pi)}{2^{-n_b+1}\pi}$ [159] for (6.10)-(6.12). In all figures, the system parameters are set to: $\bar{\gamma}_{0,e} = 10$ dB, and the ideal case of no phase errors (i.e., $n_b \rightarrow \infty$) is included as a reference in all instances. The exact values for the secrecy metrics are obtained through Monte Carlo simulations. The analytical secrecy performance metrics in the folded normal/Rayleigh (FR), Nakagami/Rayleigh (NR), and Beckmann/Rayleigh (BR) cases are included using the results in Sections 6.3.1 and 6.3.2 for the SOP and ASR, respectively. Also, analytical expressions derived in our analysis are denoted using solid lines and asymptotic expressions are represented using dashed lines.

Figs. 6.2-6.3 denote the ASR as a function of $\bar{\gamma}_{0,b}$ for different numbers of elements (i.e., n) at the RIS. Such figures explore how imperfect phase estimation, i.e, $n_b = 1$ and $n_b = 2$ affects the secrecy performance of the system. From Figs. 6.2-6.3, it can be extracted the following insights: (i) increasing the number of reflecting elements (i.e., n) allows for improving the ASR for a fixed $\bar{\gamma}_{0,b}$, thanks to the different scaling laws of the legitimate and wiretap average SNRs derived in our analysis (see, Remark 6); (ii) equivalent scalar approximations concerning FR (no phase errors) and BR (phase errors) approximate very well the real distribution regardless of the number of reflecting elements, while the NR approximation underestimates the true ASR as n decreases; (iii) asymptotic ASR formulations reveal the ASR's slope for the high SNR values; (iv) ASR expressions exhibit a linear behavior in log-scale for a wide range of SNRs, and such a range of SNRs widens with n ; (v) the performance degradation with $n_b = 2$ bits is small, which confirms that state-of-the-art solutions for RIS surfaces [167] may be enough to obtain a secrecy performance close to the case of no phase

^[2] For detailed information on such assumptions, please refer to [159]

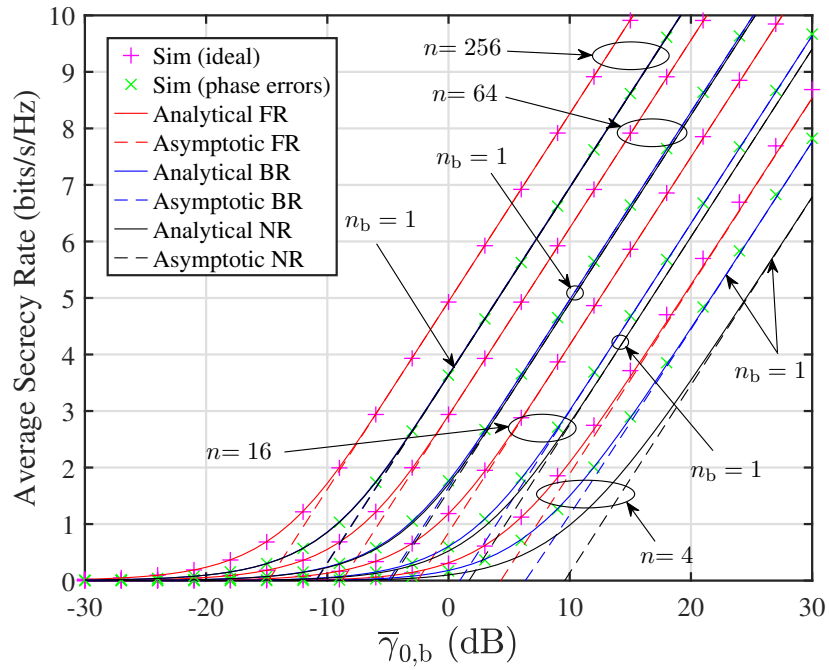


Figure 6.2: ASR as a function of $\bar{\gamma}_{0,b}$ for different values of n for $n_b = 1$. Markers correspond to the legitimate and eavesdropper channels computed with (6.2) and (6.5), respectively.

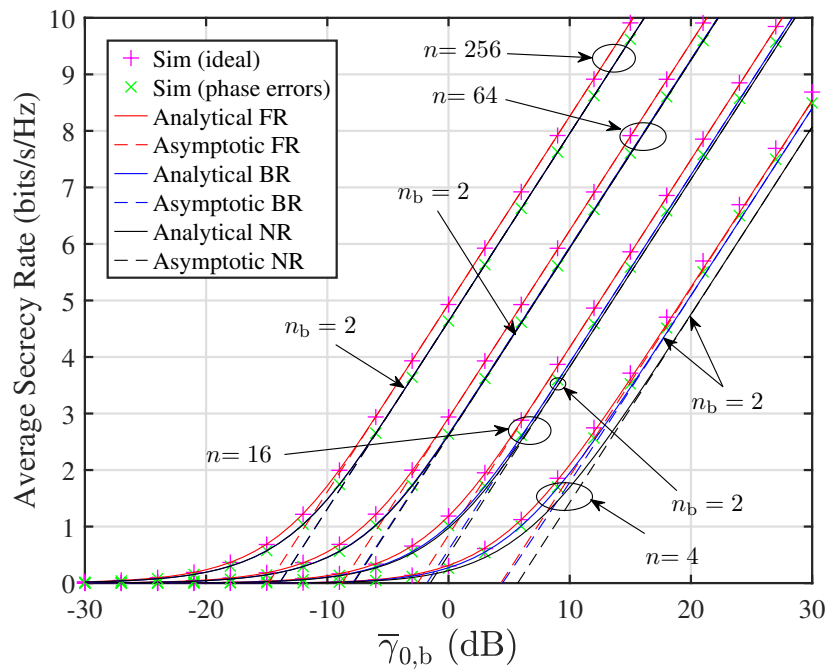


Figure 6.3: ASR as a function of $\bar{\gamma}_{0,b}$ for different values of n for $n_b = 2$. Markers correspond to the legitimate and eavesdropper channels computed with (6.2) and (6.5), respectively.

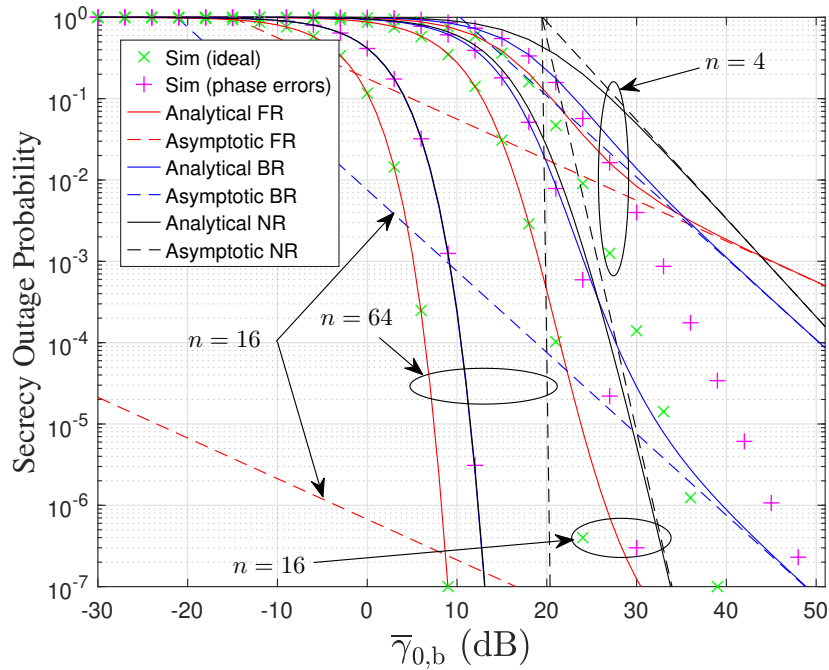


Figure 6.4: SOP as a function of $\bar{\gamma}_{0,b}$ for different values of n for $n_b = 1$. Markers correspond to the legitimate and eavesdropper channels computed with (6.2) and (6.5), respectively.

errors (i.e., ideal case); and (vi) the worst secrecy performance of the proposed approximations is achieved when the RIS has a one-bit phase shifter (i.e., $n_b = 1$). This fact corroborates that smaller n_b values mean larger phase errors.

Figs. 6.4-6.5 shows the SOP as a function of $\bar{\gamma}_{0,b}$, for different values of n . As in the previous ASR case, it is considered that the RIS have specific discrete phase shifts, i.e., $n_b = 1$ and $n_b = 2$ to evaluate the secrecy performance of the system. Here, some similar insights, as in the ASR, can be deduced from both figures: (i) for $n_b = 2$, a good secrecy performance can be attain compared to the ideal case (i.e., no phase errors), and (ii) the SOP performance deteriorates when $n_b = 1$, which means that the phase estimation in the RIS is poor. Moreover, some relevant differences are observed: while the equivalent scalar approximations work well in all instances for large n , there are substantial differences between the exact simulated results and the FR, BR, and NR cases for lower n . Regarding insights on SOP's slope, the asymptotic curves may induce confusion if not interpreted correctly. This is, while all asymptotic results are tight (i.e., they all coincide with the analytical SOP expressions for each case), the different secrecy diversity order inherent to each of the equivalent scalar approximations is translated into a different decay of the high-SNR slopes. Because of the high line-of-sight condition of the FR and BR scalar approximations, the asymptotes kick-in at very low SOP values; conversely, the NR asymptote seems to better capture the abrupt decay of the SOP for the operating range of probability values. In any case, asymptotic analyses for the SOP should be exercised with caution when using the equivalent scalar approximations, as they may not be representative of the actual behavior of the real RIS-assisted channels.

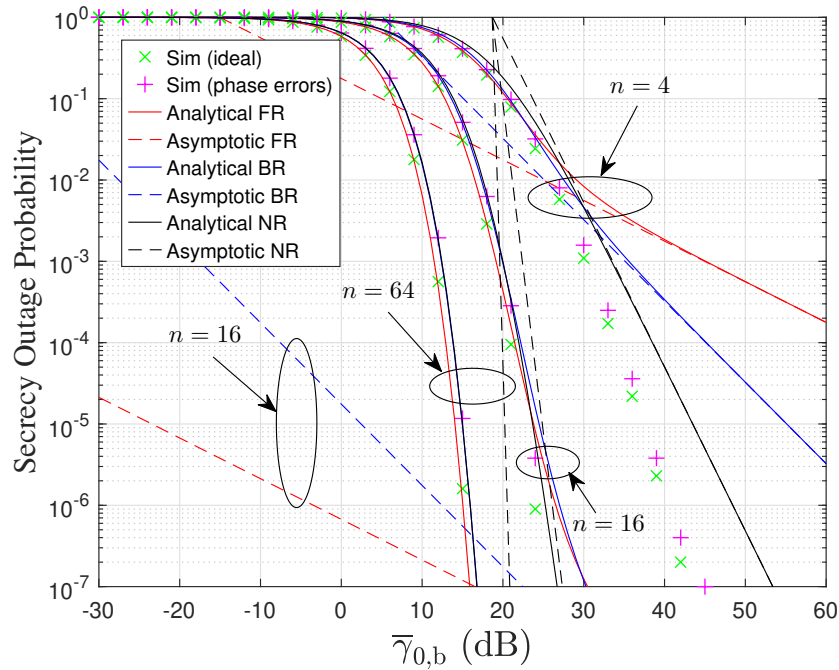


Figure 6.5: SOP as a function of $\bar{\gamma}_{0,b}$ for different values of n for $n_b = 2$. Markers correspond to the legitimate and eavesdropper channels computed with (6.2) and (6.5), respectively.

6.5 CONCLUSIONS

This chapter has provided an overview of the promising RIS technology for achieving a smart and reconfigurable environment in post-5G wireless networks. This work have formulated three approximations to capture the real secrecy performance of an RIS-aided communication with phase errors. In this context, the results have shown that even when RIS has a limited phase resolution of 2 bits, the different scaling laws for the desired and eavesdropper's SNRs allow for improving the PLS performance RIS-assisted communications. Based on this, RIS has proven useful in improving the physical layer security in future next networks. Finally, the simulation's results have validated the effectiveness of the proposed equivalent scalar channel approximations.

7 CONCLUSIONS

This chapter summarizes the general conclusions drawn from the thesis and then outlines some future research works.

7.1 THESIS CONCLUSIONS

Overall, topics including: (i) sums and ratio of RVs taken from generalized distributions; (ii) PLS over generalized fading conditions, and (iii) PLS of RIS-assisted wireless communications with imperfect phase estimation have been thoroughly explored in this thesis. Next, the major contributions of each chapter are summarized.

Chapter 3 has investigated sums and ratios of RVs taken from different types of fading channel models. The main contributions of this chapter were threefold: 1) a fast and simple approximation to the PDF of the sum of independent Nakagami- m RVs was derived by using a mixture of two Nakagami- m RVs. In this approximation, the approximate distribution parameters were estimated using an unsupervised EM learning algorithm. Furthermore, the ABEP metric over multibranch receivers was presented as an application example concerning the sums of Nakagami- m RVs; 2) a unified framework was presented to approximate the sums of generalized RVs. Specifically, the asymptotic matching method was applied to approximate the sum of κ - μ RVs. Based on the numerical results, the asymptotic matching has proven to provide an excellent fit from medium to high-SNR regime. From a practical perspective, this region is of paramount importance because it describes a wireless communication system's energy efficiency (see [117] for a nice discussion on this topic); and 3) closed-form expressions for the PDF, CDF, MGF of the ratio of two RVs envelopes taken from α - μ distributions were obtained in terms of univariate Fox H-function. Since the single Fox H-function has not yet been implemented in popular mathematical packages, this work have provided both fast convergent series expressions derived using the residues theorem and efficient implementation for the single Fox H-function in MATHEMATICA@Wolfram. Finally, to illustrate the applicability of the obtained expressions, a practical example of PLS over α - μ channels was presented.

Chapter 4 has explored the secrecy performance of the classical Wyner's wiretap model, where the main and the eavesdropper channels experience NWDP fading.

In such chapter, novel analytical expressions for the SOP, asymptotic SOP, ASC, and asymptotic ASC were derived in terms of elementary functions in the communication theory. From the SOP asymptotic analysis, useful insights into how the NWDP fading parameters of both legitimate and eavesdropper channels (e.g., K_{dB}^B , K_{dB}^E , $\alpha_{n,B}$, $\alpha_{n,E}$) affect the system performance in a high-SNR regime were also provided. Furthermore, based on the numerical results, this research has been supported the need for using ray-based fading channel models in those scenarios in which an arbitrary number of dominant specular components are considered (e.g., mm-Wave communications).

Chapter 5 has provided new equivalent representations for the κ - μ shadowed CDFs in order to derive either maximum or minimum of an arbitrary number of i.i.d. κ - μ shadowed RVs. The illustrative plots and discussions showed how different propagation factors (e.g., LOS condition, LOS fluctuation, and clustering of scattered multipath waves) impact the PLS performance over MIMO wiretap channels. Specifically, secrecy expressions such as SOP, asymptotic SOP, ASC, and Asymptotic ASC were developed in a TAS/MRC configuration. The numerical results manifested that strong LOS conditions and rich scattering waves in the legitimate path are favorable for the secrecy performance. Furthermore, it was revealed that, the asymptotic behavior depends not only on the number of antennas of the legitimate pairs but also on the clustering of scattered waves (i.e., μ_B) of the legitimate link. Conversely, the eavesdropper link's scattering environment (i.e., μ_E) plays no role in the secrecy performance of the system in the high-SNR regime.

Chapter 6 has investigated the PLS performance of a wireless communication system supported by a RIS with phase errors. Closed-form expressions for the SOP, asymptotic SOP, ASR, and asymptotic ASR were derived in terms of well-known functions. By knowing that the perfect phase estimation of the reflection phases induced by the composite channel through the RIS is unfeasible in practice; the analyzed results exhibited how the phase errors affect the secrecy performance of RIS-aided wireless communications. In this context, our analytical framework showed clear evidence that even when the RIS has a limited precision configuration of 2 bits in the estimation phase process; the ratio of the legitimate and wiretap SNRs allows for improving the PLS performance in RIS-assisted communications.

Overall, the information security at the physical layer level is an approach that relies heavily on the assumption that the channel between the transmitter and the eavesdropper is a degraded version of the channel between legitimate nodes. In this regard, the application of PLS for 5G applications is not yet a close reality, as due to the broadcast nature of the wireless medium, the legitimate channel cannot be guaranteed to be an enhanced version of the wiretap channel at all times. Nonetheless, given that the emerging new-generation environment exhibits a versatility of physical phenomena that converge in the wireless medium, our research showed that, under certain fading conditions, the PLS performance can remarkably improve in generalized fading conditions. Specifically, this work inferred that PLS techniques should be designed based on both the intrinsic features of the channel (e.g., LoS, NLoS conditions, LoS fluctuations, presence of dominant rays and clustering) and the use

of revolutionary technologies (e.g., RIS and Holographic MIMO).

Unfortunately, up to 5G, the propagation channel has been out of control of communications design engineers. In this concern, this research showed that the radio environment becomes programmable, controllable, and intelligent by leveraging the advantages of RIS technology. In fact, post-5G networks can be designed not only based on the end-points of the communications (i.e., transmitters and receivers) but also on the customization of the radio environment. Moreover, based on our findings in Chapter 6, RIS can effectively create a "dedicated" channel between two legitimate entities. Hence, PLS will finally flourish as a defense method for providing security information to upcoming wireless networks by complementing cryptography-based algorithms.

7.2 FUTURE RESEARCH DIRECTIONS

Then, a non-exhaustive list of research topics to extend the results discussed in this thesis is provided.

1. The sum of independent channel envelopes that follow NWDP distributions remains an open topic of research. Based on these results, the secrecy performance over NWDP MIMO wiretap channels is an intriguing research issue.
2. Second-order statistics, including level crossing rate and average fade duration, are still an open issue for the product and ratio of independent generalized fading channel distributions.
3. An engaging topic is to extend the asymptotic matching method to approximate sums of correlated RVs such as Nakagami- m , κ - μ , κ - μ shadowed, NWDP, among others. These approximations will allow overcoming the inherent issues of the exact statistical solutions while guaranteeing an outstanding performance for practical regimes of interest, i.e., medium to high-SNR values.
4. Nowadays, the secrecy performance has been extensively explored for the design of secure transmissions over both conventional and generalized fading channels in the context of infinite block-length. Nevertheless, the impact of having finite block-length secrecy codes on PLS performance under generalized channels is still an open field of research.
5. A most realistic wireless channel model is crucial for the performance evaluation of RIS-assisted communications. In this regard, an interesting research topic to be addressed is a propagation channel model that captures (i) key fundamentals aspects of the so-called geometric near-field of the RIS elements and (ii) spatial correlations among the RIS elements.
6. Based on the results of Chapter 6, it is the paramount importance to investigate the PLS performance of RIS-aided wireless communications over realistic propagation conditions (e.g., spatial correlation among RIS units).

8 REFERENCES

- [1] S. Haykin, *Communication Systems*, 4th ed. New York: John Wiley & Sons, 2001.
- [2] D. Tse and P. Viswanath, *Fundamentals of Wireless Communications*, Cambridge, UK: Cambridge University Press, 2005.
- [3] M. D. Yacoub, *Foundations of Mobile Radio Engineering*, Boca Raton, FL: CRC Press, 1993.
- [4] T. S. Rappaport, *Wireless Communications: Principles and Practice*, 2nd ed. New York: Prentice-Hall PTR, 1996.
- [5] G. L. Stuber, *Principles of Mobile Communication*, 2nd ed. Massachusetts: Kluwer Academic Publishers, 2001.
- [6] A. Leon Garcia, *Probability, Statistics and Random Processes for Electrical Engineering*, 3rd ed. Upper Saddle River, NJ: Prentice Hall, 2008.
- [7] E. Ezhilarasan and M. Dinakaran, "A review on mobile technologies: 3g, 4g and 5g," in *2017 Second International Conference on Recent Trends and Challenges in Computational Models (ICRTCCM)*, 2017, pp. 369–373. DOI: 10.1109/ICRTCCM.2017.90.
- [8] A. Gupta and R. K. Jha, "A survey of 5g network: Architecture and emerging technologies," *IEEE Access*, vol. 3, pp. 1206–1232, 2015. DOI: 10.1109/ACCESS.2015.2461602.
- [9] D. Liu, W. Hong, T. S. Rappaport, C. Luxey, and W. Hong, "What will 5g antennas and propagation be?" *IEEE Transactions on Antennas and Propagation*, vol. 65, no. 12, pp. 6205–6212, Dec. 2017, ISSN: 1558-2221. DOI: 10.1109/TAP.2017.2774707.
- [10] Y. J. Chun, S. L. Cotton, H. S. Dhillon, F. J. Lopez-Martinez, J. F. Paris, and S. K. Yoo, "A comprehensive analysis of 5g heterogeneous cellular systems operating over $\kappa - \mu$ shadowed fading channels," *IEEE Transactions on Wireless Communications*, vol. 16, no. 11, pp. 6995–7010, 2017. DOI: 10.1109/TWC.2017.2734080.

- [11] M. K. Samimi, G. R. MacCartney, S. Sun, and T. S. Rappaport, "28 ghz millimeter-wave ultrawideband small-scale fading models in wireless channels," in *2016 IEEE 83rd Vehicular Technology Conference (VTC Spring)*, 2016, pp. 1–6. DOI: 10.1109/VTCSpring.2016.7503970.
- [12] G. Taricco, "On the convergence of multipath fading channel gains to the rayleigh distribution," *IEEE Wireless Communications Letters*, vol. 4, no. 5, pp. 549–552, 2015. DOI: 10.1109/LWC.2015.2456066.
- [13] M. D. Yacoub, "The $\alpha - \eta - \kappa - \mu$ fading model," *IEEE Transactions on Antennas and Propagation*, vol. 64, no. 8, pp. 3597–3610, 2016. DOI: 10.1109/TAP.2016.2570235.
- [14] T. R. R. Marins, A. A. dos Anjos, V. M. R. Peñarrocha, L. Rubio, J. Reig, R. A. A. de Souza, and M. D. Yacoub, "Fading evaluation in the mm-wave band," *IEEE Transactions on Communications*, vol. 67, no. 12, pp. 8725–8738, 2019. DOI: 10.1109/TCOMM.2019.2941493.
- [15] D. Solomitckii, Q. C. Li, T. Balercia, C. R. C. M. da Silva, S. Talwar, S. Andreev, and Y. Koucheryavy, "Characterizing the impact of diffuse scattering in urban millimeter-wave deployments," *IEEE Wireless Communications Letters*, vol. 5, no. 4, pp. 432–435, 2016. DOI: 10.1109/LWC.2016.2580669.
- [16] D. He, B. Ai, K. Guan, L. Wang, Z. Zhong, and T. Kürner, "The design and applications of high-performance ray-tracing simulation platform for 5g and beyond wireless communications: A tutorial," *IEEE Communications Surveys Tutorials*, vol. 21, no. 1, pp. 10–27, 2019. DOI: 10.1109/COMST.2018.2865724.
- [17] G. D. Durgin, T. S. Rappaport, and D. A. de Wolf, "New analytical models and probability density functions for fading in wireless communications," *IEEE Transactions on Communications*, vol. 50, no. 6, pp. 1005–1015, 2002. DOI: 10.1109/TCOMM.2002.1010620.
- [18] J. M. Romero-Jerez, F. J. Lopez-Martinez, J. F. Paris, and A. J. Goldsmith, "The fluctuating two-ray fading model: Statistical characterization and performance analysis," *IEEE Transactions on Wireless Communications*, vol. 16, no. 7, pp. 4420–4432, 2017. DOI: 10.1109/TWC.2017.2698445.
- [19] J. P. Peña-Martín, J. M. Romero-Jerez, and F. J. Lopez-Martinez, "Generalized mgf of beckmann fading with applications to wireless communications performance analysis," *IEEE Transactions on Communications*, vol. 65, no. 9, pp. 3933–3943, 2017.

- [20] Y. J. Chun, "A generalized fading model with multiple specular components," Oct. 2018, arXiv:1810.05258. [Online].
- [21] J. F. Paris, "Statistical characterization of κ - μ shadowed fading," *IEEE Transactions on Vehicular Technology*, vol. 63, no. 2, pp. 518–526, 2014. DOI: 10.1109/TVT.2013.2281213.
- [22] Y. Shiu, S. Y. Chang, H. Wu, S. C. .- Huang, and H. Chen, "Physical layer security in wireless networks: A tutorial," *IEEE Wireless Communications*, vol. 18, no. 2, pp. 66–74, 2011. DOI: 10.1109/MWC.2011.5751298.
- [23] N. Yang, L. Wang, G. Geraci, M. ElKashlan, J. Yuan, and M. Di Renzo, "Safeguarding 5g wireless communication networks using physical layer security," *IEEE Communications Magazine*, vol. 53, no. 4, pp. 20–27, 2015. DOI: 10.1109/MCOM.2015.7081071.
- [24] Y. Wu, A. Khisti, C. Xiao, G. Caire, K. Wong, and X. Gao, "A survey of physical layer security techniques for 5g wireless networks and challenges ahead," *IEEE Journal on Selected Areas in Communications*, vol. 36, no. 4, pp. 679–695, 2018. DOI: 10.1109/JSAC.2018.2825560.
- [25] M. Bloch and J. Barros, *Physical-Layer Security: From Information Theory to Security Engineering*, U.K.: Cambridge Univ. Press, 2011., 2011.
- [26] H. Viswanathan and P. E. Mogensen, "Communications in the 6g era," *IEEE Access*, vol. 8, pp. 57 063–57 074, 2020. DOI: 10.1109/ACCESS.2020.2981745.
- [27] Y. Chen, P. Zhu, G. He, X. Yan, H. Baligh, and J. Wu, "From connected people, connected things, to connected intelligence," in *2020 2nd 6G Wireless Summit (6G SUMMIT)*, 2020, pp. 1–7. DOI: 10.1109/6GSUMMIT49458.2020.9083770.
- [28] V. Raghavan and J. Li, "Evolution of physical-layer communications research in the post-5g era," *IEEE Access*, vol. 7, pp. 10 392–10 401, 2019. DOI: 10.1109/ACCESS.2019.2891218.
- [29] S. Buzzi, C. D'Andrea, and C. D'Elia, "User-centric cell-free massive mimo with interference cancellation and local zf downlink precoding," in *2018 15th International Symposium on Wireless Communication Systems (ISWCS)*, 2018, pp. 1–5. DOI: 10.1109/ISWCS.2018.8491054.

- [30] H. Q. Ngo, A. Ashikhmin, H. Yang, E. G. Larsson, and T. L. Marzetta, "Cell-free massive mimo versus small cells," *IEEE Transactions on Wireless Communications*, vol. 16, no. 3, pp. 1834–1850, 2017. DOI: 10.1109/TWC.2017.2655515.
- [31] C. Huang, S. Hu, G. C. Alexandropoulos, A. Zappone, C. Yuen, R. Zhang, M. Di Renzo, and M. Debbah, "Holographic mimo surfaces for 6g wireless networks: Opportunities, challenges, and trends," *IEEE Wireless Communications*, pp. 1–8, 2020. DOI: 10.1109/MWC.001.1900534.
- [32] E. Björnson, L. Sanguinetti, H. Wymeersch, J. Hoydis, and T. L. Marzetta, "Massive mimo is a reality—what is next?: Five promising research directions for antenna arrays," *Digital Signal Processing*, vol. 94, pp. 3–20, 2019, Special Issue on Source Localization in Massive MIMO, ISSN: 1051-2004. DOI: <https://doi.org/10.1016/j.dsp.2019.06.007>. [Online]. Available: <http://www.sciencedirect.com/science/article/pii/S1051200419300776>.
- [33] E. Basar, "Reconfigurable intelligent surface-based index modulation: A new beyond mimo paradigm for 6g," *IEEE Transactions on Communications*, vol. 68, no. 5, pp. 3187–3196, 2020. DOI: 10.1109/TCOMM.2020.2971486.
- [34] W. Tang, M. Z. Chen, X. Chen, J. Y. Dai, Y. Han, M. Di Renzo, Y. Zeng, S. Jin, Q. Cheng, and T. J. Cui, "Wireless communications with reconfigurable intelligent surface: Path loss modeling and experimental measurement," *IEEE Transactions on Wireless Communications*, pp. 1–1, 2020. DOI: 10.1109/TWC.2020.3024887.
- [35] M. Nakagami, "The m -distribution - A general formula of intensity distribution of rapid fading," *Statistical Methods in Radio Wave Propagation*, vol. 26, no. 2, pp. 3–36, Apr. 1960.
- [36] J. Reig, L. Rubio, and N. Cardona, "Bivariate nakagami- m distribution with arbitrary fading parameters," *IEEE Electronic Letters*, vol. 38, no. 25, pp. 1715–1717, Dec. 2002.
- [37] M. D. Yacoub, C. R. C. M. da Silva, and J. E. V. Bautista, "Second order statistics for diversity-combining techniques in nakagami-fading channels," *IEEE Transactions on Vehicular Technology*, vol. 50, no. 6, pp. 1464–1470, Nov. 2001.
- [38] G. K. Karagiannidis and S. A. Kotsopoulos, "On the distribution of the weighted sum of l independent rician and nakagami envelopes in the presence of awgn," *KICS J. Communications Networks*, vol. 3, no. 2, pp. 26–30, Jun. 2001.

- [39] G. K. Karagiannidis, "A closed-form solution for the distribution of the sum of nakagami- m random phase vectors," *IEEE Communications Letters*, vol. 10, no. 12, pp. 828–830, Dec. 2006.
- [40] P. Dharmawansa, N. Rajatheva, and K. Ahmed, "On the distribution of the sum of nakagami- m random variables," *IEEE Transactions on Communications*, vol. 55, no. 7, pp. 1407–1416, Jul. 2007.
- [41] N. Zlatanov, Z. Hadzi-Velkov, and G. K. Karagiannidis, "An efficient approximation to the correlated nakagami- m sums and its application in equal gain diversity receivers," *IEEE Transactions on Wireless Communications*, vol. 9, no. 1, pp. 302–310, Jan. 2010.
- [42] J. Lopez-Salcedo, "Simple closed-form approximation to rician sum distributions," *IEEE Signal Processing Letters*, vol. 16, no. 3, pp. 153–155, Mar. 2009.
- [43] J. Hu and N. C. Beaulieu, "Accurate simple closed-form approximations to rayleigh sum distributions and densities," *IEEE Communications Letters*, vol. 9, no. 2, pp. 109–111, Feb. 2005.
- [44] —, "Accurate closed-form approximations to rician sum distributions and densities," *IEEE Communications Letters*, vol. 9, no. 2, pp. 133–135, Feb. 2005.
- [45] F. El Bouanani, "A new closed-form approximations for mrc receiver over non-identical weibull fading channels," in *Int. Wirel. Comm. & Mobile Comp. Conf. (IWCMC)*, Aug. 2014, pp. 4–8.
- [46] F. El Bouanani and H. Ben-Azza, "Unified analysis of egc diversity over weibull fading channels," *Intern. Journal of Commun. Syst.*, vol. 30, no. 1, pp. e2925, Feb. 2015.
- [47] F. El Bouanani, "Efficient performance evaluation for egc, mrc and sc receivers over weibull multipath fading channel," in *10th International Conference on Cognitive Radio Oriented Wireless Networks (CROWNCOM)*, Doha, Qatar, Apr. 2015, pp. 1–6.
- [48] J. C. S. Santos Filho and M. D. Yacoub, "Nakagami- m approximation to the sum of M non-identical independent nakagami- m variates," *IEEE Electronic Letters*, vol. 40, no. 15, pp. 951–952, Jul. 2004.
- [49] D. B. da Costa, M. D. Yacoub, and J. C. S. Santos Filho, "An improved closed-form approximation to the sum of arbitrary nakagami- m variates," *IEEE Transactions on Vehicular Technology*, vol. 57, no. 6, pp. 3854–3858, Nov. 2008.

- [50] J. C. S. Santos Filho and M. D. Yacoub, "Simple precise approximations to weibull sums," *IEEE Communications Letters*, vol. 10, no. 8, pp. 614–616, Aug. 2006.
- [51] —, "Highly accurate κ - μ approximation to sum of m independent non-identical rician variates," *IEEE Communications Letters*, vol. 41, no. 6, pp. 338–339, Mar. 2005.
- [52] —, "Highly accurate η - μ approximation to sum of m independent non-identical Hoyt variates," *IEEE Antennas and Wireless Propagation Letters*, vol. 4, pp. 436–438, Apr. 2005.
- [53] D. B. da Costa, M. D. Yacoub, and J. C. S. Santos Filho, "Highly accurate closed-form approximations to the sum of α - μ variates and applications," *IEEE Transactions on Wireless Communications*, vol. 7, no. 9, pp. 3301–3306, Sep. 2008.
- [54] D. B. da Costa and M. D. Yacoub, "Accurate closed-form approximations to the sum of generalized random variables and applications," in *IEEE Wireless Communications and Networking Conference (WCNC)*, 2008, pp. 785–790.
- [55] E. Illi, F. El Bouanani, and F. Ayoub, "On the distribution of the sum of Malaga M random variables and applications," *IEEE Transactions on Vehicular Technology*, pp. 1–1, Sep. 2020. DOI: 10.1109/TVT.2020.3025405.
- [56] H. Du, J. Zhang, J. Cheng, and B. Ai, "Sum of Fisher-Snedecor F random variables and its applications," *IEEE Open Journal of the Communications Society*, vol. 1, pp. 342–356, 2020. DOI: 10.1109/OJCOMS.2020.2982770.
- [57] M. Ahsen and S. A. Hassan, "On the ratio of exponential and generalized gamma random variables with applications to ad hoc SISO networks," in *2016 IEEE 84th Vehicular Technology Conference (VTC-Fall)*, Sep. 2016, pp. 1–5.
- [58] R. Annavajjala, A. Chockalingam, and S. K. Mohammed, "On a ratio of functions of exponential random variables and some applications," *IEEE Transactions on Communications*, vol. 58, no. 11, pp. 3091–3097, Nov. 2010.
- [59] S. Nadarajah and S. Kotz, "On the product and ratio of gamma and Weibull random variables," *Econometric Theory*, vol. 22, pp. 338–344, Feb. 2006.
- [60] N. T. T. P. Gia and E. Marchand, "Density of the ratio of two normal random variables and applications," *Commun. Stat., Theory Methods*, vol. 35, no. 7-9, pp. 1569–1591, Sep. 2006.

- [61] O. S. Badarneh, D. B. da Costa, M. Benjillali, and M. Alouini, "Ratio of products of fluctuating two-ray variates," *IEEE Communications Letters*, vol. 23, no. 11, pp. 1944–1948, 2019. DOI: 10.1109/LCOMM.2019.2937959.
- [62] E. J. Leonardo, D. B. da Costa, U. S. Dias, and M. D. Yacoub, "The ratio of independent arbitrary α - μ random variables and its application in the capacity analysis of spectrum sharing systems," *IEEE Communications Letters*, vol. 16, no. 11, pp. 1776–1779, Nov. 2012.
- [63] E. J. Leonardo, M. D. Yacoub, and R. A. A. de Souza, "Ratio of products of α - μ variates," *IEEE Communications Letters*, vol. 20, no. 5, pp. 1022–1025, May 2016.
- [64] C. R. N. Da Silva, N. Simmons, E. J. Leonardo, S. L. Cotton, and M. D. Yacoub, "Ratio of two envelopes taken from α - μ , η - μ , and κ - μ variates and some practical applications," *IEEE Access*, vol. 7, pp. 54 449–54 463, May 2019. DOI: 10.1109/ACCESS.2019.2907891.
- [65] C. E. Shannon, "Communication theory of secrecy systems," *Bell Syst. Tech. J.*, vol. 28, no. 4, pp. 656–715, Oct. 1949.
- [66] A. D. Wyner, "The wire-tap channel," *Bell Syst. Tech. J.*, vol. 54, no. 8, pp. 1355–1387, Oct. 1975.
- [67] I. Csiszar and J. Korner, "Broadcast channels with confidential messages," *IEEE Transactions on Information Theory*, vol. 24, no. 3, pp. 339–348, May 1978, ISSN: 1557-9654. DOI: 10.1109/TIT.1978.1055892.
- [68] S. Leung-Yan-Cheong and M. Hellman, "The gaussian wire-tap channel," *IEEE Transactions on Information Theory*, vol. 24, no. 4, pp. 451–456, Jul. 1978, ISSN: 1557-9654. DOI: 10.1109/TIT.1978.1055917.
- [69] J. Barros and M. R. D. Rodrigues, "Secrecy capacity of wireless channels," in *2006 IEEE International Symposium on Information Theory*, 2006, pp. 356–360. DOI: 10.1109/ISIT.2006.261613.
- [70] M. Bloch, J. Barros, M. R. D. Rodrigues, and S. W. McLaughlin, "Wireless information-theoretic security," *IEEE Transactions on Information Theory*, vol. 54, no. 6, pp. 2515–2534, Jun. 2008.
- [71] X. Liu, "Probability of strictly positive secrecy capacity of the rician-rician fading channel," *IEEE Wireless Communications Letters*, vol. 2, no. 1, pp. 50–53, Oct. 2013. DOI: 10.1109/WCL.2012.101812.120660.

- [72] —, “Probability of strictly positive secrecy capacity of the weibull fading channel,” in *2013 IEEE Global Communications Conference (GLOBECOM)*, Jun. 2013, pp. 659–664. DOI: 10.1109/GLOCOM.2013.6831147.
- [73] A. Shahzadi, M. G. Madiseh, and A. A. B. Shirazi, “Secret key capacity for wireless nakagami- m and suzuki fading channels,” *IJCSNS International Journal of Computer Science and Network Security*, vol. 7, no. 3, pp. 296–303, 2007.
- [74] D. Ha, T. Q. Duong, D. Tran, H. Zepernick, and T. T. Vu, “Physical layer secrecy performance over rayleigh/rician fading channels,” in *2014 International Conference on Advanced Technologies for Communications (ATC 2014)*, 2014, pp. 113–118. DOI: 10.1109/ATC.2014.7043367.
- [75] S. Iwata, T. Ohtsuki, and P. .-. Kam, “Performance analysis of physical layer security over rician/nakagami- m fading channels,” in *2017 IEEE 85th Vehicular Technology Conference (VTC Spring)*, 2017, pp. 1–6. DOI: 10.1109/VTCSpring.2017.8108517.
- [76] H. Lei, C. Gao, Y. Guo, and G. Pan, “On physical layer security over generalized gamma fading channels,” *IEEE Communications Letters*, vol. 19, no. 7, pp. 1257–1260, 2015. DOI: 10.1109/LCOMM.2015.2426171.
- [77] L. Kong, H. Tran, and G. Kaddoum, “Performance analysis of physical layer security over α - μ fading channel,” *Electronics Letters*, vol. 52, pp. 45–47, 1 Jan. 2016.
- [78] H. Lei, I. S. Ansari, G. Pan, B. Alomair, and M. Alouini, “Secrecy capacity analysis over α - μ fading channels,” *IEEE Communications Letters*, vol. 21, no. 6, pp. 1445–1448, 2017. DOI: 10.1109/LCOMM.2017.2669976.
- [79] H. Al-Hmood and H. Al-Raweshidy, “Performance analysis of physical-layer security over fluctuating beckmann fading channels,” *IEEE Access*, vol. 7, pp. 119 541–119 556, 2019. DOI: 10.1109/ACCESS.2019.2937631.
- [80] H. Zhao, Y. Liu, A. Sultan-Salem, and M. Alouini, “A simple evaluation for the secrecy outage probability over generalized- k fading channels,” *IEEE Communications Letters*, vol. 23, no. 9, pp. 1479–1483, 2019. DOI: 10.1109/LCOMM.2019.2926360.
- [81] L. Kong and G. Kaddoum, “On physical layer security over the fisher-snedecor \mathcal{F} wiretap fading channels,” *IEEE Access*, vol. 6, pp. 39 466–39 472, 2018. DOI: 10.1109/ACCESS.2018.2853700.

- [82] N. Bhargava, S. L. Cotton, and D. E. Simmons, "Secrecy capacity analysis over $\kappa - \mu$ fading channels: Theory and applications," *IEEE Transactions on Communications*, vol. 64, no. 7, pp. 3011–3024, 2016. DOI: 10.1109/TCOMM.2016.2565580.
- [83] J. M. Moualeu, D. B. da Costa, W. Hamouda, U. S. Dias, and R. A. A. de Souza, "Physical layer security over α - κ - μ and α - η - μ fading channels," *IEEE Transactions on Vehicular Technology*, vol. 68, no. 1, pp. 1025–1029, 2019. DOI: 10.1109/TVT.2018.2884832.
- [84] A. Mathur, Y. Ai, M. R. Bhatnagar, M. Cheffena, and T. Ohtsuki, "On physical layer security of α - η - κ - μ fading channels," *IEEE Communications Letters*, vol. 22, no. 10, pp. 2168–2171, 2018. DOI: 10.1109/LCOMM.2018.2860020.
- [85] W. Zeng, J. Zhang, S. Chen, K. P. Peppas, and B. Ai, "Physical layer security over fluctuating two-ray fading channels," *IEEE Transactions on Vehicular Technology*, vol. 67, no. 9, pp. 8949–8953, 2018. DOI: 10.1109/TVT.2018.2842126.
- [86] L. Wang, N. Yang, M. ElKashlan, P. L. Yeoh, and J. Yuan, "Physical layer security of maximal ratio combining in two-wave with diffuse power fading channels," *IEEE Transactions on Information Forensics and Security*, vol. 9, no. 2, pp. 247–258, 2014. DOI: 10.1109/TIFS.2013.2296991.
- [87] P. Ramírez-Espinosa, R. J. Sánchez-Alarcón, and F. J. López-Martínez, "On the beneficial role of a finite number of scatterers for wireless physical layer security," *IEEE Access*, vol. 8, pp. 105 055–105 064, 2020. DOI: 10.1109/ACCESS.2020.2999719.
- [88] A. Khisti and G. W. Wornell, "Secure transmission with multiple antennas—part ii: The mimo wiretap channel," *IEEE Transactions on Information Theory*, vol. 56, no. 11, pp. 5515–5532, 2010. DOI: 10.1109/TIT.2010.2068852.
- [89] F. Oggier and B. Hassibi, "The secrecy capacity of the mimo wiretap channel," *IEEE Transactions on Information Theory*, vol. 57, no. 8, pp. 4961–4972, 2011. DOI: 10.1109/TIT.2011.2158487.
- [90] S. Goel and R. Negi, "Guaranteeing secrecy using artificial noise," *IEEE Transactions on Wireless Communications*, vol. 7, no. 6, pp. 2180–2189, 2008. DOI: 10.1109/TWC.2008.060848.
- [91] R. Zhao, H. Lin, Y. He, D. Chen, Y. Huang, and L. Yang, "Secrecy performance of transmit antenna selection for mimo relay systems with outdated csi,"

- IEEE Transactions on Communications*, vol. 66, no. 2, pp. 546–559, 2018. DOI: 10.1109/TCOMM.2017.2747554.
- [92] Z. Chu, K. Cumanan, Z. Ding, M. Johnston, and S. Y. Le Goff, “Secrecy rate optimizations for a mimo secrecy channel with a cooperative jammer,” *IEEE Transactions on Vehicular Technology*, vol. 64, no. 5, pp. 1833–1847, 2015. DOI: 10.1109/TVT.2014.2336092.
- [93] T. Zhang, Y. Cai, Y. Huang, T. Q. Duong, and W. Yang, “Secure transmission in cognitive mimo relaying networks with outdated channel state information,” *IEEE Access*, vol. 4, pp. 8212–8224, 2016. DOI: 10.1109/ACCESS.2016.2608966.
- [94] A. Mukherjee and A. L. Swindlehurst, “Robust beamforming for security in mimo wiretap channels with imperfect csi,” *IEEE Transactions on Signal Processing*, vol. 59, no. 1, pp. 351–361, 2011. DOI: 10.1109/TSP.2010.2078810.
- [95] Z. Zhu, Z. Chu, F. Zhou, H. Niu, Z. Wang, and I. Lee, “Secure beamforming designs for secrecy mimo swipt systems,” *IEEE Wireless Communications Letters*, vol. 7, no. 3, pp. 424–427, 2018. DOI: 10.1109/LWC.2017.2780830.
- [96] P. Lin, S. Lai, S. Lin, and H. Su, “On secrecy rate of the generalized artificial-noise assisted secure beamforming for wiretap channels,” *IEEE Journal on Selected Areas in Communications*, vol. 31, no. 9, pp. 1728–1740, 2013. DOI: 10.1109/JSAC.2013.130907.
- [97] S. Sanayei and A. Nosratinia, “Antenna selection in mimo systems,” *IEEE Communications Magazine*, vol. 42, no. 10, pp. 68–73, 2004. DOI: 10.1109/MCOM.2004.1341263.
- [98] N. Yang, H. A. Suraweera, I. B. Collings, and C. Yuen, “Physical layer security of tas/mrc with antenna correlation,” *IEEE Transactions on Information Forensics and Security*, vol. 8, no. 1, pp. 254–259, 2013. DOI: 10.1109/TIFS.2012.2223681.
- [99] J. M. Moualeu, D. B. da Costa, F. J. Lopez-Martinez, W. Hamouda, T. M. N. Nkouatchah, and U. S. Dias, “Transmit Antenna Selection in Secure MIMO Systems Over $\alpha - \mu$ Fading Channels,” *IEEE Trans. Commun.*, vol. 67, no. 9, pp. 6483–6498, Sep. 2019.
- [100] L. Yang, M. O. Hasna, and I. S. Ansari, “Physical layer security for tas/mrc systems with and without co-channel interference over $\eta - \mu$ fading channels,” *IEEE Trans-*

- actions on Vehicular Technology*, vol. 67, no. 12, pp. 12 421–12 426, 2018. DOI: 10.1109/TVT.2018.2876915.
- [101] P. C. F. Eggers, M. Angjelichinoski, and P. Popovski, “Wireless channel modeling perspectives for ultra-reliable communications,” *IEEE Transactions on Wireless Communications*, vol. 18, no. 4, pp. 2229–2243, 2019. DOI: 10.1109/TWC.2019.2901788.
- [102] M. Cui, G. Zhang, and R. Zhang, “Secure wireless communication via intelligent reflecting surface,” *IEEE Wireless Commun. Lett.*, vol. 8, no. 5, pp. 1410–1414, 2019.
- [103] X. Yu, D. Xu, and R. Schober, “Enabling secure wireless communications via intelligent reflecting surfaces,” in *2019 IEEE Global Communications Conference (GLOBECOM)*, 2019, pp. 1–6.
- [104] J. Chen, Y. Liang, Y. Pei, and H. Guo, “Intelligent reflecting surface: A programmable wireless environment for physical layer security,” *IEEE Access*, vol. 7, pp. 82 599–82 612, 2019.
- [105] G. Zhou, C. Pan, H. Ren, K. Wang, A. Nallanathan, and K.K. Wong, “User cooperation for irs-aided secure swipt mimo: Active attacks and passive eavesdropping,” *arXiv preprint arXiv:2006.05347*, 2020.
- [106] D. Xu, X. Yu, Y. Sun, D. W. K. Ng, and R. Schober, “Resource allocation for secure irs-assisted multiuser miso systems,” in *2019 IEEE Globecom Workshops (GC Wkshps)*, 2019, pp. 1–6. DOI: 10.1109/GCWkshps45667.2019.9024490.
- [107] X. Guan, Q. Wu, and R. Zhang, “Intelligent reflecting surface assisted secrecy communication via joint beamforming and jamming,” *arXiv preprint arXiv:1907.12839*, Jul. 2019.
- [108] H. Yang, Z. Xiong, J. Zhao, D. Niyato, L. Xiao, and Q. Wu, “Deep reinforcement learning based intelligent reflecting surface for secure wireless communications,” *IEEE Transactions on Wireless Communications*, pp. 1–1, 2020. DOI: 10.1109/TWC.2020.3024860.
- [109] H. Shen, W. Xu, S. Gong, Z. He, and C. Zhao, “Secrecy rate maximization for intelligent reflecting surface assisted multi-antenna communications,” *IEEE Communications Letters*, vol. 23, no. 9, pp. 1488–1492, 2019. DOI: 10.1109/LCOMM.2019.2924214.

- [110] J. Chen, Y. Liang, Y. Pei, and H. Guo, "Intelligent reflecting surface: A programmable wireless environment for physical layer security," *IEEE Access*, vol. 7, pp. 82 599–82 612, 2019. DOI: 10.1109/ACCESS.2019.2924034.
- [111] X. Guan, Q. Wu, and R. Zhang, "Intelligent reflecting surface assisted secrecy communication: Is artificial noise helpful or not?" *IEEE Wireless Communications Letters*, vol. 9, no. 6, pp. 778–782, 2020. DOI: 10.1109/LWC.2020.2969629.
- [112] L. Yang, J. Yang, W. Xie, M. O. Hasna, T. Tsiftsis, and M. D. Renzo, "Secrecy performance analysis of ris-aided wireless communication systems," *IEEE Transactions on Vehicular Technology*, vol. 69, no. 10, pp. 12 296–12 300, 2020. DOI: 10.1109/TVT.2020.3007521.
- [113] M. Tahir, S. P. W. Jarot, and M. U. Siddiqi, "Wireless physical layer security using channel state information," in *International Conference on Computer and Communication Engineering (ICCCE'10)*, 2010, pp. 1–5. DOI: 10.1109/ICCCE.2010.5556862.
- [114] B. Bhushan and G. Sahoo, "Recent advances in attacks, technical challenges, vulnerabilities and their countermeasures in wireless sensor networks," *Wireless Pers. Commun.*, vol. 98, no. 2, pp. 2037–2077, Jan. 2018.
- [115] P. K. Gopala, L. Lai, and H. El Gamal, "On the secrecy capacity of fading channels," *IEEE Transactions on Information Theory*, vol. 54, no. 10, pp. 4687–4698, Oct. 2008.
- [116] V. U. Prabhu and M. R. D. Rodrigues, "On wireless channels with m-antenna eavesdroppers: Characterization of the outage probability and outage secrecy capacity," *IEEE Transactions on Information Forensics and Security*, vol. 6, no. 3, pp. 853–860, Sep. 2011.
- [117] Z. Wang and G. B. Giannakis, "A simple and general parameterization quantifying performance in fading channels," *IEEE Trans. Commun.*, vol. 51, no. 8, pp. 1389–1398, Aug. 2003.
- [118] F. Yilmaz and M. Alouini, "Novel asymptotic results on the high-order statistics of the channel capacity over generalized fading channels," in *2012 IEEE 13th International Workshop on Signal Processing Advances in Wireless Communications (SPAWC)*, 2012, pp. 389–393.
- [119] P. Billingsley, *Probability and Measures*, anniversary. Wiley Series in Probability and Statistics., 2012.

- [120] M. K. Simon and M.-S. Alouini, *Digital Communications over Fading Channels*, 2nd ed. John Wiley & Sons, Inc., 2005.
- [121] S. O. Rice, "Statistical properties of a sine wave plus random noise," *The Bell System Technical Journal*, vol. 27, no. 1, pp. 109–157, 1948. DOI: 10.1002/j.1538-7305.1948.tb01334.x.
- [122] Zhengdao Wang and G. B. Giannakis, "A simple and general parameterization quantifying performance in fading channels," *IEEE Trans. Commun.*, vol. 51, no. 8, pp. 1389–1398, Aug. 2003.
- [123] M. D. Yacoub, "The α - μ distribution: A physical fading model for the stacy distribution," *IEEE Transactions on Vehicular Technology*, vol. 56, no. 1, pp. 27–34, 2007. DOI: 10.1109/TVT.2006.883753.
- [124] D. W. M. Q. Wu and I. Sen, "5-ghz-band vehicle-to-vehicle channels: Models for multiple values of channel bandwidth," *IEEE Transactions on Vehicular Technology*, vol. 59, no. 5, pp. 2620–2625, Jun. 2010.
- [125] P. K. C. et al, "Wind-blown foliage and human-induced fading in ground-surface narrowband communications at 400 mhz," *IEEE Transactions on Vehicular Technology*, vol. 60, no. 4, pp. 1326–1336, Jun. 2011.
- [126] A. M. et al, "Statistical analysis for on-body spatial diversity communications at 2.45 ghz," *IEEE Transactions on Vehicular Technology*, vol. 60, no. 8, pp. 4014–4019, Jun. 2012.
- [127] M. D. Yacoub, "The κ - μ distribution and the η - μ distribution," *IEEE Antennas and Propagation Magazine*, vol. 49, no. 1, pp. 68–81, 2007. DOI: 10.1109/MAP.2007.370983.
- [128] F. J. Lopez-Martinez, J. F. Paris, and J. M. Romero-Jerez, "The κ - μ shadowed fading model with integer fading parameters," *IEEE Transactions on Vehicular Technology*, vol. 66, no. 9, pp. 7653–7662, 2017. DOI: 10.1109/TVT.2017.2678430.
- [129] G. D. Durgin, "Theory of stochastic local area channel modeling for wireless communications," Ph.D. dissertation, Virginia Tech, 2000.
- [130] E. Zochmann, S. Caban, C. F. Mecklenbrauker, S. Pratschner, M. Lerch, S. Schwarz, and M. Rupp, "Better than rician: Modelling millimetre wave channels as two-wave with diffuse power," *EURASIP Journal on Wireless Communications and Networking*, vol. 2019, no. 1, pp. 1–21, 2019.

- [131] Y. P. Hong, W.-J. Huang, and C. C. J. Kuo, *Cooperative communications and Networking: Technologies and System Design*, New York, USA: Springer, 2010.
- [132] Q. Wu and R. Zhang, "Towards smart and reconfigurable environment: Intelligent reflecting surface aided wireless network," *IEEE Communications Magazine*, vol. 58, no. 1, pp. 106–112, 2020. DOI: 10.1109/MCOM.001.1900107.
- [133] Ö. Özdogan, E. Björnson, and E. G. Larsson, "Using intelligent reflecting surfaces for rank improvement in mimo communications," in *ICASSP 2020 - 2020 IEEE International Conference on Acoustics, Speech and Signal Processing (ICASSP)*, 2020, pp. 9160–9164. DOI: 10.1109/ICASSP40776.2020.9052904.
- [134] E. Basar, M. Di Renzo, J. De Rosny, M. Debbah, M. Alouini, and R. Zhang, "Wireless communications through reconfigurable intelligent surfaces," *IEEE Access*, vol. 7, pp. 116 753–116 773, 2019. DOI: 10.1109/ACCESS.2019.2935192.
- [135] T. Wang, G. Chen, J. Coon, and M.-A. Badiu, "Study of intelligent reflective surface assisted communications with one-bit phase adjustments," Aug. 2020, arXiv:2008.09770. [Online].
- [136] D. G. Brennan, "Linear diversity combining techniques," *Proceedings of the IRE*, vol. 47, no. 6, pp. 1075–1102, 1959. DOI: 10.1109/JRPROC.1959.287136.
- [137] A. Papoulis and S. U. Pillai, *Probability, Random Variables, and Stochastic Processes*, 4th ed. New York, NY, USA: McGraw-Hill, 2002.
- [138] C. P. Robert and G. Casella, *Monte Carlo Statistical Methods*. New York, NY, USA: Springer, 2014.
- [139] M. Dapor, *Random Numbers. In: Transport of Energetic Electrons in Solids*. Berlin, Germany: Springer, 2014.
- [140] T. W. site, *RandomVariate function*. [Online]. Available: <http://reference.wolfram.com/language/ref/RandomVariate.html> (visited on 11/11/2020).
- [141] T. M. site, *makedist function*. [Online]. Available: <http://mathworks.com/help/stats/makedist.html> (visited on 11/11/2020).
- [142] Y. Kabalci, "An improved approximation for the nakagami- m inverse cdf using artificial bee colony optimization," *Wireless Netw.*, vol. 24, no. 2, pp. 663–669, Feb. 2018.

- [143] M. Bilim and I. Develi, "A new nakagami- m inverse cdf approximation based on the use of genetic algorithm," *Wireless Personal Commun.*, vol. 83, no. 3, pp. 2279–2287, Aug. 2015.
- [144] K. Yasin, "On the Nakagami- m inverse cumulative distribution function: Closed-form expression and its optimization by backtracking search optimization algorithm," *Wireless Personal Commun.*, vol. 91, no. 1, pp. 1–8, Jun. 2016.
- [145] O. Shechtman, *The Coefficient of Variation as an Index of Measurement Reliability. In: Methods of Clinical Epidemiology*. New York, NY, USA:Springer Heidelberg, 2013.
- [146] O. Alhussein, B. Selim, T. Assaf, S. Muhaidat, J. Liang, and G. K. Karagiannidis, "A generalized mixture of gaussians for fading channels," in *2015 IEEE 81st Vehicular Technology Conference (VTC Spring)*, 2015, pp. 1–6. DOI: 10.1109/VTCSpring.2015.7145607.
- [147] M. Blume, *Expectation maximization: A Gentle Introduction*. Tech. Univ. Munich Inst. Comp. Sci., Munich, Germany, 2002.
- [148] G. McLachlan and D. Peel, *Finite Mixture Models*. New York, NY, USA:Wiley, 2000.
- [149] Abramowitz and I. A. Stegun, *Handbook of Mathematical Functions With Formulas, Graphs, and Mathematical Tables*, 10th ed. New York, NY, USA: Dover, 1972.
- [150] E. Zedini, I. S. Ansari, and M. Alouini, "Performance analysis of mixed nakagami- m and gamma–gamma dual-hop fso transmission systems," *IEEE Photonics Journal*, vol. 7, no. 1, pp. 1–20, 2015. DOI: 10.1109/JPHOT.2014.2381657.
- [151] Y. Deng, L. Wang, M. ElKashlan, K. J. Kim, and T. Q. Duong, "Generalized selection combining for cognitive relay networks over nakagami- m fading," *IEEE Transactions on Signal Processing*, vol. 63, no. 8, pp. 1993–2006, 2015. DOI: 10.1109/TSP.2015.2405497.
- [152] P. S. Bithas, A. G. Kanatas, D. B. da Costa, P. K. Upadhyay, and U. S. Dias, "On the double-generalized gamma statistics and their application to the performance analysis of v2v communications," *IEEE Transactions on Communications*, vol. 66, no. 1, pp. 448–460, 2018. DOI: 10.1109/TCOMM.2017.2757466.
- [153] A. M. Magableh and M. M. Matalgah, "Moment generating function of the generalized α - μ distribution with applications," *IEEE Communications Letters*, vol. 13, no. 6, pp. 411–413, 2009. DOI: 10.1109/LCOMM.2009.090339.
- [154] *The wolfram functions site*, <http://functions.wolfram.com/id>, Accessed: 2020-10-20.

- [155] R. K. S. A. Mathai and H. J. Haubold, *The H-Function Theory and Applications*. Springer, 2010.
- [156] T. Bai and R. W. Heath, "Coverage and rate analysis for millimeter-wave cellular networks," *IEEE Transactions on Wireless Communications*, vol. 14, no. 2, pp. 1100–1114, 2015. DOI: 10.1109/TWC.2014.2364267.
- [157] C. Chen and A. Abdi, "Bit error rate in multipath wireless channels with several specular paths," *Electronics Letters*, vol. 14, no. 18, pp. 1046–1048, 2011.
- [158] P. Ramirez-Espinosa and F. J. Lopez-Martinez, "On the utility of the inverse gamma distribution in modeling composite fading channels," Apr. 2019, arXiv:1905.00069. [Online].
- [159] M. Badiu and J. P. Coon, "Communication Through a Large Reflecting Surface With Phase Errors," *IEEE Wireless Commun. Lett.*, vol. 9, no. 2, pp. 184–188, Feb. 2020.
- [160] E. Basar, "Transmission through large intelligent surfaces: A new frontier in wireless communications," in *2019 European Conference on Networks and Communications (EuCNC)*, Jun. 2019, pp. 112–117.
- [161] F. J. Scire, "A probability density function theorem for the modulo y values of the sum of two statistically independent processes," *Proceedings of the IEEE*, vol. 56, no. 2, pp. 204–205, Feb. 1968.
- [162] P. Beckmann, "Statistical distribution of the amplitude and phase of a multiply scattered field," *J. Res. Natl. Bur. Stand. (U. S.)-D. Radio Propagation*, vol. 66D, no. 3, pp. 231–240, Jun. 1962.
- [163] N. Bhargav, S. L. Cotton, and D. E. Simmons, "Secrecy Capacity Analysis Over κ - μ Fading Channels: Theory and Applications," *IEEE Transactions on Communications*, vol. 64, no. 7, pp. 3011–3024, Jul. 2016.
- [164] F. J. Lopez-Martinez, J. M. Romero-Jerez, and J. F. Paris, "On the Calculation of the Incomplete MGF With Applications to Wireless Communications," *IEEE Trans. Commun.*, vol. 65, no. 1, pp. 458–469, Jan. 2017.
- [165] J. Abate and W. Whitt, "Numerical Inversion of Laplace Transforms of Probability Distributions," *ORSA J. Comput.*, vol. 7, no. 1, pp. 36–43, 1995. DOI: 10.1287/ijoc.7.1.36. eprint: <https://doi.org/10.1287/ijoc.7.1.36>. [Online]. Available: <https://doi.org/10.1287/ijoc.7.1.36>.

- [166] F. R. A. Parente, F. d. P. Calmon, and J. C. S. Santos Filho, "Asymptotic system performance over generalized fading channels with application to maximal-ratio combining," *Journal of Communication and Information Systems*, vol. 35, no. 1, pp. 171–180, Jul. 2020. DOI: 10.14209/jcis.2020.18. [Online]. Available: <https://jcis.sbrt.org.br/jcis/article/view/714>.
- [167] L. D. et al., "Reconfigurable Intelligent Surface-Based Wireless Communications: Antenna Design, Prototyping, and Experimental Results," *IEEE Access*, vol. 8, pp. 45 913–45 923, 2020.
- [168] I. S. Gradshteyn and I. M. Ryzhik, *Table of Integrals, Series and Products*, 7th ed. San Diego, CA, USA: Academic Press, 2007.
- [169] E. W. Ng and M. Geller, "A table of integrals of the error functions," *Journal of Research of the National Bureau of Standards-B. Mathematical Sciences*, vol. 73B, no. 1, pp. 1–20, 1969.
- [170] R. L. Graham, D. E. Knut, and O. Patashnik, *Concrete Mathematics: A Foundation for Computer Science*, 2nd ed. Reading, MA: Addison-Wesley, 1994.
- [171] N. Bhargav, C. R. N. Da Silva, Y. J. Chun, E. J. Leonardo, S. L. Cotton, and M. D. Yacoub, "On the product of two κ - μ random variables and its application to double and composite fading channels," *IEEE Transactions on Wireless Communications*, vol. 17, no. 4, pp. 2457–2470, Apr. 2018.
- [172] M. E. Mead, "Generalized inverse gamma distribution and its application in reliability," *Communications in Statistics-Theory and Methods*, vol. 44, no. 7, pp. 1426–1435, Mar. 2015.
- [173] C. R. N. Da Silva, E. J. Leonardo, and M. D. Yacoub, "Product of two envelopes taken from α - μ , κ - μ , and η - μ distributions," *IEEE Transactions on Communications*, vol. 66, no. 3, pp. 1284–1295, Mar. 2018.
- [174] J. Romero-Jerez, F. Lopez-Martinez, J. Pena-Martin, and A. Abdi, "Stochastic fading channel models with multiple dominant specular components for 5g and beyond," May 2019, arXiv:1905.03567. [Online].
- [175] Y. A. B. A. P. Prudnikov and O. Marichev, *Integrals and Series, vol. 2: Special Functions*. Gordon and Breach, New York, 1986.
- [176] R. F. B. F. W. J. Olver D. W. Lozier, *NIST Handbook of Mathematical Functions*. U.K.: Cambridge University Press, 2010.

- [177] R. Nelson, "Expectation and fundamental theorems," in *Probability, Stochastic Processes, and Queueing Theory: The Mathematics of Computer Performance Modeling*. New York, NY: Springer New York, 1995, pp. 167–231, ISBN: 978-1-4757-2426-4. DOI: 10.1007/978-1-4757-2426-4_5. [Online]. Available: https://doi.org/10.1007/978-1-4757-2426-4_5.
- [178] V. Perim, J. D. V. Sánchez, and J. C. S. S. Filho, "Asymptotically exact approximations to generalized fading sum statistics," *IEEE Trans. Wireless Commun.*, vol. 19, no. 1, pp. 205–217, Jan. 2020.
- [179] L. Moreno-Pozas, F. J. Lopez-Martinez, J. F. Paris, and E. Martos-Naya, "The κ - μ shadowed fading model: Unifying the κ - μ and η - μ distributions," *IEEE Transactions on Vehicular Technology*, vol. 65, no. 12, pp. 9630–9641, Dec. 2016.
- [180] M. Di Renzo, F. Graziosi, and F. Santucci, "Channel capacity over generalized fading channels: A novel mgf-based approach for performance analysis and design of wireless communication systems," *IEEE Transactions on Vehicular Technology*, vol. 59, no. 1, pp. 127–149, 2010.
- [181] A. C. Moraes, D. B. da Costa, and M. D. Yacoub, "A simple, accurate approximation for the outage probability of equal-gain receivers with cochannel interference in an alpha-mu fading scenario," in *2008 IEEE Wireless Communications and Networking Conference*, 2008, pp. 54–58.

9 APPENDICES

A DERIVATION OF THE ABEP EXPRESSIONS

A.1 PROOFS OF PROPOSITION 1

ABEP Approximation for non-coherent modulations

Substituting (3.9) and (2.62) into (2.60), it arrives to

$$P_e \approx \sum_{i=1}^2 \frac{\omega_i m_i^{m_i}}{\Gamma(m_i) \Omega_i^{m_i}} \underbrace{\int_0^\infty r^{2m_i-1} \exp\left(-r^2 \left(\frac{m_i}{\Omega_i} - \frac{gE_b}{N_0}\right)\right) dr}_{I_1}. \quad (\text{A.1})$$

Here, with the aid of [168, Eq. (3.326.2)] to solve the integral in I_1 , the ABEP for non-coherent schemes can be expressed as in (3.26), which concludes the proof.

ABEP Approximation for coherent modulations

Inserting (3.9) and (2.63) into (2.60), this gets to

$$P_e \approx \sum_{i=1}^2 \frac{\omega_i m_i^{m_i}}{\Gamma(m_i) \Omega_i^{m_i}} \underbrace{\int_0^\infty r^{2m_i-1} \exp\left(-\frac{r^2 m_i}{\Omega_i}\right) \operatorname{erfc}\left(r \sqrt{gE_b/N_0}\right) dr}_{I_2}. \quad (\text{A.2})$$

Next, using [169, Eq. (4.3.9)] to solve the integral in I_2 , it follows that

$$I_2 = \left(\frac{E_b g}{N_0}\right)^{-m_i} \frac{\Gamma(2m_i) {}_2F_1\left(m_i, \frac{1}{2} + m_i; 1 + m_i; -\frac{m_i}{\frac{E_b g \Omega_i}{N_0}}\right)}{\Gamma(m_i) 4^{m_i}}. \quad (\text{A.3})$$

Replacing (A.2) into (A.3), the ABEP for coherent schemes can be expressed as in (3.27), which concludes the proof.

A.2 PROOFS OF PROPOSITION 2

ABEP expression in the low SNR regime for non-coherent modulations

By considering the Maclaurin series^[1] [149, Eq. (25.2.24)]

$$f(x) = \sum_{k=0}^n \frac{(x)^k f^{(k)}(0)}{k!} + R_n, \quad (\text{A.4})$$

where, R_n is a remainder term known as the Lagrange remainder [149, Eq. (25.2.25)]. Now, by using the second term of Maclaurin expansion in (A.4) for the denominator of (3.26), because at low SNR regime, it is assumed that $\frac{E_b}{N_0}$ in the higher order coefficients are zero. So, this gets to

$$\left(\frac{E_b g}{N_0} + \frac{m_i}{\Omega_i} \right)^{m_i} \approx \left(\frac{m_i}{\Omega_i} \right)^{m_i} + g \Omega_i \left(\frac{m_i}{\Omega_i} \right)^{m_i} \left(\frac{E_b g}{N_0} \right) + \frac{g^2 (m_i - 1) \Omega_i^2}{2 m_i} \left(\frac{m_i}{\Omega_i} \right)^{m_i} \left(\frac{E_b}{N_0} \right)^2. \quad (\text{A.5})$$

Next, by substituting (A.5) into (3.26), this yields

$$P_e \approx \frac{\frac{\omega_1}{2} \left(\frac{m_1}{\Omega_1} \right)^{m_1}}{\left(\frac{m_1}{\Omega_1} \right)^{m_1} + m_1 \left(\frac{E_b g}{N_0} \right) \left(\frac{m_1}{\Omega_1} \right)^{m_1 - 1}} + \frac{\frac{(1 - \omega_1)}{2} \left(\frac{m_2}{\Omega_2} \right)^{m_2}}{\left(\frac{m_2}{\Omega_2} \right)^{m_2} + m_2 \left(\frac{E_b g}{N_0} \right) \left(\frac{m_2}{\Omega_2} \right)^{m_2 - 1}}. \quad (\text{A.6})$$

After simple mathematical manipulations in (A.6), the expression given in (3.28) is achieved.

ABEP expression in the low SNR regime for coherent modulations

For this scenario, when $\frac{E_b}{N_0}$ in (3.27) goes to zero, the term $-\frac{1}{\frac{\Omega_i g E_b}{m_i N_0}}$ goes to ∞ , thus the Hypergeometric function ${}_2F_1(\cdot, \cdot; \cdot; \cdot)$ in (3.27) also goes to zero. Bearing this in mind, our aim is to find an expression in a closed-form that complies with the aforementioned requirements. For this purpose, by replacing the Hypergeometric Function in (3.27) by its mathematical identity given in [154, Eq. (07.24.17.0054.01)]

$${}_2F_1 \left(a, b; c; -\frac{1}{p} \right) = \left(1 + \frac{1}{p} \right)^{-a} {}_2F_1 \left(a, c - b; c; \frac{1}{p + 1} \right), \quad (\text{A.7})$$

therefore, this yields

$$P_e \approx \frac{\omega_1 \Gamma(2m_1) {}_2F_1 \left(m_1, \frac{1}{2}; 1 + m_1; \frac{1}{\frac{E_b \Omega_1 g}{N_0 m_1} + 1} \right)}{\left(1 + \frac{1}{\frac{E_b \Omega_1 g}{N_0 m_1}} \right)^{m_1} \Gamma(m_1) \left(\frac{4E_b \Omega_1 g}{N_0 m_1} \right)^{m_1}} + \frac{(1 - \omega_1) \Gamma(2m_2) {}_2F_1 \left(m_2, \frac{1}{2}; 1 + m_2; \frac{1}{\frac{E_b \Omega_2 g}{N_0 m_2} + 1} \right)}{\left(1 + \frac{1}{\frac{E_b \Omega_2 g}{N_0 m_2}} \right)^{m_2} \Gamma(m_2) \left(\frac{4E_b \Omega_2 g}{N_0 m_2} \right)^{m_2}}. \quad (\text{A.8})$$

Then, by substituting the regularized Hypergeometric function ${}_2F_1(\cdot, \cdot; \cdot; \cdot)$ by its the integral definition

^[1] In particular, the Maclaurin series is a special case of the Taylor series where the function is expanded around zero.

given in [154, Eq. (07.24.07.0001.01)] as

$${}_2F_1(a, b; c; p) = \frac{1}{\Gamma(b)\Gamma(c-b)} \int_0^1 \frac{t^{b-1} (1-t)^{-b+c-1} dt}{(1-tp)^a}, \quad (\text{A.9})$$

into (A.8), it follows that

$$P_e \approx \frac{\frac{\omega_1 \Gamma(2m_1)}{\Gamma(\frac{1}{2})\Gamma(m_1+\frac{1}{2})} \int_0^1 \frac{t^{-\frac{1}{2}} (1-t)^{m_1-\frac{1}{2}} dt}{(1-\frac{E_b \Omega_1 g}{N_0 m_1} t)^{m_1}}}{\left(1 + \frac{1}{\frac{E_b \Omega_1 g}{N_0 m_1}}\right)^{m_1} \Gamma(m_1) \left(\frac{4E_b \Omega_1 g}{N_0 m_1}\right)^{m_1}} + \frac{\frac{(1-\omega_1)\Gamma(2m_2)}{\Gamma(\frac{1}{2})\Gamma(m_2+\frac{1}{2})} \int_0^1 \frac{t^{-\frac{1}{2}} (1-t)^{m_2-\frac{1}{2}} dt}{(1-\frac{E_b \Omega_2 g}{N_0 m_2} t)^{m_2}}}{\left(1 + \frac{1}{\frac{E_b \Omega_2 g}{N_0 m_2}}\right)^{m_2} \Gamma(m_2) \left(\frac{4E_b \Omega_2 g}{N_0 m_2}\right)^{m_2}}. \quad (\text{A.10})$$

Now, performing some algebraic operations in (A.10), it arrives to

$$P_e \approx \frac{\frac{\omega_1 \Gamma(2m_1)}{\Gamma(\frac{1}{2})\Gamma(m_1+\frac{1}{2})} \int_0^1 \frac{t^{-\frac{1}{2}} (1-t)^{m_1-\frac{1}{2}} \left(1 + \frac{E_b \Omega_1 g}{N_0 m_1}\right)^{m_1} dt}{\left(1 + \frac{E_b \Omega_1 g}{N_0 m_1} t\right)^{m_1}}}{\left(1 + \frac{1}{\frac{E_b \Omega_1 g}{N_0 m_1}}\right)^{m_1} \Gamma(m_1) \left(\frac{4E_b \Omega_1 g}{N_0 m_1}\right)^{m_1}} + \frac{\frac{(1-\omega_1)\Gamma(2m_2)}{\Gamma(\frac{1}{2})\Gamma(m_2+\frac{1}{2})} \int_0^1 \frac{t^{-\frac{1}{2}} (1-t)^{m_2-\frac{1}{2}} \left(1 + \frac{E_b \Omega_2 g}{N_0 m_2}\right)^{m_2} dt}{\left(1 + \frac{E_b \Omega_2 g}{N_0 m_2} t\right)^{m_2}}}{\left(1 + \frac{1}{\frac{E_b \Omega_2 g}{N_0 m_2}}\right)^{m_2} \Gamma(m_2) \left(\frac{4E_b \Omega_2 g}{N_0 m_2}\right)^{m_2}}. \quad (\text{A.11})$$

With the purpose of simplifying the mathematical complexity in (A.11) for finding a closed-form formulation at low SNR regime, by replacing $\frac{E_b}{N_0}$ with zero in the terms corresponding to the Hypergeometric function ${}_2F_1(\cdot, \cdot; \cdot; \cdot)$. Thus, this leads to

$$P_e \approx \frac{\frac{\omega_1 \Gamma(2m_1)}{\Gamma(\frac{1}{2})\Gamma(m_1+\frac{1}{2})} \int_0^1 \frac{t^{-\frac{1}{2}} (1-t)^{m_1-\frac{1}{2}} (1+0)^{m_1} dt}{(1+0-t)^{m_1}}}{\Gamma(\frac{1}{2})\Gamma(m_1+\frac{1}{2}) \left(1 + \frac{1}{\frac{E_b \Omega_1 g}{N_0 m_1}}\right)^{m_1} \Gamma(m_1) \left(\frac{4E_b \Omega_1 g}{N_0 m_1}\right)^{m_1}} + \frac{\frac{(1-\omega_1)\Gamma(2m_2)}{\Gamma(\frac{1}{2})\Gamma(m_2+\frac{1}{2})} \int_0^1 \frac{t^{-\frac{1}{2}} (1-t)^{m_2-\frac{1}{2}} (1+0)^{m_2} dt}{(1+0-t)^{m_2}}}{\left(1 + \frac{1}{\frac{E_b \Omega_2 g}{N_0 m_2}}\right)^{m_2} \Gamma(m_2) \left(\frac{4E_b \Omega_2 g}{N_0 m_2}\right)^{m_2}}. \quad (\text{A.12})$$

After some mathematical manipulations and by solving the corresponding integrals in (A.12), it follows that

$$P_e \approx \frac{\omega_1 \Gamma(2m_1) \left[\Gamma(\frac{1}{2})\right]^2 \left(\frac{4E_b \Omega_1 g}{N_0 m_1}\right)^{-m_1}}{\Gamma(\frac{1}{2})\Gamma(m_1+\frac{1}{2}) \left(\frac{\frac{E_b \Omega_1 g}{N_0 m_1} + 1}{\frac{E_b \Omega_1 g}{N_0 m_1}}\right)^{m_1} \Gamma(m_1)} + \frac{(1-\omega_1)\Gamma(2m_2) \left[\Gamma(\frac{1}{2})\right]^2 \left(\frac{4E_b \Omega_2 g}{N_0 m_2}\right)^{-m_2}}{\Gamma(\frac{1}{2})\Gamma(m_2+\frac{1}{2}) \left(\frac{\frac{E_b \Omega_2 g}{N_0 m_2} + 1}{\frac{E_b \Omega_2 g}{N_0 m_2}}\right)^{m_2} \Gamma(m_2)}. \quad (\text{A.13})$$

Finally, by performing simple mathematical manipulations in (A.13), the expression in (3.29) is reached. This completes the proof.

A.3 PROOFS OF PROPOSITION 3

ABEP expression in the high-SNR regime for non-coherent modulations

In the high-SNR regime, it follows that P_e in (3.26) goes to zero as $\frac{E_b}{N_0}$ becomes larger. Here, our goal is to achieve an expression that meets this assumption. To attain this, one can start by using the

binomial theorem [170, Eq. (5.13)] for x, y , and $r \in \mathbb{R}$

$$(x + y)^r = x^r \left(1 + \frac{y}{x}\right)^r, \quad (\text{A.14})$$

into (3.26), therefore, this gets to

$$P_e \approx \frac{\frac{\omega_1}{2} \left(\frac{m_1}{\Omega_1 g}\right)^{m_1}}{\left(\frac{E_b}{N_0}\right)^{m_1} \left(1 + \frac{\frac{m_1}{\Omega_1}}{\frac{E_b g}{N_0}}\right)^{m_1}} + \frac{\frac{(1-\omega_1)}{2} \left(\frac{m_2}{\Omega_2 g}\right)^{m_2}}{\left(\frac{E_b}{N_0}\right)^{m_2} \left(1 + \frac{\frac{m_2}{\Omega_2}}{\frac{E_b g}{N_0}}\right)^{m_2}}. \quad (\text{A.15})$$

Now, without loss of generality, it is assumed $m_2 > m_1$. Based on this assumption, one can consider that $\left(\frac{E_b}{N_0}\right)^{m_2}$ grows to infinity more quickly than $\left(\frac{E_b}{N_0}\right)^{m_1}$ at high SNR (i.e., $\frac{E_b}{N_0}$ goes to ∞), so, this leads to

$$P_e \approx \frac{\frac{\omega_1}{2} \left(\frac{m_1}{\Omega_1 g}\right)^{m_1}}{\left(\frac{E_b}{N_0}\right)^{m_1} (1 + 0)^{m_1}} + 0. \quad (\text{A.16})$$

From (A.16), the general expression of ABEP at high SNR can be calculated as in (3.30), where $m = \min\{m_1, m_2\}$. This completes the proof.

ABEP expression in the high-SNR regime for coherent modulations

It is worth mentioning that in the high SNR regime, when $\frac{E_b}{N_0}$ in (3.27) goes to ∞ , the term $-\frac{1}{\frac{\Omega_i g E_b}{m_i N_0}}$ goes to zero and consequently the Hypergeometric function ${}_2F_1(\cdot, \cdot; \cdot; \cdot)$ in (3.27) tends to $\frac{1}{\Gamma(1+m)}$ ^[2] as will be proved below. Taking this into consideration, the first step is to substitute the Hypergeometric Function in (3.27) by (A.9), then, this gets to

$$P_e \approx \frac{\omega_1 \Gamma(2m_1) \left[\frac{1}{\Gamma(\frac{1}{2}+m_1)\Gamma(\frac{1}{2})} \int_0^1 \frac{t^{m_1-\frac{1}{2}}(1-t)^{-\frac{1}{2}} dt}{\left(1 + \frac{t}{\frac{E_b \Omega_1 g}{N_0 m_1}}\right)^{m_1}} \right]}{\Gamma(m_1) \left(\frac{4E_b \Omega_1 g}{N_0 m_1}\right)^{m_1}} + \frac{(1-\omega_1) \Gamma(2m_2) \left[\frac{1}{\Gamma(\frac{1}{2}+m_2)\Gamma(\frac{1}{2})} \int_0^1 \frac{t^{m_2-\frac{1}{2}}(1-t)^{-\frac{1}{2}} dt}{\left(1 + \frac{t}{\frac{E_b \Omega_2 g}{N_0 m_2}}\right)^{m_2}} \right]}{\Gamma(m_2) \left(\frac{4E_b \Omega_2 g}{N_0 m_2}\right)^{m_2}}. \quad (\text{A.17})$$

In this case, a procedure similar to that applied to analyze the high SNR regime of ABEP for non-coherent modulation is considered (i.e., it is assumed $m_2 > m_1$). Hence, once again, one can consider that $\left(\frac{E_b}{N_0}\right)^{m_2}$ grows to infinity more quickly than $\left(\frac{E_b}{N_0}\right)^{m_1}$ at high SNR (i.e., $\frac{E_b}{N_0}$ goes to ∞), thus, this leads to

$$P_e \approx \frac{\omega_1 \Gamma(2m_1)}{\left(\frac{E_b}{N_0}\right)^{m_1}} \left[\frac{\frac{1}{\Gamma(\frac{1}{2}+m_1)\Gamma(\frac{1}{2})} \int_0^1 \frac{t^{m_1-\frac{1}{2}}(1-t)^{-\frac{1}{2}} dt}{(1+0)^{m_1}}}{\Gamma(m_1) \left(\frac{4\Omega_1 g}{m_1}\right)^{m_1}} \right]. \quad (\text{A.18})$$

^[2] The parameter m is governed by the lower value between m_1 , and m_2 as will be seen in developing this appendix.

Herein, by solving the integral in (A.18), it follows that

$$P_e \approx \frac{\omega_1 \Gamma(2m_1)}{\left(\frac{E_b}{N_0}\right)^{m_1}} \left[\frac{\frac{1}{\Gamma(\frac{1}{2}+m_1)\Gamma(\frac{1}{2})} \times \frac{\Gamma(\frac{1}{2}+m_1)\Gamma(\frac{1}{2})}{\Gamma(1+m_1)}}{\Gamma(m_1) \left(\frac{4\Omega_1 g}{m_1}\right)^{m_1}} \right]. \quad (\text{A.19})$$

Finally, after a process of simplification in (A.19), the general formulation as in (3.31) can be attained, where $m = \min\{m_1, m_2\}$. This completes the proof.

B DERIVATION OF THE κ - μ EXPRESSIONS

B.1 PROOF OF PROPOSITION 4

Substituting the series expansion of $I_0(\cdot)$ [154, id. (03.02.02.0001.01)] and exponential function $\exp(\cdot)$ [149, Eq. (25.2.24)]

$$I_v(z) = \sum_{k=0}^{\infty} \frac{1}{\Gamma(k+v+1)k!} \left(\frac{z}{2}\right)^{2k+v}, \quad (\text{B.1a})$$

$$\exp(-z) = \sum_{k=0}^{\infty} \frac{(-1)^k z^k}{k!}. \quad (\text{B.1b})$$

into (3.32), this yields

$$\begin{aligned} f_{R_i}(r) &= \frac{2\mu_i(1+\kappa_i)^{\frac{1+\mu_i}{2}} r^{\mu_i}}{\kappa_i^{\frac{\mu_i-1}{2}} \Omega_i^{\frac{\mu_i+1}{2}} \exp(\mu_i \kappa_i)} \left(\frac{1}{\Gamma(\mu_i)} \left(\mu_i r \sqrt{\frac{\kappa_i(1+\kappa_i)}{\Omega_i}} \right)^{\mu_i-1} - \frac{1}{\Gamma(\mu_i)} \left(\frac{\mu_i(1+\kappa_i)r^2}{\Omega_i} \right) \right. \\ &\quad \times \left. \left(\mu_i r \sqrt{\frac{\kappa_i(1+\kappa_i)}{\Omega_i}} \right)^{2+\mu_i-1} + \frac{\Gamma(2+\mu_i)^{-1}}{2!2!} \left(\frac{\mu_i(1+\kappa_i)r^2}{\Omega_i} \right)^2 \left(\mu_i r \sqrt{\frac{\kappa_i(1+\kappa_i)}{\Omega_i}} \right)^{4+\mu_i-1} - \dots \right). \end{aligned} \quad (\text{B.2})$$

Now, by rewriting (B.2) in the format of (3.36), this leads to

$$f_{R_i}(r) = \sum_{n=0}^{\infty} \underbrace{\frac{2\mu_i(1+\kappa_i)^{\frac{1+\mu_i}{2}} (-1)^n \Gamma(k+\mu_i)^{-1}}{\kappa_i^{\frac{\mu_i-1}{2}} \Omega_i^{\frac{\mu_i+1}{2}} \exp(\mu_i \kappa_i) n!n!} \left(\frac{\mu_i(1+\kappa_i)}{\Omega_i} \right)^n \left(\mu_i r \sqrt{\frac{\kappa_i(1+\kappa_i)}{\Omega_i}} \right)^{2n+\mu_i-1}}_{a_{i,n}} r^{\overbrace{4n+2\mu_i-1}^{b_{i,n}}}. \quad (\text{B.3})$$

From (B.3), the coefficients of the Maclaurin series for the κ - μ case are formulated as in (3.35), thus accomplishing the proof.

B.2 DERIVATION OF THE EQUATION SYSTEM FOR κ - μ CASE

From (3.45b), the matching $\tilde{b}_0 = b_0$ with the help of (3.47b) and (3.43b) can be expressed as

$$2\tilde{\mu} - 1 = (M - 1) + \sum_{i=1}^M b_{i,0}. \quad (\text{B.4})$$

Using, (3.35b) with $n = 0$ into (B.4), this yields

$$\begin{aligned} 2\tilde{\mu} - 1 &= (M - 1) + \sum_{i=1}^M 2\mu_i - 1 \\ 2\tilde{\mu} - 1 &= M - 1 - M + 2 \sum_{i=1}^M \mu_i. \end{aligned} \quad (\text{B.5})$$

After simple mathematical simplifications in (B.5), the $\tilde{\mu}$ parameter can be formulated as in (3.49a). Next, with the help of (2.32), (3.45c) can be expressed as (3.49b). Now, using (3.35) with $n = 0$, (3.43a) can be rewritten as

$$\begin{aligned} a_0 &= \frac{\prod_{i=1}^M \left[\frac{2\mu_i(1+\kappa_i)^{\frac{1+\mu_i}{2}}}{\kappa_i^{\frac{\mu_i-1}{2}} \Omega_i^{\frac{\mu_i+1}{2}} \exp(\mu_i \kappa_i) \Gamma(\mu_i)} \left(\mu_i \sqrt{\frac{\kappa_i(1+\kappa_i)}{\Omega_i}} \right)^{\mu_i-1} \Gamma(1+2\mu_i-1) \right]}{\Gamma\left(M + \sum_{i=1}^M 2\mu_i - 1\right)} \\ &= \frac{\prod_{i=1}^M \left[\frac{2\mu_i(1+\kappa_i)^{\frac{1+\mu_i}{2}}}{\kappa_i^{\frac{\mu_i-1}{2}} \Omega_i^{\frac{\mu_i+1}{2}} \exp(\mu_i \kappa_i) \Gamma(\mu_i)} \left(\mu_i \sqrt{\frac{\kappa_i(1+\kappa_i)}{\Omega_i}} \right)^{\mu_i-1} \Gamma(2\mu_i) \right]}{\Gamma\left(2 \sum_{i=1}^M \mu_i\right)}. \end{aligned} \quad (\text{B.6})$$

Finally, by matching (B.6) with (3.47), (3.43a) is expressed as in (3.49c). This completes the proof.

C DERIVATION OF THE RATIO STATISTICS

C.1 PROOFS OF PROPOSITION 5

PDF of X

Substituting (3.58) into (3.50), it follows that

$$f_X(x) = \frac{\alpha_1 \alpha_2 x^{\frac{\alpha_1 \mu_1}{2} - 1}}{4 \beta_2^{\frac{\alpha_2 \mu_2}{2}} \beta_1^{\frac{\alpha_1 \mu_1}{2}} \Gamma(\mu_2) \Gamma(\mu_1)} \int_0^\infty y^{\frac{\alpha_2 \mu_2}{2} + \frac{\alpha_1 \mu_1}{2} - 1} G_{0,1}^{1,0} \left[\left(\frac{xy}{\beta_1} \right)^{\frac{\alpha_1}{2}} \mid 0 \right] G_{0,1}^{1,0} \left[\left(\frac{y}{\beta_2} \right)^{\frac{\alpha_2}{2}} \mid 0 \right] dy. \quad (\text{C.1})$$

After some mathematical manipulations in (C.1), it follows that

$$f_X(x) = \frac{\alpha_1 x^{\frac{\alpha_1 \mu_1}{2} - 1}}{2 \beta_2^{\frac{\alpha_2 \mu_2}{2}} \beta_1^{\frac{\alpha_1 \mu_1}{2}} \Gamma(\mu_2) \Gamma(\mu_1)} \underbrace{\int_0^\infty w^{\mu_2 + k \mu_1 - 1} G_{10,1}^{1,0} \left[\frac{w}{\beta_2^{\frac{\alpha_2}{2}}} \mid 0 \right] G_{0,1}^{1,0} \left[\frac{w^k}{\left(\frac{x}{\beta_1} \right)^{-\frac{\alpha_1}{2}}} \mid 0 \right] dw}_{I_1}, \quad (\text{C.2})$$

where $w = y^{\alpha_2/2}$ and recalling that $k = \frac{\alpha_1}{\alpha_2}$. Then, by using [154, Eq. (07.34.21.0012.01)], I_1 in (C.2) can be solved in a straightforward manner as

$$I_1 = \left(\frac{1}{\beta_2^{\frac{\alpha_2}{2}}} \right)^{-(\mu_2 + k \mu_1)} H_{1,1}^{1,1} \left[\left(\frac{x \beta_2}{\beta_1} \right)^{\frac{\alpha_2}{2}} \mid \begin{matrix} (1 - \mu_2 - k \mu_1, k) \\ (0, 1) \end{matrix} \right]. \quad (\text{C.3})$$

Finally, by replacing I_1 into (C.2), the expression in (3.60) can be obtained.

CDF of X

Replacing (3.58) and (3.59) into (3.51), this leads to

$$F_X(x) = \frac{\alpha_2 x^{\frac{\mu_1 \alpha_1}{2}}}{2 \beta_2^{\frac{\alpha_2 \mu_2}{2}} \beta_1^{\frac{\alpha_1 \mu_1}{2}} \Gamma(\mu_2) \Gamma(\mu_1)} \int_0^\infty y^{\frac{\alpha_2 \mu_2}{2} + \frac{\alpha_1 \mu_1}{2} - 1} G_{0,1}^{1,0} \left[\left(\frac{y}{\beta_2} \right)^{\frac{\alpha_2}{2}} \mid 0 \right] G_{1,2}^{1,1} \left[\left(\frac{xy}{\beta_1} \right)^{\frac{\alpha_1}{2}} \mid \begin{matrix} 1 - \mu_1 \\ 0, -\mu_1 \end{matrix} \right] dy. \quad (\text{C.4})$$

Here, a similar procedure as in the derivation of the PDF of X is employed. That is, by replacing

$w = y^{\alpha_Y/2}$ and $k = \frac{\alpha_1}{\alpha_2}$ into (C.4), it follows that

$$F_X(x) = \frac{x^{\frac{\mu_1 \alpha_1}{2}}}{\beta_2^{\frac{\alpha_2 \mu_2}{2}} \beta_1^{\frac{\alpha_1 \mu_1}{2}} \Gamma(\mu_2) \Gamma(\mu_1)} \underbrace{\int_0^\infty w^{\mu_1 k + \mu_2 - 1} G_{I_2, 0, 1}^{1, 0} \left[\frac{w}{\beta_Y^{\frac{\alpha_Y}{2}}} \middle| 0 \right] G_{1, 2}^{1, 1} \left[\left(\frac{x}{\beta_1} \right)^{\frac{\alpha_1}{2}} w^k \middle| \begin{matrix} 1 - \mu_1 \\ 0, -\mu_X \end{matrix} \right]}_{I_2} dw. \quad (C.5)$$

Now, by using [154, Eq.(07.34.21.0009.01)], I_2 in (C.5) can be solved in a straightforward manner as

$$I_2 = \left(\frac{1}{\beta_2^{\frac{\alpha_2}{2}}} \right)^{-(\mu_1 k + \mu_2)} H_{2, 2}^{1, 2} \left[\left(\frac{x \beta_2}{\beta_1} \right)^{\frac{\alpha_1}{2}} \middle| \begin{matrix} (1 - \mu_1, 1), (1 - \mu_1 k - \mu_2, k) \\ (0, 1), (-\mu_1, 1) \end{matrix} \right]. \quad (C.6)$$

Finally, substituting (C.6) into (C.5), a closed-form expression for the CDF of $X = \gamma_1 / \gamma_2$ can be calculated as in (3.61). This completes the proof.

MGF of X

Replacing $f_X(x)$ given as in (3.60) into (3.53), this leads to

$$\mathcal{M}_X(s) = \frac{\alpha_1}{2\Gamma(\mu_2)\Gamma(\mu_1)} \left(\frac{\beta_2}{\beta_1} \right)^{\frac{\alpha_1 \mu_1}{2}} \int_0^\infty x^{\frac{\alpha_1 \mu_1}{2} - 1} e^{-sx} H_{1, 1}^{1, 1} \left[\left(\frac{x \beta_2}{\beta_1} \right)^{\frac{\alpha_1}{2}} \middle| \begin{matrix} (1 - \mu_2 - k\mu_1, k) \\ (0, 1) \end{matrix} \right] dx. \quad (C.7)$$

Substituting the Fox H-function in (C.7) by its Mellin-Barnes type contour integral as in [155, Eq. (1.2)], interchanging the order of integrations, and performing some simplifications, this gets to

$$\begin{aligned} \mathcal{M}_X(s) &= \frac{\alpha_1 \left(\frac{\beta_2}{\beta_1} \right)^{\frac{\alpha_1 \mu_1}{2}}}{2\Gamma(\mu_2)\Gamma(\mu_1)} \int_0^\infty x^{\frac{\alpha_1 \mu_1}{2} - 1} \exp(-sx) \frac{1}{2\pi j} \int_C \Gamma(z) \Gamma(\mu_2 + k\mu_1 - kz) \left[\left(\frac{x \beta_2}{\beta_1} \right)^{\frac{\alpha_1}{2}} \right]^{-z} dz dx \\ &= \frac{\alpha_1 \left(\frac{\beta_2}{\beta_1} \right)^{\frac{\alpha_1 \mu_1}{2}}}{2\Gamma(\mu_2)\Gamma(\mu_1)j} \frac{1}{2\pi j} \int_C \Gamma(z) \Gamma(\mu_2 + k\mu_1 - kz) \left[\left(\frac{\beta_2}{\beta_1} \right)^{\frac{\alpha_1}{2}} \right]^{-z} \underbrace{\int_0^\infty x^{\frac{\alpha_1 \mu_1}{2} - \frac{z \alpha_1}{2} - 1} \exp(-sx) dx}_{I_3} dz \end{aligned} \quad (C.8)$$

Here, with the help of [168, Eq. (3.351.3)], I_3 can be solved as

$$I_3 = s^{-\frac{\mu_1 \alpha_1}{2} + \frac{\alpha_1 z}{2}} \Gamma \left(\frac{\mu_1 \alpha_1}{2} - \frac{\alpha_1 z}{2} \right). \quad (C.9)$$

Thus, (C.8) can be formulated as

$$\mathcal{M}_X(s) = \frac{\alpha_1 \left(\frac{\beta_2}{\beta_1} \right)^{\frac{\alpha_1 \mu_1}{2}} s^{-\frac{\alpha_1 \mu_1}{2}}}{2\Gamma(\mu_2)\Gamma(\mu_1)} \underbrace{\frac{1}{2\pi j} \int_C \Gamma(z) \Gamma(\mu_2 + k\mu_1 - kz) \Gamma \left(\frac{\mu_1 \alpha_1}{2} - \frac{\alpha_1 z}{2} \right) \left[\left(\frac{\beta_2}{s \beta_1} \right)^{\frac{\alpha_1}{2}} \right]^{-z} dz}_{I_4} \quad (C.10)$$

Then, by substituting I_4 in (C.10) by its corresponding Fox H-function with the use of [155, Eq. (1.2)], the expression in (3.62) is obtained, thus accomplishing the proof.

Higher Order Moments of X

The n -th order moment for a RV X is defined as (3.52). However, to calculate the n -th moment of the ratio of squared α - μ distributed RVs, $X = \gamma_1/\gamma_2$, the identity for the product of two statistically independent RVs is employed, i.e., $\mathbb{E}[(\gamma_1\gamma_2)^n] = \mathbb{E}[\gamma_1^n] \mathbb{E}[\gamma_2^n]$ [171]. Now, for the case of the ratio of two squared RVs, the approach is interested in solving $\mathbb{E}[(\gamma_1/\gamma_2)^n]$, thus is necessary to determine the n -th moment of the inverse of a RV γ_2 . To this end, let us define $A = 1/\gamma_2 = 1/R_2^2$, such that $\mathbb{E}[(\gamma_1 A)^n] = \mathbb{E}[\gamma_1^n] \mathbb{E}[A^n]$. Thus, by determining the moments of $\mathbb{E}[\gamma_1^n]$ and $\mathbb{E}[A^n]$, the higher order moments of $\mathbb{E}[X^n]$ can be found. In order to compute $\mathbb{E}[A^n]$, it is defined Y_2 as the inverse of the envelope R_2 , i.e., $Y_2 = 1/R_2$. Hence, the moments of A can be determined by considering $\mathbb{E}[A^n] = \mathbb{E}[Y_2^{2n}]$ [53].

First, it is defined the n -th moment of the envelope of an α - μ RV. Then, from [123], it follows that

$$\mathbb{E}[R^n] = \Omega^n \frac{\Gamma(\mu + n/\alpha)}{\mu^{n/\alpha} \Gamma(\mu)}. \quad (\text{C.11})$$

Next, by substituting (C.11) into $\mathbb{E}[\Upsilon_1^n] = \mathbb{E}[R_1^{2n}]$, this yields

$$\mathbb{E}[\gamma_1^n] = \Omega_1^{2n} \frac{\Gamma(\mu_1 + 2n/\alpha_1)}{\mu_1^{2n/\alpha_1} \Gamma(\mu_1)}. \quad (\text{C.12})$$

Recalling that Y_2 is the inverse of envelope R_2 with PDF given in (2.27). Therefore, the PDF of Y_2 can be expressed as in [172, Eq. (4)] by

$$f_{Y_2}(y) = \frac{\alpha_2 \Omega_2^{\mu_2 \alpha_2} y^{-1 - \alpha_2 \mu_2}}{\mu_2^{\mu_2} \Gamma(\mu_2)} \exp\left(-\frac{\Omega_2^{\alpha_2}}{\mu_2 y^{\alpha_2}}\right). \quad (\text{C.13})$$

From (C.13), the n -th moment $\mathbb{E}[Y_2^n]$ can be expressed as [172]

$$\mathbb{E}[Y_2^n] = \Omega_2^n \frac{\Gamma(\mu_2 - n/\alpha_2)}{\mu_2^{n/\alpha_2} \Gamma(\mu_2)}, \quad n > \mu_2 \alpha_2. \quad (\text{C.14})$$

Then, by inserting (C.14) into $\mathbb{E}[A^n] = \mathbb{E}[Y_2^{2n}]$, it follows that

$$\mathbb{E}[A^n] = \Omega_2^{2n} \frac{\Gamma(\mu_2 - 2n/\alpha_2)}{\mu_2^{2n/\alpha_2} \Gamma(\mu_2)}, \quad n > \mu_2 \alpha_2. \quad (\text{C.15})$$

Finally, by inserting (C.14) and (C.15) into $\mathbb{E}[X^n] = \mathbb{E}[\Upsilon_1^n] \mathbb{E}[A^n]$, the formulation in (3.63) is reached, thus completing the proof.

C.2 REPRESENTATION OF THE FOX-H FUNCTION AS A SUM OF RESIDUES

Here, for illustration purposes, the Fox H-functions in (3.60)-(3.62) are expressed as a sum of residues [173]. Therefore, by defining the Fox H-function as in [155, Eq. (1.1)], it follows that

$$H_{p,q}^{m,n}[z] = H_{p,q}^{m,n} \left[z \left| \begin{matrix} (a_1, A_1), \dots, (a_p, A_p) \\ (b_1, B_1), \dots, (b_q, B_q) \end{matrix} \right. \right] = \frac{1}{2\pi i} \int_{\mathcal{C}} \Theta(s) z^{-s} ds, \quad (\text{C.16})$$

where $m, n, p, q \in \mathbb{N}$, with $0 \leq n \leq p$, $1 \leq m \leq q$, $z \in \mathbb{C}$. Here

$$\Theta(s) = \frac{\left\{ \prod_{j=1}^m \Gamma(b_j + B_j s) \right\} \left\{ \prod_{j=1}^n \Gamma(1 - a_j - A_j s) \right\}}{\left\{ \prod_{j=m+1}^q \Gamma(1 - b_j - B_j s) \right\} \left\{ \prod_{j=n+1}^p \Gamma(a_j + A_j s) \right\}}. \quad (\text{C.17})$$

An empty product is always interpreted as unity, $A_i, B_j \in \mathbb{R}^+$, $a_i, b_j \in \mathbb{C}$, $i = 1, \dots, p$; $j = 1, \dots, q$. In addition, $\mathcal{C} = (c - i\infty, c + i\infty)$ is a contour of integration separating the poles of $\Gamma(1 - a_j - A_j s)$, $j = 1, \dots, n$ from those of $\Gamma(b_j + B_j s)$, $j = 1, \dots, m$. On the other hand, the contour integral \mathcal{C} in (C.16) can be obtained by the sum of residues technique, evaluated at all poles of $\Theta(s)$ [155]. Hence,

$$\frac{1}{2\pi i} \int_{\mathcal{C}} \Theta(s) z^{-s} ds = \sum_{h=0}^{\infty} \lim_{s \rightarrow \pm \chi(h)} (s \pm \chi(h)) \Theta(s) z^{-s}, \quad (\text{C.18})$$

where $\chi(h)$ is a specific pole of $\Theta(s)$. Now, using (C.16) and (C.17), H_2 in (3.61) can be rewritten as

$$H_2 = \frac{1}{2\pi i} \int_{\mathcal{C}} \frac{\Gamma(s) \Gamma(\mu_1 - s) \Gamma(k\mu_1 + \mu_2 - ks) z^{-s} ds}{\Gamma(1 + \mu_1 - s)}, \quad (\text{C.19})$$

where the suitable contour \mathcal{C} separates all the poles of $\Gamma(s)$ to the left from those of $\Gamma(\mu_1 - s)$ and $\Gamma(k\mu_1 + \mu_2 - ks)$ to the right. Then, it is possible to evaluate (C.19) as the sum of residues, as follows

$$H_2 = S_1 + S_2, \quad (\text{C.20})$$

where, the analysis of the Fox H-function given in (C.19) has been split into two sums of residues^[1], according to the following ranges of values of k : (i) $\chi(h) = -h$, for $k \leq 1$; (ii) $\chi(h) = \mu_1 + h$ and $\chi(h) = \frac{k\mu_1 + \mu_2 + h}{k}$, for $k \geq 1$. Now, by using (C.18) and the condition for $k \leq 1$ into (C.19), the term S_1 can be formulated as

^[1] It is worth mentioning that S_1 corresponds to the sum of residues with respect to the pole of $\Gamma(s)$. On the other hand, S_2 corresponds to the sum of residues regarding the poles of $\Gamma(\mu_1 - s)$ and $\Gamma(k\mu_1 + \mu_2 - ks)$.

$$\begin{aligned}
S_1 &= \sum_{h=0}^{\infty} \lim_{s \rightarrow -h} \frac{\Gamma(s)\Gamma(\mu_1 - s)\Gamma(k\mu_1 + \mu_2 - ks)}{(s+h)^{-1}\Gamma(1 + \mu_1 - s)z^s} \\
&= \sum_{h=0}^{\infty} \frac{z^h \Gamma(k(h + \mu_1) + \mu_2)}{(-1)^h (h + \mu_1)\Gamma(1 + h)}. \tag{C.21}
\end{aligned}$$

Likewise, by using (C.18) and the condition for $k \geq 1$ into (C.19), the term S_2 can be expressed as

$$\begin{aligned}
S_2 &= - \sum_{h=0}^{\infty} \lim_{s \rightarrow h + \mu_1} \frac{\Gamma(s)\Gamma(\mu_1 - s)\Gamma(k\mu_1 + \mu_2 - ks)}{(s - h - \mu_1)^{-1}\Gamma(1 + \mu_1 - s)z^s} - \sum_{h=0}^{\infty} \lim_{s \rightarrow \frac{k\mu_1 + \mu_2 + h}{k}} \frac{\Gamma(s)\Gamma(\mu_1 - s)\Gamma(k\mu_1 + \mu_2 - ks)}{\left(s - \frac{k\mu_1 + \mu_2 + h}{k}\right)^{-1}\Gamma(1 + \mu_1 - s)z^s} \\
&= \sum_{h=0}^{\infty} \frac{z^{-h - \mu_1} \Gamma(h + \mu_1) \Gamma(-hk + \mu_2)}{(-1)^{h-2} \Gamma(1 - h) h!} + \sum_{h=0}^{\infty} \frac{z^{-\frac{h}{k} - \mu_1 - \frac{\mu_2}{k}} \Gamma\left(\frac{-h - \mu_2}{k}\right) \Gamma\left(\frac{h + k\mu_1 + \mu_2}{k}\right)}{(-1)^{h-2} \Gamma\left(\frac{-h + k - \mu_2}{k}\right) k h!}. \tag{C.22}
\end{aligned}$$

By following a similar procedure as in the solution for H_2 , the series representation for H_1 and H_3 can be obtained as in (3.64) and (3.66), respectively.

C.3 MATHEMATICA IMPLEMENTATION FOR THE SINGLE FOX H-FUNCTION

Tabla C.1: MATHEMATICA®IMPLEMENTATION OF THE FOX-H FUNCTION

```

(*H-Fox Function*)
Clear all;
FOX::InconsistentCoeffs = "Inconsistent coefficients!";
FOX[z_,a_,b_] := Module[{},
(*where "z" is the argument of the Fox H Function, "a" and "b" are the
coefficient sequences of Fox H Function defined as:
a={{a1,A1},...,{an,An}},{{an+1,An+1},...,{ap,Ap}}
b={{b1,B1},...,{bm,Bm}},{{bm+1,Bm+1},...,{bq,Bq}}*)
(*Computation of  $\theta(s)$ , See Eq. (32) *)
Pa=Function[s,Product[Gamma[1-a[[1,n,1]]-s a[[1,n,2]]],{n,1,Length[a[[1]]]}];
Pb=Function[s,Product[Gamma[b[[1,n,1]]+s b[[1,n,2]]],{n,1,Length[b[[1]]]}];
Qa=Function[s,Product[Gamma[a[[2,n,1]]+s a[[2,n,2]]],{n,1,Length[a[[2]]]}];
Qb=Function[s,Product[Gamma[1-b[[2,n,1]]-s b[[2,n,2]]],{n,1,Length[b[[2]]]}];
Theta=Function[s,Pa[s]Pb[s]/Qa[s]/Qb[s]];
(*Countour limiters (Depends on numerator of  $\theta(s)$ )*
var[Gamma[x_]]:=x;
var[Times[x_,y_]]:={var[Times[x]],var[Times[y]]};
RPoles=var[Pa[s]];
LPoles=var[Pb[s]];
ArrayPa=ConstantArray[0,Length[a[[1]]];
ArrayPb=ConstantArray[0,Length[b[[1]]];
If[Length[a[[1]]]==1,ArrayPa[[1]]=s/.Solve[RPoles==0,s],For[i=1,i<=Length[a[[1]]],
i++,ArrayPa[[i]]=s/.Solve[RPoles[[i]]==0,s]];
If[Length[b[[1]]]==1,ArrayPb[[1]]=s/.Solve[LPoles==0,s],For[j=1,j<=Length[b[[1]]],
j++,ArrayPb[[j]]=s/.Solve[LPoles[[j]]==0,s]];
(*Assignments*)
epsilon=Max[ArrayPb]+0.1;
R=Min[ArrayPa]-0.1;
W=80;
(*Evaluation*)
Print["Numerical Integration:"];
value= $\frac{1}{2\pi i}$ NIntegrate[Theta[s](z)-s,
{s,epsilon-I W,R-epsilon-I W,R-epsilon+I W,epsilon+I W},
MaxRecursion->55];
(*Returning back the value*)
Return[value];];

```

D DERIVATION OF THE SECRECY METRICS FOR THE NWDP FADING MODEL

D.1 PROOFS OF PROPOSITION 6

D.1.1 SOP

Substituting (4.1) into (2.5), this leads to

$$\begin{aligned} \text{SOP} = & \underbrace{\sum_{z_B=0}^{\infty} C_{z_B} \sum_{k_B=0}^{z_B} \frac{(-1)^{k_B}}{k_B!} \binom{z_B}{k_B} \frac{1}{\bar{\gamma}_E} \sum_{z_E=0}^{\infty} C_{z_E}}_{C_1} \int_0^{\infty} \exp\left(-\frac{\gamma_E}{\bar{\gamma}_E}\right) L_{z_E}\left(\frac{\gamma_E}{\bar{\gamma}_E}\right) \\ & \times \Upsilon\left(k_B + 1, \frac{(\tau\gamma_E + \tau - 1)}{\bar{\gamma}_B}\right) d\gamma_E. \end{aligned} \quad (\text{D.1})$$

Using the series representation of the incomplete lower function [168, Eq. (8.352.1)]

$$\Upsilon(1 + n, x) = n! \left[1 - \exp(-x) \left(\sum_{m=0}^n \frac{x^m}{m!} \right) \right] \quad (\text{D.2})$$

into (D.1), the SOP can be rewritten as

$$\begin{aligned} \text{SOP} = & \underbrace{C_1 k_B! \int_0^{\infty} \exp\left(-\frac{\gamma_E}{\bar{\gamma}_E}\right) L_{z_E}\left(\frac{\gamma_E}{\bar{\gamma}_E}\right) d\gamma_E}_{I_1} - C_1 k_B! \sum_{q=0}^{k_B} \frac{1}{q!} \left(\frac{1}{\bar{\gamma}_B}\right)^q \underbrace{\int_0^{\infty} \exp\left(-\frac{\gamma_E}{\bar{\gamma}_E}\right)}_{I_2} \\ & \times \underbrace{L_{n_E}\left(\frac{\gamma_E}{\bar{\gamma}_E}\right) \exp\left(-\frac{\tau\gamma_E + \tau - 1}{\bar{\gamma}_B}\right) (\tau\gamma_E + \tau - 1)^q}_{I_2} d\gamma_E. \end{aligned} \quad (\text{D.3})$$

Here, with the help of [168, Eq. (7.414.6)] the value of the integral I_1 is $\bar{\gamma}_E$ when $z_E = 0$ or zero otherwise (i.e., $z_E \neq 0$). In the former case, when $z_B \rightarrow \infty$, the T_1 term can be approximated as

$$T_1 = \sum_{z_B=0}^{\infty} C_{z_B} \sum_{k_B=0}^{z_B} \frac{(-1)^{k_B}}{k_B!} \binom{z_B}{k_B} \frac{1}{\bar{\gamma}_E} \sum_{z_E=0}^{\infty} C_{z_E} k_B! \bar{\gamma}_E \approx 1. \quad (\text{D.4})$$

Next, by using [168, Eq. (1.111)]

$$(a+x)^n = \sum_{k=0}^n \binom{n}{k} x^k a^{n-k} \quad (\text{D.5})$$

into (D.3), I_2 can be expressed as

$$I_2 = \sum_{a=0}^q \binom{q}{a} (\tau-1)^{q-a} \tau^a \exp\left(-\frac{\tau-1}{\bar{\gamma}_B}\right) \underbrace{\int_0^\infty L_{z_E}\left(\frac{\gamma_E}{\bar{\gamma}_E}\right) \gamma_E^a \exp\left(-\frac{\gamma_E}{\bar{\gamma}_E} - \frac{\tau\gamma_E}{\bar{\gamma}_B}\right) d\gamma_E}_{I_3}. \quad (\text{D.6})$$

Then, by solving I_3 with the help of [168, Eq. (7.414.7)]

$$\int_0^\infty \exp(-st) t^\beta L_n^\alpha(t) dt = \frac{\Gamma(\beta+1)\Gamma(\alpha+n+1)}{n!\Gamma(\alpha+1)} s^{-\beta-1} {}_2F_1\left(-n, \beta+1; \alpha+1; \frac{1}{s}\right) \quad (\text{D.7})$$

the I_3 term is solved as

$$I_3 = \left(\frac{1}{\bar{\gamma}_E} + \frac{\tau}{\bar{\gamma}_B}\right)^{-1-a} \Gamma(1+a) {}_2F_1\left(1+a, -z_E, 1, \frac{\bar{\gamma}_B}{\bar{\gamma}_B + \bar{\gamma}_E\tau}\right). \quad (\text{D.8})$$

Finally, by combining (D.3) to (D.8), the SOP can be formulated as in (4.4), which concludes the proof.

D.1.2 SOP_A

Substituting (4.1) into (2.6), this leads to

$$\text{SOP}_A = \underbrace{\sum_{z_B=0}^\infty C_{z_B} \sum_{k_B=0}^{z_B} \frac{(-1)^{k_B}}{k_B!} \binom{z_B}{k_B} \frac{1}{\bar{\gamma}_E} \sum_{z_E=0}^\infty C_{z_E}}_{C_1} \int_0^\infty \exp\left(-\frac{\gamma_E}{\bar{\gamma}_E}\right) L_{z_E}\left(\frac{\gamma_E}{\bar{\gamma}_E}\right) \Upsilon\left(k_B+1, \frac{\tau\gamma_E}{\bar{\gamma}_B}\right) d\gamma_E. \quad (\text{D.9})$$

Again, by using (D.2) into (D.9), the SOP_A can be reformulated as

$$\text{SOP}_A = \underbrace{C_1 k_B! \int_0^\infty \exp\left(-\frac{\gamma_E}{\bar{\gamma}_E}\right) L_{z_E}\left(\frac{\gamma_E}{\bar{\gamma}_E}\right) d\gamma_E}_{I_4} - C_1 k_B! \sum_{q=0}^{k_B} \frac{1}{q!} \left(\frac{1}{\bar{\gamma}_B}\right)^q \tau^q \underbrace{\int_0^\infty \exp\left(-\frac{\gamma_E}{\bar{\gamma}_E}\right)}_{I_5} \times \underbrace{L_{z_E}\left(\frac{\gamma_E}{\bar{\gamma}_E}\right) \exp\left(-\frac{\tau\gamma_E}{\bar{\gamma}_B}\right) \gamma_E^q d\gamma_E}_{I_5}. \quad (\text{D.10})$$

Here, note that I_4 is equivalent to I_1 . Therefore, the T_2 term of the SOP_A (i.e., $C_1 k_B! \bar{\gamma}_E$) can be approximated to unity, as discussed in the previous proof. On the other hand, by using [168,

Eq. (7.414.7)], I_5 can be solved in closed-form fashion as

$$I_5 = \left(\frac{1}{\bar{\gamma}_E} + \frac{\tau}{\bar{\gamma}_B} \right)^{-1-q} \Gamma(1+q) {}_2F_1 \left(-z_E, 1+q, 1, \frac{\bar{\gamma}_B}{\bar{\gamma}_B + \bar{\gamma}_E \tau} \right). \quad (\text{D.11})$$

Finally, by replacing (D.11) and (D.10), the SOP_A is reached as in (4.5), which completes the proof.

D.2 PROOFS OF PROPOSITION 7

D.2.1 SOP^∞

In the following, two approaches are used to calculate the asymptotic SOP.

D.2.1.1 Keeping $\bar{\gamma}_E$ Fixed and $\bar{\gamma}_B \rightarrow \infty$ (Approach I)

In order to approximate (4.1b) as $\bar{\gamma}_B \rightarrow \infty$, the following relationship is employed for the lower incomplete gamma function $\Upsilon(a, x) \simeq x^a/s$ as $x \rightarrow 0$. Therefore, (4.1b) can be asymptotically expressed by

$$F_B(\gamma_B) \simeq \sum_{z_B=0}^{\infty} C_{z_B} \sum_{k_B=0}^{z_B} \frac{(-1)^{k_B}}{(k_B+1)!} \binom{z_B}{k_B} \left(\frac{\gamma_B}{\bar{\gamma}_B} \right)^{k_B+1}. \quad (\text{D.12})$$

Substituting (D.12) and (4.1a) into (2.6), it follows that

$$\begin{aligned} \text{SOP}^\infty &\simeq \sum_{z_B=0}^{\infty} C_{z_B} \sum_{k_B=0}^{z_B} \frac{(-1)^{k_B}}{(k_B+1)!} \binom{z_B}{k_B} \left(\frac{1}{\bar{\gamma}_E} \right) \left(\frac{\tau}{\bar{\gamma}_B} \right)^{k_B+1} \\ &\times \sum_{z_E=0}^{\infty} C_{z_E} \underbrace{\int_0^\infty \gamma_E^{k_B+1} \exp\left(-\frac{\gamma_E}{\bar{\gamma}_E}\right) L_{z_E}\left(\frac{\gamma_E}{\bar{\gamma}_E}\right) d\gamma_E}_{I_6} \end{aligned} \quad (\text{D.13})$$

Next, with the aid of (D.7) to solve I_6 in (D.13), the asymptotic SOP can be expressed as in (4.6), which concludes the proof.

D.2.1.2 Keeping $\bar{\gamma}_E$ Fixed and $\bar{\gamma}_B \rightarrow \infty$ (Approach II)

From [174, Eq. (10)], (4.1b) can be asymptotically formulated as

$$F_B(\gamma_B) \simeq \frac{K_{N_B} + 1}{\bar{\gamma}_B} \gamma_B \mathbb{E}_{P_{N_B}} \left[\exp\left(-\frac{P_{N_B}}{\Omega_B}\right) \right], \quad (\text{D.14})$$

where P_{N_B} is given as in [174, Eq. (6)] by

$$\begin{aligned} P_{N_B} &= \Omega_{N_B} + 2 \sum_{\Delta_{N_B}} V_{l,B} V_{s,B} \cos(\theta_{l,B} - \theta_{s,B}) \\ &= \Omega_{N_B} + 2f(\theta), \end{aligned} \quad (\text{D.15})$$

with $\{(l, s) : l < s, l = 1 \dots N_B - 1, s = 2 \dots N_B\}$. Now, using [20, Eq. (44)]

$$L_n^\beta(t) = \sum_{i=0}^n (-1)^i \binom{n+\beta}{n-i} \frac{t^i}{i!} \quad (\text{D.16})$$

to expand the Laguerre polynomial in (4.1a), it follows that

$$f_E(\gamma_E) = \frac{1}{\bar{\gamma}_E} \exp\left(-\frac{\gamma_E}{\bar{\gamma}_E}\right) \sum_{z_E=0}^{\infty} C_{z_E} \sum_{h=0}^{z_E} \frac{(-1)^h}{h!} \binom{z_E}{z_E-h} \left(\frac{\gamma_E}{\bar{\gamma}_E}\right)^h. \quad (\text{D.17})$$

Next, by substituting (D.17) and (D.14) into (2.6), this gets to

$$\begin{aligned} \text{SOP}^\infty &\simeq \frac{K_{N_B} + 1}{\bar{\gamma}_B} \exp(-K_{N_B}) \mathbb{E}_\theta \left[\exp\left(-\frac{2f(\theta)}{\Omega_B}\right) \right] \left(\frac{1}{\bar{\gamma}_E}\right)^{h+1} \sum_{z_E=0}^{\infty} C_{z_E} \sum_{h=0}^{z_E} \frac{(-1)^h}{h!} \binom{z_E}{z_E-h} \\ &\quad \times \underbrace{\int_0^\infty \gamma_E^h (\tau \gamma_E + \tau - 1) \exp\left(-\frac{\gamma_E}{\bar{\gamma}_E}\right) d\gamma_E}_{I_7}. \end{aligned} \quad (\text{D.18})$$

Finally, by using [168, Eq. (3.351.3)]

$$\int_0^\infty x^n \exp(-\mu x) dx = \Gamma(n+1) \mu^{-n-1} \quad (\text{D.19})$$

to solve I_7 , the asymptotic SOP is attained as in (4.7). This completes the proof.

D.3 PROOF OF PROPOSITION 8

Firstly, (4.1a) can be rewritten as

$$f_i(\gamma_i) = \frac{1}{\bar{\gamma}_i} \exp\left(-\frac{\gamma_i}{\bar{\gamma}_i}\right) \left(C_0 L_0\left(\frac{\gamma_i}{\bar{\gamma}_i}\right) + \sum_{z_i=1}^{\infty} C_{z_i} L_{z_i}\left(\frac{\gamma_i}{\bar{\gamma}_i}\right) \right). \quad (\text{D.20})$$

Here, by using the identity $L_0^\beta(x) = 1$ [168, Eq. (8.97.3)] and obtaining C_0 term from (4.3), (D.20) can be expressed by

$$f_i(\gamma_i) = \frac{1}{\bar{\gamma}_i} \exp\left(-\frac{\gamma_i}{\bar{\gamma}_i}\right) \left(1 + \sum_{z_i=1}^{\infty} C_{z_i} L_{z_i}\left(\frac{\gamma_i}{\bar{\gamma}_i}\right) \right). \quad (\text{D.21})$$

Next, plugging (D.21) for $i = B$ into (2.10), it follows that

$$\bar{C}_B = \frac{1}{\bar{\gamma}_B \ln 2} \left[\underbrace{\int_0^\infty \ln(1 + \gamma_B) \exp\left(-\frac{\gamma_B}{\bar{\gamma}_B}\right) d\gamma_B}_{I_8} + \sum_{z_B=1}^\infty C_{z_B} \underbrace{\int_0^\infty \ln(1 + \gamma_B) \exp\left(-\frac{\gamma_B}{\bar{\gamma}_B}\right) L_{z_B}\left(\frac{\gamma_B}{\bar{\gamma}_B}\right) d\gamma_B}_{I_9} \right]. \quad (D.22)$$

Employing the identities [168, Eq. (4.337.2)], [175, Eq. (2.19.6.5)]

$$\int_0^\infty \exp(-\mu x) \ln(1 + \beta x) dx = \frac{1}{\mu} \exp\left(\frac{\mu}{\beta}\right) \mathbb{E}_1\left(\frac{\mu}{\beta}\right), \quad (D.23a)$$

$$\int_0^\infty \exp(-\mu x) \ln(1 + x) L_z(\mu x) dx = -\Gamma(z) U(1 + z, 2, c). \quad (D.23b)$$

the integrals in I_8 , and I_9 can be solved in closed-form fashion, respectively. Next, for convenience, (4.1b) is expanded as

$$F_i(\gamma_i) = \overbrace{C_0 \Upsilon\left(1, \frac{\gamma_i}{\bar{\gamma}_i}\right)}^{T_3} + \sum_{z_i=1}^\infty C_{z_i} \sum_{k_i=0}^{z_i} \frac{(-1)^{k_i}}{k_i!} \binom{z_i}{k_i} \Upsilon\left(k_i + 1, \frac{\gamma_i}{\bar{\gamma}_i}\right). \quad (D.24)$$

Here, by substituting $z_i = 0$ into (4.3), it follows that $C_0 = 1$. Then, by replacing the lower incomplete gamma function, i.e., $\Upsilon(\cdot, \cdot)$ in T_3 by its series representation given in (D.2), (D.24) can be rewritten as

$$F_i(\gamma_i) = 1 - \exp\left(-\frac{\gamma_i}{\bar{\gamma}_i}\right) + \sum_{z_i=1}^\infty C_{z_i} \sum_{k_i=0}^{z_i} \frac{(-1)^{k_i}}{k_i!} \binom{z_i}{k_i} \Upsilon\left(k_i + 1, \frac{\gamma_i}{\bar{\gamma}_i}\right). \quad (D.25)$$

Substituting (D.25) for $i \in \{B, E\}$ into (2.11), it follows that

$$\begin{aligned} \mathcal{L}(\bar{\gamma}_B, \bar{\gamma}_E) &= \frac{1}{\ln 2} \left[\underbrace{\int_0^\infty \frac{\exp\left(-\gamma_E \left(\frac{1}{\bar{\gamma}_B} + \frac{1}{\bar{\gamma}_E}\right)\right)}{(1 + \gamma_E)} d\gamma_E}_{I_{10}} - \sum_{z_E=1}^\infty C_{z_E} \sum_{k_E=0}^{z_E} \frac{(-1)^{k_E}}{k_E!} \binom{z_E}{k_E} \underbrace{\int_0^\infty \frac{\exp\left(-\frac{\gamma_E}{\bar{\gamma}_B}\right)}{(1 + \gamma_E)} d\gamma_E}_{I_{11}} \right. \\ &\quad \times \underbrace{\Upsilon\left(k_E + 1, \frac{\gamma_E}{\bar{\gamma}_E}\right) d\gamma_E}_{I_{11}} - \sum_{z_B=1}^\infty C_{z_B} \sum_{k_B=0}^{z_B} \binom{z_B}{k_B} \frac{(-1)^{k_B}}{k_B!} \underbrace{\int_0^\infty \frac{\exp\left(-\frac{\gamma_E}{\bar{\gamma}_E}\right)}{(1 + \gamma_E)} \Upsilon\left(k_B + 1, \frac{\gamma_E}{\bar{\gamma}_B}\right) d\gamma_E}_{I_{12}} \\ &\quad + \sum_{z_B=1}^\infty C_{z_B} \sum_{k_B=0}^{z_B} \frac{(-1)^{k_B}}{k_B!} \binom{z_B}{k_B} \sum_{z_E=1}^\infty C_{z_E} \sum_{k_E=0}^{z_E} \frac{(-1)^{k_E}}{k_E!} \binom{z_E}{k_E} \underbrace{\int_0^\infty \frac{1}{(1 + \gamma_E)} \Upsilon\left(k_B + 1, \frac{\gamma_E}{\bar{\gamma}_B}\right) d\gamma_E}_{I_{13}} \\ &\quad \left. \times \underbrace{\Upsilon\left(k_E + 1, \frac{\gamma_E}{\bar{\gamma}_E}\right) d\gamma_E}_{I_{13}} \right]. \quad (D.26) \end{aligned}$$

With the help of [168, Eq. (3.352.4)]

$$\int_0^{\infty} \frac{\exp(-\mu x)}{x + \beta} dx = \exp(\mu\beta) \mathbf{E}_1(\mu\beta). \quad (\text{D.27})$$

the integral I_{10} in (D.26) can be solved straightforwardly. Then, by using (D.2) to expand the lower incomplete gamma function in I_{11} , this yields

$$I_{11} = k_E! \underbrace{\int_0^{\infty} \frac{\exp\left(-\frac{\gamma_E}{\bar{\gamma}_B}\right)}{(1 + \gamma_E)} d\gamma_E}_{I_{14}} - k_E! \sum_{w=0}^{k_E} \frac{1}{w!} \left(\frac{1}{\bar{\gamma}_E}\right)^w \underbrace{\int_0^{\infty} \frac{\gamma_E^w \exp\left(-\gamma_E \left(\frac{1}{\bar{\gamma}_B} + \frac{1}{\bar{\gamma}_E}\right)\right)}{(1 + \gamma_E)} d\gamma_E}_{I_{15}}. \quad (\text{D.28})$$

Here, it is used (D.27), and [168, Eq. (3.353.5)], so

$$\int_0^{\infty} \frac{x^k \exp(-\mu x)}{1 + x} dx = \exp(\mu) \Gamma(1 + k) \Gamma(-k, \mu) \quad (\text{D.29})$$

to solve I_{14} , and I_{15} , respectively. Again, by expanding the lower incomplete gamma function in I_{12} with the use of (D.2), this yields

$$I_{12} = k_B! \underbrace{\int_0^{\infty} \frac{\exp\left(-\frac{\gamma_E}{\bar{\gamma}_E}\right)}{(1 + \gamma_E)} d\gamma_E}_{I_{16}} - k_B! \sum_{d=0}^{k_B} \frac{1}{d!} \left(\frac{1}{\bar{\gamma}_B}\right)^d \underbrace{\int_0^{\infty} \frac{\gamma_E^d \exp\left(-\gamma_E \left(\frac{1}{\bar{\gamma}_B} + \frac{1}{\bar{\gamma}_E}\right)\right)}{(1 + \gamma_E)} d\gamma_E}_{I_{17}}. \quad (\text{D.30})$$

By using (D.27), and (D.29), both I_{16} , and I_{17} can be evaluated in closed-form fashion, respectively. Now, to find a closed-form solution of I_{13} in (D.26), a series expansion of $\Upsilon(\cdot, \cdot)$ [176, Eq. (8.5.1)] is employed, so

$$\Upsilon(a, z) = a^{-1} z^a {}_1F_1(1, 1 + a, z). \quad (\text{D.31})$$

For convenience, ${}_1F_1(\cdot, \cdot, \cdot)$ in (D.31) is expressed as [176, Eq. (13.2.2)]

$${}_1F_1(a, b, z) = \sum_{s=0}^{\infty} \frac{(a)_s}{(b)_s s!} z^s. \quad (\text{D.32})$$

Next, by substituting (D.31) and (D.32) into (D.26), I_{13} can be rewritten as

$$I_{13} = \frac{(k_E + 1)^{-1}}{(k_B + 1)} \left(\frac{1}{\bar{\gamma}_B}\right)^{k_B+1} \left(\frac{1}{\bar{\gamma}_E}\right)^{k_E+1} \sum_{g=0}^{\infty} \frac{(1)_g}{g! (k_B + 2)_g} \left(\frac{1}{\bar{\gamma}_B}\right)^g \sum_{c=0}^{\infty} \frac{(1)_c}{c! (k_E + 2)_c} \times \underbrace{\left(\frac{1}{\bar{\gamma}_E}\right)^c \int_0^{\infty} \frac{\gamma_E^{k_B+k_E+g+c+2}}{1 + \gamma_E} \exp\left(-\gamma_E \left(\frac{1}{\bar{\gamma}_B} + \frac{1}{\bar{\gamma}_E}\right)\right) d\gamma_E}_{I_{18}}. \quad (\text{D.33})$$

Similar to the evaluation of I_{17} , (D.29) is used to calculate I_{18} . Finally, by combining (D.22) and (D.26) with the respective substitutions, the ASC can be formulated as in (4.9), which concludes the proof.

D.4 PROOF OF PROPOSITION 9

From [20, Eq. (26)], the n -th moment of the NWDP model is given by

$$\mathbb{E}[\gamma_B^g] = \bar{\gamma}_B^g \Gamma(1+g) \sum_{z_B=0}^{\infty} C_{z_B} {}_2F_1(-z_B, g+1; 1; 1), \quad (\text{D.34})$$

where for convenience in our analysis, the series representation of ${}_2F_1(\cdot, \cdot; \cdot; \cdot)$ [149, Eq. (15.1.1)] is used, so

$${}_2F_1(a, b; c; z) = \sum_{s=0}^{\infty} \frac{(a)_s}{(b)_s s!} z^s. \quad (\text{D.35})$$

Next, by plugging (D.34) into (2.15), the normalized moments of the RV γ_B is expressed by

$$\mathcal{M}(\mu) = \Gamma(1+\mu) \sum_{z_B=0}^{\infty} C_{z_B} \sum_{b=0}^{\infty} \frac{(-z_B)_b (\mu+1)_b}{b! (1)_b}. \quad (\text{D.36})$$

Here, taking the derivative of (D.36) with respect to g , and setting g equal to zero, it follows that

$$\left. \frac{d\mathcal{M}(g)}{dg} \right|_{g=0} = \sum_{z_B=0}^{\infty} C_{z_B} \sum_{b=0}^{\infty} \frac{(-z_B)_b}{b!} \psi(1+b) \quad (\text{D.37})$$

Then, by replacing (D.37) into (2.13), $\bar{C}_B^{\bar{\gamma}_B \rightarrow \infty}$ can be formulated in a simple form as

$$\bar{C}_B^{\bar{\gamma}_B \rightarrow \infty} = \log_2(\bar{\gamma}_B) + \log_2(e) \sum_{z_B=0}^{\infty} C_{z_B} \sum_{b=0}^{\infty} \frac{(-z_B)_b}{b!} \psi(1+b). \quad (\text{D.38})$$

Now, by substituting (D.21) for $i = E$ into (2.10), it gets to

$$\bar{C}_E = \frac{1}{\ln 2\bar{\gamma}_E} \left(\underbrace{\int_0^{\infty} \ln(1+\gamma_E) \exp\left(-\frac{\gamma_E}{\bar{\gamma}_E}\right) d\gamma_E}_{I_{19}} + \sum_{z_E=1}^{\infty} C_{z_E} \underbrace{\int_0^{\infty} \ln(1+\gamma_E) \exp\left(-\frac{\gamma_E}{\bar{\gamma}_E}\right) L_{z_E}\left(\frac{\gamma_E}{\bar{\gamma}_E}\right) d\gamma_E}_{I_{20}} \right) \quad (\text{D.39})$$

Next using (D.23a) and (D.23b) to solve I_{19} and I_{20} , \bar{C}_E can be obtained in a simple way. Finally, by plugging (D.38) and (D.39) into (2.12), the asymptotic ASC is attained as in (4.10). This completes the proof.

E DERIVATION OF THE SECRECY METRICS FOR THE κ - μ SHADOWED FADING MODEL

E.1 PROOF OF PROPOSITION 10

Since the MRC receiver scheme is employed in the system configuration, the instantaneous SNR at Bob can be expressed as

$$\gamma_B = \sum_{l=1}^{N_B} \gamma_{k^*,l}. \quad (\text{E.1})$$

Now, using (5.7), the CDF of γ_B can be formulated as

$$F_{\gamma_B}(\gamma_B) = \left(F_{\gamma_1}(\gamma_B) \right)^{N_A}, \quad (\text{E.2})$$

where

$$\gamma_1 = \sum_{l=1}^{N_B} \gamma_{k,l}, \quad (\text{E.3})$$

with $\gamma_{k,l}$ denoting the instantaneous received SNR of the link between a single transmitting k -th antenna at Alice and the l -th receive antenna at Bob. In dealing with i.i.d. channels, the CDF of γ_1 can be obtained by following the same methodology used for (5.11), and (5.12), i.e.,

$$\sum_{l=1}^{N_B} \gamma_{k,l}(\bar{\gamma}, \kappa_B, \mu_B, m_B) = \gamma_1(N_B \bar{\gamma}, \kappa_B, N_B \mu_B, N_B m_B). \quad (\text{E.4})$$

Based on (E.4), by substituting $\bar{\gamma}$, μ , m , and κ by $N_B \bar{\gamma}$, $N_B \mu_B$, $N_B m_B$, and κ_B , respectively into (5.1b) and (5.2b), so the resulting CDFs of γ_1 are given by

□ **if** $m_B < \mu_B$

$$F_{\gamma_1}(\gamma_B) = 1 - \sum_{j=1}^{\eta_B} A_{1,j}^B \exp\left(-\frac{\gamma_B}{\Delta_1^B}\right) \sum_{r=0}^{\eta_B-j} \frac{1}{r!} \left(\frac{\gamma_B}{\Delta_1^B}\right)^r - \sum_{j=1}^{\nu_B} A_{2,j}^B \exp\left(-\frac{\gamma_B}{\Delta_2^B}\right) \sum_{r=0}^{\nu_B-j} \frac{1}{r!} \left(\frac{\gamma_B}{\Delta_2^B}\right)^r, \quad (\text{E.5})$$

where $\eta_B = N_B(\mu_B - m_B)$, and $\nu_B = N_B m_B$.

□ **If** $m_B \geq \mu_B$

$$F_{\gamma_1}(\gamma_B) = 1 - \sum_{j=0}^{\beta_B} B_j^B \exp\left(-\frac{\gamma_B}{\Delta_2^B}\right) \sum_{r=0}^{\nu_B-j-1} \frac{1}{r!} \left(\frac{\gamma_B}{\Delta_2^B}\right)^r, \quad (\text{E.6})$$

where $\beta_B = N_B(m_B - \mu_B)$. However, the resulting CDFs in (E.5) and (E.6) become intractable in developing (E.2), if not impossible. Therefore, such CDFs of γ_1 are reformulated from its original forms to equivalent expressions by changing the indices of the sums and rearranging some of the terms, so, this yields

□ **If** $m_B < \mu_B$

$$F_{\gamma_1}(\gamma_B) = 1 - \sum_{j=1}^{\eta_B} \left(\frac{\gamma_B}{\Delta_1^B}\right)^{\eta_B-j} \frac{\exp\left(-\frac{\gamma_B}{\Delta_1^B}\right)}{(\eta_B-j)!} \sum_{z=\eta_B+1-j}^{\eta_B} A_{1,\eta_B+1-z}^B - \sum_{j=1}^{\nu_B} \left(\frac{\gamma_B}{\Delta_2^B}\right)^{\nu_B-j} \frac{\exp\left(-\frac{\gamma_B}{\Delta_2^B}\right)}{(\nu_B-j)!} \sum_{z=\nu+1-j}^{\nu} A_{2,\nu_B+1-z}^B, \quad (\text{E.7})$$

where $\eta_B = N_B(\mu_B - m_B)$, and $\nu_B = N_B m_B$.

□ **If** $m_B \geq \mu_B$

$$F_{\gamma_1}(\gamma_B) = 1 - \sum_{j=0}^{\nu_B-1} \left(\frac{\gamma_B}{\Delta_2^B}\right)^{\nu_B-1-j} \frac{\exp\left(-\frac{\gamma_B}{\Delta_2^B}\right)}{(\nu_B-1-j)!} \sum_{z=\beta_B+1-\mathcal{T}(j)}^{\beta_B} B_{\beta_B-z}^B, \quad (\text{E.8})$$

where $\beta_B = N_B(m_B - \mu_B)$, the coefficients marked with superscripts B (e.g., Δ_1^B) are associated to the fading parameters at Bob, and

$$\mathcal{T}(j) = \begin{cases} j + 1, & \text{for } 0 \leq j \leq \beta_B \\ \beta_B + 1, & \text{otherwise.} \end{cases}$$

It is worth mentioning that the CDFs in (E.5) for $m_B < \mu_B$ and (E.6) for $m_B \geq \mu_B$ are equivalent to (E.7) and (E.8), respectively. However, unlike (E.5) and (E.6), the CDFs given in (E.7) and (E.8) are mathematically tractable to perform the multinomial expansion in (E.2). In what follows, with the help of (E.7) and (E.8), the CDF of γ_B given in (E.2) is derived for $m_B < \mu_B$ and $m_B \geq \mu_B$.

□ If $m_B < \mu_B$

Substituting (E.7) into (E.2), we get

$$F_{\gamma_B}(\gamma_B) = \left(1 - \left(\sum_{j=1}^{\eta_B} \left(\frac{\gamma_B}{\Delta_1^B} \right)^{\eta_B-j} \frac{\exp\left(-\frac{\gamma_B}{\Delta_1^B}\right)}{(\eta_B-j)!} \sum_{z=\eta_B+1-j}^{\eta_B} A_{1,\eta_B+1-z}^B \right. \right. \\ \left. \left. - \sum_{j=1}^{\nu_B} \left(\frac{\gamma_B}{\Delta_2^B} \right)^{\nu_B-j} \frac{\exp\left(-\frac{\gamma_B}{\Delta_2^B}\right)}{(\nu_B-j)!} \sum_{z=\nu_B+1-j}^{\nu} A_{2,\nu_B+1-z}^B \right) \right)^{N_A}. \quad (\text{E.9})$$

Next, by applying the binomial expansion (D.5) twice in (E.9), this yields

$$F_{\gamma_B}(\gamma_B) = \sum_{k=0}^{N_A} (-1)^k \binom{N_A}{k} \sum_{c=0}^k \binom{k}{c} \underbrace{\left(\sum_{j=1}^{\eta_B} \left(\frac{\gamma_B}{\Delta_1^B} \right)^{\eta_B-j} \frac{\exp\left(-\frac{\gamma_B}{\Delta_1^B}\right)}{(\eta_B-j)!} \sum_{z=\eta_B+1-j}^{\eta_B} A_{1,\eta_B+1-z}^B \right)^{k-c}}_{T_1} \\ \times \underbrace{\left(\sum_{j=1}^{\nu_B} \left(\frac{\gamma_B}{\Delta_2^B} \right)^{\nu_B-j} \frac{\exp\left(-\frac{\gamma_B}{\Delta_2^B}\right)}{(\nu_B-j)!} \sum_{z=\nu_B+1-j}^{\nu} A_{2,\nu_B+1-z}^B \right)^c}_{T_2}. \quad (\text{E.10})$$

Next, by using the multinomial theorem [149, Eq. (24.1.2)]

$$(x_1 + x_2 + \dots + x_m)^n = \sum_{k_1+k_2+\dots+k_m=n} \frac{n!}{k_1!k_2!\dots k_m!} \prod_{1 \leq t \leq m} x_t^{k_t} \quad (\text{E.11})$$

for both terms T_1 and T_2 , it follows that

$$T_1 = \sum_{\rho(c, \nu_B)} \frac{c!}{p_1! \dots p_{\nu_B}!} \left[\prod_{q=1}^{\nu_B} \left(\frac{\left(\frac{1}{\Delta_2^B}\right)^{\nu_B-q}}{(\nu_B-q)!} \sum_{z=\nu_B+1-q}^{\nu_B} A_{2,\nu_B+1-z}^B \right)^{p_q} \right] \\ \times \exp\left(-\gamma_B \left(\frac{k-c}{\Delta_1^B}\right)\right) \gamma_B^{\sum_{q=1}^{\nu_B} (\nu_B-q)p_q} \quad (\text{E.12})$$

$$T_2 = \sum_{\rho(k-c, \eta_B)} \frac{(k-c)!}{s_1! \dots s_{\eta_B}!} \left[\prod_{t=1}^{\eta_B} \left(\frac{\left(\frac{1}{\Delta_1^B}\right)^{\eta_B-t}}{(\eta_B-t)!} \sum_{z=\eta_B+1-t}^{\eta_B} A_{1,\eta_B+1-z}^B \right)^{s_t} \right] \\ \times \exp\left(-\gamma_B \left(\frac{c}{\Delta_2^B}\right)\right) \gamma_B^{\sum_{t=1}^{\eta_B} (\eta_B-t)s_t}, \quad (\text{E.13})$$

where $\eta_B = N_B(\mu_B - m_B)$, $\nu_B = N_B m_B$ and based on (E.11), it follows that $\rho(k-c, \eta_B) = \{(s_1, s_2, \dots, s_{\eta_B})\}$, for $s_t \in \mathbb{N}$, $\sum_{t=1}^{\eta_B} s_t = k-c$, and similarly $\rho(c, \nu_B) = \{(p_1, p_2, \dots, p_{\nu_B}) : p_q \in \mathbb{N}, \sum_{q=1}^{\nu_B} p_q = c\}$. Then, by substituting (E.12) and (E.13) into (E.10), the CDF of γ_B can be formulated as in (5.13), which concludes the proof.

□ **If** $m_B \geq \mu_B$

Replacing (E.8) into (E.2), it follows that

$$F_{\gamma_1}(\gamma_B) = \left(1 - \sum_{j=0}^{\nu_B-1} \left(\frac{\gamma_B}{\Delta_2^B} \right)^{\nu_B-1-j} \frac{\exp\left(-\frac{\gamma_B}{\Delta_2^B}\right)}{(\nu_B-1-j)!} \sum_{z=\beta_B+1-\mathcal{T}(j)}^{\beta_B} B_{\beta_B-z}^B \right)^{N_A}. \quad (\text{E.14})$$

Again, by applying the binomial expansion in (D.5), this leads to

$$F_{\gamma_B}(\gamma_B) = \sum_{k=0}^{N_A} (-1)^k \binom{N_A}{k} \underbrace{\left(\sum_{j=1}^{\nu_B} \left(\frac{\gamma_B}{\Delta_2^B} \right)^{\nu_B-j} \frac{\exp\left(-\frac{\gamma_B}{\Delta_2^B}\right)}{(\nu_B-j)!} \sum_{z=\beta_B+1-\mathcal{T}(j-1)}^{\beta_B} B_{\beta_B-z}^B \right)^k}_{T_3}. \quad (\text{E.15})$$

Here, by invoking the multinomial expansion given in (E.11) into (E.15), T_3 can be expressed as

$$T_3 = \sum_{\rho(k, \nu_B)} \frac{k!}{s_1! \cdots s_{\nu_B}!} \left[\prod_{t=1}^{\nu_B} \left(\frac{\left(\frac{1}{\Delta_2^B}\right)^{\nu_B-t}}{(\nu_B-t)!} \sum_{z=\beta_B+1-\mathcal{T}(j-1)}^{\beta_B} B_{\beta_B-z}^B \right)^{s_t} \right] \exp\left(-\gamma_B \left(\frac{k}{\Delta_2^B}\right)\right) \gamma_B^{\sum_{t=1}^{\nu_B} (\nu_B-t)s_t}. \quad (\text{E.16})$$

where $\rho(k, \nu_B) = \left\{ (s_1, s_2, \dots, s_{\nu_B}) : s_t \in \mathbb{N}, \sum_{t=1}^{\nu_B} s_t = k \right\}$ and $\beta_B = N_B(m_B - \mu_B)$. Finally, by substituting (E.16) into (E.15), the CDF of γ_B can be expressed as in (5.14). This completes the proof.

E.2 PROOF OF PROPOSITION 12

□ If $m_i < \mu_i$ for $i \in \{B, E\}$

Substituting (5.11a) and (5.13) into (2.5), this gets to

$$\begin{aligned}
 \text{SOP} &= \sum_{k=0}^{N_A} (-1)^k \binom{N_A}{k} \sum_{c=0}^k \binom{k}{c} \sum_{\rho(k-c, \eta_B)} \frac{(k-c)!}{s_1! \cdots s_{\eta_B}!} \left[\prod_{t=1}^{\eta_B} \left(\frac{\left(\frac{1}{\Delta_1^B}\right)^{\eta_B-t}}{(\eta_B-t)!} \sum_{z=\eta_B+1-t}^{\eta_B} A_{1, \eta_B+1-z}^B \right)^{s_t} \right] \\
 &\times \sum_{\rho(c, \nu_B)} \frac{c!}{p_1! \cdots p_{\nu_B}!} \left[\prod_{q=1}^{\nu_B} \left(\frac{\left(\frac{1}{\Delta_2^B}\right)^{\nu_B-q}}{(\nu_B-q)!} \sum_{z=\nu_B+1-q}^{\nu_B} A_{2, \nu_B+1-z}^B \right)^{p_q} \right] \exp\left(-\frac{(\tau-1)(k-c)}{\Delta_1^B}\right) \\
 &\times \exp\left(-\frac{(\tau-1)c}{\Delta_2^B}\right) \left[\sum_{j=1}^{\eta_E} \frac{A_{1,j}^E}{(\eta_E-j)!} \left(\frac{\eta_E-j+1}{\omega_{A_1}^E}\right)^{\eta_E-j+1} \int_0^\infty (\tau\gamma_E + \tau - 1)^{\sum_{t=1}^{\eta_B} (\eta_B-t)s_t + \sum_{q=1}^{\nu_B} (\nu_B-q)p_q} \right. \\
 &\times \underbrace{\gamma_E^{\eta_E-j} \exp\left(-\gamma_E \left(\frac{\tau(k-c)}{\Delta_1^B} + \frac{\tau c}{\Delta_2^B} + \frac{\eta_E-j+1}{\omega_{A_1}^E}\right)\right)}_{T_4} d\gamma_E + \sum_{j=1}^{\nu_E} \frac{A_{2,j}^E}{(\nu_E-j)!} \left(\frac{\nu_E-j+1}{\omega_{A_2}^E}\right)^{\nu_E-j+1} \int_0^\infty \underbrace{\gamma_E^{\nu_E-j}}_{T_5} \\
 &\times \left. (\tau\gamma_E + \tau - 1)^{\sum_{t=1}^{\eta_B} (\eta_B-t)s_t + \sum_{q=1}^{\nu_B} (\nu_B-q)p_q} \exp\left(-\gamma_E \left(\frac{\tau(k-c)}{\Delta_1^B} + \frac{\tau c}{\Delta_2^B} + \frac{\nu_E-j+1}{\omega_{A_1}^E}\right)\right) d\gamma_E \right]. \tag{E.17}
 \end{aligned}$$

Next, with the aid of (D.5), T_4 and T_5 can be rewritten by

$$\begin{aligned}
 T_4 &= \sum_{b=0}^{\sum_{t=1}^{\eta_B} (\eta_B-t)s_t + \sum_{q=1}^{\nu_B} (\nu_B-q)p_q} \binom{\sum_{t=1}^{\eta_B} (\eta_B-t)s_t + \sum_{q=1}^{\nu_B} (\nu_B-q)p_q}{b} (\tau-1)^{\sum_{t=1}^{\eta_B} (\eta_B-t)s_t + \sum_{q=1}^{\nu_B} (\nu_B-q)p_q - b} \\
 &\times \underbrace{\tau^b \int_0^\infty \gamma_E^{\eta_E-j+b} \exp\left(-\gamma_E \left(\frac{\tau(k-c)}{\Delta_1^B} + \frac{\tau c}{\Delta_2^B} + \frac{\eta_E-j+1}{\omega_{A_1}^E}\right)\right) d\gamma_E}_{I_1}. \tag{E.18}
 \end{aligned}$$

$$\begin{aligned}
 T_5 &= \sum_{b=0}^{\sum_{t=1}^{\eta_B} (\eta_B-t)s_t + \sum_{q=1}^{\nu_B} (\nu_B-q)p_q} \binom{\sum_{t=1}^{\eta_B} (\eta_B-t)s_t + \sum_{q=1}^{\nu_B} (\nu_B-q)p_q}{b} (\tau-1)^{\sum_{t=1}^{\eta_B} (\eta_B-t)s_t + \sum_{q=1}^{\nu_B} (\nu_B-q)p_q - b} \\
 &\times \underbrace{\tau^b \int_0^\infty \gamma_E^{\nu_E-j+b} \exp\left(-\gamma_E \left(\frac{\tau(k-c)}{\Delta_1^B} + \frac{\tau c}{\Delta_2^B} + \frac{\nu_E-j+1}{\omega_{A_1}^E}\right)\right) d\gamma_E}_{I_2}. \tag{E.19}
 \end{aligned}$$

Then, by using (D.19), I_1 and I_2 can be solved as

$$I_1 = \left(\frac{\tau(k-c)}{\Delta_1^B} + \frac{\tau c}{\Delta_2^B} + \frac{\eta_E-j+1}{\omega_{A_1}^E}\right)^{-1-(\eta_E-j+b)} \Gamma(1 + \eta_E - j + b). \tag{E.20}$$

$$I_2 = \left(\frac{\tau(k-c)}{\Delta_1^B} + \frac{\tau c}{\Delta_2^B} + \frac{\nu_E - j + 1}{\omega_{A_1}^E} \right)^{-1 - (\nu_E - j + b)} \Gamma(1 + \nu_E - j + b). \quad (\text{E.21})$$

Then, by combining (E.17) to (E.21), the SOP can be expressed as in (5.17), which concludes the proof.

□ **If** $m_i \geq \mu_i$ for $i \in \{B, E\}$

Substituting (5.12a) and (5.14) into (2.5), this gets to

$$\begin{aligned} \text{SOP} &= \sum_{k=0}^{N_A} (-1)^k \binom{N_A}{k} \exp\left(-k \frac{(\tau-1)}{\Delta_2^B}\right) \sum_{\rho(k, \nu_B)} \frac{k!}{s_1! \cdots s_{\nu_B}!} \left[\prod_{t=1}^{\nu_B} \left(\frac{\left(\frac{1}{\Delta_2^B}\right)^{\nu_B-t}}{(\nu_B-t)!} \sum_{z=\beta_B+1-\mathcal{T}(j-1)}^{\beta_B} B_{\beta_B-z}^B \right)^{s_t} \right] \\ &\quad \times \sum_{j=0}^{\beta_E} \frac{B_j^E}{\nu_E - j - 1} \left(\frac{\nu_E - j}{\omega_B^E} \right)^{\nu_E - j} \underbrace{\int_0^\infty \gamma_E^{\nu_E - j - 1} \exp\left(-\gamma_E \left(\frac{k\tau}{\Delta_2^B} + \frac{\nu_E - j}{\omega_B^E} \right)\right) (\tau\gamma_E + \tau - 1)^{\sum_{t=1}^{\nu_B} (\nu_B - t)s_t} d\gamma_E}_{T_6}. \end{aligned} \quad (\text{E.22})$$

Again, by using the binomial expansion (D.5), T_6 can be rewritten as

$$T_6 = \sum_{b=0}^{\sum_{t=1}^{\nu_B} (\nu_B - t)s_t} \binom{\sum_{t=1}^{\nu_B} (\nu_B - t)s_t}{b} \tau^b (\tau - 1)^{\sum_{t=1}^{\nu_B} (\nu_B - t)s_t} \underbrace{\int_0^\infty \gamma_E^{\nu_E - j - 1 + b} \exp\left(-\gamma_E \left(\frac{k\tau}{\Delta_2^B} + \frac{\nu_E - j}{\omega_B^E} \right)\right) d\gamma_E}_{I_3}. \quad (\text{E.23})$$

Then, by using (D.19), I_3 can be solved as

$$I_3 = \left(\frac{k\tau}{\Delta_2^B} + \frac{\nu_E - j}{\omega_B^E} \right)^{-1 - (\nu_E - j - 1 + b)} \Gamma(1 + \nu_E - j - 1 + b). \quad (\text{E.24})$$

Finally, by combining (E.22) to (E.24), the SOP can be formulated as in (5.18). This concludes the proof.

E.3 PROOF OF PROPOSITION 13

Keeping $\bar{\gamma}_E$ Fixed and $\bar{\gamma}_B \rightarrow \infty$ Firstly, by using the asymptotic-matching method proposed in Section 3.1.3, the CDF of a κ - μ shadowed RV given in (5.1b) and (5.2b) can be approximated by a gamma distribution with CDF

$$F_X^G(x) \approx \frac{\Upsilon(\alpha, \frac{x}{\lambda})}{\Gamma(\alpha)}, \quad (\text{E.25})$$

where the shape parameters α and λ are given in terms of the κ - μ shadowed fading parameters as

$$\alpha = \mu, \quad (\text{E.26a})$$

$$\lambda = \frac{\bar{\gamma}}{(1 + \kappa)\mu} \left(\frac{(m + \kappa\mu)^m}{m^m} \right)^{\frac{1}{\mu}}. \quad (\text{E.26b})$$

Now, in order to asymptotically approximate (E.25), the following relationship $\Upsilon(a, x) \simeq x^a/a$ as $x \rightarrow 0$ is used, thus

$$F_X^G(x) \simeq \frac{1}{\alpha\Gamma(\alpha)} \left(\frac{x}{\lambda} \right)^\alpha. \quad (\text{E.27})$$

Then, by using (E.27), any CDF in (5.1b) and (5.2b) can be expressed asymptotically by

$$F_\gamma(\gamma) = \frac{\gamma^\mu}{\mu\Gamma(\mu)} \left(\frac{\mu(1 + \kappa)}{\bar{\gamma}} \right)^\mu \frac{m^m}{(m + \kappa\mu)^m}. \quad (\text{E.28})$$

Next, substituting (E.28) into (E.4) with $\bar{\gamma} \rightarrow N_B\bar{\gamma}_B$, $\mu \rightarrow N_B\mu_B$, $m \rightarrow N_B m_B$, and $\kappa \rightarrow \kappa_B$ [21, Proposition 1], the CDFs given in (E.5) and (E.6) can asymptotically approximate by

$$F_1(\gamma_B) \simeq \left(\frac{m_B^{N_B m_B} (1 + \kappa_B)^{N_B \mu_B} \mu_B^{N_B \mu_B - 1} \gamma_B^{N_B \mu_B}}{N_B \bar{\gamma}_B^{N_B \mu_B} (m_B + \kappa_B \mu_B)^{N_B m_B} \Gamma(N_B \mu_B)} \right). \quad (\text{E.29})$$

Plugging (E.29) into (E.2), this yields

$$F_B(\gamma_B) \simeq \left(\frac{m_B^{N_B m_B} (1 + \kappa_B)^{N_B \mu_B} \mu_B^{N_B \mu_B - 1} \gamma_B^{N_B \mu_B}}{N_B \bar{\gamma}_B^{N_B \mu_B} (m_B + \kappa_B \mu_B)^{N_B m_B} \Gamma(N_B \mu_B)} \right)^{N_A}. \quad (\text{E.30})$$

Inserting (E.30) together with the PDF of the Eavesdropper given in [21, Eq. (4)] by ^[1]

$$\begin{aligned} f_{\gamma_E}(\gamma_E) &= \frac{(\mu_E N_E)^{N_E \mu_E} (N_E m_E)^{N_E m_E} (1 + \kappa_E)^{N_E \mu_E}}{\Gamma(N_E \mu_E) N_E \bar{\gamma}_E (N_E \mu_E \kappa_E + N_E m_E)^{m_E}} \exp\left(-\frac{\mu_E (1 + \kappa_E) \gamma_E}{\bar{\gamma}_E}\right) \left(\frac{\gamma_E}{N_E \bar{\gamma}_E}\right)^{N_E \mu_E - 1} \\ &\quad \times {}_1F_1\left(N_E m_E, N_E \mu_E, \frac{\mu_E^2 \kappa_E (1 + \kappa_E) \gamma_E}{\bar{\gamma}_E (\mu_E \kappa_E + m_E)}\right) \end{aligned} \quad (\text{E.31})$$

^[1] Since the eavesdropper uses MRC receiver, by substituting $\bar{\gamma} \rightarrow N_E \bar{\gamma}_E$, $\mu \rightarrow N_E \mu_E$, $m \rightarrow N_E m_E$, and $\kappa \rightarrow \kappa_E$ into [21, Eq. (4)].

into (2.6), it follows that

$$\begin{aligned} \text{SOP}^\infty &\simeq \left(\frac{m_B^{N_B m_B} (1 + \kappa_B)^{N_B \mu_B} \mu_B^{N_B \mu_B - 1} \tau^{N_B \mu_B}}{N_B \bar{\gamma}_B^{N_B \mu_B} (m_B + \kappa_B \mu_B)^{N_B m_B} \Gamma(N_B \mu_B)} \right)^{N_A} \frac{\mu_E^{N_E \mu_E} m_E^{N_E m_E} (1 + \kappa_E)^{N_E \mu_E}}{\Gamma(N_E \mu_E) \bar{\gamma}_E^{N_E \mu_E} (\mu_E \kappa_E + m_E)^{N_E m_E}} \\ &\times \underbrace{\int_0^\infty \gamma_E^{N_E \mu_E + N_A N_B \mu_B - 1} \exp\left(-\frac{\gamma_E \mu_E (1 + \kappa_E)}{\bar{\gamma}_E}\right) {}_1F_1\left(N_E m_E, N_E \mu_E, \frac{\gamma_E \kappa_E \mu_E^2 (1 + \kappa_E)}{\bar{\gamma}_E (m_E + \kappa_E \mu_E)}\right) d\gamma_E}_{I_4}. \end{aligned} \quad (\text{E.32})$$

Finally, using [168, Eq. (7.522.9)]

$$\int_0^\infty x^{\rho-1} \exp(-\beta x) {}_1F_1(a, b, cx) dx = \beta^{-\rho} \Gamma(\rho) {}_2F_1\left(a, \rho, b, \frac{c}{\beta}\right) \quad (\text{E.33})$$

the integral I_4 in (E.32) is solved in closed-form as

$$I_4 = \left(\frac{\mu_E (1 + \kappa_E)}{\bar{\gamma}_E} \right)^{-N_A N_B \mu_B} \Gamma(N_A N_B \mu_B + N_E \mu_E) {}_2F_1\left(N_E m_E, N_A N_B \mu_B + N_E \mu_E, N_E \mu_E, \frac{\kappa_E \mu_E}{m_E + \kappa_E \mu_E}\right). \quad (\text{E.34})$$

Finally, by substituting (E.34) into (E.32), the SOP^∞ for TAS/MRC configuration can be formulated as in (5.19). This completes the proof.

E.4 PROOFS OF PROPOSITION 14

□ **If** $m_i < \mu_i$ for $i \in \{B, E\}$

Inserting (5.13) in (2.9), the result is

$$\begin{aligned} \bar{C}_B &= \frac{1}{\ln 2} \sum_{k=1}^{N_A} (-1)^{k+1} \binom{N_A}{k} \sum_{c=0}^k \binom{k}{c} \sum_{\rho(c, \nu_B)} \frac{c!}{p_1! \cdots p_{\nu_B}!} \left[\prod_{q=1}^{\nu_B} \left(\frac{\left(\frac{1}{\Delta_2^B}\right)^{\nu_B - q}}{(\nu_B - q)!} \sum_{z=\nu_B+1-q}^{\nu_B} A_{2, \nu_B+1-z}^B \right)^{p_q} \right] \\ &\times \sum_{\rho(k-c, \eta_B)} \frac{(k-c)!}{s_1! \cdots s_{\eta_B}!} \left[\prod_{t=1}^{\eta_B} \left(\frac{\left(\frac{1}{\Delta_1^B}\right)^{\eta_B - t}}{(\eta_B - t)!} \sum_{z=\eta_B+1-t}^{\eta_B} A_{1, \eta_B+1-z}^B \right)^{s_t} \right] \underbrace{\int_0^\infty \frac{\exp\left(-\frac{\gamma_E c}{\Delta_2^B}\right)}{(1 + \gamma_E)} d\gamma_E}_{I_5} \\ &\times \underbrace{\exp\left(-\gamma_E \left(\frac{k-c}{\Delta_1^B}\right)\right) \gamma_E^{\sum_{t=1}^{\eta_B} (\eta_B - t) s_t + \sum_{q=1}^{\nu_B} (\nu_B - q) p_q}}_{I_5} d\gamma_E. \end{aligned} \quad (\text{E.35})$$

Here, by using (D.29), the integral in I_5 can be solved in closed-form fashion as

$$I_5 = \exp\left(\frac{k-c}{\Delta_1^B} + \frac{c}{\Delta_2^B}\right) \Gamma\left(1 + \sum_{t=1}^{\eta_B} (\eta_B - t) s_t + \sum_{q=1}^{\nu_B} (\nu_B - q) p_q\right) \\ \times \Gamma\left(-\sum_{t=1}^{\eta_B} (\eta_B - t) s_t - \sum_{q=1}^{\nu_B} (\nu_B - q) p_q, \frac{\Delta_2^B (k-c) + \Delta_1^B c}{\Delta_1^B \Delta_2^B}\right). \quad (\text{E.36})$$

Then, by substituting (5.13) together with (5.11b) into (2.11), it follows that

$$\mathcal{L}(\bar{\gamma}_B, \bar{\gamma}_E) = \sum_{k=1}^{N_A} (-1)^{k+1} \binom{N_A}{k} \sum_{c=0}^k \binom{k}{c} \sum_{\rho(c, \nu_B)} \frac{c!}{p_1! \cdots p_{\nu_B}!} \left[\prod_{q=1}^{\nu_B} \left(\frac{\left(\frac{1}{\Delta_2^B}\right)^{\nu_B - q}}{(\nu_B - q)!} \sum_{z=\nu_B+1-q}^{\nu_B} A_{2, \nu_B+1-z}^B \right)^{p_q} \right] \\ \times \frac{1}{\ln 2} \sum_{\rho(k-c, \eta_B)} \frac{(k-c)!}{s_1! \cdots s_{\eta_B}!} \left[\prod_{t=1}^{\eta_B} \left(\frac{\left(\frac{1}{\Delta_1^B}\right)^{\eta_B - t}}{(\eta_B - t)!} \sum_{z=\eta_B+1-t}^{\eta_B} A_{1, \eta_B+1-z}^B \right)^{s_t} \right] \left(\sum_{j=1}^{\eta_E} A_{1,j}^E \sum_{r=0}^{\eta_E - j} \frac{1}{r!} \right) \\ \times \underbrace{\left(\frac{1}{\Delta_1^E} \right)^r \int_0^\infty \exp\left(-\gamma_E \left(\frac{k-c}{\Delta_1^B} + \frac{c}{\Delta_2^B} + \frac{1}{\Delta_1^E} \right)\right) \frac{1}{(1+\gamma_E)^{\gamma_E}} \gamma_E^{r + \sum_{t=1}^{\eta_B} (\eta_B - t) s_t + \sum_{q=1}^{\nu_B} (\nu_B - q) p_q} d\gamma_E}_{I_6} \\ + \underbrace{\sum_{j=1}^{\nu_E} A_{2,j}^E \sum_{r=0}^{\nu_E - j} \frac{1}{r!} \left(\frac{1}{\Delta_2^E} \right)^r \int_0^\infty \exp\left(-\frac{\gamma_E}{\Delta_2^E}\right) \exp\left(-\gamma_E \left(\frac{k-c}{\Delta_1^B} + \frac{c}{\Delta_2^B} \right)\right) \frac{1}{(1+\gamma_E)}}_{I_7} \\ \times \underbrace{\gamma_E^{r + \sum_{t=1}^{\eta_B} (\eta_B - t) s_t + \sum_{q=1}^{\nu_B} (\nu_B - q) p_q} d\gamma_E}_{I_7}. \quad (\text{E.37})$$

Again, by using (D.29), both I_6 and I_7 can be evaluated in closed-form fashion as

$$I_6 = \exp\left(\frac{k-c}{\Delta_1^B} + \frac{c}{\Delta_2^B} + \frac{1}{\Delta_1^E}\right) \Gamma\left(-r - \sum_{t=1}^{\eta_B} (\eta_B - t) s_t - \sum_{q=1}^{\nu_B} (\nu_B - q) p_q, \frac{k-c}{\Delta_1^B} + \frac{c}{\Delta_2^B} + \frac{1}{\Delta_1^E}\right) \\ \times \Gamma\left(1 + r + \sum_{t=1}^{\eta_B} (\eta_B - t) s_t + \sum_{q=1}^{\nu_B} (\nu_B - q) p_q\right) \quad (\text{E.38})$$

$$I_7 = \exp\left(\frac{k-c}{\Delta_1^B} + \frac{c}{\Delta_2^B} + \frac{1}{\Delta_2^E}\right) \Gamma\left(-r - \sum_{t=1}^{\eta_B} (\eta_B - t) s_t - \sum_{q=1}^{\nu_B} (\nu_B - q) p_q, \frac{k-c}{\Delta_1^B} + \frac{c}{\Delta_2^B} + \frac{1}{\Delta_2^E}\right) \\ \times \Gamma\left(1 + r + \sum_{t=1}^{\eta_B} (\eta_B - t) s_t + \sum_{q=1}^{\nu_B} (\nu_B - q) p_q\right). \quad (\text{E.39})$$

Finally, by substituting (E.35) and (E.37) into (2.8), the \bar{C}_S can be expressed as in (5.21). This completes the proof.

□ If $m_i \geq \mu_i$ for $i \in \{B, E\}$

Plugging (5.14) in (2.9), it follows that

$$\begin{aligned} \bar{C}_B = & \frac{1}{\ln 2} \sum_{k=1}^{N_A} (-1)^{k+1} \binom{N_A}{k} \sum_{\rho(k, \nu_B)} \frac{k!}{s_1! \cdots s_{\nu_B}!} \left[\prod_{t=1}^{\nu_B} \left(\frac{\left(\frac{1}{\Delta_2^B}\right)^{\nu_B-t}}{(\nu_B-t)!} \sum_{z=\beta_B+1-\mathcal{T}(j-1)}^{\beta_B} B_{\beta_B-z}^B \right)^{s_t} \right] \\ & \times \underbrace{\int_0^\infty \frac{1}{(1+\gamma_E)} \exp\left(-\gamma_E \left(\frac{k}{\Delta_2^B}\right)\right) \gamma_E^{\sum_{t=1}^{\nu_B} (\nu_B-t)s_t} d\gamma_E}_{I_8}. \end{aligned} \quad (\text{E.40})$$

With the aid of (D.29), I_8 can be evaluated in exact closed-form as

$$I_8 = \exp\left(\frac{k}{\Delta_2^B}\right) \Gamma\left(1 + \sum_{t=1}^{\nu_B} (\nu_B-t)s_t\right) \Gamma\left(-\sum_{t=1}^{\nu_B} (\nu_B-t)s_t, \frac{k}{\Delta_2^B}\right). \quad (\text{E.41})$$

Next, inserting (5.12b) and (5.14) into (2.11) yields

$$\begin{aligned} \mathcal{L}(\bar{\gamma}_B, \bar{\gamma}_E) = & \frac{1}{\ln 2} \sum_{k=1}^{N_A} (-1)^{k+1} \binom{N_A}{k} \sum_{\rho(k, \nu_B)} \frac{k!}{s_1! \cdots s_{\nu_B}!} \left[\prod_{t=1}^{\nu_B} \left(\frac{\left(\frac{1}{\Delta_2^B}\right)^{\nu_B-t}}{(\nu_B-t)!} \sum_{z=\beta_B+1-\mathcal{T}(j-1)}^{\beta_B} B_{\beta_B-z}^B \right)^{s_t} \right] \\ & \times \sum_{j=0}^{\beta_E} B_j^E \sum_{r=0}^{\nu_E-j-1} \frac{1}{r!} \left(\frac{1}{\Delta_2^E}\right)^r \underbrace{\int_0^\infty \exp\left(-\frac{\gamma_E}{\Delta_2^E}\right) \frac{1}{(1+\gamma_E)} \exp\left(-\frac{\gamma_E k}{\Delta_2^B}\right) \gamma_E^{\sum_{t=1}^{\nu_B} (\nu_B-t)s_t+r} d\gamma_E}_{I_9}. \end{aligned} \quad (\text{E.42})$$

Similar to the evaluation of I_8 , the identity (D.29) is used to calculate I_9 , thus

$$I_9 = \exp\left(\frac{k}{\Delta_2^B} + \frac{1}{\Delta_2^E}\right) \Gamma\left(1+r + \sum_{t=1}^{\nu_B} (\nu_B-t)s_t\right) \Gamma\left(-r - \sum_{t=1}^{\nu_B} (\nu_B-t)s_t, \frac{k}{\Delta_2^B} + \frac{1}{\Delta_2^E}\right). \quad (\text{E.43})$$

Finally, by substituting (E.40) and (E.42) into (2.8), the \bar{C}_S can be formulated as in (5.20), which concludes the proof.

E.5 PROOFS OF PROPOSITION 15

□ If $m_i < \mu_i$ for $i \in \{B, E\}$

Here, the aim is to express \bar{C}_S^∞ in the form of (2.12). For this purpose, \bar{C}_E and $\bar{C}_B^{\bar{\gamma}_B \rightarrow \infty}$ are derived

below. Inserting (5.11b) in (2.9), this yields

$$\begin{aligned} \bar{C}_E = & \frac{1}{\ln 2} \left(\sum_{j=1}^{\eta_E} A_{1,j}^E \sum_{r=0}^{\eta_E-j} \frac{1}{r!} \left(\frac{1}{\Delta_1^E} \right)^r \underbrace{\int_0^\infty \exp\left(-\frac{\gamma_E}{\Delta_1^E}\right) \frac{\gamma_E^r}{(1+\gamma_E)} d\gamma_E}_{I_{10}} + \sum_{j=1}^{\nu_E} A_{2,j}^E \sum_{r=0}^{\nu_E-j} \frac{1}{r!} \left(\frac{1}{\Delta_2^E} \right)^r \right. \\ & \left. \times \underbrace{\int_0^\infty \exp\left(-\frac{\gamma_E}{\Delta_2^E}\right) \frac{\gamma_E^r}{(1+\gamma_E)} d\gamma_E}_{I_{11}} \right). \end{aligned} \quad (\text{E.44})$$

Recalling (D.29), both I_{10} and I_{11} are given by

$$I_{10} = \exp\left(\frac{1}{\Delta_1^E}\right) \Gamma\left(-r, \frac{1}{\Delta_1^E}\right) \Gamma(1+r), \quad (\text{E.45a})$$

$$I_{11} = \exp\left(\frac{1}{\Delta_2^E}\right) \Gamma\left(-r, \frac{1}{\Delta_2^E}\right) \Gamma(1+r). \quad (\text{E.45b})$$

Now, to express $\bar{C}_B^{\gamma_B \rightarrow \infty}$ as (2.13), it is defined the g -th moment of a RV X as [6, Eq. (4.39)]

$$\mathbb{E}[x^g] = \int_0^\infty x^g f_X(x) dx, \quad (\text{E.46})$$

where $f_X(x)$ is the PDF of the RV X . Using (5.15) into (E.46), the g -th moment of the RV γ_B is given by

$$\begin{aligned} \mathbb{E}[\gamma_B^g] = & \underbrace{\sum_{k=1}^{N_A} (-1)^k \binom{N_A}{k} \sum_{c=0}^k \binom{k}{c} \sum_{\rho(c, \nu_B)} \frac{c!}{p_1! \cdots p_{\nu_B}!} \left[\prod_{q=1}^{\nu_B} \left(\frac{\left(\frac{1}{\Delta_2^B}\right)^{\nu_B-q}}{(\nu_B-q)!} \sum_{z=\nu_B+1-q}^{\nu_B} A_{2, \nu_B+1-z}^B \right)^{p_q} \right]}_{C_1} \\ & \times \underbrace{\sum_{\rho(k-c, \eta_B)} \frac{(k-c)!}{s_1! \cdots s_{\eta_B}!} \left[\prod_{t=1}^{\eta_B} \left(\frac{\left(\frac{1}{\Delta_1^B}\right)^{\eta_B-t}}{(\eta_B-t)!} \sum_{z=\eta_B+1-t}^{\eta_B} A_{1, \eta_B+1-z}^B \right)^{s_t} \right]}_{C_1} \underbrace{\int_0^\infty \exp\left(-\gamma_B \left(\frac{k-c}{\Delta_1^B}\right)\right)}_{I_{12}} \\ & \times \underbrace{\exp\left(-\frac{\gamma_B c}{\Delta_2^B}\right) \gamma_B^{-1+g+\sum_{t=1}^{\eta_B} (\eta_B-t)s_t + \sum_{q=1}^{\nu_B} (\nu_B-q)p_q} \left(\left(\frac{\sum_{t=1}^{\eta_B} (\eta_B-t)s_t + \sum_{q=1}^{\nu_B} (\nu_B-q)p_q}{\sum_{t=1}^{\eta_B} (\eta_B-t)s_t + \sum_{q=1}^{\nu_B} (\nu_B-q)p_q} \right)^{T_7} \right)}_{I_{12}} \\ & \underbrace{\left(-\frac{\gamma_B c}{\Delta_2^B} + \frac{\gamma_B (c-k)}{\Delta_1^B} d\gamma_B \right)}_{I_{12}}. \end{aligned} \quad (\text{E.47})$$

Next, it is considered the following two cases to solve I_{12} in (E.47).

□ **When** $T_7 = 0$

In this case, with the help of (D.19) and (5.6) with $\bar{\gamma} \rightarrow N_B \bar{\gamma}_B$, $\mu \rightarrow N_B \mu_B$, $m \rightarrow N_B m_B$, and $\kappa \rightarrow \kappa_B$, I_{12} can be expressed as

$$I_{12} = -\bar{\gamma}_B^g \left(\frac{c + kC_2C_3 - cC_2C_3}{C_3} \right)^{-g} \Gamma(1+g). \quad (\text{E.48})$$

where $C_2 = N_B \mu_B (1 + \kappa_B)$ and $C_3 = \frac{\mu_B \kappa_B + m_B}{N_B m_B \mu_B (1 + \kappa_B)}$. Then, by substituting (E.48) into (E.47), and the resulting expression in (2.15), it follows that

$$\mathcal{M}(g) = -C_1 \left(\frac{c + kC_2C_3 - cC_2C_3}{C_3} \right)^{-g} \Gamma(1+g). \quad (\text{E.49})$$

Taking the derivative of (E.49), this gets to

$$\frac{d\mathcal{M}(g)}{dg} = C_1 \left(kC_2 + c \left(-C_2 + \frac{1}{C_3} \right) \right)^{-g} \Gamma(1+g) \left(\mathcal{C} + \ln \left(kC_2 + c \left(-C_2 + \frac{1}{C_3} \right) \right) \right). \quad (\text{E.50})$$

Substituting (E.50) into (2.14), it follows that

$$t = -\log_2(e) C_1 \left(\mathcal{C} + \ln \left(kC_2 + c \left(-C_2 + \frac{1}{C_3} \right) \right) \right). \quad (\text{E.51})$$

Finally, by inserting (E.51) into (2.13), this yields

$$\bar{C}_B^{\bar{\gamma}_B \rightarrow \infty} \approx \log_2(N_B \bar{\gamma}_B) + \log_2(e) C_1 \left(\mathcal{C} + \ln \left(kC_2 + c \left(-C_2 + \frac{1}{C_3} \right) \right) \right). \quad (\text{E.52})$$

□ **When** $T_7 \neq 0$

Here, again with the help of (D.19) and (5.6) with $\bar{\gamma} \rightarrow N_B \bar{\gamma}_B$, $\mu \rightarrow N_B \mu_B$, $m \rightarrow N_B m_B$, and $\kappa \rightarrow \kappa_B$, I_{12} can be expressed as

$$I_{12} = -\bar{\gamma}_B^g g \left(\frac{c + kC_2C_3 - cC_2C_3}{C_3} \right)^{-g-T_7} \Gamma(g+T_7). \quad (\text{E.53})$$

Next, by plugging (E.53) into (E.47), and the resulting expression in (2.15), this yields

$$\mathcal{M}(g) = -C_1 g \left(\frac{c + kC_2C_3 - cC_2C_3}{C_3} \right)^{-g-T_7} \Gamma(g + T_7). \quad (\text{E.54})$$

Taking the derivative of (E.54), this leads to

$$\begin{aligned} \frac{d\mathcal{M}(g)}{dg} = & -C_1 \left(\frac{c - cC_2C_3 + C_2C_3k}{C_3} \right)^{-g-T_7} \left(\Gamma(g + T_7) - g\Gamma(g + T_7) \ln \left(\frac{c - cC_2C_3 + C_2C_3k}{C_3} \right) \right. \\ & \left. + g\Gamma(g + T_7)\psi(g + T_7) \right). \end{aligned} \quad (\text{E.55})$$

Inserting (E.55) into (2.14), this yields

$$t = -\log_2(e)C_1 \left(- \left(\frac{c - cC_2C_3 + C_2C_3k}{C_3} \right)^{-T_7} \Gamma(T_7) \right). \quad (\text{E.56})$$

Next, by inserting (E.56) into (2.13), this yields

$$\bar{C}_B^{\bar{\gamma}_B \rightarrow \infty} \approx \log_2(N_B \bar{\gamma}_B) + \log_2(e)C_1 \left(- \left(\frac{c - cC_2C_3 + C_2C_3k}{C_3} \right)^{-T_7} \Gamma(T_7) \right). \quad (\text{E.57})$$

Replacing (E.44) together with (E.52) and (E.57) into (2.12), \bar{C}_S^∞ is attained as in (5.22). This completes the proof.

□ If $m_i \geq \mu_i$ for $i \in \{B, E\}$

Again, the goal is to express \bar{C}_S^∞ in the form of (2.12). To this end, \bar{C}_E and $\bar{C}_B^{\bar{\gamma}_B \rightarrow \infty}$ are derived below.

Firstly, substituting (5.12b) into (2.9), it follows that

$$\bar{C}_E = \frac{1}{\ln 2} \sum_{j=0}^{\beta_E} B_j^E \sum_{r=0}^{\nu_E - j - 1} \frac{1}{r!} \left(\frac{1}{\Delta_2^E} \right)^r \underbrace{\int_0^\infty \exp\left(-\frac{\gamma_E}{\Delta_2^E}\right) \frac{\gamma_E^r}{(1 + \gamma_E)} d\gamma_E}_{I_{13}}. \quad (\text{E.58})$$

Again, making use of (D.29), I_{13} is computed in a closed-form as

$$I_{13} = \exp\left(\frac{1}{\Delta_2^E}\right) \Gamma(1 + r) \Gamma\left(-r, \frac{1}{\Delta_2^E}\right). \quad (\text{E.59})$$

Here, a similar steps to obtain $\overline{C}_B^{\overline{\gamma}_B \rightarrow \infty}$ as in the previous case is performed. Therefore, using (5.16) into (E.46), the g -th moment of the RV γ_B is given by

$$\mathbb{E} [\gamma_B^g] = \underbrace{\sum_{k=1}^{N_A} (-1)^k \binom{N_A}{k} \sum_{\rho(k, \nu_B)} \frac{k!}{s_1! \cdots s_{\nu_B}!} \left[\prod_{t=1}^{\nu_B} \left(\frac{\left(\frac{1}{\Delta_2^B}\right)^{\nu_B - t}}{(\nu_B - t)!} \sum_{z=\beta_B+1-\mathcal{T}(j-1)}^{\beta_B} B_{\beta_B-z}^B \right)^{s_t} \right]}_{C_4} \times \underbrace{\int_0^\infty \exp\left(-\frac{k\gamma_B}{\Delta_2^B}\right) \gamma_B^{-1+g+\sum_{t=1}^{\nu_B} (\nu_B - t)s_t} \left(\sum_{t=1}^{\nu_B} (\nu_B - t)s_t - \frac{k\gamma_B}{\Delta_2^B} \right)^{\overbrace{\sum_{t=1}^{\nu_B} (\nu_B - t)s_t}_{T_8}}}_{I_{14}} d\gamma_B. \quad (\text{E.60})$$

Next, it is considered the following two cases to solve I_{14} in (E.60).

□ **When $T_8 = 0$**

In this case, with the help of (D.19) and (5.6) with $\overline{\gamma} \rightarrow N_B \overline{\gamma}_B$, $\mu \rightarrow N_B \mu_B$, $m \rightarrow N_B m_B$, and $\kappa \rightarrow \kappa_B$, I_{14} can be expressed as

$$I_{14} = -\overline{\gamma}_B^g \left(\frac{k}{C_3}\right)^{-g} \Gamma(1+g). \quad (\text{E.61})$$

Next, by substituting (E.61) into (E.60), and the resulting expression in (2.15), it follows that

$$\mathcal{M}(g) = -C_4 \left(\frac{k}{C_3}\right)^{-g} \Gamma(1+g). \quad (\text{E.62})$$

Taking the derivative of (E.62), this yields

$$\frac{d\mathcal{M}(g)}{dg} = C_4 \left(\frac{k}{C_3}\right)^{-g} \Gamma(1+g) \left(\ln\left(\frac{k}{C_3}\right) - \psi(1+g) \right). \quad (\text{E.63})$$

Inserting (E.63) into (2.14), it follows that

$$t = -\log_2(e) C_4 \left(\mathcal{C} + \ln\left(\frac{k}{C_3}\right) \right). \quad (\text{E.64})$$

Substituting (E.64) into (2.13), this yields

$$\overline{C}_B^{\overline{\gamma}_B \rightarrow \infty} \approx \log_2(N_B \overline{\gamma}_B) + \log_2(e) C_4 \left(\mathcal{C} + \ln\left(\frac{k}{C_3}\right) \right). \quad (\text{E.65})$$

□ **When** $T_8 \neq 0$

Here, again with the help of (D.19) and (5.6) with $\bar{\gamma} \rightarrow N_B \bar{\gamma}_B$, $\mu \rightarrow N_B \mu_B$, $m \rightarrow N_B m_B$, and $\kappa \rightarrow \kappa_B$, I_{12} can be expressed as

$$I_{14} = -\bar{\gamma}_B^g g \left(\frac{k}{C_3} \right)^{-g-T_8} \Gamma(g+T_8). \quad (\text{E.66})$$

Then, by plugging (E.66) into (E.60), and the resulting expression in (2.15), this gets to

$$\mathcal{M}(g) = -g C_4 \left(\frac{k}{C_3} \right)^{-g-T_8} \Gamma(g+T_8). \quad (\text{E.67})$$

Taking the derivative of (E.67), this yields

$$\frac{d\mathcal{M}(g)}{dg} = -C_4 \left(\frac{k}{C_3} \right)^{-g-T_8} \Gamma(g+T_8) \left(1 - g \ln \left(\frac{k}{C_3} \right) + g\psi(g+T_8) \right). \quad (\text{E.68})$$

Inserting (E.68) into (2.14), it follows that

$$t = -\log_2(e) C_4 \left(\frac{k}{C_3} \right)^{-g-T_8} \Gamma(g+T_8). \quad (\text{E.69})$$

Next, substituting (E.69) into (2.13), this gets to

$$\bar{C}_B^{\bar{\gamma}_B \rightarrow \infty} \approx \log_2(N_B \bar{\gamma}_B) + \log_2(e) C_4 \left(\frac{k}{C_3} \right)^{-g-T_8} \Gamma(g+T_8). \quad (\text{E.70})$$

Finally, by replacing (E.58) together with (E.65) and (E.70) into (2.12), \bar{C}_S^∞ is formulated as in (5.23). This completes the proof.

F PROOF OF THEOREM 1

Knowing that if X is a random variable with expectation $\mathbb{E}[X]$ and Y is another random variable distributed on the same probability space of X , then [177]

$$\mathbb{E}\{X\} = \mathbb{E}\{\mathbb{E}\{X|Y\}\}. \quad (\text{F.1})$$

Next, from (6.2), it is defined the set $Z = \{H_{i,1}, H_{i,b}, \Theta_i\}$. Now, using the law of total expectation in (F.2) on the set Z , the total expectation of (6.2) and (6.5) can be reformulated as

$$\mathbb{E}\{H_b H_e\} = \mathbb{E}\{\mathbb{E}\{H_b H_e|Z\}\}. \quad (\text{F.2})$$

Here, note that H_b is constant when conditioned to Z , so that it can be taken off the inner expectation operation as

$$\mathbb{E}\{H_b H_e\} = \mathbb{E}\{H_b \mathbb{E}\{H_e|Z\}\}. \quad (\text{F.3})$$

Then, by expanding the inner expectation in (F.3) with respect to (6.5), and noting that $H_{i,1}$ are constant when conditioned to Z , it follow that

$$\mathbb{E}\{H_e|Z\} = \frac{1}{n} \sum_{i=1}^n |H_{i,1}| \mathbb{E}\{|H_{i,e}| e^{j\Psi_i}\}. \quad (\text{F.4})$$

Here, based on the results given in [161], the distribution of Ψ_i is uniform in any interval of length 2π provided that $\angle H_{i,e}$ is uniformly distributed in the same interval. Now, under the mild assumption that $|H_{i,e}|$ and $e^{j\Psi_i}$ are independent, which is the case for instance of $|H_{i,e}|$ being Rayleigh distributed, it follows that

$$\mathbb{E}\{H_e|Z\} = 0. \quad (\text{F.5})$$

Therefore, the independence between H_b and H_e is stated.

G DERIVATION OF THE SOP AND THE ASYMPTOTIC SOP EXPRESSIONS

The derivation of the SOP and the Asymptotic SOP analytical expressions for the FN/Rayleigh (FR), Nakagami/Rayleigh (NR) and Beckmann/Rayleigh (BR) scenarios are provided here.

G.1 PROOF OF LEMMA 1

G.1.1 SOP_{FR}

From [164, Corollary 5], an alternative formulation of the SOP for the FN/Rayleigh case is given by

$$\text{SOP}_{\text{FR}} = F_{\gamma_b}(\tau - 1) + \exp\left(\frac{\tau-1}{\tau\bar{\gamma}_e}\right) \mathcal{M}_{\gamma_b}^u\left(-\frac{1}{\tau\bar{\gamma}_e}, \tau - 1\right), \quad (\text{G.1})$$

where $\tau = 2^{R_S}$, and $F_{\gamma_b}(\cdot)$ is the κ - μ CDF distribution with $\kappa = K$ and $\mu_{\kappa-\mu} = 1/2$ given by [163, Eq. (3)]

$$F_{\gamma_b}(\gamma) = 1 - Q_{0.5}\left(\sqrt{K}, \sqrt{\frac{(1+K)\gamma}{\bar{\gamma}_b}}\right). \quad (\text{G.2})$$

and

$$\mathcal{M}_{\gamma_b}^u(-1/\tau, \tau - 1) = \mathcal{M}_{\gamma_b}(-1/\tau) - \mathcal{M}_{\gamma_b}^l(-1/\tau, \tau - 1), \quad (\text{G.3})$$

$\mathcal{M}_{\gamma_b}(\cdot)$, $\mathcal{M}_{\gamma_b}^u(\cdot, \cdot)$, and $\mathcal{M}_{\gamma_b}^l(\cdot, \cdot)$ are the conventional moment generating function (MGF), the upper-incomplete MGF, and the lower-incomplete (IMGF) of the RV γ_b , which follows a squared κ - μ distribution, respectively [164, Eq. (3)]. From [164, Table I], it follows that

$$\begin{aligned} \mathcal{M}_{\gamma_b}^l(s, z) &= \frac{(1/2)^{1/2}(1+K)^{1/2}}{(1/2(1+K) - \bar{\gamma}_b s)^{1/2}} \exp\left(\frac{1/2K\bar{\gamma}_b s}{1/2(1+K) - \bar{\gamma}_b s}\right) \\ &\times \left[1 - Q_{1/2}\left(\sqrt{\frac{1/2K(1+K)}{1/2K(1+K) - \bar{\gamma}_b s}}, \sqrt{2\left(\frac{1+K}{2\bar{\gamma}_b s} - s\right)z}\right) \right] \end{aligned} \quad (\text{G.4})$$

$$\mathcal{M}_{\gamma_b}(s) = \frac{(1/2)^{1/2}(1+K)^{1/2}}{1/2(1+K) - \bar{\gamma}_b s} \exp\left(\frac{K\bar{\gamma}_b s}{(1+K) - \bar{\gamma}_b s}\right). \quad (\text{G.5})$$

Then, by combining (G.1) to (G.5), the SOP_{FR} can be expressed as in (6.18). This completes the proof.

G.1.2 $\text{SOP}_{\text{FR}}^{\infty} (\bar{\gamma}_b \rightarrow \infty)$

By using the asymptotic approach given in [178], the CDF of a κ - μ RV can be asymptotically approximate as

$$F_{\gamma_b}(\gamma_b) \simeq \frac{\exp(-K\mu) \gamma_b^{\mu} K^{\frac{1-\mu}{2}} (1+K)^{\frac{1+\mu}{2}} \bar{\gamma}_b^{\frac{-1-\mu}{2}}}{\Gamma(\mu) \left(\mu \sqrt{\frac{K(1+K)}{\bar{\gamma}_b}}\right)^{1-\mu}}, \quad (\text{G.6})$$

Then, by substituting (G.6) together with the Exponential PDF given in (6.16) into (2.5), this yields

$$\text{SOP}_{\text{FR}}^{\infty} \simeq \frac{\exp(-K\mu) K^{\frac{1-\mu}{2}} (1+K)^{\frac{1+\mu}{2}} \bar{\gamma}_b^{\frac{-1-\mu}{2}}}{\Gamma(\mu) \left(\mu \sqrt{\frac{K(1+K)}{\bar{\gamma}_b}}\right)^{1-\mu}} \underbrace{\int_0^{\infty} (\gamma_e \tau + \tau - 1)^{\mu} \exp\left(\frac{\gamma_e}{\bar{\gamma}_e}\right) d\gamma_e}_{I_1}. \quad (\text{G.7})$$

Finally, by solving the integral I_1 with the aid of the mathematical software package Wolfram Mathematica, and then setting $\kappa = K$ and $\mu = 1/2$, the $\text{SOP}_{\text{FR}}^{\infty}$ can be formulated as (6.19). This concludes the proof.

G.2 PROOF OF LEMMA 2

G.2.1 SOP_{BR}

Recalling [164, Corollary 5], the SOP given in (2.5) for the Beckmann/Rayleigh case can be reformulated as

$$\text{SOP}_{\text{BR}} = F_{\gamma_b}(\tau - 1) + \exp\left(\frac{\tau-1}{\tau\bar{\gamma}_e}\right) \mathcal{M}_{\gamma_b}^u\left(-\frac{1}{\tau\bar{\gamma}_e}, \tau - 1\right), \quad (\text{G.8})$$

where $F_{\gamma_b}(\cdot)$ is the squared Beckmann CDF [164, Eq. (7)] , which can be computed with the aid of Matlab code developed in appendix I. Furthermore, the $\mathcal{M}_{\gamma_b}^u(\cdot, \cdot)$ [164, Eq. (3)] of the RV γ_b , which follows a squared Beckmann distribution can be computed by using the Matlab code given in appendix J. Such algorithm was implemented with the help of the inverse Laplace transformation [165] as proposed in [164, Eq.4].

G.2.2 SOP_{BR}[∞] ($\bar{\gamma}_b \rightarrow \infty$)

Substituting the MGF of the squared Beckmann distribution [120, Eq. (2.41)]

$$\begin{aligned} \mathcal{M}_{\gamma_b}(s) &= \frac{(1+q^2)(1+K)}{\sqrt{((1+q^2)(1+K) - 2q^2\bar{\gamma}_b s)((1+q^2)(1+K) - 2\bar{\gamma}_b s)}} \\ &\quad \times \exp\left(\frac{(1+q^2)K\bar{\gamma}_b s}{(1+q^2)(1+K) - 2\bar{\gamma}_b s}\right). \end{aligned} \quad (\text{G.9})$$

into [122, Proposition 3] with $d = 1$ ^[1], this yields

$$\begin{aligned} \text{SOP}_{\text{BR}}^\infty &\simeq \lim_{s \rightarrow \infty} \frac{s(1+q^2)(1+K)(\bar{\gamma}_e \tau + \tau - 1)}{\sqrt{((1+q^2)(1+K) - 2q^2\bar{\gamma}_b s)((1+q^2)(1+K) - 2\bar{\gamma}_b s)}} \\ &\quad \times \exp\left(\frac{(1+q^2)K\bar{\gamma}_b s}{(1+q^2)(1+K) - 2q^2\bar{\gamma}_b s}\right). \end{aligned} \quad (\text{G.10})$$

Finally, by performing the limit in (G.10) with the aid of Wolfram Mathematica, the SOP_{BR} can be expressed in closed-form fashion as in (6.21). This completes the proof.

G.3 PROOF OF LEMMA 3

G.3.1 SOP_{NR}

Again, by making use of [164, Corollary 5], the SOP given in (2.5) for the Nakagami-Rayleigh case can be reformulated as

$$\text{SOP}_{\text{NR}} = F_{\gamma_b}(\tau - 1) + \exp\left(\frac{\tau-1}{\tau\bar{\gamma}_e}\right) \mathcal{M}_{\gamma_b}^u\left(-\frac{1}{\tau\bar{\gamma}_e}, \tau - 1\right), \quad (\text{G.11})$$

where $F_{\gamma_b}(\cdot)$ is the squared Nakagami- m CDF given as in [99, Eq. (3)] by

$$F_{\gamma_b}(\gamma) = \frac{\Upsilon\left(m, \frac{m\gamma}{\bar{\gamma}_b}\right)}{\Gamma(m)}. \quad (\text{G.12})$$

Next, from [164, Eq. (2)], the $\mathcal{M}_{\gamma_b}^u(\cdot, \cdot)$ in (G.11) is defined as

$$\mathcal{M}_{\gamma_b}^u\left(-\frac{1}{\tau\bar{\gamma}_e}, \tau - 1\right) = \underbrace{\int_{\tau-1}^{\infty} \exp\left(-\frac{1}{\tau\bar{\gamma}_e}\gamma_b\right) f_{\gamma_b}(\gamma_b) d\gamma_b}_{T_1} \quad (\text{G.13})$$

^[1] Setting $d = 1$ is because in a single-input single-output communication system over the Beckmann fading channel, diversity order equals unity.

by substituting (6.14) into (G.13), T_1 term is expressed as

$$T_1 = \frac{m^m}{\Gamma(m)\bar{\gamma}_b^m} \underbrace{\int_{\tau-1}^{\infty} x^{m-1} \exp\left(-x\left(\frac{m}{\bar{\gamma}_b} + \frac{1}{\tau\bar{\gamma}_e}\right)\right) dx}_{I_2}. \quad (\text{G.14})$$

Employing [168, Eq. (3.351.2)], I_2 can be expressed in simple exact closed-form. Finally, by combining (G.11)-(G.14), the SOP_{NR} can be attained as in (6.22). This completes the proof.

G.3.2 $\text{SOP}_{\text{NR}}^{\infty} (\bar{\gamma}_b \rightarrow \infty)$

From [99, Eq. (21)], the $\text{SOP}_{\alpha-\mu}^{\infty}$ for a MIMO system over $\alpha-\mu$ fading channels, is given by

$$\begin{aligned} \text{SOP}_{\alpha-\mu}^{\infty} = & \frac{2^{\frac{R_S M_A M_B \alpha_B \mu_B}{2}} \Gamma\left(M_E \mu_E + M_A M_B \mu_B \frac{\alpha_B}{\alpha_E}\right) \mu_B^{M_A(M_B \mu_B - 1)} M_B^{M_A(M_B \mu_B - M_B \mu_B \alpha_B / 2 - 1)}}{\Gamma(M_E \mu_E) \Gamma(M_A M_B \mu_B) \mu_E^{M_A M_B \mu_B \frac{\alpha_B}{\alpha_E}} M_E^{M_A M_B \mu_B \left(\frac{\alpha_B}{\alpha_E} - \frac{\alpha_B}{2}\right)}} \\ & \times \left(\frac{\bar{\gamma}_e}{\bar{\gamma}_b}\right)^{M_A M_B \mu_B \alpha_B / 2} \end{aligned} \quad (\text{G.15})$$

where M_i for $i \in \{A, B, E\}$ are the number of antennas at the source, destination, and the eavesdropper. Also, μ_i, α_i for $i \in \{A, B, E\}$ denote the fading parameters of the $\alpha-\mu$ fading channel. Now, knowing that the Nakagami-Rayleigh case is a particular case of $\alpha-\mu$ distribution, the system parameters are set $M_A = M_B = M_E = 1$, $\mu_B = m$, $\mu_E = 1$, and $\alpha_B = \alpha_E = 2$. Therefore, the $\text{SOP}_{\text{NR}}^{\infty}$ is obtained as in (6.23). This completes the proof.

H DERIVATION OF THE ASR AND THE ASYMPTOTIC ASR EXPRESSIONS

Here, mathematical expressions of the ASR, and the Asymptotic ASR for the FN/Rayleigh (FR), Nakagami/Rayleigh (NR) and Beckmann/Rayleigh (BR) scenarios are derived.

H.1 PROOF OF LEMMA 4

H.1.1 ASR_{S-FR}

By replacing [149, Eq. (9.6.10)] into the κ - μ PDF given in (6.13), this gets to

$$f_{\gamma_b}(\gamma) = \frac{\mu(1+K)^{\frac{\mu+1}{2}} \gamma^{\frac{\mu-1}{2}}}{K^{\frac{\mu-1}{2}} \bar{\gamma}_b^{\frac{\mu+1}{2}} \exp(\mu K)} \exp\left(-\frac{(1+K)\gamma\mu}{\bar{\gamma}_b}\right) \sum_{z=0}^{\infty} \frac{1}{z! \Gamma(\mu+z)} \left(\mu \sqrt{\frac{K(K+1)}{\bar{\gamma}_b}}\right)^{\mu-1+2z}. \quad (\text{H.1})$$

Next, by replacing (H.1) into (2.10), the average secrecy capacity of the main link is given by

$$\begin{aligned} \bar{C}_B &= \frac{\mu(1+K)^{\frac{\mu+1}{2}}}{\ln(2) K^{\frac{\mu-1}{2}} \bar{\gamma}_b^{\frac{\mu+1}{2}} \exp(\mu K)} \sum_{z=0}^{\infty} \frac{1}{z! \Gamma(\mu+z)} \int_0^{\infty} \gamma^{\frac{\mu-1}{2}} \ln(1+\gamma) \exp\left(-\frac{(1+K)\gamma\mu}{\bar{\gamma}_b}\right) \\ &\quad \times \left(\mu \sqrt{\frac{K(K+1)}{\bar{\gamma}_b}}\right)^{\mu-1+2z} d\gamma. \end{aligned} \quad (\text{H.2})$$

Using the Meijer's G-function $G_{p,q}^{m,n}[\cdot]$ representations of both $\exp(\cdot)$ [154, id. (01.03.26.0004.01)] and $\ln(\cdot)$ [154, id. (01.04.26.0003.01)], this leads to

$$\begin{aligned} \bar{C}_B &= \frac{1}{\ln 2} \frac{\mu(1+K)^{(\mu+1)/2}}{K^{(\mu-1)/2} \bar{\gamma}_b^{(\mu+1)/2} \exp(\mu K)} \sum_{z=0}^{\infty} \frac{1}{z! \Gamma(\mu+z)} \left(\mu \sqrt{\frac{K(K+1)}{\bar{\gamma}_b}}\right)^{\mu-1+2z} \\ &\quad \times \underbrace{\int_0^{\infty} \gamma_b^{\mu+z-1} G_{2,2}^{1,2} \left[\gamma_b \middle| \begin{matrix} 1, 1 \\ 1, 0 \end{matrix} \right] G_{0,1}^{1,0} \left[\frac{\gamma_b \mu (1+K)}{\bar{\gamma}_b} \middle| \begin{matrix} - \\ 0 \end{matrix} \right] d\gamma_b}_{I_1} \end{aligned} \quad (\text{H.3})$$

Here, I_1 can be solved with the help of [154, id. (07.34.21.0011.01)]. Next, by replacing [163, Eq. (28)] into the κ - μ CDF given in (G.2), it follows that

$$F_{\gamma_b}(\gamma) = 1 - \sum_{l=0}^{\infty} \frac{(2K\mu)^l \Gamma\left(\mu + l, \frac{(1+K)\mu\gamma}{\bar{\gamma}_b}\right)}{l! \Gamma(\mu + l) 2^l \exp(K\mu)}. \quad (\text{H.4})$$

Now, from (6.16), the exponential CDF can be expressed as

$$F_{\gamma_e}(\gamma) = 1 - \exp\left(-\frac{\gamma}{\bar{\gamma}_e}\right), \quad (\text{H.5})$$

Substituting (H.4) and (H.5) into (2.11), it follows that

$$\mathcal{L}(\bar{\gamma}_b, \bar{\gamma}_e) = \frac{1}{\ln 2} \sum_{l=0}^{\infty} \frac{(\mu K)^l}{l! \exp(\mu K)} \sum_{z=0}^{\mu+l-1} \frac{1}{z!} \left(\frac{\mu(1+K)}{\bar{\gamma}_b}\right)^z \underbrace{\int_0^{\infty} \frac{\gamma_e^z}{1+\gamma_e} \exp\left(-\gamma_e \left(\frac{1}{\bar{\gamma}_e} + \frac{\mu(1+K)}{\bar{\gamma}_b}\right)\right) d\gamma_e}_{I_2} \quad (\text{H.6})$$

With the aid of [168, Eq. (3.353.5)], I_2 can be evaluated in exact fashion. Next, by substituting (H.3) and (H.6) into the definition of the ASR, i.e., [99, Eq. (29)]

$$\bar{\mathcal{R}}_S = \bar{\mathcal{C}}_B - \mathcal{L}(\bar{\gamma}_b, \bar{\gamma}_e), \quad (\text{H.7})$$

and then setting $\mu = 1/2$, the $\bar{\mathcal{R}}_{S\text{-FN}}$ can be formulated as in (6.24), which concludes the proof.

H.1.2 ASR_{S-FR}[∞] ($\bar{\gamma}_b \rightarrow \infty$)

An alternative formulations of the ASR and asymptotic ASR given in (2.8) and (2.12), respectively, can be expressed as in [99] by

$$\mathcal{R}_S \approx \bar{\mathcal{C}}_B - \bar{\mathcal{C}}_E + \mathcal{G}_Z(\bar{\gamma}_b, \bar{\gamma}_e), \quad (\text{H.8})$$

$$\mathcal{R}_S^\infty \approx \bar{\mathcal{C}}_B - \bar{\mathcal{C}}_E, \quad (\text{H.9})$$

$$\approx \log_2(\bar{\gamma}_b) - t - \bar{\mathcal{C}}_E, \quad (\text{H.10})$$

where t is given by (2.14), and

$$\mathcal{G}_Z(\bar{\gamma}_b, \bar{\gamma}_e) = \frac{e^{1/\bar{\gamma}_e}}{\ln 2} \int_0^1 \frac{1}{u} e^{-1/(u\bar{\gamma}_e)} \mathcal{M}_{\gamma_b}\left(\frac{-1}{u\bar{\gamma}_e}\right) du, \quad (\text{H.11})$$

in which $\mathcal{M}_{\gamma_b}(\cdot)$ is the conventional MGF of γ_b . From [179, Eq. (22)], the $\mathcal{G}_Z(\bar{\gamma}_b, \bar{\gamma}_e)$ term for the Folded Normal-Rayleigh case can be calculated directly as

$$\mathcal{G}_Z(\bar{\gamma}_b, \bar{\gamma}_e) = -\log_2(e)\psi(\mu) + \log_2(\mu) + \log_2(1+K) - K \log_2(e) {}_2F_2(1, 1; 2, \mu+1; -\mu K). \quad (\text{H.12})$$

Now, by replacing the Exponential PDF given in (6.16) into (2.10), the average capacity of the eavesdropper link, \bar{C}_E , can be expressed as

$$\bar{C}_E = \frac{1}{\bar{\gamma}_e \ln 2} \underbrace{\int_0^\infty \ln(1 + \gamma_e) \exp\left(-\frac{\gamma_e}{\bar{\gamma}_e}\right) d\gamma_e}_{I_3}. \quad (\text{H.13})$$

Here, employing [168, Eq. (4.337.2)], the integral in I_3 can be expressed in simple exact closed-form. Then, by substituting (H.12) by setting $\mu = 1/2$ together with (H.13) into (H.10), the $\bar{\mathcal{R}}_{S-FN}^\infty$ can be attained as in (6.25). This completes the proof.

H.2 PROOF OF LEMMA 5

H.2.1 ASR_{S-BR}

An equivalent expression of (2.10) can be expressed as in [180, Eq. (7)] by

$$\bar{C}_B = \frac{1}{\ln 2} \int_0^\infty E_1(x) \phi_{\gamma_b}(x) dx. \quad (\text{H.14})$$

where $\phi_{\gamma_b}(\cdot)$ is the generalized MGF of the Beckmann given in [19, Eq. (6)] with $r \rightarrow \infty$ and $n = 1$ as

$$\begin{aligned} \phi_{\gamma_b}(s) = & \frac{1}{\left[\left(\frac{(1+q^2)}{(1+K)^{-1}} - 2s\bar{\gamma}_b\right) \left((1+K)(1+q^2) - 2q^2s\bar{\gamma}_b\right)\right]^{5/2}} \left[\frac{(1+q^2)}{(1+K)^{-1}}\right] \\ & \times \exp\left(-\frac{K\bar{\gamma}_b(1+q^2)x}{(1+K)(1+q^2) - 2q^2s\bar{\gamma}_b}\right) \bar{\gamma}_b \left((1+K)(1+q^2) - 2s\bar{\gamma}_b\right) \\ & \times \left(\frac{(1+q^2)^3}{(1+K)^{-3}} - \frac{2(1+q^2)}{(1+K)^{-1}} \left(K + (3+K)q^2 + q^4\right) s\bar{\gamma}_b - 8q^4s^2\bar{\gamma}_b^2\right). \end{aligned} \quad (\text{H.15})$$

Now, by replacing (H.15) in (H.14), this leads to

$$\begin{aligned} \bar{C}_B = & \frac{1}{\ln 2} \int_0^\infty \frac{E_1(x)}{\underbrace{\left[\left(\frac{(1+q^2)}{(1+K)^{-1}} + 2x\bar{\gamma}_b\right) \left((1+K)(1+q^2) + 2q^2x\bar{\gamma}_b\right)\right]^{5/2}}_{f_1'(x)}} \left[\frac{(1+q^2)}{(1+K)^{-1}}\right] \\ & \times \int_0^\infty \underbrace{\exp\left(-\frac{K\bar{\gamma}_b(1+q^2)x}{(1+K)(1+q^2) + 2q^2x\bar{\gamma}_b}\right) \bar{\gamma}_b \left((1+K)(1+q^2) + 2x\bar{\gamma}_b\right)}_{f_1(x)} \\ & \times \int_0^\infty \underbrace{\left(\frac{(1+q^2)^3}{(1+K)^{-3}} + \frac{2(1+q^2)}{(1+K)^{-1}} \left(K + (3+K)q^2 + q^4\right) x\bar{\gamma}_b + 8q^4x^2\bar{\gamma}_b^2\right)}_{f_1(x)} dx. \end{aligned} \quad (\text{H.16})$$

Here, one can rewrite the integral in (H.16) as

$$I_4 = \int_0^{\infty} \exp(-x) f_1(x) dx, \quad (\text{H.17})$$

where $f_1(x) = \exp(x) f_1'(x)$. Now, according to the Gauss-Laguerre quadrature (QLQ) method [149, Eq. (25.4.45)], I_4 can be closely approximated by a weighted sum as

$$I_4 \approx \sum_{i=1}^h w_i f_1(k_i), \quad (\text{H.18})$$

in which k_i is the i -th zero of the Laguerre polynomial $L_h(x)$ [149, Eq. (22.2.13)], and $w_i = l_i \times [(h+1)L_{h+1}(k_i)]^{-2}$. Then, by substituting the conventional MGF of the Beckmann distribution given in (G.9) with $s = -1/(u\bar{\gamma}_e)$ into (H.11), it follows that

$$\mathcal{G}_Z(\bar{\gamma}_b, \bar{\gamma}_e) = \frac{e^{1/\bar{\gamma}_e}}{\ln 2} \int_0^1 \frac{1}{u} e^{-1/(u\bar{\gamma}_e)} \underbrace{e^{-\frac{K(1+q^2)\bar{\gamma}_b}{2\bar{\gamma}_b+(1+K)(1+q^2)u\bar{\gamma}_e}} (1+K)(1+q^2)(u\bar{\gamma}_e)}_{f_2(u)} \frac{du}{\sqrt{\left(\frac{2}{\bar{\gamma}_b} + \frac{(1+q^2)u\bar{\gamma}_e}{(1+K)^{-1}}\right) \left(\frac{2q^2}{\bar{\gamma}_b} + \frac{(1+q^2)u\bar{\gamma}_e}{(1+K)^{-1}}\right)}} \quad (\text{H.19})$$

In order to solve the integral in (H.18), a change of variables $u = 1 - e^{-w}$ is performed, so that the original integration limits are transformed of $(0, 1)$ to $(0, \infty)$. Therefore, the integral in (H.18) can be rewritten as

$$I_5 = \int_0^{\infty} \exp(-w) f_2(w) dw, \quad (\text{H.20})$$

where $f_2(w) = f_2'(1 - e^{-w})$. Again, making use of QLQ method [149, Eq. (25.4.45)], I_5 can be closely approximated by a weighted sum as

$$I_5 \approx \sum_{i=1}^r w_i f_2(l_i), \quad (\text{H.21})$$

where l_i, r and w_i are defined in a similar way as in (H.18). Finally, by substituting (H.13), (H.16), and (H.19) into (H.8), the $\bar{\mathcal{R}}_{\text{S-BR}}$ can be obtained as in (6.28). This completes the proof.

H.2.2 ASR $_{\text{S-BR}}^{\infty}$ ($\bar{\gamma}_b \rightarrow \infty$)

Inserting (H.13) and (H.16) into (H.9), the asymptotic ASR for the Beckmann/Rayleigh case, i.e., $\bar{\mathcal{R}}_{\text{S-BR}}^{\infty}$ can be approximated as in (6.29), which completes the proof.

H.3 PROOF OF LEMMA 6

H.3.1 ASR_{S-NR}

Employing the identity [168, Eq. (8.352.6)]

$$\Upsilon(n, x) = (n-1)! \left(1 - \exp(-x) \sum_{z=0}^{n-1} \frac{x^z}{z!} \right), \quad (\text{H.22})$$

for the lower incomplete gamma function in the squared Nakagami- m CDF given in (G.12), this leads to

$$F_{\gamma_b}(\gamma) = 1 - \exp\left(-\frac{m\gamma}{\bar{\gamma}_b}\right) \sum_{z=0}^{m-1} \frac{1}{z!} \left(\frac{m\gamma}{\bar{\gamma}_b}\right)^z. \quad (\text{H.23})$$

Substituting (H.23) into (2.9), it follows that

$$\bar{C}_B = \frac{1}{\ln 2} \sum_{z=0}^{m-1} \frac{1}{z!} \left(\frac{m}{\bar{\gamma}_b}\right)^z \underbrace{\int_0^\infty \frac{\gamma_b^z}{1 + \gamma_b} \exp\left(-\frac{m\gamma_b}{\bar{\gamma}_b}\right) d\gamma_b}_{I_6}. \quad (\text{H.24})$$

With the aid of [168, Eq. (3.353.5)], I_6 can be evaluated in exact closed-form. Now, substituting the exponential CDF given in (H.5) and the squared Nakagami- m CDF given in (H.23) into (2.11), this yields

$$\mathcal{L}(\bar{\gamma}_b, \bar{\gamma}_e) = \frac{1}{\ln 2} \sum_{z=0}^{m-1} \frac{1}{z!} \left(\frac{m}{\bar{\gamma}_b}\right)^z \underbrace{\int_0^\infty \frac{\gamma_b^z}{1 + \gamma_b} \exp\left(-\gamma_b \left(\frac{m}{\bar{\gamma}_b} + \frac{1}{\bar{\gamma}_e}\right)\right) d\gamma_b}_{I_7}. \quad (\text{H.25})$$

Similar to the evaluation of I_6 , the identity [168, Eq. (3.353.5)] is used to calculate I_7 . Finally, by combining (H.24) and (H.25) into (2.8), the $\bar{\mathcal{R}}_{S-NR}$ can be formulated as in (6.30), which concludes the proof.

H.3.2 ASR_{S-NR}[∞] ($\bar{\gamma}_b \rightarrow \infty$)

Here, the goal is to find an asymptotic ASR expression as in (H.10) for the Nakagami-Rayleigh case. Hence, from [181, Eq. (16)] by setting $\mu_{\alpha-\mu} = m$ and $\alpha = 2$, the $\mathcal{M}(g)$ of the Nakagami- m distribution needed in (2.14) can be formulated as

$$\mathcal{M}(g) = \frac{\Gamma(m+g)}{m^g \Gamma(m)}. \quad (\text{H.26})$$

Next, taking the derivative of (H.26) with respect to g , it follows that

$$\mathcal{M}'(g) = \frac{\Gamma(g+m) (-\ln(m) + \psi(g+m))}{m^g \Gamma(m)} \quad (\text{H.27})$$

Then, by setting $g = 0$ in (H.27) and then substituting the resulting expression into (2.14), this gets to

$$t = -\log_2(e) (-\ln(m) + \psi(m)). \quad (\text{H.28})$$

Finally, by replacing (H.28) and (H.13) into (H.10), the $\overline{\mathcal{R}}_{\text{S-NR}}^\infty$ is attained as in (6.31). This completes the proof.

I MATLAB CODE FOR BECKMANN CDF

```
1 %-----
- % CDF of the SNR Beckmann distribution
- % Definitions
- % omega: the mean power of the SNR Beckman distribution
5 % g: the random variable
- %-----
- function [cdf] = CDFBeckmann(K,q,omega,g)
- th0=0;
- mu2=0;
10 mu1=sqrt(K*omega./(K+1));
- sigma2=sqrt(omega./((K+1).*(q.^2+1)));
- sigma1=q*sqrt(omega./((K+1).*(q.^2+1)));
- A=sqrt(mu1.^2+mu2.^2);
- integrand=@(theta)(1./(2*fgamma(theta,sigma1,sigma2)).*(1-exp(- ...
15 fgamma(theta,sigma1,sigma2).*g+sqrt(g).*frho(A,sigma1,sigma2,...
- th0,theta)))+frho(A,sigma1,sigma2,th0,theta).*sqrt(pi)./(4.*...
- fgamma(theta,sigma1,sigma2).^(1.5)).*exp(frho(A,sigma1,...
- sigma2,th0,theta).^2./(4.*fgamma(theta,sigma1,sigma2))).*...
- (erf(frho(A,sigma1,sigma2,th0,theta)./(2*sqrt(fgamma(theta,...
20 sigma1,sigma2)))))+erf((2*fgamma(theta,sigma1,sigma2).*sqrt(g)...
- frho(A,sigma1,sigma2,th0,theta))./(2.*sqrt(fgamma(theta,...
- sigma1,sigma2))))));
- cdf=1./(2*pi*sigma1.*sigma2).*exp(-A.^2.*fgamma(th0,sigma1,...
- sigma2)).*integral(integrand,0,2*pi,'ArrayValued',true);
25 end
- function z=fgamma(th,sigma1,sigma2)
- z=cos(th).^2./(2*sigma1.^2)+sin(th).^2./(2*sigma2.^2);
- end
- function z=frho(A,sigma1,sigma2,th0,th)
30 z=A.*(cos(th).*cos(th0)./(sigma1.^2)+sin(th).*sin(th0)./(sigma2.^2));
- end
```

J MATLAB CODE FOR UPPER INCOMPLETE MOMENT GENERATION FUNCTION OF THE BECKMANN DISTRIBUTION

```

1 function y=uIMGFBeckmann(K,q,omega,s,z)
- %-----
- %Definitions
- %z: the random variable
5 %omega: the mean power of the SNR Beckmann Distribution
- %-----
- N=1e4;
- A=15;
- % Inverse Laplace Transform
10 C=exp(A/2) ./ z;
- alphainv=[0.5,ones(1,N-1)];
- n=0:N-1;
- p=(A+2*pi*i*n)/(2*z);
- y1=(-1).^n.*alphainv.*real(1./p.*MGFbeckmann(K,q,omega,s-p));
15 y=C.*sum(y1);
- y=MGFbeckmann(K,q,omega,s)-y;
- end
- function MGF = MGFbeckmann(K,q,omega,s)
- aux=exp(K.*(1+q.^2).*omega.*s./((1+q.^2).(1+K)-2.*q.^2.*omega.*s));
20 MGF=(1+q.^2).(1+K)./(sqrt((1+q.^2).(1+K)-2.*q.^2.*omega.*s)).*...
- sqrt((1+q.^2).(1+K)-2*omega.*s)).*aux;
- end

```